

UNIVERSITÉ PARIS XIII - SORBONNE PARIS NORD
École Doctorale Sciences, Technologies, Santé Galilée

Continuous-wave operating conditions of organic solid-state lasers: the role of triplet states

THÈSE DE DOCTORAT

présentée par

Anthony DALL'AGNOL

Laboratoire de Physique des Lasers

pour l'obtention du grade de
DOCTEUR EN PHYSIQUE

soutenue le 26 janvier 2023 devant le jury d'examen composé de :

CLAVIER Gilles, Directeur de recherche CNRS Rapporteur
RIBIERRE Jean-Charles, Professor Rapporteur
D'ALEO Anthony, Chargé de recherche CNRS Examineur
BRETENAKER Fabien, Professeur des universités Examineur
ISHOW Éléna, Professeure des universités Examinatrice
CHÉNAIS Sébastien, Professeur des universités Directeur de thèse
FORGET Sébastien, Professeur des universités Co-directeur de thèse

Abstract

The last five years have been the witnesses of many breakthroughs regarding organic solid-state lasers (OSSLs). However, the demonstration of a continuous-wave (CW) lasing emission remains a challenge that is essential to overcome in order to reach practical applications. A part of this limitation arises from a well-defined triplet state that is specific to organic molecules, to which atoms on the fluorescence energy level are promoted *via* intersystem crossing (ISC) $S_1 \rightarrow T_1$. Although triplet states do not participate in light emission for most compounds, an irretrievable accumulation of T_1 atoms whose lifetimes are much longer than the fluorescence have always caused the premature death of the laser by depletion of the gain medium ground state, intermolecular interactions or absorption of photons by triplet excitons.

Current efforts towards the achievement of CW lasing mostly focus on tailoring the photophysical properties of molecules to reduce the influence of triplet state atoms. Recently, a lasing operation during a quasi-CW 30 ms excitation was reported using BSBCz and then its derivatives in a low-threshold optical resonator, which was ascribed to the low triplet creation yield of the molecules and the removal of parasite absorptions, emphasizing the importance of properties characterizations in organic gain media. Although this achievement has been well explained in the framework of triplet dynamics, few studies have investigated the role of the resonator.

The purpose of this thesis is then twofold: first, the presentation of an experimental protocol to characterize triplet state lifetimes and other triplet-related interactions such as ISC, singlet-triplet annihilation (STA) and triplet-triplet annihilation (TTA) in organic thin films thanks to photoluminescence transients. Because this method is simple, requires neither expensive apparatus nor a spectral resolution, we believe it has the potential to become a useful tool for material properties screening. In a second time, the requirements for OSSLs to achieve CW lasing are investigated with the help of numerical simulations of rate equations and analytical reasonings. By explicitly taking into account the role of the resonator, this work provides a broader view regarding the influences of optical and photophysical losses regarding the lasing pulse duration.

Keywords: organic lasers, continuous-wave lasing, photophysical constant measurements, BSBCz

Résumé en français

Ces cinq dernières années ont été les témoins de grandes avancées dans le domaine des lasers organiques solides (OSSLs). Cependant, la démonstration d'une émission laser continue est toujours un défi qu'il est essentiel de relever pour viser des applications pratiques. Une partie des limitations provient d'une spécificité de molécules organiques: un état triplet T_1 vers lequel les atomes sur le niveau de fluorescence sont transférés *via* un croisement inter-système $S_1 \rightarrow T_1$. Même si ces atomes dans l'état triplet ne participent pas à l'émission de lumière pour la plupart des composés, leur rapide accumulation sur ce niveau dont la durée de vie est bien plus longue que la fluorescence a toujours entraîné la mort prématurée de l'émission laser, à cause d'une dépopulation de l'état fondamental et d'interactions intermoléculaires.

Actuellement, les efforts déployés pour atteindre une émission laser continue consistent principalement à améliorer les propriétés des molécules pour réduire l'influence de ces état triplets. C'est ainsi que récemment, une émission laser durant le temps d'une excitation quasi-continue de 30 ms a été publiée en utilisant du BSBCz implémenté dans un résonateur à très bas seuil, qui a été expliquée par le faible taux de création de triplets par la molécule et la suppression d'absorption parasites, soulignant l'importance de la caractérisation des milieux à gain organiques. Bien que ce succès ait été beaucoup étudié et expliqué à travers le prisme des triplets, peu d'études se sont intéressées au rôle du résonateur.

Le but de cette thèse est alors double. Premièrement, le développement d'une méthode d'évaluation des constantes photophysiques relatives aux triplets tel que leur temps de vie, les taux de croisement inter-système, d'annihilation singulet-triplet (STA) et triplet-triplet (TTA) à l'aide de transitoires de photoluminescence. Cette expérience ne nécessitant pas d'appareils coûteux ni de résolution spectrale, nous pensons qu'elle pourrait être un outil très utile pour caractériser et comparer différentes molécules et leurs propriétés. Dans un deuxième temps, les conditions des OSSLs pour obtenir une émission continue sont étudiées théoriquement par des simulations numériques d'équation de taux et des démonstrations analytiques. En prenant explicitement en compte le rôle de la cavité dans les différentes dynamiques, cette thèse apporte une vue plus large sur les influences des pertes optiques et photophysiques sur les durées d'impulsions lasers.

Mots clés: lasers organiques, émission continue, mesure de constantes photo-

Contents

Abstract	iii
Résumé en français	v
Introduction	1
1 Fundamentals of organic lasers	5
1.1 The concepts behind lasers	5
1.1.1 Laser peculiarities	5
1.1.2 Fundamentals components	6
1.1.3 Light-matter interaction	7
1.1.3.1 Einstein coefficients	7
1.1.3.2 Population inversion	8
1.1.4 Lasers dynamics	10
1.1.4.1 Fluorescence and laser emission	10
1.1.4.2 Requirements to achieve lasing	11
1.1.4.3 Jablonski-Perrin diagram of a four-level configuration	13
1.1.5 Different resonators	14
1.1.6 Applications	15
1.1.7 Summary	16
1.2 Introduction to organic electronics	18
1.2.1 Organic molecules	18
1.2.1.1 Molecular orbitals and conjugated systems	18
1.2.1.2 Electronic transitions and excited states	20
1.2.1.3 Nature of charges in organic semiconductors	22
1.2.2 Jablonski-Perrin diagram of organic systems	23
1.2.3 First excited singlet state: lifetime and luminescence quantum yield	23
1.2.4 First excited triplet state	25
1.2.4.1 The generation of triplet excitons	25
1.2.4.2 Lifetime	28
1.2.4.3 Triplet absorption	29
1.2.4.4 Thermally activated delayed fluorescence	29

1.2.5	Energy transfers	31
1.2.5.1	Förster type	31
1.2.5.2	Dexter type	34
1.2.6	Bi-exciton mechanisms in organic semiconductors	34
1.2.6.1	Singlet-triplet annihilation	34
1.2.6.2	Triplet-triplet annihilation	35
1.2.6.3	Singlet-singlet annihilation	36
1.2.7	Some applications of organic electronics	37
1.2.8	Summary	39
1.3	Organic semiconductors lasers	39
1.3.1	Liquid dyes lasers	40
1.3.2	Thin film based organic lasers	41
1.3.2.1	Limiting the population of the triplet state	42
1.3.2.2	Preventing environmental influences	45
1.3.3	State-of-the-art	46
1.3.3.1	Molecular engineering	46
1.3.3.2	Resonator engineering	49
1.3.3.3	Towards true continuous-wave lasing	50
2	Measurement of triplet state lifetime and triplet-related constants in organic thin films	53
2.1	Introduction	53
2.1.1	State-of-the-art regarding triplet state characterization	54
2.1.1.1	Triplet excited state lifetime	54
2.1.1.2	Intersystem crossing and triplet formation quantum yields	56
2.1.1.3	Triplet-triplet-annihilation	57
2.1.1.4	Singlet-triplet annihilation	59
2.1.2	Aims of this work	61
2.2	Methods	61
2.2.1	Experimental setup	61
2.2.2	Preparation of the thin films	63
2.2.3	Characterization of thin films	64
2.2.3.1	Absorption	65
2.2.3.2	Emission	65
2.2.3.3	Fluorescence lifetime	65
2.2.4	Photoluminescence transients analysis on C521T films	66
2.2.4.1	Triplet lifetime and intersystem crossing	66
2.2.4.2	STA and TTA rates at different concentrations	68
2.2.4.3	Summary	73
2.2.5	Discussions on the method	74
2.2.5.1	Requirements	74

2.2.5.2	Transient absorption spectroscopy measurements	76
2.2.5.3	Avoid pump-induced degradation of the sample during measurements	78
2.2.5.4	Temperature or triplets?	78
2.2.5.5	Pump power density dependency of the triplet lifetime	80
2.2.5.6	On the temporal discrimination of STA from TTA	81
2.3	Results for other compounds	87
2.3.1	Triplet state lifetimes	88
2.3.1.1	Solid PMMA films	88
2.3.1.2	Comparison with liquid dye solution	90
2.3.2	Intersystem crossing	91
2.3.3	Bi-molecular interaction rates	92
2.3.4	CBP:BSBCz 200 nm encapsulated films	97
2.4	Conclusions	99
3	Continuous-wave lasing conditions of organic lasers	101
3.1	Motivations	101
3.2	Previous investigations	102
3.3	Theoretical framework	104
3.3.1	System of equations	105
3.3.1.1	Energy states populations	105
3.3.1.2	Photon density	106
3.3.2	Limits and approximations	107
3.3.3	Resonator	108
3.3.4	Methods	109
3.3.4.1	Numerical algorithms	109
3.3.4.2	Theoretical analysis: the example of the four-level system	112
3.4	Results	116
3.4.1	Enabling the generation of triplet excitons	116
3.4.2	Other losses mechanisms	121
3.4.2.1	Singlet-triplet annihilation	121
3.4.2.2	Triplet absorption	128
3.4.2.3	Summary	131
3.4.3	CW lasing: A new hope	134
3.4.3.1	Triplet-triplet annihilation	135
3.4.3.2	Triplet state lifetime	140
3.4.3.3	Thermally activated delayed fluorescence	142
3.5	Conclusions	145

4 On the discrepancy regarding BSBCz lasing pulse duration in different resonators	149
4.1 Introduction	149
4.2 Results	150
Conclusion	155
Appendices	159
List of figures	185
List of tables	193
Bibliography	195

Introduction

Notably driven by an important growth of **O**rganic-**L**ight **E**mitting **D**iode (OLED) displays in the imaging market for the last ten years, the interest regarding organic light emitting devices from the public, the industry or the academic world has never been stronger. As of today, organic compounds are also used to make solar cells [1] that now exhibit a power conversion efficiency up to 17% [2], transistors usable for instance to detect and to track heat sources [3, 4] or even lasers [5, 6]. The use of organic materials to replace inorganic ones has many advantages: one of them being the thousands of compounds capable of light emission in the visible region of the electromagnetic spectrum enable the obtention of every color. This is why the red, green, blue pixels of an OLED panel are said to emit their own light, as opposed to LCD displays that use liquid crystals to modulate the white emission of LEDs, hence the impossibility to achieve true black in those screen as well as thinner basels. They are also much cheaper since they do not need the extraction and fabrication processes of inorganic semiconductors, making these materials more environmentally friendly. Indeed, a simple ink jet printing on a substrate is enough to obtain a proper light emitting medium thanks to, for most molecules, their processability in solution. The possibility to use organic molecules in thin amorphous films allows a great mechanical flexibility that OLEDs, monitors, as well as smartphones are more and more taking advantage of. Foldable displays such as Samsung newest Galaxy Fold or LG forthcoming foldable televisions are worth being mentioned as examples.

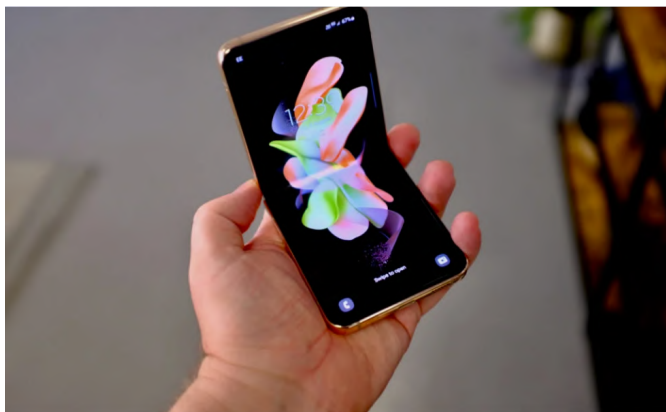


Figure 1: Galaxy Flip 4

Organic Solid-State Lasers (OSSLs) on the other hand still face many challenges to overcome in order to target practical applications. Although it always depends on the context, lasers in general have to fulfill a basic set of conditions to be useful in many relevant applications. The most important one is the ability for the laser gain medium to be excited by electrical excitation (as opposed optical excitation) in order to be integrated wherever it is needed: barcode scanners, printers, computer mouses, facial recognition sensors and so on. Furthermore, for applications involving any kind of data transmission, it has to endure a high enough repetition rate without any sign of degradation or instability. Lasers providing the Internet throughout optical fibers are an obvious yet relevant application in this context.

As of today however, OSSLs have failed to reach practical applications, except for a few niche ones such as explosive detection [7], or to expose counterfeit bank notes [8]. These difficulties arise from the inherent presence of a triplet state T_1 , whose energy is lower than that of the excited singlet state S_1 , from which fluorescence and therefore stimulated emission occur. As depicted on Figure 2, the T_1 state is populated in time by **InterSystem Crossing (ISC)** $S_1 \rightarrow T_1$ [9, 10] at a rate k_{ISC} (s^{-1}), which is caused by a relativistic effect known as spin-orbit coupling. Since the de-excitation of molecules in the triplet state to the ground state S_0 (from which photons are absorbed) is quantum-mechanically forbidden, they exhibit a very long lifetime compared to the fluorescence and do not participate in the light emission for most compounds. Therefore, the ground state is quickly depleted, leading to a population inversion that can no longer be maintained, and ending the lasing emission. Besides, an important fraction of triplet states enable additional mechanisms such as **Singlet-Triplet Annihilation (STA)** or **Triplet Absorption (TA)** that also influence the fluorescence by quenching either the S_1 population or directly the photon density inside the resonator, respectively. This is why OSSLs have for a long time been limited to lasing pulse that lasted only tens to hundreds of nanoseconds.

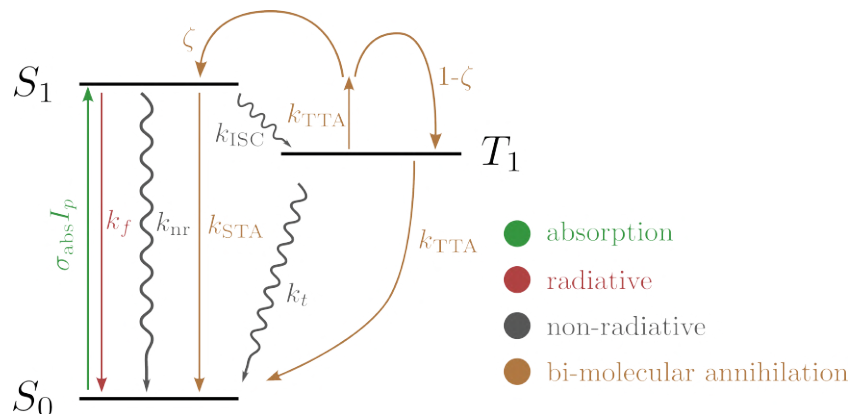


Figure 2: Illustration of the three level electronic configuration of organic molecules.

Overcoming these limitations and thus achieving **C**ontinuous-**W**ave (CW) lasing is often designated as first step towards electrical excitation and the above-mentioned applications that goes with it. Current efforts to overcome the influence of triplet molecules therefore logically consists in tailoring the photophysical properties of molecules to reduce the production of triplets and/or to limit their interaction with other molecules or photons [11, 12, 13]. This is how, in 2017, Sandanayaka *et al.* reported a 30 ms lasing in a **D**istributed **F**eed**B**ack (DFB) resonator using a blended CBP:BSBCz thin film as a gain medium [5]. This three orders of magnitude breakthrough in duration was ascribed to a reduced triplet formation quantum yield generation and to the absence of TA, thanks to a weak overlap between the lasing and triplet absorption spectrum [14]. It was also shown that a proper management of heat removal inside the film played a role in this achievement but, nevertheless, these results showed that photophysical properties are of the utmost importance. After that, similar results were obtained using derivatives of BSBCz, namely BSFCz [15] and BSBCz-EH [16]. Later, the same group reported the longest lasing pulse ever for an optically pumped OSSL: up to one second [6], which represents another two orders of magnitude improvement. The only difference with previous reports is that this achievement was not ascribed to some properties of the emissive molecule, as the same BSBCz was used in a similar thin film, but to the enhanced quality of the resonator that led to a significant reduction of its lasing threshold.

The purpose of this thesis is then twofold: first, the development of an experimental protocol presented in Chapter 2 to characterize triplet state lifetimes and other triplet-related mechanisms such as ISC, STA, and **T**riplet-**T**riplet **A**nnihilation (TTA) in organic thin films, since we have seen that it was crucial to properly estimate such constants when aiming at longer lasing pulses. These parameters play key roles in controlling the lasing pulse duration and at the same time, the reports on proper measurements for those is very scarce. Moreover, it could help to better understand the reasons behind the ms lasing pulses obtained with BSBCz and derivatives. In Chapter 3, the requirements for OSSLs to achieve CW lasing are investigated with the help of numerical simulations of rate equations and analytical reasonings, to unravel whether or not the resonator plays a role in the lasing emission and if so, to what extent compared to molecular properties of gain media. In chapter 4, we take advantage of our setup and our numerical algorithms to explain why lasing pulses lasted less than one microsecond in a **V**ertical-**C**avity **S**urface-**E**mitting **L**aser (VCSEL) configuration, whereas CW lasing was achieved in a DFB with a much lower lasing threshold.

Since this work is halfway between laser and organic electronics, Chapter 1 provides an introduction to the notions required to understand the thesis. A first succinct review of the fundamentals of lasers is presented in which their working, dynamics and the different regimes of light emissions are discussed. The second part is devoted to the field of organic electronics: the difference between organic

and inorganic compounds, the requirements to absorb and emit light, and different mechanisms related to intra- and inter-molecular interactions in organic gain media are presented.

Chapter 1

Fundamentals of organic lasers

1.1 The concepts behind lasers

The purpose of this section is not to parse in details the physics of lasers¹, but to provide for the reader an overview of how they work, how they are made and to what extent this technology intervenes everywhere in our lives. Moreover, a good understanding of their dynamics will be helpful to understand the context of this work and some chapters. In this introduction, the uniqueness of laser emission will be discussed, followed by the fundamental components of any lasing device. Then, the main processes ruling interactions between light radiation and matter will be presented, alongside the conditions required to obtain a laser beam.

1.1.1 Laser peculiarities

A LASER, for **L**ight **A**mplification by **S**timulated **E**mission of **R**adiation, is a device that creates and amplifies coherent light radiation. They are used to emit light at wavelengths that are mostly located in three distincts regions of the electromagnetic spectrum: the ultraviolet, the visible, and the infrared. The light emitted by a laser exhibits many properties that differentiates it from other sources such as lamps or **L**ight **E**mitting **D**iodes (LED). An important one is their coherence, namely spatial and temporal. First, spatial coherence allows the light to be collimated over long distance, hence the *beam* terminology. Thanks to this property, beams can also be focused on very tight spots, generating high power densities that can be useful in numerous applications. On the other hand, lasers usually have a very narrow emission, as shown in Figure 1.5, due to their temporal coherence. This property can be used, for instance, to create ultrashort pulses that can reach a few femtoseconds.

¹A reference on this matter is the book of A.E.Siegman [17], still highly relevant 35 years after its publishing.

1.1.2 Fundamentals components

A laser eventually boils down to a set of three elements: a gain medium to amplify light radiation, an external energy source to *feed* the gain medium and a resonator to turn this amplifier into an oscillator, as illustrated in Figure 1.1.

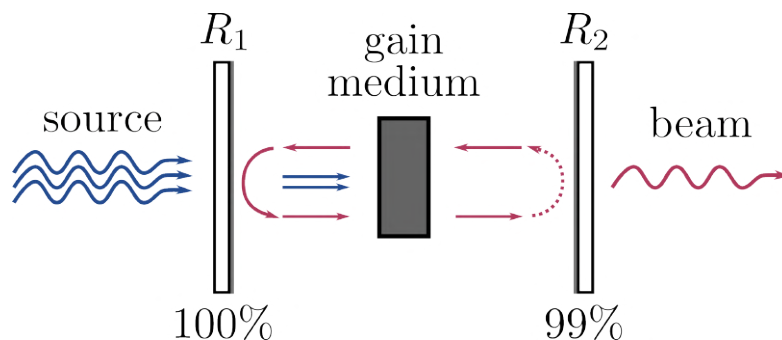


Figure 1.1: Fabry-Pérot cavity with a gain medium between two mirrors R_1 and R_2 and their reflectivities at the lasing wavelength. Pump photons are in blue, stimulated ones are in red.

The gain medium refers to a medium that have a certain density of atoms that will interact with incoming light radiations. It is so central to lasing systems that most of them are named after their gain medium composition *e.g.* Ti:Sapphire [18], Nd:YAG [19] ... Gain media exist in liquid, solid and gaz. Liquid organic dyes gain media were widely popular decades ago but required a circular flow of the fluids (and the heavy machinery for the maintenance that goes with it) to keep the solution safe from permanent photodegradation. Furthermore, liquid dyes were often linked to potential health issues. Gazeous lasers have been introduced very shortly after the very first laser and have been extensively studied until the beginning of the century, from Hélium-Néon and CO_2 systems, to chemical ones using hydrogen fluoride for instance [20]. As research progressed and could offer more and more stability in solid-state gain media, they gradually replaced liquid and gazeous ones in research or in the industry, as they do not need any management system and are much less dangerous than certain gaz whilst being much more compact.

The external source of energy allows the creation of photons by a process called spontaneous emission (see Section 1.1.3). Pumping sources can be sorted into three categories: optical, electrical and chemical. In the first case, the external energy is brought by photons coming from a flash lamp, a LED, or often a secondary laser. Incoming photons are then absorbed by the gain medium, resulting in the promotion of an electron to a higher excited energy state, which can undergo (non)radiative de-excitation afterwards. Light emission can also be achieved by a chain of chemical reaction that lead to very powerful but very consuming emissions [21, 22, 23]. However, devices aiming to be used at large scale are *pumped* by the mean of electrical stimulations, where the excited energy levels are populated by electron-hole pairs (see Section 1.1.5). Because, in this configuration, you do not

need anything to excite the gain medium but a current source, it has always been the method of choice when compactness and cost are required, for telecommunications or the reading of CDs. In this thesis, we will be mostly interested by optical and electrical pumping.

Last but not least, the cavity is of the utmost importance, since it constrains a portion of the light emitted by the gain medium between physical boundaries so that photons can circle back inside to be amplified again. These boundaries, in most cases, will be high-reflectivity mirrors but can also be naturally created by a difference of refractive indexes of the gain medium and its surrounding environment *e.g.* ambient air. The simplest one is referred as a **Fabry-Pérot** (FP) cavity, which consists of two mirrors around the gain medium (see Figure 1.1). The entry mirror R_1 lets the pump pass through and is 100% reflective at the lasing wavelength, whereas R_2 , the *output coupler*, lets a portion of the amplified light out, forming the laser beam.

1.1.3 Light-matter interaction

1.1.3.1 Einstein coefficients

Although the first laser was reported in 1960 [24], the principles of the interactions between light and matter that could enable lasing were described by Albert Einstein more than forty years before [25]. Three processes, required to understand how lasers work, are illustrated in Figure 1.2: stimulated emission which was mentioned earlier, the absorption of a photon, and spontaneous emission. To explain those, we will consider a system containing only two levels of energy E_1 (referred to as the lower level or ground state) and E_2 (the upper level or excited state). For the purpose of the demonstration, the light source will have a frequency ν_l that perfectly matches the energy of this two-level model so that $h\nu_l = E_2 - E_1$.

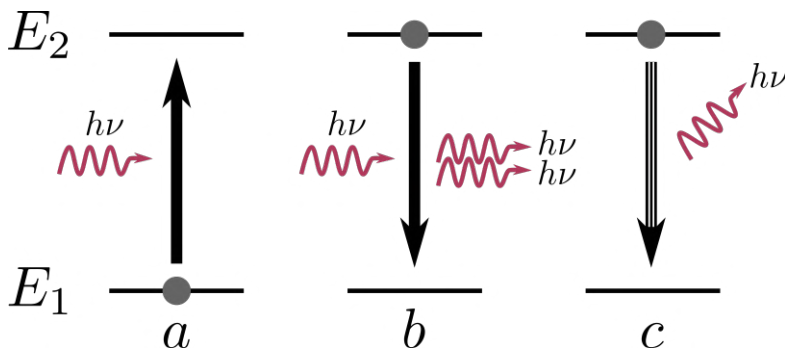


Figure 1.2: Illustration of a) photon absorption, b) photon duplication by stimulated emission, c) spontaneous emission of a photon. $E_{1,2}$ are two arbitrary atomic energy levels.

When this light passes through the gain medium, some of its photons will be absorbed by atoms located on the ground state, since their energy matches

the one of the system. Atoms that have absorbed photons will be transferred to the excited state, here E_2 , at the femtosecond scale. Then, a decay to the lower level can be induced by an other incoming photon, resulting in the emission of a second photon which has the same properties as the incident one *i.e.* same phase, direction, frequency: the initial photon has been duplicated. At last, it is also probable for this atom lying on the excited state to decay spontaneously and emit a photon at the same frequency ν_l , but its phase and direction will be purely random².

Moreover, there are also ways for excited atoms to de-excite spontaneously without emitting photons. This so-called non-radiative de-excitation is due to vibration and/or rotation of the molecules composing the gain medium. It is important to highlight that all of these interactions can happen at the same time and therefore are in competition. When, for instance, an atom reached the E_2 state, it will be preferable in the framework of lasers that its de-excitation generates a second photon to feed the beam than none. All of the mentioned pathways to the ground state E_1 are ruled by rates in s^{-1} which directly depend on material properties.

1.1.3.2 Population inversion

Prior to this competition between de-excitation processes, a problem subsists: since the photon absorption and the duplication of one *via* stimulated emission are reciprocal, their probability are exactly equal. Meaning that in order to promote stimulated emission over absorption, the number of atoms lying on the upper state has to be superior to the number of atoms onto the lower state. This requirement is commonly referred to as *population inversion*, it is expressed in Equation 1.1.

$$\Delta N = N_2 - N_1 > 0 \quad (1.1)$$

The distribution of atoms in a two level sytem at the **Local Thermodynamics Equilibrium** (LTE) is written as Equation 1.2, where k_b is the Boltzmann's constant and T the temperature inside the gain medium. In this configuration, it is straightforward to see that the ratio N_2/N_1 will never be superior or equal to unity, therefore no lasing will ever be observed.

$$N_2 = N_1 \times \exp \left[\frac{-(E_2 - E_1)}{k_b T} \right] \quad (1.2)$$

To overcome this limitation, there is one fundamental requirement: the energy of the lasing transition must be smaller than the one of the absorption transition. A useful example, pictured on Figure 1.3.a, is the *four-level* configuration on which

²Although it is not related to this thesis, it is interesting to mention that what we call spontaneous emission is actually an approximation. As it is stimulated by the void quantum fluctuations.

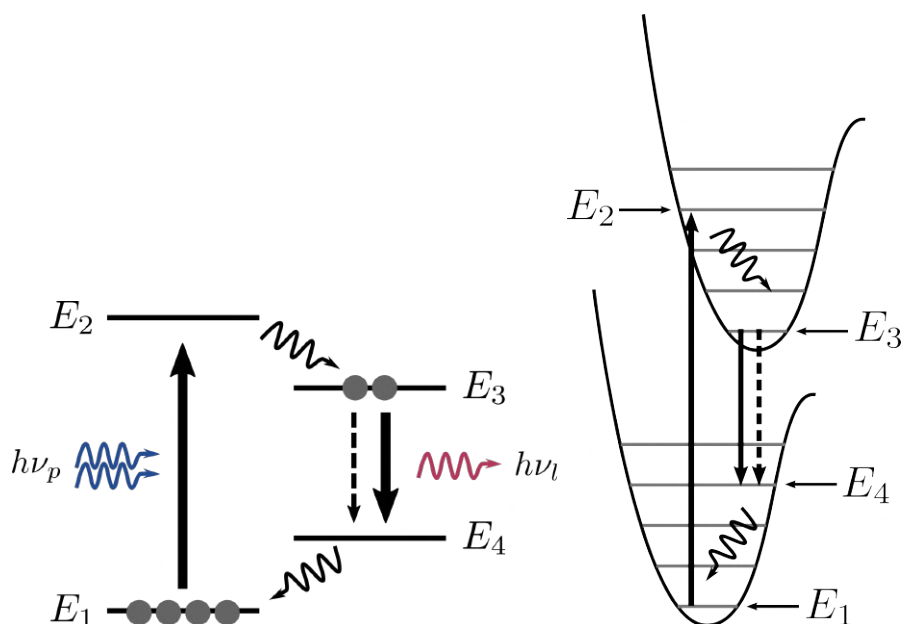


Figure 1.3: Left: Illustration of a four-level electronic system with non-radiative de-excitation (curved), spontaneous emission (dashed), absorption and stimulated emission (bold). $\nu_{l,p}$ are the laser and pump transition frequency, respectively.

efficient lasers are based on. In this setup, E_1 the ground state is pumped by photons whose energies match the $E_1 \rightarrow E_2$ transition. They can then decay non-radiatively very quickly to E_3 , at the picosecond scale. Since E_4 is not populated in the first place, the population is said to be inverted on this transition, allowing an efficient stimulated emission. Finally, atoms circle back to the ground state and absorb more photons to feed the population inversion.

The energy difference between pump and lasing photons explains why the fluorescence of the gain medium will always be shifted to the red compared to the absorption, as smaller energies result in higher wavelengths. This phenomenon is known as Stokes shift, which is illustrated on Figure 1.4 in the case of the coumarin 521T. This molecule absorbs very well around 450 nm and will emit photons at 510 nm. The Stokes-Shift is a very important characteristics of gain media, since the overlap between the two spectra will rule the strength of many processes that will be described later.

This simple representation of a four-level system makes it seem like each one is not related to another, but the reality is more complex than that. Figure 1.3.b shows a more realistic representation of the molecular configuration of such systems. In fact, E_1 and E_4 both are vibrational sub-levels of the electronic ground state (often denoted by S_0) whereas E_2 and E_3 belong to the excited electronic state referred to as S_1 ³. More precisely, E_3 and E_1 are the lowest vibrational levels of S_1 and S_0 , respectively. Besides, this representation allows one to understand

³The reason for this S notation will be discussed in details in Section 1.2.1.2

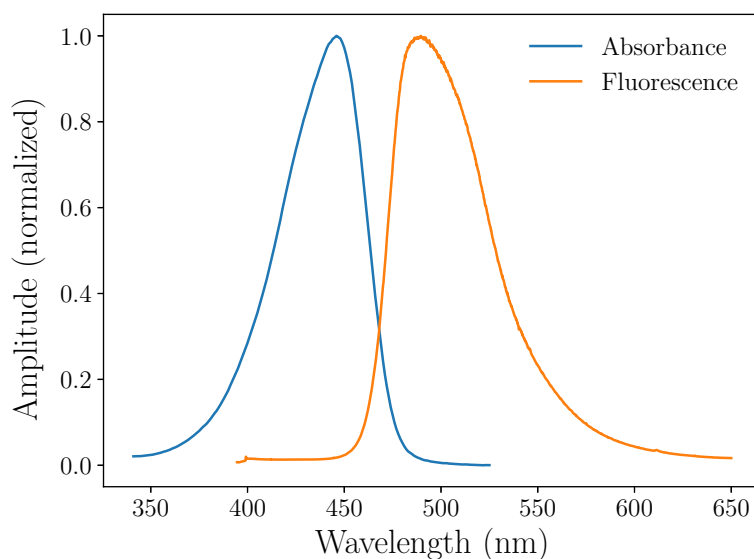


Figure 1.4: Illustration of the Stokes-Shift of molecules: the example of coumarin 521T. This molecule absorbs around 450 nm and emit at 510 nm.

the different time scales in play, as a process from two vibrational levels of the same electronic state is much faster than a transition involving two different ones.

1.1.4 Lasers dynamics

1.1.4.1 Fluorescence and laser emission

Lasing emission is based on the stimulated emission of photons with an energy $h\nu_l$, where ν_l is the frequency of the lasing transition. But, as illustrated in Figure 1.2, this interaction requires at the beginning photons whose energies are the same. Then, the only solution for an atom lying on the upper level of the lasing transition (E_3 on Figure 1.3) when there are not enough lasing photons available is to de-excite *via* spontaneous emission.

This emission is commonly referred to as fluorescence. The resulting photons will be emitted in a purely random direction, as discussed in Section 1.1.3. The frequency of fluorescence is not fixed, as it occurs between the lowest vibrational state of the upper level and some sub-levels of the ground state (Figure 1.3.b). This explains why the fluorescence spectrum of a gain medium is so broad, as illustrated in Figure 1.5. The multiplicity of sub-levels implies that spontaneous emission can occur within a wide range of frequencies *i.e.* a wide range of wavelengths.

The same logic applies for the ground state absorption of a photon, as atoms will be promoted from the lowest sub-level E_1 to an arbitrary sub-level of the excited state, as pictured on Figure 1.6.

To undergo stimulated emission inside the gain medium, one would have to make use of the photons emitted at the lasing frequency *via* spontaneous emis-

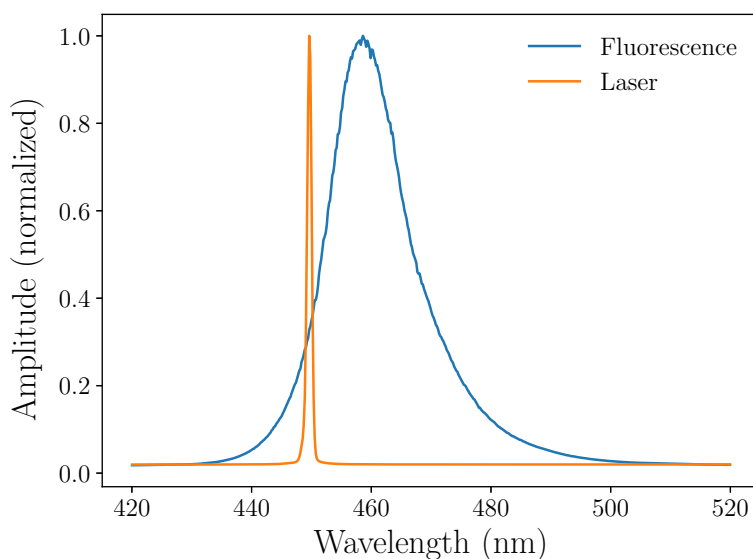


Figure 1.5: Emission spectrum of a commercial 450 nm diode used in Chapter 2 recorded before (blue) and after (orange) its lasing threshold. The lasing spectrum appears much narrower than the fluorescence emission.

sion. This is precisely the role of the cavity. In Figure 1.1 for instance, the cavity is made of two mirrors that reflect photons whose directions are roughly along the pump axis, so that they circle back inside the gain medium to be duplicated. Since duplicated (or stimulated) photons will have the same frequency, phase and direction than the original one, it is straightforward to understand why spontaneous emission is said to be the seed of lasing, as stimulated emission cannot exist without fluorescence.

1.1.4.2 Requirements to achieve lasing

For a system to achieve lasing, the losses of the cavity have to be overcome by the gain generated from the active medium. In other words, the number of stimulated photons must outnumber lost ones. The configuration in which the gain is exactly balanced by the effects of losses after one round trip inside the cavity is known as the lasing threshold. To illustrate this, we will once again take the example of the plano-plano resonator sketched on Figure 1.1. Two sources of loss will be considered here: the ones coming from the cavity, which are modeled after the reflectivities $R_{1,2}$ of the mirrors, and the losses due to the gain medium, that will be gathered under the term α (cm^{-1}). Potential material losses are ground reabsorption or scattering. Those are usually not controlled by experimenters as they depend on intrinsic molecular properties.

The gain of the active medium G can be expressed by the ratio of the output optical power (the laser beam) and the pump power. However, it is often more useful to work with its linear gain g (cm^{-1}), the relation between G and g being

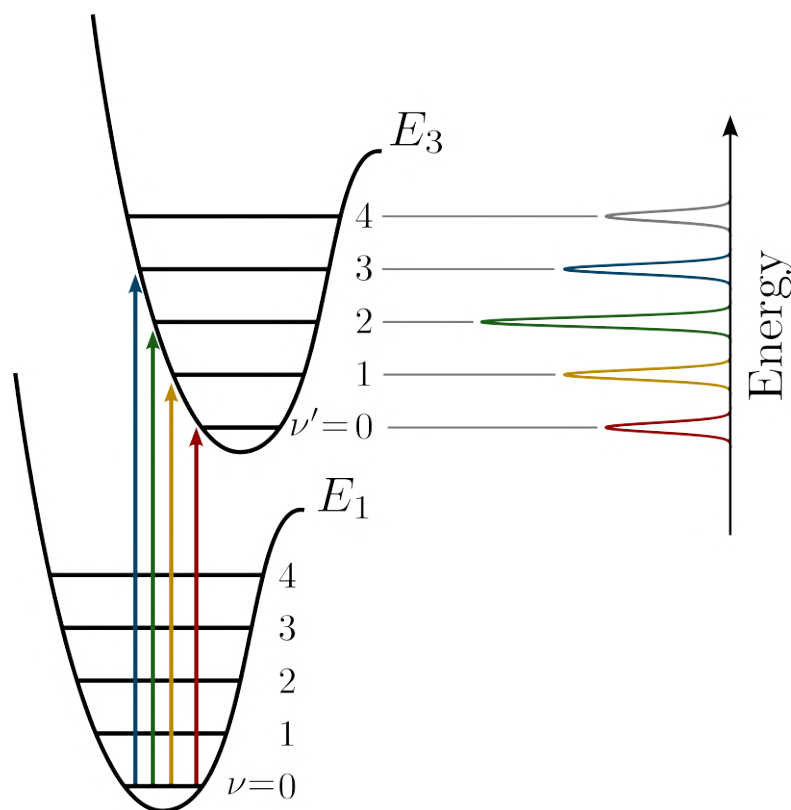


Figure 1.6: Illustration of the broadness of absorption spectra

written in Equation 1.3 where l is the length of the active medium.

$$G = e^{gl} \quad (1.3)$$

Because for each round trip, some photons are lost *via* the mirrors while some are lost *via* the active medium, the latter has to stimulate enough photons to at least equalize the losses and hence keep the population inversion alive: The intensity inside the cavity must then remain the same after one round trip. Equation 1.4 models this intensity starting for instance just before the output coupler (R_2). P is the starting power at a given point inside the resonator, P_{rt} is the power after one round trip. The terms R_1 and R_2 reflect the losses of the mirrors whereas $e^{2g_{\text{th}}l}$ and $e^{-2\alpha l}$ reflect the two passes of the intensity through the active medium, with photons emission for the former, and absorption for the latter.

$$P_{\text{rt}} = PR_1R_2e^{2g_{\text{th}}l}e^{-2\alpha l} \rightarrow R_1R_2e^{2g_{\text{th}}l}e^{-2\alpha l} = 1 \quad (1.4)$$

When in steady-state configuration, $P = P_{\text{rt}}$. This allows the simple derivation from Equation 1.4 of the linear gain required for the laser to be stable:

$$g_{\text{th}} = \alpha - \frac{1}{2l} \ln(R_1R_2) \quad (1.5)$$

The term R_1R_2 is always inferior to unity so that both terms contribute to

increase the threshold. It is interesting to mention the case where the cavity is made of perfect mirrors ($R_1 = R_2 = 1$). In this configuration, the discussion about the compensation of the overall losses by the gain becomes much easier on the mind, since Equation 1.5 can be written as a simple balance between g and α :

$$g - \alpha = 0 \quad (1.6)$$

Three regimes can be listed from Equation 1.5: If $g < g_{\text{th}}$, the laser cannot oscillate since more photons are lost than created by stimulated emission. When $g = g_{\text{th}}$, the production of stimulated photons is just enough to balance the losses, the lasing threshold is reached. If $g > g_{\text{th}}$, the intensity inside the cavity increases at each round trip. It would seem like the intensity could grow indefinitely but this is not the case. In fact, the more stimulated photons inside the cavity, the less gain will be available, as the population inversion per second is limited. This phenomenon is called the *gain saturation*.

1.1.4.3 Jablonski-Perrin diagram of a four-level configuration

Until now, the discussion was mostly focused on the optical intensity coming out of the output coupler. However, it is useful to study the origins of this intensity (*i.e.* the photon density) inside the resonator: the dynamics of the energy state populations. To study the flow of atom between different states, a system composed of a lower level of energy S_0 and a higher one S_1 will be used. S_0 and S_1 correspond to the lasing transition and are perfectly analogous to E_3 and E_4 in Figure 1.3.

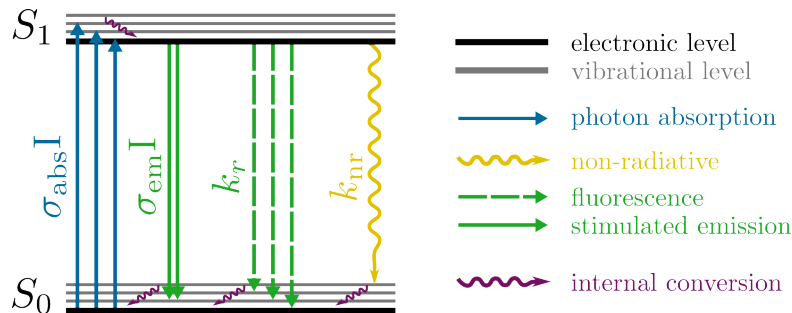


Figure 1.7: Jablonski-Perrin diagram of a typical two-level system.

Figure 1.7 displays a typical Jablonski diagram containing every processes taken into account from and to each atomic level. This representation is usually used to provide a graphical view of the equations modeling a given system. However, since the four-level configuration will be used as a reference in Chapter 3, the equations governing the population of the different electronic states and their temporal evolution will be presented afterwards.

1.1.5 Different resonators

Although the concepts of laser were discussed in this introduction using a plano-plano (Fabry-Pérot) cavity as illustration because of its simplicity and also because it is enough to cover the fundamentals, this particular configuration is rarely used nowadays, whether it is in research laboratory or in more practical cases. Therefore, other types of resonator that are massively used will be presented in this subsection.

One point that was intentionally left aside is the fact that the classical FP cavity is said to be unstable. It can be easily understood with geometrical optics, as the only photon that are sure to stay between the two parallel mirrors are the one emitted perfectly normal to the face of the mirror, otherwise they will deviate from the cavity axis at each reflection and eventually propagate outside the cavity. This makes plano-plano cavity very sensitive to the least variation (and thus the most difficult to align), which also has for a consequence the support of a limited number of spatial modes. To stabilize this resonator and obtain diffraction-limited beams alongside well-defined lasing modes, a solution is to use spherical mirrors as sketched on Figure 1.9 to focus the photon between the mirrors after each reflection.

The **Vertical-Cavity Surface-Emitting Laser** (VCSEL) is one of the most used resonator [26]. The beam is obtained by excitation of a material sandwiched between two mirrors often composed an alternation of $\lambda/2$ and $\lambda/4$ layers. Its emission is normal to the top surface, making it a prime candidate for massive production, since it can easily be tested at many stages of its fabrication process. This, coupled with the addition of electrode in between for electrical stimulation allows VCSELs to be used in every applications where compactness is required: bar-codes reading, computer mouses, laser printers.

An extension of the VCSEL referred to as VECSEL (where the E stands of External) is also interesting to present. It consists of VCSEL in an external configuration, meaning that there is empty space between the gain medium and the output coupler. Even though these resonators do not have as much practical usages as their compact counterpart above-mentioned because of bulkiness and a higher lasing threshold, they are used to achieve very high power densities [27, 28]. Moreover, the free space inside the cavity can be used to put elements inside to have insights on the beam properties or to tune the emission wavelength with dispersive elements [29]. A tuning of the wavelength can also be obtained by adjusting the length of the cavity [30].

Last but not least, the **Distributed FeedBack** (DFB) laser can be distinguished from other cavities by its unique feedback mechanism, which is said to be distributed. As pictured on Figure 1.8, the gain medium is deposited on a substrate (silica is often used) and contains a periodical structure or diffraction grating. The feedback, distributed along the whole grating, arises from the spatial modulation of the refractive index, which acts as highly selective mirror. One key advantage

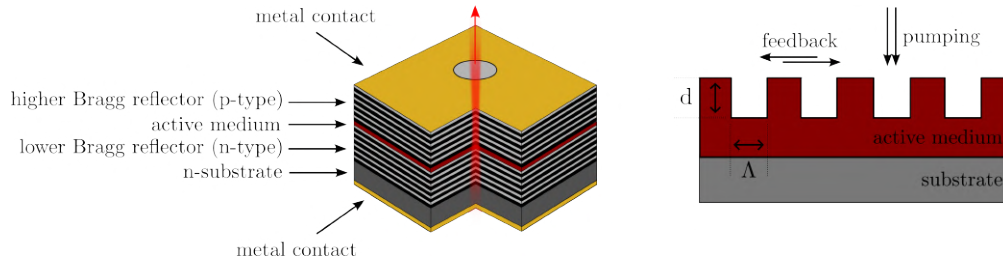


Figure 1.8: (left) **V**ertical-**C**avity **S**urface-**E**mitting **L**aser (VCSEL) and (right) **D**istributed **F**eed**B**ack (DFB) resonator.

of DFB is that their emission wavelength is easily tunable, since it is ruled by the following relation [6]:

$$m\lambda_b = 2n_{\text{eff}}\Lambda \quad (1.7)$$

where m is a positive integer designating the diffraction order, λ_b is the lasing wavelength of the device, n_{eff} is the effective refraction index of the medium, and Λ is the period of the grating.

DFBs exhibit much lower lasing threshold than the one of previously mentioned cavities thanks to their feedback mechanism, which allow them to be massively used, notably for data communication, since gratings are easily integrable in fibers for instance [31].

1.1.6 Applications

A extensive review of laser applications would not be relevant here, as they really are used everywhere around us nowadays. Besides, numerous interesting reviews or books have already been written focusing on certain fields, such as surgery [32] or communication in space [33, 34] Instead, I would like to highlight two applications that I found quite interesting during my PhD.

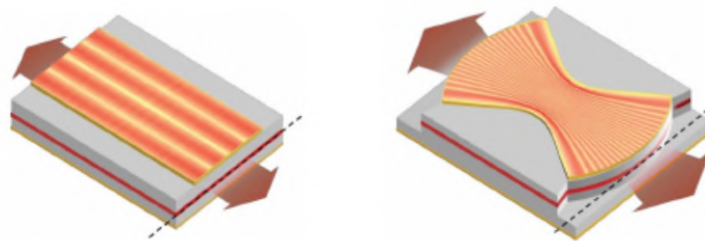


Figure 1.9: Left) a classical, unstable Fabry-Pérot resonator in which only low-order transverse modes are supported. Right) Specially designed stable cavity with curved mirrors to support high-order transverse modes. Figure taken from Reference [35].

The first one is linked to **R**andom **N**umber **G**enerators (RNG), which is a very important field of research, especially when it comes to data that require a certain level of encryption that computers cannot offer⁴. On this matter, Kim *et al.* recently reported a record of 250 terabits (250×10^{12} bits) using a chip-scale laser [35]. While the production of random, non-reproducible sequence of numbers is possible thanks to the fundamental randomness of spontaneous emission, which adds stochastic noise on the intensity recording, the parallelization of this protocol is achieved thanks to the design of a stable cavity replacing the classical Fabry-Pérot resonator. As pictured on Figure 1.9, their design allows the support of much more transverse modes, leading to proportionally more random sequences, since they show that the different modes inside the resonator are not at all correlated.

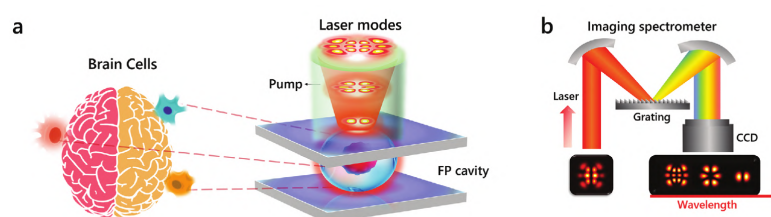


Figure 1.10: (a) Schematic of single-cell laser, where different types of brain cells were sandwiched within a FP microcavity. Laser modes emit from the FP cavity upon excitation. (b) Schematic of hyperspectral imaging setup. Hyperspectral images of laser modes were obtained using an imaging spectrometer, in which a CCD was used to record the laser modes with different wavelengths after the laser emission beam was diffracted by a grating Figure taken from Reference [36].

I would like at last to cite the work of Qiao *et al.* [36] who, with brain cells sandwiched inside a FP cavity and artificial intelligence were able to discriminate different types of cells, which as one can imagine has tons a potential applications in biology and medicine. To do so, they took advantage of the so called lens effect induced by cells inside the resonator, which leads to spatial modes (see Figure 1.10.a) that differ from one cell to another because of their structural difference. Then, they use the frequency distribution of spatial modes (Figure 1.10.b) as an input for a neural network to know whether this is a neuron or an astrocyte (among other possibilities).

1.1.7 Summary

The fundamental principles regarding the dynamics of lasers have been described in this section. First, the role of each primary component required to obtain a laser beam have been discussed, from the gain medium via which spontaneous photons

⁴One very good example is the public company Cloudflare, which helps fasten the internet requests and is responsible for the security of around 20 wt.% of Internet's websites. To ensure non-reproducible security keys, they use a whole wall of 80's like lava lamps and transform with a simple camera and two different computers the creation and destruction of bubbles in 1 and 0.

are emitted to the cavity, which transforms the whole device into an oscillator by constraining a certain portion of the spontaneous photons between two physical boundaries. These components are illustrated on Figure 1.1 and are discussed more in details in the corresponding section.

Then, the main processes ruling the interaction between light radiation and the amplifying medium have been addressed. Notably, it has been shown that for one system to achieve lasing, the number of stimulated photons must outnumber the number of absorbed ones, meaning that there must be a population inversion between two energy levels. Since this cannot be satisfied in a system at LTE, a solution referred to as a four-level system has been discussed. As illustrated on Figure 1.3, it requires an electronic configuration that allows the excitation of ground states atoms via a more energetic transition than the lasing transition (In the illustrated case: $h\nu_p > h\nu_l$ where p refers to the pump and l the lasing transition). This system works very efficiently because the fluorescence spectrum of the lasing transition does not overlap totally with the absorption spectrum, resulting in a very low reabsorption. This difference of energy, called the Stokes-shift, is pictured on Figure 1.4.

In addition, we have seen the following general rule to achieve lasing: the gain has to overcome the losses. More precisely, the density of photons generated by stimulated emission from the amplifying medium (quantified by the linear gain g) has to be more important than the photons lost either through the mirrors or by mechanisms inside the gain medium such as reabsorption. This criteria is modeled as Equation 1.5. If the linear gain of the medium is not enough to overcome the mentioned losses, then lasing cannot occur as stimulated emission will never provide enough photons.

Finally, several different types of optical resonators with very different working principles were presented, all of them are sketched on Figure 1.8. The DFB, with its very unique feedback mechanism that allows much lower thresholds than any other cavities presented in this work. The VCSEL, which consists of two plane mirrors compressed in a sandwich configuration on the gain medium to minimize the cavity losses and decrease its lasing threshold. Its configuration allowing an excitation of the gain medium via current flowing through electrodes, it is the resonator of choice for mass production and large applications such as barcodes reading or Apple's Face ID™. Also, an extension of the VCSEL referred to as VECSEL because of the empty space left between the gain medium and the output coupler has been presented. This structure is found to be very useful to study the properties of the light emitted thanks to the possibility to put, for instance, dispersive inside the cavity.

1.2 Introduction to organic electronics

The second part of the introduction is devoted to the field of organic electronics, since it is the most important one regarding this thesis. First, the nature of organic compounds and their difference with inorganic ones regarding charge conduction and electronic configurations are described. Then, important properties of different excited states of energy are presented, followed by an extensive discussion on the so-called T_1 state and the related intermolecular interactions.

1.2.1 Organic molecules

It is generally assumed that organic compounds are referred to as organic because they are mostly composed of carbon with hydrogen, alongside heteroatoms such as nitrogen [9, 37]. Some reports only referred to carbon atoms that are covalently bond [38] while some choose to define organic chemistry as the opposite of its inorganic counterpart, excluding all compounds without C-H bonds [10]. In fact, there is no clear consensus in the definition of an organic molecule, as exceptions can always be found to prove one wrong.

The only thing that really matters is that organic molecules are all articulated around a backbone of carbon bonds, and as it will be discussed, their properties are mostly driven by the electronic configuration of carbon. Since four electrons are available per carbon atoms to bound to other atoms, the number of reported organic compounds reaches several millions [39]. Examples of simple organic compounds are presented on Figure 1.11.

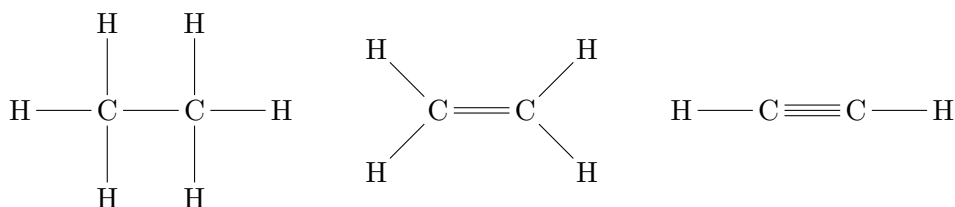


Figure 1.11: Chemical formula of ethane (left), ethylene (center), and ethyne (right).

1.2.1.1 Molecular orbitals and conjugated systems

The optical properties of one molecule is mostly driven by the electronic configuration of carbon atoms, it is therefore useful to understand how this very abundant compound behaves in the framework of organic molecules. For an unbonded carbon on the ground state, its electrons are arranged in the $1s^2 2s^2 2p^2$ configuration, meaning that the 1s- and 2s-orbitals are filled whereas two out of three 2p-orbitals are only occupied by one electron, as sketched on Figure 1.12 (top left). Then, the 2s- and 2p-orbitals will participate in the formation of more complex orbitals when bonds are formed with other atoms, which will result in the *hybridization* of the

molecular orbitals. Although numerous hybrid orbitals can be formed, this introduction will focus on three hybridizations using as an example the three molecules mentioned from Figure 1.11, as their description is sufficient to understand the main relevant mechanisms for this thesis.

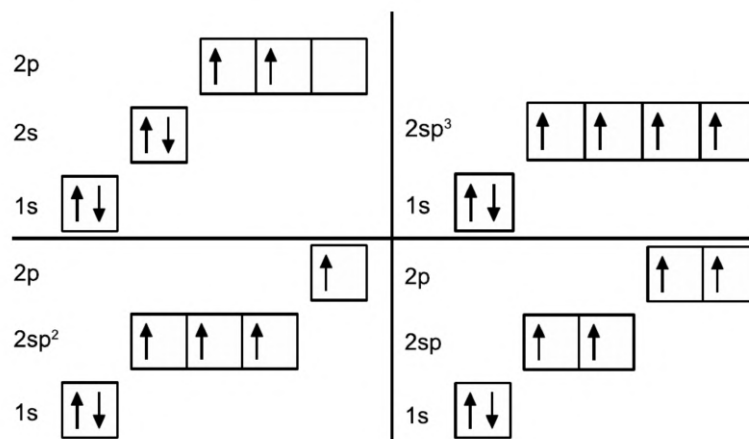


Figure 1.12: Electron configuration of carbon: ground state (top left), sp^3 - (top right), sp^2 - (down left) and sp -hybridization (down right). For the ground state, the 1s- and the 2s- orbitals are occupied by two electrons and two 2p-orbitals are occupied by one electron. Hybrid orbitals are formed by superposition of s- and p-orbitals. Figure taken from Reference [38].

In the case of ethane (C_2H_6), both carbons form four single bonds either with hydrogen or between each other. For this molecule, carbons exhibit a sp^3 -hybridization, and the resulting bonds are referred to as σ -bonds, because of the axial overlap between the orbitals of each atoms. The binding energy of single bonds is very strong and σ -electrons are said to be localized. Therefore, compounds that only exhibit σ -bonds are found to be good insulators thanks to their ground state configuration at room temperature. A good example of a well-known molecule that matches this description is the polyéthylène (C_2H_4)_n.

For ethylene (Figure 1.11 (center)), carbons exhibit a sp^2 -hybridization: the sp^2 orbitals are arranged in a trigonal planar geometry whereas the unhybridized $2p_z$ orbital is perpendicular to the molecule plane. What makes this configuration more interesting is the lateral overlaps between the $2p_z$ orbitals, which are referred to as π -bonds. Since the overlap between the wavefunctions is only partial, the bond is much weaker than its σ counterpart. Ethyne (Figure 1.11 (right)) is somehow similar to ethylene, except for the triple bonds between carbons resulting in one strong σ bond and two π -bond from the 2p-orbitals, whose sp -hybridized configuration is shown on Figure 1.12.

When a molecule exhibits an alternation of single and double bonds on the same plan, it is referred to as a conjugated material, as illustrated on Figure 1.13. More precisely, because of the partial overlap of $2p_z$ -orbitals along the whole carbon backbone of the molecule, it is called a π -conjugated system. Of course,

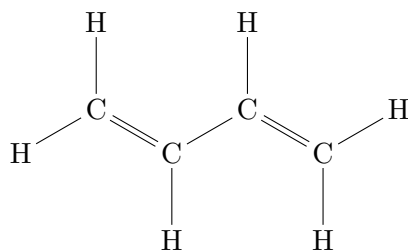


Figure 1.13: Topological representation of the butadi-1,3-diene, for which the alternation of single and double bonds allows the delocalization of the π -electrons to be along the whole carbon backbone of the molecule thanks to the overlap between 2p-orbitals.

for long carbon chains (known as polymers), it happened that some part of the molecule does not lie on the same plan as others, the whole compound is then only partially conjugated and this part will account for its optical properties.

1.2.1.2 Electronic transitions and excited states

The absorption of a photon by a π -conjugated compound will result in the promotion of the molecule to a higher-lying energetic state, also referred to as an excited state. The state from which the molecule absorbs this photon is one of lower energy, usually the lowest, which is referred to as the ground state.

The main transitions allowed in organic media are pictured on Figure 1.14 with the electronic configuration of the formaldehyde molecule as an example. The nature of the transition differs depending on the energy of the absorbed photon. For instance, a delocalized π -electron can be promoted to a so called antibonding orbital π^* if the energy of the photon matches the energy difference: this is a π - π^* transition. Also, a molecule composed of heteroatoms (oxygen in this case) may also present what is called n orbitals. The n -electrons are weakly bonded to the molecule structure but can still trigger its promotion to an antibonding π^* orbital. This transition is denoted n - π^* and is, with its π - π^* counterpart, the most relevant transition regarding an optical excitation, considering the weakness of π -bonds. Considering a typical energy gap of around 2.5 eV between the π - and the π^* -orbitals in organic compounds, they are found to behave as semiconductor materials and can be treated as their inorganic counterparts.

On the other hand, σ -electrons can also be promoted to a π^* - and σ^* -orbital *via* σ - π^* and σ - σ^* transitions, respectively. However, the covalent bonds resulting from the complete overlap of sp^2 -hybridized molecules are so strong that the energy required to trigger such transitions is usually located in the deep ultraviolet [40], which is above most organic molecule dissociation energies [37]. Therefore, they fall out of the scope of this thesis and will not be taken into account in further photophysical analysis.

On Figure 1.14 are denoted the two main energy levels for the physics of organic electronics: the **H**ighest **O**ccupied **M**olecular **O**rbital (HOMO) and the **L**owest

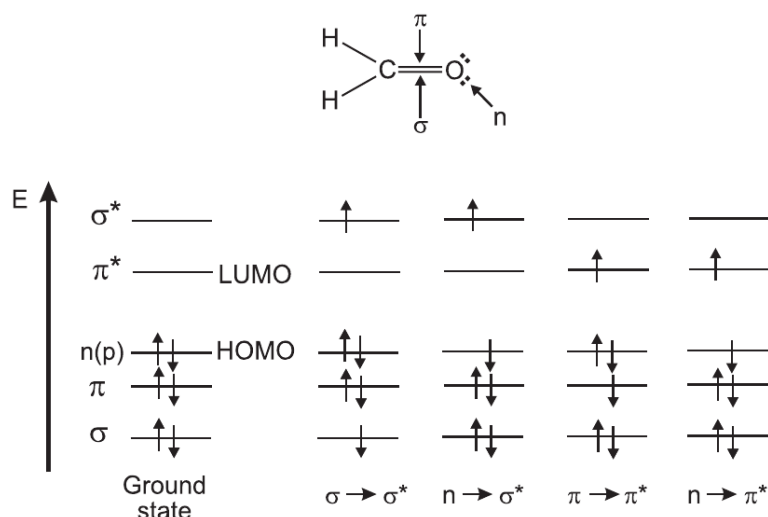


Figure 1.14: Energy levels of molecular orbitals in formaldehyde and possible electronics transitions. Figure taken from Reference [40].

Unoccupied Molecular Orbital (LUMO). The molecule is said to be in an excited state when an electron from the HOMO is promoted to the LUMO. In virtue of the spin selection rule, electrons going through electronic transitions have their spin angular momentum unchanged, the total spin number S (the sum of all spins in the system) then accounts for 0 and the multiplicity of spin $M = 2S + 1$ equals 1. Hence, the ground state and the related excited states are referred to as singlet states (S_0 for the ground, then S_1 , S_2 , and so on for the higher-lying excited states). An absorption of a photon by a molecule in the ground state that results in its promotion to the LUMO will be called a singlet-singlet ($S_0 \rightarrow S_1$) transition.

However, as it will be described in Section 1.2.4.1, the spin of the excited electron is in some conditions allowed to reverse, resulting in a total spin number of 1 ($|+\frac{1}{2}\rangle + |+\frac{1}{2}\rangle$) and a multiplicity M of 3. These are the triplet states, whose energies are very close to each other at room temperature, and inferior to the S_1 state according to first Hund rule (also known as the multiplicity rule) [41].

Triplet states can also be understood in terms of wavefunctions definition. Considering that nuclei are much heavier than electrons, their dynamics is said to be proportionally slower: This is the Born-Oppenheimer approximation [42]. In this framework, the total wavefunctions of the molecule ψ can be decomposed into two independent parts: the spatial wavefunction ψ_s , and the electronic spin wavefunction ψ_e .

$$\psi = \psi_e \psi_s \quad (1.8)$$

In addition, Pauli's exclusion principle states that the whole molecular wavefunction has to be antisymmetric when two electrons are exchanged. Only two possibilities allow the system to fulfill this requirement: Either the spatial wavefunction is symmetric and its spin counterpart is antisymmetric, or the opposite.

If we take the first case and a two electrons system whose nuclear coordinates are \mathbf{r}_1 and \mathbf{r}_2 , ψ can be expressed in the form of $\psi(\mathbf{r}_1, \mathbf{r}_2; S, m_s)$ as:

$$\psi(\mathbf{r}_1, \mathbf{r}_2; 0, 0) = \psi_s^{\text{sym}} \times (\alpha_1\beta_2 - \alpha_2\beta_1) \quad (1.9)$$

where $\alpha = |\uparrow\rangle$ ($m_s = +\frac{1}{2}$) and $\beta = |\downarrow\rangle$ ($m_s = -\frac{1}{2}$) for the electron 1 and 2, respectively. This is the wavefunction of the singlet state mentioned earlier. When, on the other hand, the spatial wavefunction is antisymmetric, it results three expressions for ψ arising from the three possible projections m_s of the electronic spin (1, 0, -1):

$$\begin{cases} \psi(\mathbf{r}_1, \mathbf{r}_2; 1, 1) & = \psi_s^{\text{antisym}} \times \alpha_1\alpha_2 \\ \psi(\mathbf{r}_1, \mathbf{r}_2; 1, 0) & = \psi_s^{\text{antisym}} \times (\alpha_1\beta_2 + \alpha_2\beta_1) \\ \psi(\mathbf{r}_1, \mathbf{r}_2; 1, -1) & = \psi_s^{\text{antisym}} \times \beta_1\beta_2 \end{cases} \quad (1.10)$$

These are the wavefunctions of the three states that are all denoted by T_1 because of how close they are energetically. Molecules in a triplet spin state and their influence on the physics of organic media will be discussed in details all along this thesis, as their well-defined spin state is one of the key difference with the physics of inorganic materials.

1.2.1.3 Nature of charges in organic semiconductors

It has been stated in the previous subsection that for most organic compounds, their HOMO and the LUMO are located within the π - and π^* -orbitals, respectively. Since the energy of σ -bonds are much more important, the overall influence of σ -electrons can be neglected when working with electronic transition from a photon absorption, leaving π - π^* the only relevant transition to be taken into account.

The absorption of a photon from a π -molecule results in the generation of an electron-hole⁵ pair (referred to as an exciton) whose binding energy is expressed as:

$$E = \frac{e^2}{4\pi\epsilon_0\epsilon_r d} \quad (1.11)$$

with e the elementary charge, ϵ_0 the dielectric constant of vacuum, ϵ_r the molecule dielectric constant, and d the average distant between the electron and the hole.

A small dielectric constant in organic compounds and the localization of the electron-hole pair on one molecule leads to a very strong binding energy (0.1 - 1 eV), making them very stable at room temperature. Therefore, excitons in organic crystals, polymers and semiconductors can be described in the picture Frenkel excitons, as opposed to Wannier-Mott ones, whose binding energy are much lower

⁵The *hole* denotes the absence of electron in the HOMO, which will pair with the promoted electron on the LUMO.

than k_bT (≈ 10 meV) since their radius is usually larger than the crystal lattice [37, 38]. This strong binding energy allows us to describe the whole photophysics within the exciton picture. For instance, a molecule promoted to an excited singlet state will be referred to as a S_1 (or singlet excited) exciton.

1.2.2 Jablonski-Perrin diagram of organic systems

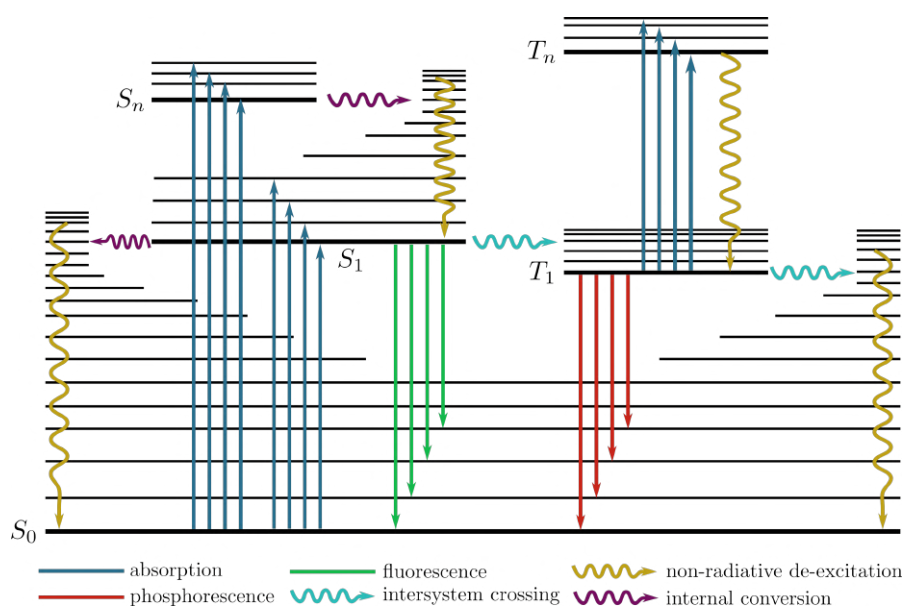


Figure 1.15: Jablonski-Perrin diagram of organic molecules.

1.2.3 First excited singlet state: lifetime and luminescence quantum yield

Once an exciton is formed in the first excited singlet state S_1 , two routes exist towards a relaxation to the ground state S_0 : by the emission of a photon or because of vibrations and/or rotations of the molecule. As discussed in Section 1.1.4, the emission of a photon can be stimulated by another photon or spontaneous. However, molecular properties will only be discussed in the absence of lasing here.

When an S_1 exciton undergoes spontaneous de-excitation, it emits one photon in a pure random direction, phase and polarization: this is fluorescence. The rate at which it occurs is denoted by k_r (s^{-1}) and is closely related to the singlet-singlet absorption cross section *via* the following formula [43, 44]:

$$k_r = \frac{8\pi c n_e^3}{n_a} \frac{\int_{\sigma_{em}} f(\lambda) d\lambda}{\int_{\sigma_{em}} f(\lambda) \lambda^3 d\lambda} \int_{\sigma_{abs}} \frac{\sigma_{abs}(\lambda)}{\lambda} d\lambda \quad (1.12)$$

where n_e and n_a are the average refractive index in the emission and absorption spectral regions, respectively. f is the λ -dependent fluorescence emission spectrum,

whereas σ_{abs} and σ_{em} are the absorption and emission cross sections of the $S_0 \rightarrow S_1$ transition. Because the spontaneous de-excitation of an excited exciton can end on any vibrational sub-level of the ground state, the fluorescence spectrum of one compound is not narrow, as discussed in Section 1.1.4 and Figure 1.6. Besides, giving the important density of rotational and vibrational level of π -conjugated systems, some molecules fluorescence spectra can span over 100 nm.

On the other hand, the non-radiative de-excitation of an exciton is referred to as *internal conversion*, the rate at which it occurs is denoted by k_{nr} . Since it is related to the possibilities for molecules to vibrate and rotate, k_{nr} can be greatly influenced by environmental parameters such as the temperature of the gain medium [45], or the solvent in which it is diluted [46, 47]. Typical k_{nr} values reported in the literature scale between 10^8 and 10^9 s⁻¹ [47, 48, 49]. Taking both pathways into account, the equation ruling the singlet density can be written as:

$$\frac{dS_1}{dt} = -(k_r + k_{\text{nr}})S_1(t) \quad (1.13)$$

and be solved to reach the following exponential dynamics:

$$S_1(t) = e^{-(k_r+k_{\text{nr}})t} = e^{-t/\tau_f} \quad (1.14)$$

where $\tau_f = (k_r + k_{\text{nr}})^{-1}$. Although τ_f is always referred to as the fluorescence lifetime, it accounts for both radiative and non-radiative decay. Moreover, it represents a very important quantity to evaluate whether a molecule could achieve a high luminescence (from a singlet-singlet transitions) efficiency or not. Indeed, a low excited state lifetime means that singlet excitons have less time to be transferred to a dark triplet state *via* intersystem crossing (discussed in details in Section 1.2.4.1) or by the means of other processes. Most fluorescence lifetime scale at a few nanoseconds, as presented in Table 1.1 for different molecules.

material	τ_f (ns)	solvent	references
CBP:BSBCz	1.28	thin film	[14]
BSFCz	0.86	toluene	[15]
Rhodamine 123	1.92	ethanol	[50]
Rhodamine 19	4.16	methanol	[51]
Rhodamine 6G	3.7	ethanol	[52, 53]
DCM	2.18	DMSO	[54]

Table 1.1: Some fluorescence lifetimes reported in the literature for different organic compounds.

Another useful characteristics of light emitting compounds is their **PhotoLuminescence Quantum Yield** (PLQY), which describes more efficiently the capabilities of one molecule to emit light. It is defined as [37, 38, 40]:

$$\phi_F = \frac{k_r}{k_r + k_{nr}} = \frac{\tau_f}{\tau_{rad}} \quad (1.15)$$

and can go from 0 to 1. It consists of an intuitive ratio between the radiative decay from S_1 to S_0 and all other de-excitation processes. If k_r is equal to k_{nr} , the molecule will have a PLQY of 50%. In the case of highly fluorescent compounds for instance, which have by definition a weak **Spin-Orbit Coupling** (SOC) or a short fluorescence lifetime, it generally scales much lower than k_{nr} and therefore, do not influence much their PLQYs. On the other hand, k_r and k_{nr} can decrease by three orders of magnitude in the case of organo-metallic complexes such as *far*-Ir(F₂ppy)₃ in which they have been measured around 10⁵ s⁻¹ in different solvents [55]. It should also be highlighted that ϕ_F does not take into account stimulated emission in the possible decay channels, as it is always measured in absence of lasing for a better comparison with other materials.

The higher ϕ_F , the better, since it means that a greater proportion of excitons on the S_1 state will be useful to the luminescence. Among other parameters that can influence PLQYs, there is the concentration of active molecule in the gain medium. Indeed, when the density of chromophores inside the active volume becomes important, a so-called *concentration quenching* occurs, meaning that numerous intermolecular processes leading to non-radiative decay arise thanks to this high density and as a result, the luminescence of the material can be dramatically impacted.

For instance, it can lead to what is called π -stacking⁶, where the 2p_z orbitals of several molecules stack each other, which decreases the overall gain medium luminescence [58]. These types of quenching obviously depends on the conformation of the molecule, as one fully planar will tend to stack more easily. Moreover, a high concentration can lead to more collision between active molecules [59], which can facilitate non-radiative de-excitations. It is especially relevant in liquid configurations where molecules have much more degrees of freedom than in solid thin films.

1.2.4 First excited triplet state

1.2.4.1 The generation of triplet excitons

The generation of triplets originates from two distinct methods: An optical excitation of the gain medium or by the use of an electrical current. In the first case, the building of the triplet population arises from, at first, the absorption of a photon by the ground state S_0 whose energy matches the $S_0 \rightarrow S_1$ transition. In

⁶The term π -stacking itself and the intuitive image that comes with it is somewhat misleading and are still a matter of debate, as stacking of aromatic units seems incompatible with the electrostatic repulsions of each compound [56, 57]. Other stacking do occur under high concentration, but are not that simple and must lead to an attraction between two or more molecules.

the case of electrical injection though, triplets accumulate thanks to the creation of electron-hole pairs. Both approaches are sketched on Figure 1.16.

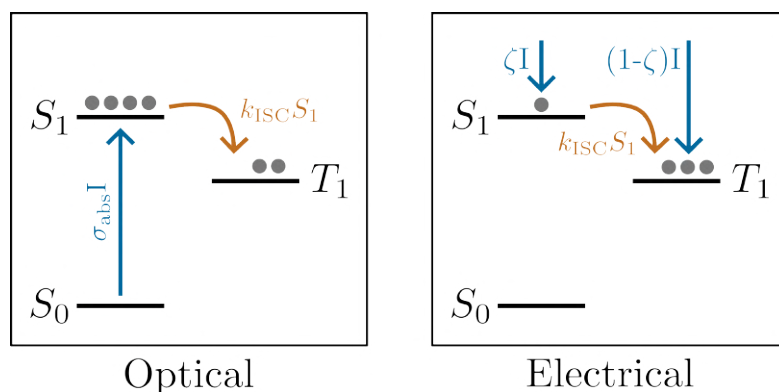


Figure 1.16: Illustration of two methods to pump gain media: Optical injection (left) where the S_1 state is filled by ground state absorption and triplets are only generated *via* intersystem crossing, and electrical current injection (right) where excitons are created from the removal of electrons from their orbital

Optical injection

As stated, the building of the triplet population by optical injection requires in the first place a certain density of singlet excitons. The first and most important interaction giving rise to triplets is referred to as **InterSystem Crossing (ISC)** [9, 60, 61], it can be represented as on Figure 1.17 (left) and by the following simple process:



where S_1 denotes the first excited singlet state (which is populated by ground state photon absorption) and T_1 the first excited triplet state, whose energy level is lower so that ISC is in direct competition with the de-excitation roads from S_1 to S_0 .

The reason for this non-zero probability of a transition between two electronic states with different spins comes from a relativistic effect known as **Spin-Orbit Coupling (SOC)**. In a semi-classical view, SOC can be described as the interaction between the magnetic field generated from the motion of an electron around its nucleus and the one generated from its spin. Thus, k_{ISC} can be expressed as:

$$k_{\text{ISC}} = \frac{2\pi}{h} |\langle \psi_{T_1} | H_{\text{SOC}} | \psi_{S_1} \rangle|^2 [\text{FCWD}] \quad (1.17)$$

where ψ_{S_1} and ψ_{T_1} denotes the singlet and triplet state wavefunctions, respectively. H_{SOC} is the SOC hamiltonian between both states, and FCWD accounts for the **Franck-Condon Weighted Density**, meaning that there must be an overlap between the wavefunctions of the states involved for ISC to be efficient. More, this

interaction can also be seen in terms of pure, well defined electronic states, which in the case of a pronounced SOC is no longer accurate. Instead, the triplet state is mixed with singlet ones is written as [9]:

$$|\tilde{T}_1\rangle = |T_1\rangle + \sum_n \frac{\langle S_n | H_{\text{SOC}} | T_1 \rangle}{E(T_1) - E(S_n)} |S_n\rangle \quad (1.18)$$

where \tilde{T}_1 denotes the excited triplet state perturbed by SOC while S_n is the unperturbed n th singlet state. The same development could be applied to the ground state S_0 , but the effect of SOC on it would be negligible since the energy difference between these two states is quite large. A direct consequence of this perturbation is that the scalar product $\langle \tilde{T}_1 | S_1 \rangle$ no longer vanishes, opening the way to previously forbidden transitions.

Since H_{SOC} is directly proportional to Z^4 the atomic charge, the most efficient way to increase ISC is *via* the implementation of heavy atoms inside the gain medium [37, 9]. In fact, organometallic complexes (Platinum, Iridium, and so on) are widely used in phosphorescent light emitting diodes, as it allows one to easily reach an emission efficiency close to unity from the triplet state [62, 63, 64, 65]. Typical intersystem crossing rates scale around 10^7 s^{-1} [66, 67, 68] but can be orders of magnitude higher when heavy atoms are incorporated, as in the case of $\text{Ir}(\text{piq})_3$, for which Hedley *et al.* reported that ISC occurs within less than 100 fs after the initial excitation [69].

Moreover, it has been shown by Jian *et al.* that ISC could be increased thanks to the presence of molecular aggregates in the gain medium [70], paving the way for a more efficient phosphorescence.

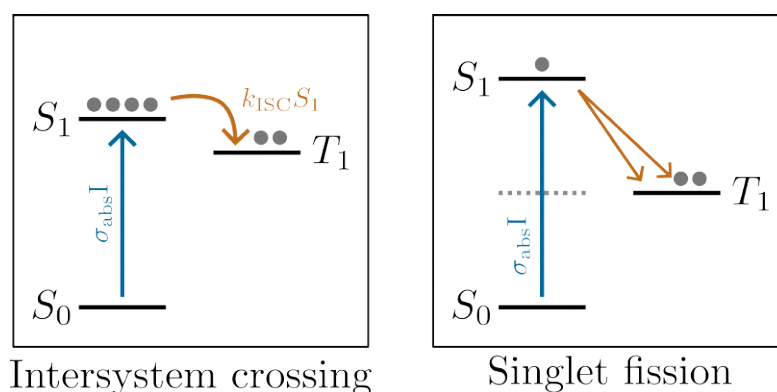


Figure 1.17: Illustration of two methods to generate triplet excitons: Intersystem crossing (left) where singlets are transferred to the triplet state at a fixed rate k_{ISC} , and singlet fission (right), where the energy of one singlet is split in half to produce two triplets because $\Delta E_{\text{SS}} \geq 2 \times \Delta E_{\text{ST}}$.

An other way to populate the triplet state, firstly described in 1965 to explain the photophysics of anthracene [71], is called **S**inglet **F**ission (SF), whereby the energy of an excited singlet state is split into two, producing two T_1 excitons. SF is

illustrated on Figure 1.17 (right) and even though it involves more complex routes [72, 73], it is usually summarized as [74, 38, 37]:



SF has been observed after that in tetracene [75, 76] and in other molecular complexes with similar structures [77]. Because there are a lot of restrictions on the molecule conformations, recent approaches towards practical applications use computational methods to explore whether or not different structures would exhibit singlet fission [78, 79]. Although there is still no clear roadmap, it is commonly admitted that an efficient SF is only possible if the energy of the S_1 is at least twice the energy of the T_1 state, drastically limiting the number of potential SF friendly materials.

Electrical injection

Contrarily to the generation of triplets *via* ground state absorption followed by ISC or SF, they can also be formed after an electrical excitation of the gain medium. A current injection through electrodes will result in the placing or the removing of electrons in the entire active volume. Then, electrons and holes can diffuse until they are attracted to each other to recombine on an active site and emit a photon. Following spin statistics mathematics, 25% of the recombinations will produce a singlet state, while the remaining 75% will be triplets (see Equation 1.10).

Considering the high proportion of triplets, electrical stimulation represents an easier solution when aiming at the emission of light from the triplet state, as it does not require additional direct or indirect methods to harvest singlets. Besides, ISC still occurs from S_1 to T_1 , which improves the overall efficiency. Fluorescent materials on the other hand rely on additional processes to harvest the triplets back to the S_1 level to obtain luminescence.

1.2.4.2 Lifetime

In theory, the very same description could be applied to the T_1 state as what has been done for the S_1 state, since the former is also prone to radiative and non-radiative processes to relax towards the ground state. However, because of the quantum mechanically forbidden nature of the $T_1 \rightarrow S_0$ transition, the emission cross section of most compounds (especially fluorescent ones) scale so low compared to those of S-S transitions that it is not counted as a relevant pathway [80, 81, 82, 83]. Thus, the triplet lifetime of organic molecules τ_t will only account for the non-radiative de-excitation in this work.

These negligible emission cross sections are the reason why excited triplet states are often referred to as *dark* states. Of course, light cannot be emitted from these states but more importantly, excitons located on this energy level are trapped for

very long times because of the low probability for one to de-excite even non-radiatively back to the ground state, causing an impactful depletion of the ground state. Hence, the lifetime of this dark state T_1 is typically three to five orders of magnitude higher than the fluorescence lifetime, as presented in Table 1.2 for different, well known fluorescent and phosphorescent compounds.

material	τ_T (ms)	references
BSBCz	0.175	[14]
DCM	0.031	[84]
PPIX	0.390	[85]
Alq ₃	0.17	[86]
Alq ₃ :DCM	1.55	[86]
4-hydroxycoumarin	700	[87]

Table 1.2: Some triplet state lifetimes reported in the literature for different compounds.

1.2.4.3 Triplet absorption

An exciton lying on the T_1 state also has the possibility to absorb a photon and be promoted to a higher-lying state referred to as T_n ⁷. This process, known as **Triplet Absorption (TA)** or triplet-triplet absorption, is also represented on Figure 1.15. Since $T_1 \rightarrow T_n$ transitions are allowed thanks to the spin of the two states involved, triplet absorption cross sections are found to be of the same order of magnitude as singlet-singlet transitions ($\approx 10^{-16}$ cm²) in most organic compounds [37, 38].

We will see that this is of paramount interest when it comes to achieving lasing under long-pulsed excitation, as the non-linear nature of lasing regimes makes them very sensitive to photon losses inside the cavity.

1.2.4.4 Thermally activated delayed fluorescence

Although ISC and TA are common to the vast majority of π -conjugated materials, some of them exhibit properties that allows other phenomena to occur, this is the case of the so-called **Thermally Activated Delayed Fluorescence (TADF)** materials. What distinguishes these compounds from others is their small energy gap between the first excited singlet and triplet states. Whereas typical energy gaps ΔE_{ST} scale around 0.7 eV [9, 37, 38], the gap of TADF materials is usually lower than 200 meV [88]. With an energy difference much closer to k_bT , **Reverse InterSystem Crossing (RISC)**, which is the perfect opposite of ISC, becomes allowed.

⁷Higher-lying triplet excited states are denoted with a n because of the difficulty to probe their structure with enough precision.



Here, k_{RISC} denotes the fixed rate (s^{-1}) at which triplets are upconverted back to the fluorescence level. In the last decade, these materials have been the center of a significant attention within the organic device community as it represents a very promising route for 100% fluorescence efficiency [89]. As shown on Figure 1.18, the most popular approach for the design of TADF materials consists of getting a really poor overlap between donor and acceptor molecules of the chromophores by setting them apart and on different plans, hence the common use of twisted molecules [90].

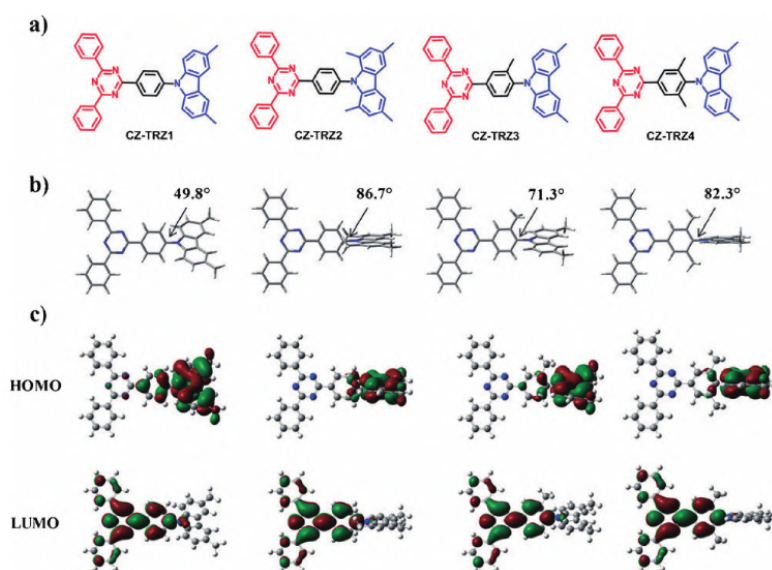


Figure 1.18: Chemical structures, optimized geometries, and theoretically calculated frontier molecular orbitals for Cz-TRZ derivatives. Figure taken from Reference [90].

This poor overlap between the LUMO and HOMO band has for consequence the decrease of the energy difference between S_1 and T_1 states, which eases RISC process since k_{RISC} can be expressed in terms of gap law:

$$k_{\text{RISC}} \propto \exp \left[-\frac{\Delta E_{\text{ST}}}{k_b T} \right] \quad (1.21)$$

with k_b the Boltzmann's constant and T the temperature of the gain medium.

The delayed nature of the fluorescence of TADF materials comes from the need of a populated triplet state for RISC to be efficient. In the case of a very brief excitation (ns), the fluorescence of a normal molecule will vanish within a few nanoseconds, depending on its fluorescence lifetime. But, because triplets generated by ISC from this brief excitation have a very long lifetime, they can be upconverted back to S_1 for a long time after the excitation through RISC, leading

to a longer (but much weaker) light emission. The delayed fluorescence induced by RISC is illustrated on Figure 1.19, where k_{RISC} can be evaluated from the temporal integral of the delayed light emission.

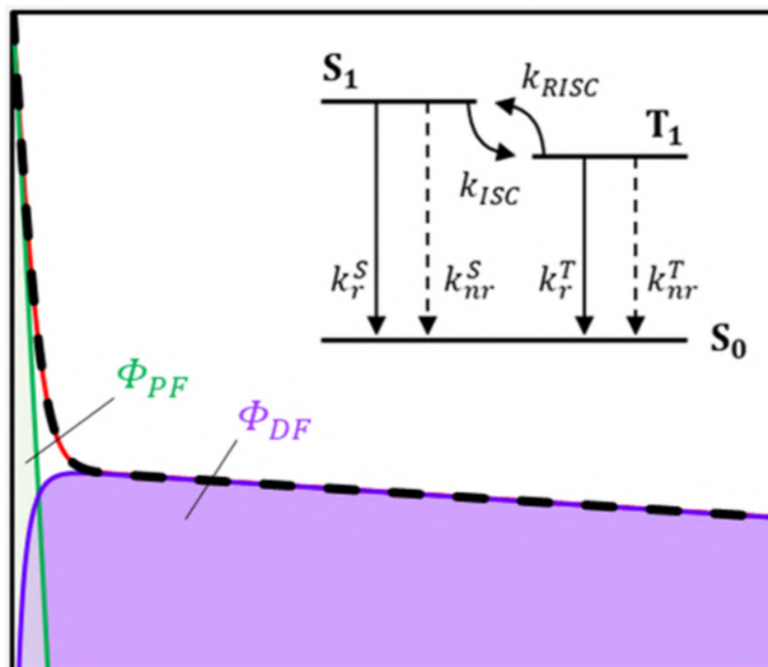


Figure 1.19: Illustration of the delayed fluorescence induced by reverse intersystem crossing. Figure taken from Reference [88].

1.2.5 Energy transfers

Several processes that rely on absorption or different types of transitions from one state to another have already been presented. However, the photophysics of π -conjugated systems is more complex, as the multiplicity of spin states allows interactions between excitons to occur that are all ruled by two types of energy transfers: Förster and Dexter transfers. The purpose of this subsection is then to present both in order to understand the origin of interactions that will be investigated further in this work.

1.2.5.1 Förster type

An excited donor molecule (D^*) can interact at long range with an energy accepting molecule (A) *via* a **F**luorescent **R**esonant **E**nergy **T**ransfer (FRET) or simply a Förster transfer [40]. This non-radiative dipole-dipole interaction has been theorized in 1948 by Förster [91]. As illustrated in Figure 1.20, the excited donor is quenched by transferring its energy to an accepting site, promoting the latter to a higher-lying electronic state.

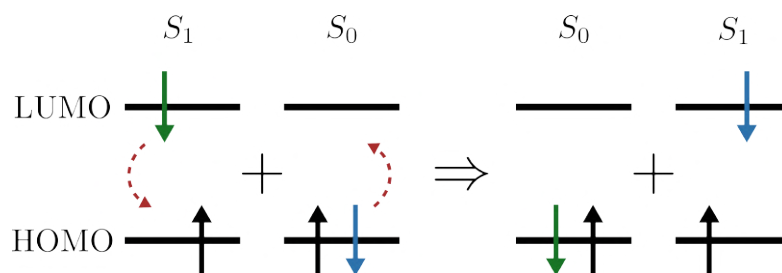


Figure 1.20: Förster energy transfer between two singlet state excitons. The first molecule is quenched from the fluorescence level (\$S_1\$) to the ground state (\$S_0\$) by transferring its energy to a ground state molecule, hence promoting it to the \$S_1\$ state.

The probability for a molecule to be transferred from an initial state i to a final state f by a FRET mechanism is based on Fermi's golden rule [92], where in Equation 1.23 $\langle i|H'|f\rangle$ is the interaction matrix element of the perturbation H' between two eigenstates of the system.

$$\Gamma_{i \rightarrow f} = \frac{2\pi}{\hbar} |\langle f|H'|i\rangle|^2 \delta(E_f - E_i) \quad (1.23)$$

The Dirac function⁸ implies that the energies of the states involved have to match in order for the probability Γ not to vanish. Therefore, there must be an overlap between the emission spectrum of the donor and the absorption spectrum of the acceptor for a Förster transfer to be efficient, as sketched on Figure 1.21. An evaluation of the matrix element coupled with the integration of both spectra allows the total FRET rate to be expressed as Equation 1.24 [40], where τ_D is the fluorescence lifetime of the donor in the absence of acceptor and r the distance between the two molecules.

$$k_{\text{FRET}} = \frac{1}{\tau_D} \left(\frac{R_0}{r} \right)^6 \quad (1.24)$$

R_0 the *Förster radius* is defined as the distance for which a spontaneous de-excitation of the donor and an energy transfer to the acceptor are equally probable, it is expressed as [93, 37]:

$$R_0^6 = \frac{2.07 \times 10^4}{128\pi^5 \mathcal{N}_A} \frac{\kappa^2 \phi_D}{n^4} \int \frac{f_D(\lambda) \epsilon_A(\lambda) \lambda^4 d\lambda}{f_D(\lambda) \epsilon_A(\lambda) \lambda^4 d\lambda} \quad (1.25)$$

where κ is the orientation factor of the molecules, ϕ_D the fluorescence quantum yield of the donor, \mathcal{N}_A the Avogadro constant, and n the average refraction index

⁸A more accurate expression would take into account the density of state of the electronic levels, as many combinations of sub-levels satisfy this energy difference.

of the gain medium where the spectra overlap. $\overline{f_D(\lambda)}$ is the normalized fluorescence spectrum of the donor and $\epsilon(\lambda)$ the molar absorption coefficient of the acceptor.

The efficiency ρ of this transfer defined in Equation 1.26 is mostly driven by the ratio r/R_0 , reaching 50% when $r = R_0$ and quickly decreasing when the distance between the molecules becomes important. As a matter of fact, the r^6 dependency prevents such transfers from happening beyond 10nm in organic compounds, and every measured or calculated R_0 in different molecules scale between 1 and 10 nm [40]. This theoretical dependency over r has been confirmed for the first time in 1967 by Wilchek *et al.* using Tryptophyl [94].

$$\rho = \left[1 + \left(\frac{r}{R_0} \right)^6 \right]^{-1} \quad (1.26)$$

Förster transfers are especially important in so-called host-guest systems where two light-sensitive molecules are mixed together in a solution or in a solid film. Figure 1.21 shows the general idea:

1. The first molecule (the donor) is excited at a given wavelength accordingly to its absorption spectrum (here, in blue).
2. Considering the Stokes shift between its emission and absorption spectra, it will then emit photons at longer wavelengths.
3. Thanks to the overlap (in grey) between the emission spectrum of the donor and the absorption spectrum of the second molecule (the acceptor). Photons emitted in the green will be absorbed immediately by accepting molecules.
4. The final result is an emission from a molecule in the red, coming from the excitation of an other molecule in the blue.

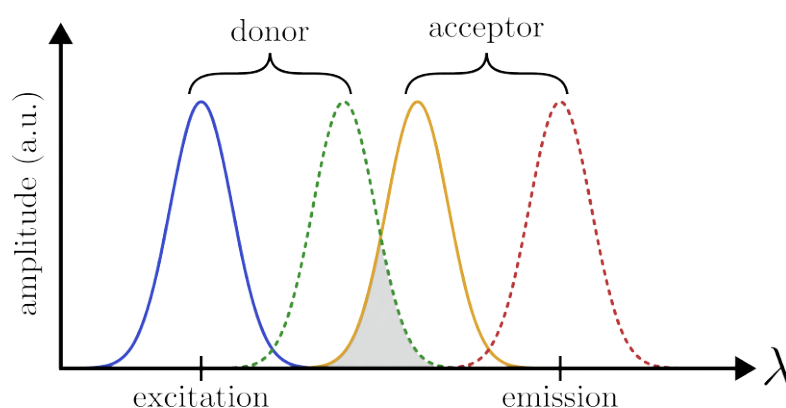


Figure 1.21: Illustration of Förster transfer in host-guest systems. Higher emission wavelengths are reachable with the same excitation source thanks to the overlap (colored in grey) between the donor emission spectrum and the acceptor absorption spectrum. Dashed lines: emission spectra ; Solid lines: absorption spectra.

1.2.5.2 Dexter type

Dexter transfer, on the other hand, is a short range interaction whereby an excited donor D^* and an acceptor A simultaneously exchange charge carriers (an electron from the former, a hole from the latter) [95]. This process is sketched on Figure 1.22 and its rate is expressed in Equation 1.27. Because it decreases exponentially with r the distance between the two molecules [38], it can only happen if there is a spatial overlap of the exciton wavefunctions. The typical distance for a Dexter exchange is therefore no more than 1 nm in most cases,

$$k_{\text{DEXT}} \propto \exp\left(\frac{-2r}{L}\right) \quad (1.27)$$

where L is related to the average distance between molecules inside the gain medium [38].

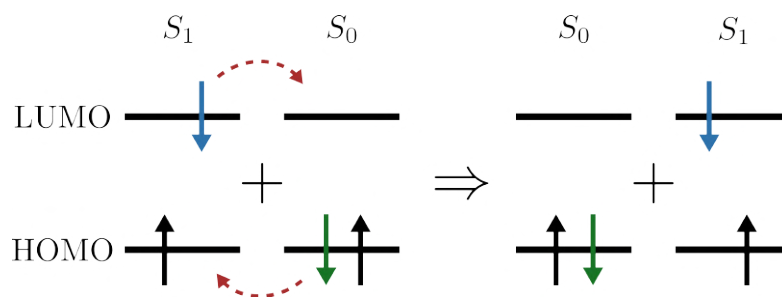


Figure 1.22: Dexter energy transfer between two singlet state excitons, where two molecules simultaneously exchange a charge carrier, transferring their energy to the other.

Although its finality is the same as a Förster transfer, the fact it does not have to be dipole-allowed means that transitions between singlet and triplet states are probable.

1.2.6 Bi-exciton mechanisms in organic semiconductors

In this section, some of the most important bi-exciton interactions (which are based after either Förster or Dexter exchange) occurring in organic media under electrical or optical stimulation will be presented.

1.2.6.1 Singlet-triplet annihilation

Singlet-Triplet Annihilation (STA) is described as a dipole-dipole interaction between an excited singlet state S_1 and a triplet state T_1 . As expressed in Equation 1.28, the singlet exciton is transferred to the ground state (without the emission of a photon) at a rate k_{STA} ($\text{cm}^3 \cdot \text{s}^{-1}$) whereas the triplet exciton is promoted to a higher excited triplet state of energy T_n [96].



Then, the T_n exciton quickly de-excites in a non-radiative way back to the first excited triplet state, as this is the most efficient pathway [9].



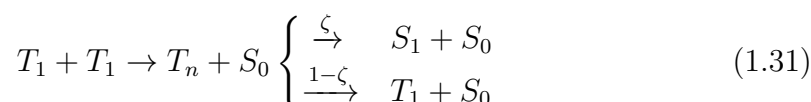
STA can therefore be modeled as:

$$\frac{dS_1}{dt} = -k_{\text{STA}}S_1T_1 \quad (1.30)$$

Both transitions $S_1 \rightarrow S_0$ and $T_1 \rightarrow T_n$ being allowed by the spin selection rule, STA can be described within the framework of long range Förster interactions. As such, it is proportional to the overlap between the fluorescence emission and triplet absorption spectra of the molecule, without the need for the wavefunctions to overlap.

1.2.6.2 Triplet-triplet annihilation

Triplet-Triplet Annihilation (TTA) occurs between two excitons located on the triplet state of energy T_1 of a molecule, it was described for the first time as a delayed fluorescence in highly concentrated anthracene solutions [97]. Because it involves more complex roads, TTA cannot be described by a simple graphic representation such as STA, but can be simplified and written as Equation 1.31 [96].



When two triplet excitons interact, one of them is promoted to a higher-excited T_n state whereas the other is transferred instantly to the ground state S_0 . It is attributed to the promoted exciton a probability ζ ($0 \leq \zeta \leq 1$) to get transferred by a cascade of non-radiative de-excitations to the fluorescence level S_1 , and a probability $1 - \zeta$ to circle back to T_1 . Therefore, TTA is seen as a loss for the triplet population and shall be modeled as Equation 1.32 [38].

$$\frac{dT_1}{dt} = -2k_{\text{TTA}}T_1^2 + (1 - \zeta)k_{\text{TTA}}T_1^2 = -(1 + \zeta)k_{\text{TTA}}T_1^2 \quad (1.32)$$

The first term represents the initial annihilation of two triplets at a rate k_{TTA} ($\text{cm}^3 \cdot \text{s}^{-1}$) and the second stands for the proportion $1 - \zeta$ of higher-lying excitons that circle back to the T_1 state.

This interaction involves a forbidden $T_1 \rightarrow S_0$ transition. Hence, it can only be explained by a Dexter mechanism, meaning that both wavefunctions have to overlap for TTA to be efficient, as discussed in Section 1.2.5.2. Its strength will

mostly be driven by the density of active molecule inside the gain medium, so that the probability for molecules to be at very close range no longer vanishes. This is why it is thought to have an influence on the population dynamics only in highly concentrated solid films or solutions [9]. The excitation power density has also to be taken into account: the density of triplet excitons created by intersystem crossing or other pathways has to be high enough so that when two molecules or more *collide*, TTA can occur.

The proportion ζ of singlets generated by TTA is often set to 0.25 [82, 98, 74, 80, 99] by analogy to the spin statistics of an exciton created by the spin of an electron-hole pair. However, as stated before, Equation 1.31 is a simplification of the real consequences of the collision of two triplets and therefore fails at precisely describing the whole process. Indeed, the collision of two triplet state wavefunctions results in charges distributed accordingly to the following spin statistics [100, 9]:

$$\frac{1}{9}S + \frac{1}{3}T + \frac{5}{9}Q \quad (1.33)$$

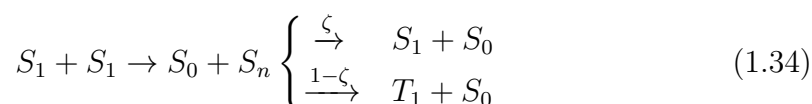
where S is the singlet state, T the triplet state, and Q a quintet state. If this last spin state has not been mentioned earlier, it is because **Density Functional Theory** (DFT) calculations indicate that a so called quintet level of energy is not compatible with most organic compounds due to its high endergonicity [101, 99]. Therefore, it is usually assumed in the framework of organic light emitting devices that charges annihilated *via* TTA do result in the spin statistics of Equation 1.33, and that the portion on the quintet state relaxes instantly considering its non-stability with time [102]. Hence, the overall spin statistics after having taken this assumption into account ends with 75% of triplets and 25% of singlets.

The most complete and recent description of triplet-triplet annihilation and its spin statistics has been provided by Clark *et al.* [100]. In their work, they included various factors that are thought to influence the value of ζ such as the orientation between active molecules, the energy of the first excited triplet state, and reach values for ζ going from 0.2 to 0.66, affecting the overall excitons populations dynamics.

Regardless of the value of ζ , it is straightforward to picture why TTA is of the utmost importance in many systems, since it contributes to the quenching of the triplet population and at the same time to the filling of the fluorescence level. It is especially impactful where triplets are abundant, such as for electrical stimulations.

1.2.6.3 Singlet-singlet annihilation

Singlet-Singlet Annihilation (SSA) describes an interaction between two singlet excitons [103, 104] which can be summarized by the following reaction:



Here, a S_1 exciton transfer its energy to the second and then relaxes to the ground state. The later gets promoted to a higher-lying S_n state, and then can circle back to the fluorescence or relax onto the triplet state T_1 . The probability that it circles back is denoted ζ , hence the $(1 - \zeta)$ probability to generate a triplet state. The value of ζ is assumed in many studies to be ruled by spin-statistics rules in electrical excitation configuration ($\frac{1}{4}S_1 + \frac{3}{4}T_1$) [96, 74].

SSA is modeled in the singlet equation similarly to TTA for the triplet equation:

$$\frac{dS_1}{dt} = -(2 - \zeta)k_{\text{SSA}}S_1^2 \quad (1.35)$$

Relevant principles of intermolecular interactions have been covered in this section. This introduction to the world of organic electronics ends with the brief presentation of a couple of applications that take advantage of the photophysics above-mentioned, and that I personally found quite interesting to discuss during my studies.

1.2.7 Some applications of organic electronics

Recently, continuous-wave phosphorescent tags for imaging applications have been developed. More, they are found to be easily programmable thanks to a monitoring of the oxygen local concentration [105, 106]. First, the oxygen is quench locally using masks and a strong UV source. Reineke *et al.* showed that with a second low power UV source it was possible to excitate continuously triplet excitons to obtain phosphorescence, since they are not quench by oxygen any longer. The only requirements was for the material to have, of course, a high phosphorescence quantum yield ϕ_T and a short triplet state lifetime. To cancel the emission and/or change the image, one just has to turn off the UV excitation so that oxygen can diffuse homogeneously inside the gain medium.

Because the photoactivation of proteins in biological tissues requires visible light radiation that cannot propagate easily in such media, triplet-triplet annihilation is used with metal complexes [107] or more biocompatible moisture like hydrogels [108] to upconvert NIR radiation (which penetrates through skin more easily) to a blue emission, capable of proteine activation. Moreover, the recent progresses regarding the use of hydrogels has numerous potential applications in optogenetics and the non-destructive analysis of deep tissues. Regarding biomedical applications, Huang *et al.* reported the use of organic scintillators as X-ray detectors coming from irradiated samples [109]. They showed that using organic compounds allow the reduction of X-ray doses by a factor of 167 compared to standard detection techniques.

Obviously, the application of organic electronics that comes instantly in mind is **Organic Light Emitting Diodes (OLEDs)**, as it has literally revolutionized the imaging industry, from the first Samsung AMOLED display in 2009 and the first 55" OLED TV in 2012, to the foldable TVs and mobile screens aiming at a mass commercialization within the next few years. Even though this technology seems rather recent in our lives, its roots can be traced back into the 1950's with the works of Bernarose *et al.* [110, 111, 112], who were the first to report luminescence from an organic compound under electrical stimulations. The technology was improved to a closer version of what is done today by Pope *et al.* a few years later [113, 114, 115], especially regarding the charges injection.

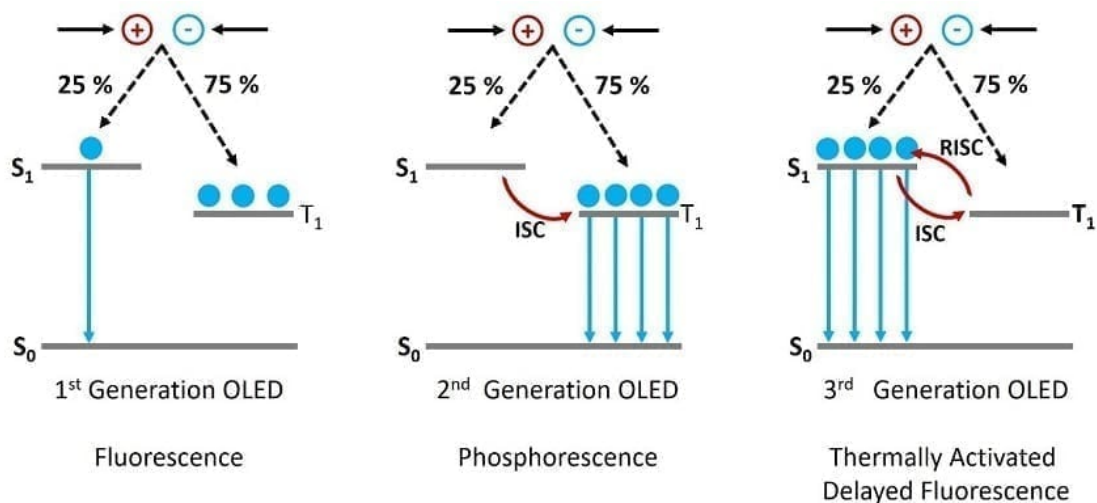


Figure 1.23: Illustration of the different generations of OLED and what mechanisms are used to emit light. Figure taken from Edinburgh Instruments website.

As pictured on Figure 1.23, what is now called the first generation of OLED relied on simple fluorescent emitters that were excited by the means of electrodes. However, we have seen in this introduction that a huge portion of excitons formed by electron-hole pair recombinations ended up on dark triplet states. This explains why, whether it is red, green, or blue, this generation has never exhibited an interesting efficiency and/or brightness. To overcome the triplet problem, researchers decided to embrace these long lived excitons by the use of novel, highly phosphorescent materials, coupled with metal complexes inside the gain medium to enhance ISC *via* spin-orbit coupling, as described in Section 1.2.4.1. But, since the light emission from triplets is usually largely red-shifted from the fluorescence, no material that could provide an efficient blue emission has ever been found, contrarily to red and green emitters. Therefore, the second generation always had to work with inefficient, blue emitters from the previous generation to cover all the spectrum. In 2012 however, Adachi *et al.* reported the first efficient OLED covering the whole visible spectrum without using phosphorescence [89]. Instead, they used a TADF material to harvest the 75% excitons on the triplet state to

the fluorescence, as discussed in Section 3.4.3.3. These progresses constitutes the more recent generation of OLED to date.

1.2.8 Summary

Thanks to partial overlaps of unhybridized π -orbitals along single and double carbon bonds chains, π -conjugated materials allow the excitation of delocalized electrons through π - π^ transitions and their diffusion along the carbon backbone of the molecule. But, because of OSCs lower dielectric constant and the localization on one active site of the electron-hole pair formed by the absorption of a photon, the resulting quasi-particle referred to as an exciton has a binding energy much higher than k_bT at room temperature, making it quite stable and allowing us to treat the photophysics of excited states in OSCs within the exciton framework.*

Contrarily to their inorganic counterparts, OSCs exhibit a well defined triplet state T_1 whose energy is lower than the one of the S_1 state. Besides, the energy difference ΔE_{ST} between both states scales around 0.7 eV in most compounds, meaning that the T_1 state has to be taken into account in the physics of OSCs. In addition to the classical fluorescence, a direct consequence for excitons located on the S_1 state is that they can be transferred to the triplet state via intersystem crossing. Moreover, the forbidden nature of the $T_1 \rightarrow S_0$ results in a very long triplet state lifetime, meaning that S_1 excitons that could be useful for luminescence are trapped, hence the dark state terminology.

From the T_1 state, many processes that excitons can undergo whilst trapped have been described. First, it can undergo triplet absorption by absorbing a photon if its energy is appropriate, which will be interesting to study when coupled with a cavity and lasing photons propagating back and fourth inside the gain medium. Then, T_1 excitons can also interact with other molecules located on other active molecules under certain conditions. If the ground state absorption spectrum overlaps with the triplet absorption one, STA can occur at long range and quench the S_1 density. On the other hand, TTA can occur between two T_1 excitons at close range if there is an overlap between both molecular wavefunctions. Because this mechanism fills the S_1 population and also artificially reduces the triplet state lifetime, it has been described as a promising route to harvest more excitons for light emitting devices. At last, a novel class of materials, exhibiting TADF, has been depicted, as their conformation results in a very small energy gap between the S_1 and T_1 state. The consequence is the possibility for this materials to upconvert very efficiency triplets back to the fluorescence thanks to reverse intersystem crossing.

1.3 Organic semiconductors lasers

Because the capabilities of organic molecules to conduct charge carriers had been discovered back in 1950 by Akamatu *et al.* [116], it was only a question of time

before the first luminescence coming from an organic compound is reported. It happened 16 years later (six years after the invention by Maiman of the first Ruby laser [24]) when Helfrich *et al.* electrically pumped anthracene crystals and observed luminescence, which was explained by the recombination of electron-hole pairs [117], as described in Section 1.2.4.1. Surprisingly, the first organic laser was reported just one year after that, optically pumped by a Q-switched ruby laser of a liquid solution of phthalocyanine [118].

However, as discussed in Section 1.2.1.2, organic compounds have the peculiarity to exhibit a well defined, dark triplet state whose lifetime is much longer than the fluorescence (see Section 1.2.2). Thus, the fast accumulation of triplets with time makes the population inversion no longer possible and as a result, causes the premature death of the lasing pulse. Exciton annihilation losses coupled with important elevations of temperature had prevented in the first place organic lasers to operate in a continuous-wave regime [119, 120, 121], regardless of the gain medium configuration.

1.3.1 Liquid dyes lasers

A solution to overcome the triplet and temperature problem has been proposed in 1970 with a liquid solution of Rhodamine 6G as the gain medium [122]. The breakthrough here did not rely on molecular properties but rather on a novel setup idea. The problem being that molecules in the pumping volume were trapped in dark states or bleached by thermal effects, Peterson *et al.* introduced a flowing configuration of the solution to continuously renew the pool of relaxed molecules available to undergo ground state absorption $S_0 \rightarrow S_1$. Such a setup is schematically illustrated on Figure 1.24. Since molecules trapped on the T_1 state are moved out of the pumping volume for a long time (long enough for them to de-excite back to the ground state non-radiatively) and replaced by S_0 molecules, triplets are no longer part of the problem. In addition, the constant replacement of molecules allows for the heat generated by vibrations of the active molecules to be dissipated very efficiently, resulting in no more processes to quench the population inversion and thus, an endless lasing emission. This setup was largely used after that to obtain CW emission from other organic compounds [123] such as coumarin derivatives [124], exploring emission wavelengths that could not be obtained from inorganic semiconductors.

It has been stated in Section 1.2.2 that the fluorescence spectrum of organic compounds could be much broader than most of their inorganic counterparts, mostly because of an important density of sub-levels due to vibrations/rotations possibilities of long carbon atoms chains. As such, organic lasers were prime candidate for modelocking, as the width of the pulse that can be obtained is inversely proportional to the number of lasing modes [17]. One requirement is a lasing pulse duration longer than the build-up time of the mode-locking, which has been solved

by the flowing circulation of the molecules in the case of liquid dyes. This regime has allowed in the 70's the achievement of the very first picosecond lasing pulses [125, 126, 127], followed by the first sub-picosecond emission two years later with the help of a liquid saturable absorber [128].

Moreover, researchers quickly took advantage of organic molecules broad emission spectra to obtain very tunable lasing emission, thanks to the addition inside the cavity of dispersive elements that shift the wavelength of the lasing peak [129, 130, 131]. This is useful for applications where a small range of wavelengths is required, as well as when a very specific wavelength is needed. For instance, tunable dye lasers have allowed the study of the fine structure of sodium *via* a high-resolution spectroscopy setup [132]. More practical, it has also allowed researchers to reach a 577 nm emission to treat port wine stains without any nonselective destruction of tissue [133], which was occurring with the initial setup used to treat this disease, namely the ruby laser invented by Maiman [134]. The clever setup of Telle and Tang even allowed the shifting of the lasing wavelength at the nanosecond scale [135], which is fast enough to be used in transient recovery studies.

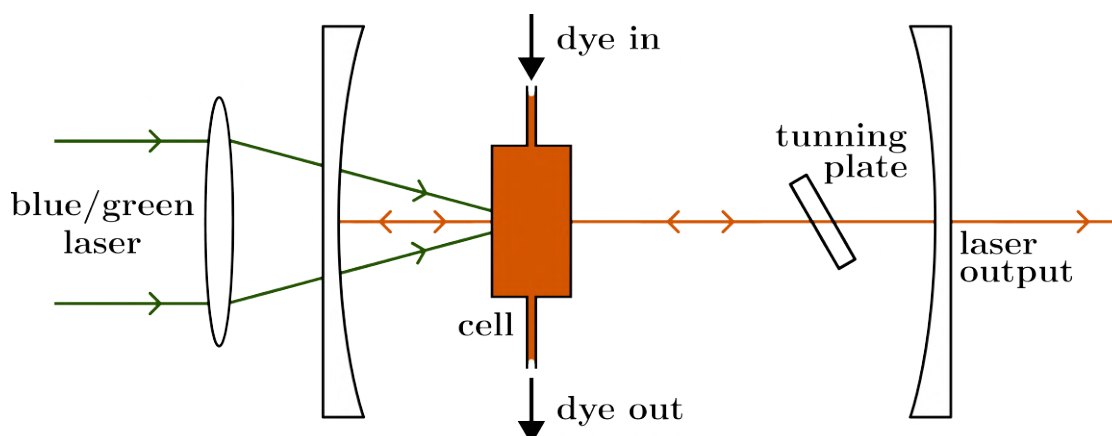


Figure 1.24: Schematic representation of a circular flowing configuration of the gain medium. This setup allows a constant pool of active molecule on the ground state, ready to absorb pump photons and to undergo fluorescence and stimulated emission. The portion of molecules being promoted to the T_1 state *via* intersystem crossing is moved away for a long enough time so that they can de-excite to the ground state. A tuning plate (often a grating acting as cavity mirror) is used to shift the wavelength of the lasing peak in tunable sources.

1.3.2 Thin film based organic lasers

The beginning of this section makes it seem like organic lasers were only studied in liquid configurations for thirty years but they were not. As a matter of fact, the first **Organic Solid State Laser** (OSSL) was reported as early as 1967 by Soffer and McFarland [131] using rhodamine 6G (whose lasing capabilities had already been established in liquid state) incorporated in a solid Poly(methyl methacrylate)

(PMMA) "plastic" film. Their work was quickly followed by Peterson and Snavely [136] who included an interesting, pioneering discussion about the role of triplets in solid gain media compared to liquid ones. In fact, Rh6G has for a long time been the molecule of choice to study the properties of OSSs [137, 138, 139] thanks to its very high gain and high PLQY. In addition to Rh6G and its derivatives, numerous papers also reported lasing from coumarin derivatives [140, 138, 141].

The advantages of solid-state gain media over liquid ones are obvious: compact, not toxic or carcinogenic like dyes in solution, and easier to maintain on an experiment table. However, OSSs have one major flaw: a very poor photostability, especially under intense excitation [142, 143]. Whether it is attributed to photodegradation of higher-lying excited states [143] or to the fast accumulation of triplet excitons [144, 145], lasing pulses achieved by OSSs did not last longer than hundreds of nanoseconds. It was for instance showed by Popov [143] using a PMMA:Rh6G blended film that an increase of the pump repetition rate resulted in a dramatic decreasing of the lasing efficiency, which was attributed to the weak heat dissipation of the gain material. This is why OSSs were not considered attractive during twenty years and therefore, were not studied a lot until novel solutions were provided in the 90's.

The development of conjugated polymers with photoluminescence quantum yields comparable to those of liquid dyes and their easier availability led to the very first organic laser based on solid semiconductors in 1996 [146]. In this report, Tessler *et al.* used poly(phenylene-vinylene) (PPV) in a high-Q microcavity to obtain a spectrally narrow emission *via* optical excitation. More, they showed that the emission of PPV mainly arose from intrachain species and therefore that these compounds were suitable for electrical stimulations, paving the way towards the long awaited organic laser diode. Their pioneer work inspired many teams afterwards to obtain lowest lasing thresholds, higher photostabilities and higher luminescence efficiencies by combining PPV with other molecules. Diaz-Garcia *et al.* used poly(2-butyl, 5-(2'-ethyl-hexyl)-1,4-phenylene vinylene) (BuEH-PPV) in planar waveguides and microcavities to conclude that the lasing threshold of both was very similar. BBEHP- [147, 148] and MEH-PPV [149, 150, 151, 86] have also been extensively studied and eventually led to the lowest lasing threshold ever reported (See Table 3.1 in Chapter 3 for details).

1.3.2.1 Limiting the population of the triplet state

Even with a rebirth of interest for OSSs thanks to the mentioned developments and the progresses towards Organic Solid-state Laser Diodes (OSLDs) (= OSSs pumped *via* current injection), the lasing pulse durations were still limited to hundreds of nanoseconds due to triplet building-up and heat generation. The first concept to actively address these difficulties was to emulate the flowing configuration of dye solutions by using a gain medium with a rotating wheel [152], so that excitation pulses would not hit twice in a row the same active volume (considering

the low repetition rate of 10 Hz). Although the heat having more time to dissipate and triplets to relax back to the ground state provided improvements in terms of photostability, the lasing outputs were very noisy and the whole mechanical device not so convenient.

Triplet quenchers

A more reliable solution was found to be the addition of other compounds inside the host matrix to ensure the de-activation or the trapping of triplets. Oxygen for instance has been used as a triplet *quencher* in thin films [153] and in liquid solutions [154, 155] to enhance the photostability of the gain medium by direct interactions between active molecules in a triplet state and oxygen atoms (whose ground states are also triplet states). However, the easy conversion of oxygen from their unique triplet ground state to reactive singlet state is found to be detrimental for the gain material, because of photo-oxydation [156].

Rather than to quench triplet excitons, Zhang and Forrest proposed [157] the concept of triplet *manager* using 9,10-di(naphtha-2-yl)anthracene (ADN) as the manager incorporated in a AlQ_3 :DCM solid film. The difference with a triplet quencher is not only semantic, as the mechanism completely differ from the simple quenching of active molecules in a triplet state (see Figure 1.25). Instead, T_1 excitons generated *via* ISC after ground state absorption $S_0 \rightarrow S_1$ from the host or the guest are being removed from the guest emissive molecules to the lowest triplet state in energy (ADN in this case) by a cascade of Dexter interactions. In the meantime, S_1 excitons that manage to reach the guest S_1 state *via* a cascade of Förster transfer are not quenched by triplets since they are removed.

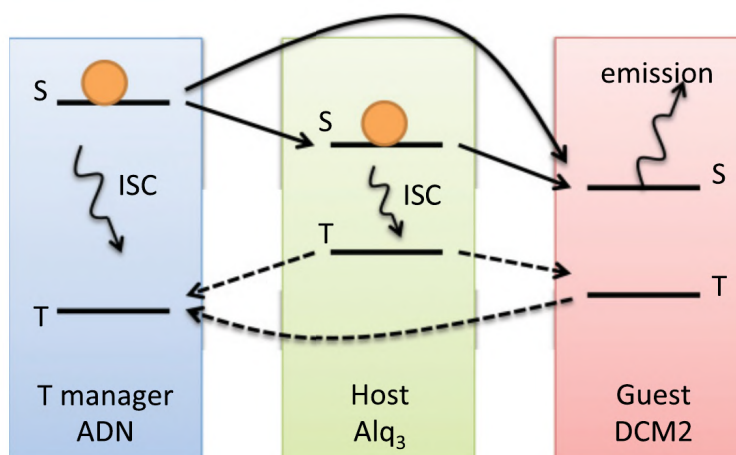


Figure 1.25: Graphical representation of the different pathways for excitons (S: singlets, T: triplets) inside the gain medium during the excitation. Figure taken from Reference [157].

As expected, there are a few requirements for this system to be efficient: the

triplet manager must have the lowest triplet- and the highest singlet-energy. Its triplet absorption $T_1 \rightarrow T_n$ must also be shifted from the one of the guest molecules in order for the trapped T_1 excitons not to contribute to optical losses. Also, the triplet manager has to have a triplet lifetime that is much shorter than the one of the emissive molecule, otherwise the problem is just shifted, but not solved. Thanks to this novel concept, Zhang and Forrest were able to show with a numerical model [157] that the lasing threshold of the device was reduced by an order of magnitude and that lasing pulses emitted from DCM2 could reach 100 μs , three orders of magnitude longer than usual triplet limited emissions. The same team later implemented this exact composition of molecules in an OLED configuration and reported a complete deletion of singlet-triplet annihilation during excitation, leading to more than 100% improvement of their device external quantum efficiency [158]. The same observations have been reported by Matsuchima *et al.* when comparing bis[(N-carbazole)styryl]biphenyl (BSBCz) (see Figure 1.26) thin films with and without ADN [159], notably a PL lifetime (in terms of stability) extended by two orders of magnitude when pumping at very low pump fluence ($< 1 \text{ W}\cdot\text{cm}^{-2}$).

On the other hand, anthracene derivatives are known to have very long triplet lifetimes of $\approx 20 \text{ ms}$ [160], so that the triplet accumulation is just relocated from the emissive- to the manager-sites. Although the emission is not quenched, the ground state eventually is also depleted in a non-negligible way. The most efficient triplet manager/quencher as of today is found to be **C**yclo**O**cta**T**etraene (COT), whose triplet lifetime has been estimated around 100 μs [161] which is not so different from usual triplet lifetime of fluorescent compounds (Section 1.2). This has been successfully used with solutions of rhodamine [162] for which an increase in the lasing efficiency with the COT concentration was reported, as well as fluorecein dyes [163].

To overcome COT limitations (only liquid at room temperature), Mai *et al.* reported just two years ago a modified version of COT: the mCP:COT [16]. With its implementation in BSBCz-EH⁹ thin film, they showed a net improvement of the photoluminescence during 400 μs for only 5 wt.% of mCP:COT inside the BSBCz-EH matrix, which has been attributed to the suppression of STA.

Intrinsic molecular properties

As it has been described, overcoming the inherent flaws of organic compounds with other compounds provided many interesting and useful results. Another approach however relies on the design of molecules that intrinsically exhibit *good* photophysical properties. The perfect example to illustrate this philosophy is the work of Rabe *et al.* [165] who reported the first **Q**uasi-**C**ontinuous **W**ave (qCW) lasing

⁹A solution processable version of BSBCz obtained without changing the pristine molecule but the addition of alkyl chains on both sides of the backbone to make it processable where BSBCz cannot be [164].

in an OSSL using an engineered version of poly(9,9-dioctylfluorene) (PFO) containing 6,6-(2,2-octyloxy-1,1-binaphthalene) bi-naphthyl (BN-PFO) spacer groups. They managed to achieve stable lasing outputs up to a repetition rate f_r of 1 MHz ($\tau_r = 1/f_r = 1 \mu\text{s}$), much higher than the previous state-of-the-art (5 kHz) [166], and also high enough to be considered qCW in many applications. This breakthrough has been ascribed to the optimization of the grating of the DFB resonator, but mostly to the large angle between naphthalene units of BN-PFO, preventing the accumulation of triplets with time thanks to a reduced overlap between the emission and the triplet absorption.

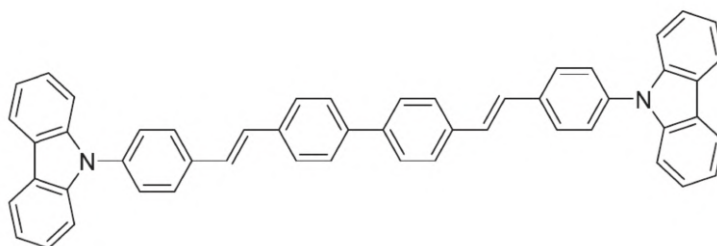


Figure 1.26: Chemical structure of bis[(N-carbazole)styryl]biphenyl (BSBCz).

More recently, Sandanayaka *et al.* [14] reported a lasing operation up to 8 MHz using 4,4'-bis(N-carbazolyl)-1,1'-biphenyl (CBP) blended with 6 wt.% of BSBCz in a DFB resonator. Thanks to the limited overlap between the triplet absorption spectrum and the lasing frequency [167], the high PLQY and low fluorescence lifetime of BSBCz [167], no triplet quencher was necessary. Moreover, this combination allowed lasing thresholds as low as $275 \text{ W}\cdot\text{cm}^{-2}$ (the lowest reported for qCW OSSLs), making BSBCz the most promising candidate for CW excitation and potentially for the long awaited OSLD.

1.3.2.2 Preventing environmental influences

The protection of solid gain media from outside defects also met some progresses in the meantime, notably thanks to the use of encapsulation. This process consists of sealing the device from environmental influences (oxygen, water, moisture). In the case of OLEDs, the encapsulation was ensured by epoxy and cover glass deposited by **C**hemical **V**apor **D**eposition (CVD) [168] or **P**hysical **V**apor **D**eposition (PVD) [169] on the bottom emitter of OLEDs. Although glass does not affect the properties of the emitter or the emitted light, these methods were found to be not robust enough and as such, were improved by **A**tomic **L**ayer **D**eposition (ALD) of aluminium oxide [170], which led to more than 1000 hours at 85°C without any signs of degradation.

In the case of organic lasers however, the encapsulation of the gain medium requires much more attention, especially in the case of DFB which were (and still

are) commonly used to achieve low-threshold lasing emissions. As discussed in Section 1.1.5, DFBs feedback mechanism consists of a spatial modulation of the refractive index (the grating) acting as very fine mirrors. Therefore, special cares must be taken when choosing encapsulating materials with these resonators, as their refractive index can modify the device properties when filling the grating of the device. The first encapsulated DFB was reported by Richardson *et al.* [171] in 2007. They used a commercially available adhesive that they degassed and drop casted directly on their MEH-PPV gain medium. Thanks to the uniform coverage of the MEH-PPV, its optical transparency and its compatibility with the index contrast of the grating, they showed that the lifetime of their device was extended by a factor of 2500 compared to the unencapsulated one.

1.3.3 State-of-the-art

Each breakthrough mentioned previously is in a certain way at the origin of the state-of-the-art that will be presented in this subsection, which will be followed by the most recent leads on how to improve what have been done.

1.3.3.1 Molecular engineering

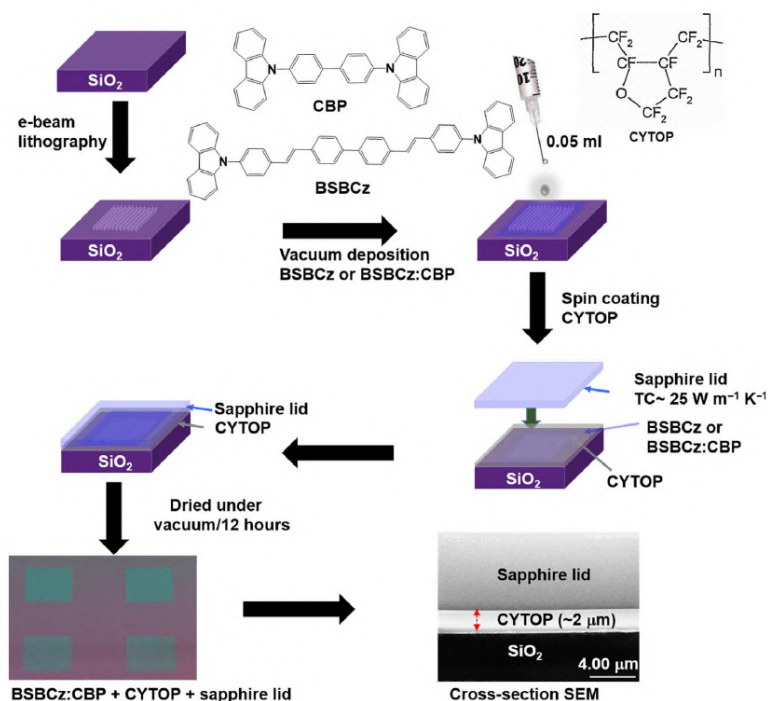


Figure 1.27: Fabrication method of the organic DFB laser with BSBCz as a gain medium, which is sandwiched between a glass substrate and a 2 μm layer of CYTOP to encapsulate it. A thick layer of Sapphire is deposited on top of the CYTOP to ensure an efficient heat conductivity. Figure taken from Reference [14].

Following their work on BSBCz, Sandanayaka *et al.* managed to reach an outstanding repetition rate of 80 MHz as well as a qCW emission during 30 ms [5] using once again a CBP film blended with BSBCz. The difference between their previous setup [165] lies in the thermal management of their devices. Indeed, as pictured on Figure 1.27, the BSBCz (or CBP:BSBCz) active medium is sandwiched between a silica substrate and a thin layer of encapsulating material. Here, CYTOP, a chemically robust, optically transparent fluoropolymer, is used to prevent oxygen and other sources of environmental quenching to penetrate into the amorphous films. On top of that, a thick layer of Sapphire is applied to ensure that heat is dissipated with high efficiency thanks to its very high thermal conductivity of $25 \text{ W.m}^{-1}.\text{K}^{-1}$. Regarding the heat dissipation, they mentioned that their encapsulating material CYTOP should be replaced in further studies by one with a higher thermal conductivity, since the broadening of the lasing peak after 500 pulses of 30 ms (Figure S12.B of their paper: from 3.4 to 10 nm) is ascribed to thermal degradation of the gain medium under such high intensities ($I_p = 2 \text{ kW.cm}^{-2}$).

Moreover, they found out in the case of a neat BSBCz film that no lasing pulses longer than $100 \mu\text{s}$ could be achieved, a limitation ascribed to concentration quenching as discussed in Section 1.2. It should also be noticed that in the case of their CBP:BSBCz (20 wt.%) film, Sandanayaka *et al.* needed to increase the pump power density from 0.2 to 2 kW.cm^{-2} to achieve lasing pulses of $800 \mu\text{s}$ and 30 ms, respectively. This finding suggests that although more intensity means more quenching because of more triplets, an increase of the excitation duration could allow one optimized device such as DFBs to shift from a pulsed emission regime to a (q)CW one. The fact that their mix-order encapsulated DFB exhibits a lasing threshold as low as $\approx 10 \text{ W.cm}^{-2}$ but that they needed to increase the pump power to a few kW.cm^{-2} to achieve qCW lasing is consistent with the theoretical paper of Zhang and Forrest on ADN as a triplet manager [157] mentioned earlier, in which they discussed the existence of two distinct thresholds: one to achieve population inversion, and a second one to achieve a CW excitation. Their system also shows that in a lossless resonator (*i.e.* with a very high quality factor Q), the two thresholds would become one.

One conclusion that could need clarification is the working of their OSSL after 500 excitations of 30 ms. Indeed, the only figures related to this particular point are Figure S12A and S12B: an emission spectrum averaged over the 500 excitation pulses, and the temporal evolution of the lasing intensity. For the former, a broadening of the spectrum is clearly visible with a FWHM going from 3 to 10 nm after 10 and 500 pulses, respectively. Regarding the temporal evolution of the lasing intensity, reports indicate a decrease of $\approx 80\%$ for 500 pulses compared to 10 pulses, however it is not indicated if these spectra are average over time or recorded after the last excitation. Because in the case of $100 \mu\text{s}$ at 100 W.cm^{-2} a decrease of $\approx 4\%$ is observable for encapsulated mix-order DFB (Figure 4D), it

could be useful to know how, pulse by pulse, the lasing intensity evolves in the case of much longer and powerful excitations (30 ms at $2 \text{ kW}\cdot\text{cm}^{-2}$).

In a more recent report, similar results were obtained by Mai *et al.* with a solution-processed BSBCz derivative (bis(N-carbazolylstyryl)-9,9-dihexylfluorene (BSFCz)) blended in a wide band-gap host (tris(4-carbazoyl-9-yl-phenyl)amine (TCTA)). BSFCz is not to be confused with BSBCz-EH: the latter had for only purpose to make BSBCz solution processable without altering the properties of the pristine BSBCz molecule. The former however is only inspired by the chemical structure of BSBCz but was engineered to enhance its properties, as well as making it processable in solutions.

BSFCz blended with TCTA was implemented in the same DFB as Sandanayaka *et al.* [5] (same grating, encapsulation, and thermal management) to achieve qCW lasing during a 10 ms excitation at $420 \text{ W}\cdot\text{cm}^{-2}$, which is similar in duration to the state-of-the-art but with a slightly lower threshold (I_p^{th} was $500 \text{ W}\cdot\text{cm}^{-2}$ for 10 ms excitation with BSBCz). Moreover, the lifetime of the DFB emission with a 6 wt.% BSFCz gain medium was measured at about 13 minutes under excitations of 10 ms at $2 \text{ kW}\cdot\text{cm}^{-2}$ (Figure 8), which is about four times more intense than its "qCW threshold" of $420 \text{ W}\cdot\text{cm}^{-2}$. It would have been interesting to see how this lifetime evolved in the case of a more important excitation duty cycle, since it has been set to 10 % in the paper, which gives about 90 ms for the heat to dissipate between each 10 ms excitation.

To prove that these results also depend on the reduced overlap between the lasing/ASE peak and the triplet absorption (similarly to BSBCz), they compared the lasing intensity of BSFCz with bis(N-carbazolyl)styryl-ter(9,9-dihexylfluorene) (BSTFCz) [172], which has a very similar chemical structure and exhibits the same ASE threshold in the mix-order DFB resonator. The only meaningful difference with BSFCz is a more pronounced overlap between lasing peak and the triplet absorption band. Although neither a temporal profile of the lasing intensity nor a streak camera recording is provided for the BSTFCz DFB, its emission spectrum after a 1 ms excitation at $2 \text{ kW}\cdot\text{cm}^{-2}$ (Figure S22 of the paper) indicates that lasing is no longer the main process occurring. Indeed, contrarily to BSFCz whose lasing emission is still well defined and narrow, the one of BSTFCz became much broader, and much closer to ASE mixed with fluorescence.

We can cite the work of Karunathilaka *et al.* [173] who also used a mix-order DFB resonator with a film of BSBCz blended with 2,6-dicyano-1,1-diphenyl- $\lambda^5\sigma^4$ -phosphinine (DCNP), an organic green dye. Indeed, and surprisingly, BSBCz is here not used as the emissive material but is *demoted* to the role of triplet manager, whereas stimulated emission arises from DCNP molecules. This host-guest system is made possible thanks to the relatively small ΔE_{ST} of DCNP ($\approx 0.44 \text{ eV}$). Triplets generated following photoexcitation are then relegated to the BSBCz site *via* Dexter transfer. Thanks to the low overlap between DCNP emission peak and BSBCz triplet absorption, triplets are no longer part of the problem

regarding the population inversion. They reported a 10 ms true CW emission¹⁰, ascribed to the very efficient management of triplets, in addition to a good thermal management. Contrarily to previous reports on BSBCz or BSFCz, they show that the lasing threshold of 75 W.cm^{-2} does not depend on the duration of the excitation (which is expected since a lasing threshold is in the first place fixed by the resonator), every temporal profiles corresponding to long ms excitation is indicated to be recorded for a pump fluence of 3.5 kW.cm^{-2} . Nevertheless, their results open the way to more CW excitation friendly material, considering the now wider choice of host material.

1.3.3.2 Resonator engineering

Even though the design of new molecules and the customization of existing ones to overcome the current limitations had gained a lot of attraction for the last decade, only a few papers explored the influence of the resonator in the lasing pulse duration and worked on novel structures that could exhibit lower lasing thresholds.

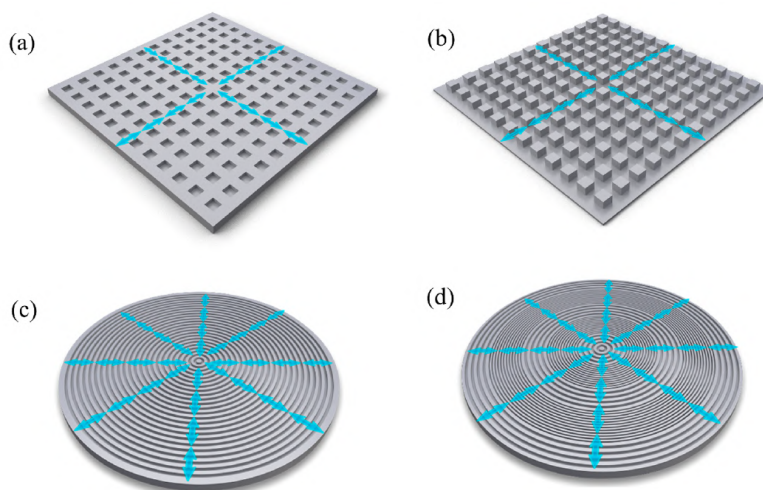


Figure 1.28: 2D DFB resonator structures were designed to improve laser performance. (a) Second-order 2D square lattice, (b) second-order 2D cross double, (c) circular second order, and (d) circular mixed-order grating structures. Arrows represent the feedback directions of each structure. All these 2D DFBs provide a surface-emitting laser. Figure taken from Reference [6].

On this matter, the work of Senevirathe *et al.* [6] is the most important. In their recent paper, they designed four different DFB resonators illustrated on Figure 1.28 to study their influences on the lasing threshold in short- and long-pulse excitation. The same CBP film doped with 6 wt.% of BSBCz was chosen

¹⁰The difference between long pulse (qCW) and true CW excitation is not clear in this paper, as it consists in both cases in a 10 ms excitation.

as gain medium for each. First, they managed to obtain for the circular mix-order DFB a lasing threshold of only $0.015 \mu\text{J}\cdot\text{cm}^{-2}$ (≈ 6 times lower than the previous reports in more conventional mix-order DFBs [5]), which is attributed to the multiple directions from which the light feedback mechanism takes place, as illustrated with the blue arrows on Figure 1.28. Then, they show that under long-pulse 1 second excitation at $1 \text{ kW}\cdot\text{cm}^{-2}$ (and at a repetition rate of 0.01 Hz), the circular mix-order DFB still exhibits a FWHM of 0.4 nm, showing the solidity of the lasing regime. This breakthrough is directly ascribed to the reduced peak power required to achieve such long lasing emission.

Furthermore, they show *via* streak camera recordings that after non-stop "true" CW excitation (100 pulses of 1 s with a duty cycle of 1), the laser still works, even though its intensity has been irretrievably quenched by either chemical or thermal degradation of BSBCz or CBP molecules. However, they report an excitation power of $43 \text{ W}\cdot\text{cm}^{-2}$, which seem inconsistent with the $\text{kW}\cdot\text{cm}^{-2}$ peak power required to achieve one second laser in the first place. As of today, these results constitute the longest lasing operation ever reported for organic solid-state lasers, and were made possible thanks to years of progresses regarding molecular design improvements and thermal management. Moreover, this paper really emphasizes that not only the gain medium should be taken into account, but also the resonator in which it is implemented.

1.3.3.3 Towards true continuous-wave lasing

The results presented with BSBCz and its derivatives are important in many ways. However, all reports pointed out that improvements will be necessary in further studies to achieve a truly continuous-wave lasing emission in organic solid-state lasers and/or their electrical stimulation. In this section, some of the leads that have been explored to go further than the state-of-the-art are discussed.

Although BSBCz already exhibited desirable properties (PLQY close to unity in blended films, high radiative rate $> 10^8 \text{ s}^{-1}$, and a strikingly low ASE threshold of $0.22 \mu\text{J}\cdot\text{cm}^{-2}$), weak points in its chemical structure have been identified and could be responsible, alongside thermal degradation, for the death of the lasing after 30 ms. Indeed, it has been indicated in some reports that stilbene units might undergo *cis-trans* isomerization due to the twisted structure of the triplet states at C=C bonds [174, 175]. To study the potential influence of such mechanism, Oyama *et al.* introduced two compounds based on bisphenylbenzofuran (BPBF), namely BPBFCz1 and BPBFCz2 [11], whose chemical structures are really close to the one of BSBCz besides the incorporation of furan rings. While these new molecules exhibit similar properties, and even a greater radiative decay rate than the original BSBCz, reports showed great improvements for both BPBFCz regarding their photostability with time. When BSBCz films photoluminescence had decreased by 80% after 2000 seconds of continuous excitation, the PL of BPBFCz1 and BPBFCz2 films had decreased by only 50 and 40% after 4000 and 5000 seconds,

respectively. Furthermore, the ASE duration is also found to last much longer, up to 3 times with BPBFCz1 than for BSBCz. These results indicate clearly that there is again room for many improvements regarding molecular engineering, and that the *cis-trans* isomerization should be taken into account, even for semiconductors already exhibiting outstanding properties. In addition, the higher decomposition temperature of BPBFCz compounds might decrease the formation of impurities during thermal evaporation and potentially have additional positive income on their photostability.

Another method to overcome *cis-trans* isomerization of BSBCz has been found to be the addition of naphthalene units onto its carbon chains so that triplet states will not be located on the stilbene groups anymore [12]. They show that this method does not sacrifice the properties of the pristine material except for slight red-shift of the emission towards the green. On the other hand, the prevention of isomerization allows the presented compounds to incredibly extend the PL and the ASE duration. Besides, this red-shifted emission makes them the most efficient green emitters, with properties that are much better than commonly used coumarin derivatives to emit at these wavelengths.

Rather than focusing on the synthesis of novel molecules, Ou *et al.* [176] published an interesting paper about theoretical calculations on numerous recently used molecules to identify the best candidates for OSLEDs (based on their reported ASE threshold under optical excitation). To do so, they used DFT and Time-Dependent DFT (TDDFT) to compute the materials electronic structure and a self-developed package referred to as MOMAP, a molecular properties prediction package to evaluate photophysical properties. Based on the gathering of several criteria (a low k_{ISC} to limit the influence of triplet excitons, a high stimulated emission cross section, a high-lying singlet excited state, a short triplet excited state lifetime, a limited overlap between emission and triplet absorption, a high electron/hole mobility), they show that only three molecules arise as prime candidates to realize the first OSLED: BSBCz that has been already mentioned, CzPVSBF which also contains carbazole units and exhibited a very low ASE threshold of only 220 W.cm^{-2} , and BP3T which had been designated as a good candidate of OSLED as early as 2005 [177]. Of course, they mentioned that during their study in 2020, other interesting molecules had been synthesized and should be worth screening too. They also discuss the possibility to use this theoretical method to build photophysical properties database that could one day be used as inputs for more advanced machine learning models, which could provide new insights.

Chapter 2

Measurement of triplet state lifetime and triplet-related constants in organic thin films

2.1 Introduction

In the previous chapter, the influence of triplet states on the exciton densities and on the photon density was addressed. Considering their importance in the photophysics of organic media, it is crucial to measure the constants controlling the generation of these dark states and subsequent quenching mechanisms in order to have a clearer view of one compound regarding its lasing possibilities, as discussed in Section 1.3. Furthermore, the measurements of constants such as τ_t , k_{ISC} , k_{STA} , and k_{TTA} is also motivated by the modeling of the CW lasing requirements presented in Chapter 3, for which such parameters are used as inputs in population rate equations. However, their evaluation usually requires complex and/or expensive setups because of the difficulty to isolate one phenomenon from the influence of others.

In this chapter, we introduce a protocol that allows one to obtain a complete set of data for a molecule in solid- or liquid-state. With the help of photoluminescence transients at different concentrations and a simple pump-probe like experiment, we are able to extract the triplet lifetime of the gain medium as well as ISC, STA, TTA rates. Although each step of this characterization is directly inspired by previous works, our approach to combine several methods into one allows us to determine each of the above-mentioned constants by numerical fit with only one adjustable parameter at a time as graphically summarized on Figure 2.17, which has not been reported elsewhere before. Key advantages of this work are its low cost, its simplicity and the fact that a spectral resolution is not required at any step.

This study begins with an introduction to different methods used nowadays to characterize the constants related to the triplet state T_1 . Then, the protocol is

presented in detail with the example of plastic films blended with coumarin 521T as an example. The setup and gain medium preparation will also be addressed. This will be followed by a discussion regarding some key points of the method. At last, results obtained with other compounds will be presented.

2.1.1 State-of-the-art regarding triplet state characterization

2.1.1.1 Triplet excited state lifetime

Measuring the triplet lifetime of phosphorescent compounds is straightforward, as one just has to excite the gain medium with a short pulse and record the afterglow with a detector and an oscilloscope [178, 179]. The same method is used to measure the lifetime of the S_1 state in fluorescent molecules, except that the shorter timescale requires a ps pump pulse or a time correlated photon counting setup to evaluate τ_f . The evaluation of τ_t in compounds that do not emit light from the triplet state however demands more reflection, as it is only possible *via* indirect pathways.

The most common method to evaluate the lifetime of excited states (S_n or T_n with $n \geq 0$) is known as a **T**ransient **A**bsorption **S**pectroscopy (TAS) [180, 181, 182, 183], where the gain medium is excited by a high-energy brief pump pulse (\approx fs-ns, depending on the processes investigated) followed by a less intense second excitation: the probe. While the pump intense peak power and short temporal width allows at the same time the limitation of the material photobleaching and the creation of triplet excitons *via* ISC, the probe comes after a delay Δ_t and induces triplet absorption $T_1 \rightarrow T_n$, which is then observable on the absorption spectrum.

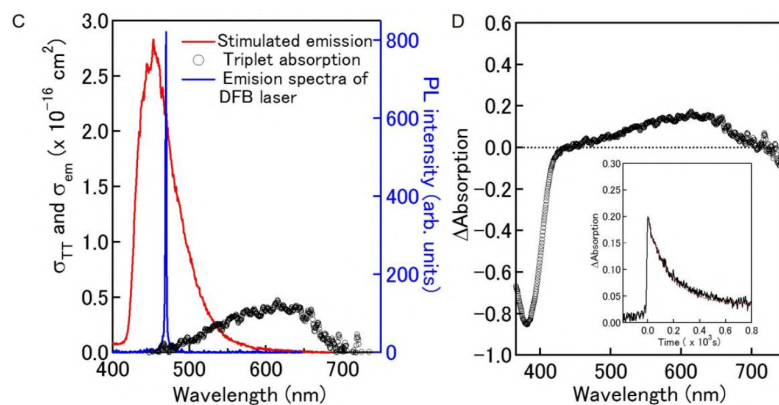


Figure 2.1: (left) Stimulated emission and triplet absorption cross section spectra of BSBCz. Emission spectra of DFB laser were measured from the BSBCz neat film above the threshold. (right) Triplet absorption spectra were measured in a solution containing BSBCz under Ar. Figure taken from Reference [5].

A typical output is presented on Figure 2.1 (right), where the difference in absorption after a fixed delay between pump and probe was recorded from 350 to 800 nm, leading to a transient absorption spectrum of the gain medium (ground state depletion is negative, triplet absorption is positive). On the other hand, one can focus the measurement at a certain wavelength and shift Δ_t in order to study how the differential absorbance evolves with time, leading to the lifetime of the triplet state (inset of Figure 2.1.D).

However, the variations of absorbance $\Delta A/A$ (where A is the gain medium absorbance before the pump) using this method are often at the mOD (10^{-3} OD) level if not less for fluorescent compounds¹. Therefore, this method is also known to require expensive apparatus, whether it is the pump that has to be very stable in time and in intensity, or the detector that has to be highly resolved.

A portion of the method presented in this chapter is inspired by the work of Kogan *et al.* [85], which was itself inspired by the protocol introduced by Sanden *et al.* a few years before [184], in which they analyze the triplet temporal dynamics *via* fluorescence recovery kinetics. First, a pump pulse is used to generate long-lived triplets through intersystem crossing. Then, using a second pulse after an adjustable delay, the fluorescence intensity is recorded again and compared to the one at the end of the first pulse. The triplet lifetime can then be traced back easily since the fluorescence intensity is directly proportional to the ground state, whose density is related to the depletion of the triplet state. By elongating the delay between pump and probe, they obtain an image of the ground state density recovery and fit this dynamics with a monoexponential whose lifetime is in fact τ_t the T_1 state lifetime.

To our knowledge, their work has not been used yet for organic semiconductor characterization, but because oxygen easily interacts with triplet excitons, it has been widely used in the microscopy field, notably to image spatially and temporally the oxygen concentration of biological tissues [185, 186], which have been applied for the detection of cancer cells thanks to their altered oxygen consumption [187], or to understand the metabolism of muscle cells during contraction [188].

A similar time-resolved technique to study triplets is the **P**ulse **T**rain **F**luorescence (PTF) technique [189]. The principle is to use the pulse train of a mode-locked Nd:YAG (70 ps, separated by 13.2 ns at 532 nm) that acts as sequential pump-probe pulses allowing a monitoring of the triplets dynamics at the ns scale. By fitting the difference in fluorescence pulse after pulse with a three-level system (S_0 , S_1 , and T_1), they obtain k_{ISC} the generation rate constant of triplets. Since they do not take into account a triplet lifetime *i.e.* assume that triplets do not relax back to the ground state during the pulse train, they cannot estimate the triplet lifetime of their gain media. This approach seems surprising, especially when working with liquid solutions in which the non-radiative channel of excited states are intuitively

¹For gain media with heavy-atoms, the SoC is stronger and therefore is the ISC. The triplet absorption is then easier to detect.

enhanced. Moreover, by implementing k_{ISC} only *via* the fluorescence lifetime ($\tau_f^{-1} = \tau^{-1} + \tau_{\text{ISC}}^{-1}$) in the equations, the setup only allows the measurement of ISC rates that are close of higher than τ^{-1} , hence the use of organo-metallic complexes such as ZnTMPP.

A different approach known as **F**luorescence **C**orrelation **S**pectroscopy (FCS) allows the study of several transient states, notably triplet states, *via* the analysis of the fluctuations of the fluorescence with time [190]. Assuming that ISC occurs at much slower time scales than the fluorescence, the excitons promoted to the T_1 state at a time t will cause variations in the fluorescence intensity. The triplet state lifetime is then estimated by fitting the correlation function $G(\tau)$ of the output transients by an analytical formula, and this is the biggest limitation of FCS. Indeed, in addition to require a very high resolution setup and a great electronic (and/or pumping) noise cancellation, the system has to be modeled as a set of linear rate equations such as this one to be solved

$$\frac{d}{dt} \begin{bmatrix} S_1 \\ T_1 \\ S_0 \end{bmatrix} = \begin{bmatrix} -k_f - k_{\text{ISC}} & 0 & R_p \\ k_{\text{ISC}} & -k_t & 0 \\ k_f & k_t & -R_p \end{bmatrix} \begin{bmatrix} S_1 \\ T_1 \\ S_0 \end{bmatrix} \quad (2.1)$$

(where R_p is the pumping rate (s^{-1})) so that the following eigenvalues can be derived²

$$\left\{ \begin{array}{l} \lambda_1 = 0 \\ \lambda_2 \approx -k_f \\ \lambda_3 = -\frac{k_f + k_{\text{ISC}} + R_p + k_t}{2} + \frac{\kappa}{2} \end{array} \right. \quad (2.2)$$

where $\kappa = (k_f^2 + k_{\text{ISC}}^2 + k_t^2 + R_p^2 + 2k_f k_{\text{ISC}} + 2k_f R_p - 2k_f k_t - 2k_{\text{ISC}} R_p - 2k_{\text{ISC}} k_t - 2R_p k_t)^{1/2}$. The values can then be used to compute the complete fluorescence autocorrelation function of the transients.

Although for illustration purposes we ignore the spatial component of the fluorescence detected, it shows that in order for the method to be useful, no intermolecular processes can occur since cross or quadratic terms ($S_1 T_1$ for STA, T_1^2 for TTA) would make the system unsolvable. Thus, FCS has been proven useful only in the case of liquid gain media [191, 192], where no STA or TTA is thought to happen because of the increased non-radiative de-excitation pathway for triplet excitons to the ground state, and a longer diffusion length of the active molecules.

2.1.1.2 Intersystem crossing and triplet formation quantum yields

King *et al.* measured k_{ISC} in liquid- and solid-state using a femtosecond transient setup to probe the recovery of the ground state after an initial, brief pump exci-

²The complete derivation of the eigenvalues of the system is provided in Section 4.2.

tation [193]. To be more precise, they deduce the triplet formation quantum yield ϕ_T of the gain medium from these transients and calculate k_{ISC} from the relation:

$$k_{\text{ISC}} = \phi_T k_f \quad (2.3)$$

where k_f is the inverse of the fluorescence lifetime. They assume that the influence of ISC is isolated from bi-molecular interactions or degradation of the sample (especially in solid state) by pumping at the lowest possible intensity whilst keeping a sufficient **S**ignal to **N**oise **R**atio (SNR). This direct proportionality between k_{ISC} and the triplet formation quantum yield ϕ_T is often used to quantify ISC [194, 195, 196].

To explain the breakthroughs achieved with BSBCz in solid thin films in terms of CW lasing and electrical pumping [14, 5], Sandanayaka *et al.* measured the excitation power dependence of its transient absorption in a solution of dichloromethane. ϕ_T was then evaluated at 0.04 by comparison with a solution of benzophenone in benzene as a reference (Reference [14]). This value, combined with a fluorescence lifetime of 1.28 ns in thin film, yields an ISC rate constant of $3.1 \times 10^7 \text{ s}^{-1}$ (Equation 2.3) which is, as discussed in Section 1.2.4.1, usual for organic compounds.

k_{ISC} can also be predicted theoretically. Shuai *et al.* reported constants of several well-known molecules thanks to **T**ime-**D**ependent **D**ensity **F**unctional **T**heory (TDDFT) and a self-developed molecular analysis package [176]. Interestingly, their results designate BSBCz as a promising candidate for electrical pumping thanks to among other criteria a very low k_{ISC} of $6 \times 10^4 \text{ s}^{-1}$, which is consistent with the *negligible* ISC mentioned in the previous paragraph, although much lower than the above-mentioned experimentally measured value.

2.1.1.3 Triplet-triplet-annihilation

Triplet-triplet annihilation has been described in Section 1.2.6.2 as a Dexter "collision" mechanism between two triplet excitons that generates in a reduced proportion singlet excitons. As with every phenomenon that entirely depends on triplet states, TTA is quite easy to quantify in phosphorescent media, as it can be directly monitored on the luminescence emitted from the T_1 state. However, fluorescent compounds exhibit a dark triplet state, there are therefore only two ways to observe the influence of TTA and/or estimate k_{TTA} : by monitoring the **D**elayed **F**luorescence (DF) induced by TTA (often referred to as TTA-UC for **U**p-**C**onversion) or *via* indirect methods. Both are discussed in the next two paragraphs.

Detection of TTA induced fluorescence

As soon as 1967, Johnson *et al.* [197] used the influence of an external magnetic field on the triplet state energies to study the DF of anthracene crystals. By

showing that the integrated intensity varied with the strength of the magnetic field applied, they eventually reached the conclusion that the mechanism in play had to emerge from triplet states, hence TTA. Their conclusion was consistent with a theoretical study on this topic that had been done not so long after [198].

k_{TTA} was also estimated *via* temporal traces of the fluorescence after an initial excitation by Baldo *et al.* [199] with PtOEP and Ir(ppy)₃ in different host materials and Bachilo *et al.* [200] using TPP, Zn-TPP and C₇₀. Of course, for TTA to be detectable without the need for any expensive or complicated apparatus but a fluorescence transient, the compound must exhibit a high triplet formation quantum yield ϕ_T in order for the **D**elayed **F**luorescence (DF) to be strong enough. This is why the compounds investigated in both studies contain heavy atoms, leading to a more important spin-orbit coupling and thus more triplets *via* ISC. To illustrate this requirement, the setup of Bachilo *et al.* [200] was employed to detect the DF of C₇₀, but without any success because of its lower triplet formation quantum yield.

Their papers also contain interesting discussions about the different dynamics regarding P-type (TTA) and E-type (TADF) DF and how to discriminate one over the other. Indeed, the dynamics leading the delayed fluorescence from TTA and from TADF are different since both mechanisms are very different, therefore the modeling differs.

The work of Shukla *et al.* [201] is similar to the previous papers, except that they estimate k_{TTA} by fitting the transient luminescence of a solid-state gain medium under electrical excitation. Doing so in their case yields TTA rates of 6×10^{-11} and 2×10^{-10} cm³.s⁻¹ for the blended and the neat film, respectively. These very high values, along with similarly high values of k_{STA} (1.4×10^{-9} and 7.3×10^{-9} cm³.s⁻¹) could be explained by the more important proportion of triplet generated *via* current injection compared to optical excitation. That would also be supported by the increase in both STA and TTA rates from doped to neat configurations, ascribed to a more important triplet density. It could also be linked to k_{STA} and k_{TTA} both being adjustable parameters to fit only tens of ns luminescence transients, since they show for instance by theoretical prediction that many combinations of those rate would yield the same current density threshold.

Probing TTA from indirect pathways

Whether the DF is induced by TADF or TTA, there is a need of a apparatus that provides a high-sensitivity to fluorescence over several decades and/or one that counts photons. Therefore, most papers interested in TTA work through the recording of indirect routes to study it, especially in fluorescent compounds. Actually, the probing of other triplet-related transitions (triplet absorption $T_1 \rightarrow T_n$, non-radiative relaxation) combined with numerical fit to predict k_{TTA} is the commonly used method. Since the triplet equation differs in the presence of TTA by the addition of a quadratic term (Equation 2.4), the T_1 density is no longer

ruled by a unique lifetime since the solution is no longer monoexponential.

Lehnhardt *et al.* [86] used a pump-probe experiment with F8BT:MEH-PPV and Alq₃:DCM films where the delay between pump and probe is longer than the fluorescence lifetime to exclude STA from the dynamics. A spatial separation of the pump and the probe allows the monitoring of the triplet population by probing the triplet absorption with a similar setup as the one presented on Figure 2.2. Then, using the following triplet equation:

$$\frac{dn_T}{dt} = n_0 - \frac{n_T}{\tau_T} - \frac{1}{2}k_{\text{TTA}} \times n_T^2 \quad (2.4)$$

where n_T is the triplet population density (m^{-3}), τ_T the triplet state lifetime (s), and k_{TTA} the TTA rate ($\text{m}^3 \cdot \text{s}^{-1}$). n_0 is the triplet generation rate (s^{-1}), and is set to zero for long enough delays between pump and probe. In their experiment, a long pump pulse creates triplet excitons *via* intersystem crossing, followed by a brief probe that creates a fluorescence burst. Then, photons emitted from this burst propagate through the pumped area and eventually reach the detector. By varying the delay between pump and probe, we can access the strength of the $T_1 \rightarrow T_n$ absorption with time to fit the triplet population depletion dynamic. In their report, they reached values of $6.2 \times 10^{-13} \text{cm}^3 \cdot \text{s}^{-1}$ and $400 \mu\text{s}$ for k_{TTA} and τ_T in the F8BT:MEH-PPV film, respectively, emphasizing the importance of TTA in fluorescent compounds under high intensity excitation. Also, triplet lifetimes of investigated films are found to be much longer when it comes to host-guest systems than for monomolecular gain medium (0.17 ms for Alq₃, 1.55 ms for Alq₃:DCM), which was logically ascribed to a reduced TTA rate.

Hale *et al.* [202] studied the triplet dynamics in MEH-PPV (material evoked in Section 1.3) thin films using a two-photon spectroscopy apparatus and obtained by fitting the photoelectron spectrum a TTA constant of $10^{-14} \text{cm}^3 \cdot \text{s}^{-1}$, alongside a typical interaction distance interaction between triplets of 0.5 nm, which is consistent with the Dexter nature of TTA (Section 1.2.6.2).

At last, one can measure TTA absolute quantum yields (without any reference such as PtOEP or DPA) using integrating spheres and TCSPC in liquid- [203] or solid-state [204] configurations.

2.1.1.4 Singlet-triplet annihilation

k_{STA} is among if not the trickiest constant to experimentally evaluate in organic gain media. Because its influence is proportional to both singlet and triplet population densities, it is then very demanding to isolate STA from other mechanisms. Indeed, it can only occur during the excitation (electrical or optical) so that intersystem crossing, $S_1 \rightarrow S_n$ transitions, and fluorescence have to be taken into account, but at the same time triplet-related processes such as TTA or triplet absorption might blur its influence as well. Hence, very few experimental papers reporting proper values of k_{STA} can be found, as opposed to TTA for instance

which just has to be recorded after the excitation.

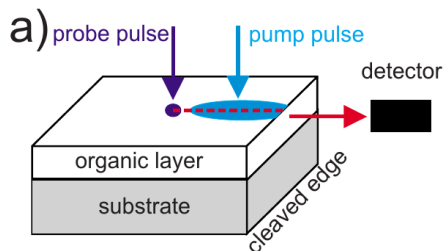


Figure 2.2: Setup for TA measurement introduced by Lehnhardt *et al.* [145].

Lehnhardt *et al.* [145] studied the influence of TA and STA on the pulse duration of an OSSL based on a F8BT:MEH-PPV host-guest system. To separate the respective influence of TA from STA and vice-versa, they used two different pump-probe experiments. The first one, used to evaluate the triplet absorption cross section is depicted in Figure 2.2 taken from their paper, is done by spatially separating the pump and the probe. The probe pulse generates light which propagates through a waveguide structure towards the cleaved edge and has to pass the region where triplets have been generated by the pump pulse. Since the exciton typical diffusion length (5-8 nm) is much shorter than the distance between the pump and the probe (0.1 mm), only photons (as opposed to excitons), will propagate and therefore only TA will occur. The sensitivity of the TA detection is ensured by the long interaction path length (0.5 mm). Then, the STA measurement is done by removing the spatial separation of both pulses and by replacing the SiO₂ layer by a silicon substrate whose absorption is much higher, preventing guided modes presence during the measurement.

Although TA is ruled out, probing during the excitation does not allow a complete removal of TTA and as such, the fitting of the transients (and therefore the estimation of k_{STA}) has to be done with k_{TTA} as an additional adjustable parameters (if we assumed that k_{ISC} taken from other references is correct). Doing so has given values of 4×10^{-7} and $1.5 \times 10^{-12} \text{ cm}^3 \cdot \text{s}^{-1}$ for k_{STA} and k_{TTA} , respectively. This limitation regarding the fitting procedure might explain the surprisingly high STA rate constant reported here.

Another method to evaluate STA rate constants in organic solutions and solid films relies on the analysis of **PhotoLuminescence** (PL) transients, and parts of the experiment presented in this thesis are largely inspired after related works [157, 154]. The principle is to excite the gain medium and monitor its fluorescence with time. Doing so, Zhang and Forrest, and Adachi *et al.* have notably shown that the abrupt decrease of the PL that was observed could be interpreted in terms of singlet quenching, and more precisely in terms of interactions between singlet and triplet excitons. Zhang and Forrest [157] compared PL transients of a gain medium containing, or not, a triplet quencher inside the host matrix, in addition to the emissive molecules. They managed to obtain drastic improvements thanks

to this additional compound, which was attributed to a quicker de-excitation of the triplets from the manager molecules and therefore less STA. The complete absence of STA, justified by a fluorescence transients that is proportional to the pump profile, has also been reported by Adachi *et al.* [154] by comparing N₂ and O₂ bubbling of CBP:EHCz solutions. They reported a complete removal of singlet quenching with the second option, thanks to dioxygen molecules actively quenching emissive molecules in an excited triplet state. However, as stated before, it is not trivial to obtain precise rate constants for such interactions, and this method is not exception. If it is true that the comparison between two configurations is sufficient to conclude on the removal of singlet-triplet annihilation, the number of adjustable parameters required to fit the PL transients is too important to obtain more precise informations on the related rates.

2.1.2 Aims of this work

Several methods used to measure the photophysical constants of organic gain media have been presented. Whether they rely on direct or indirect measurements, most of the protocols require in the first place an expensive apparatus (fs resolution detector, streak camera, TCSPC, and so on). For some constants and especially when it comes to bi-exciton processes, estimations are done by numerical fitting procedures that cannot always be reliable, either because the mechanism of interest is blurred by others or because the system of equations just contains too many adjustable parameters.

The main idea of this work is to gather some of the ideas presented above in a single setup that would enable a simultaneous measurement of τ_t , k_{ISC} , k_{STA} , and k_{TTA} without the use of a brief, intense excitation, and without a sub-ns/ns detector or a spectral resolution.

2.2 Methods

2.2.1 Experimental setup

The excitation source is a simple commercial laser diode (5W at 450 nm) controlled by a 4A current monitor (Thorlabs, LDC240C). The output power of the laser diode is controlled by a $\lambda/2$ waveplate and a **Polarization Beam Splitter** (PBS) (Thorlabs, CCM1-PBS251/M). A secondary $\lambda/2$ waveplate is placed after the PBS to control the polarization of the diode beam to be horizontal to match with the **Acousto-Optic Modulator** (AOM) requirements.

The beam is then directed to the AOM (Gooch & Housego, I-M110-2C10B6-3-GH26) controlled by a RF driver (Gooch & Housego, A35110-S-1/50-p4k7u). Two function generators (Agilent, 33500B) allow an easy customization of the delay between two pulses as well as their duration. The optimization of the diffraction

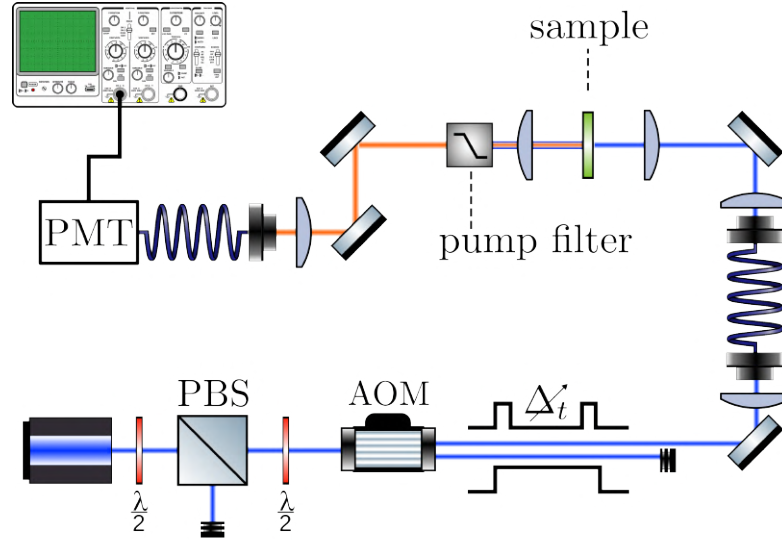


Figure 2.3: Experimental setup used in this work

efficiency is ensured by the beam polarization and the spatial overlap between the beam and the crystal of the AOM.

The portion of the pump that is not diffracted is removed using a standard beam blocker, whereas the pulsed signal is injected into a $400 \mu\text{m}$ optical fiber to obtain a top-hat profile. At the end of the fiber, the beam is collimated and then focused on the sample using a microscope objective (M-APO 20x, Mitutoyo) whose working distance (20 mm) is much longer than its focal length (10 mm). Following the excitation of the sample, an image of its luminescence is done by collimating and focusing it in a fiber, linked to a **PhotoMultiplier Tube** (PMT) (Thorlabs, PMTSS). The luminescence is visualised on a 100 MHz, $2.5 \text{ GB}\cdot\text{s}^{-1}$ Tektronix oscilloscope. To remove the pump from the data, a low-pass filter was placed before the detection.

Other diodes (Jtech, 1W at 405 nm) were used to work with BSBCz films because it does not absorb at 450 nm. A few changes on the initial setup must be done for it to work: the PBS must be replaced (Thorlabs, PBS12-405-HP) alongside the waveplates according to the diode emission.

Contrarily to other pump-probe experiments where the gain medium is excited by a brief and intense pulse (see Section 2.1.1) followed by a white, much less intense pulse to probe its absorption after a certain delay and build a triplet absorption spectrum, this experiment only needs the temporal recording of two pulses to work.

At first, a μs initial excitation (the pump) is absorbed by the gain medium, and its **PhotoLuminescence** (PL) is recorded by a PMT and an oscilloscope. It can be seen ending at $t = t_1$ on Figure 2.4 and will always end at $t = 0$ in every subsequent figures. Then, the gain medium PL is recorded again when a second

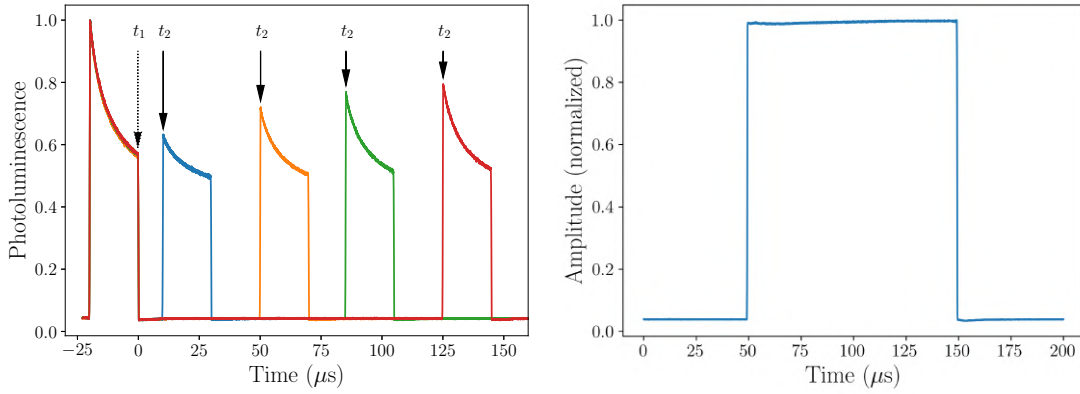


Figure 2.4: (left) Photoluminescence transients of a PMMA:C521T (32 wt.%) 17 μm thin film recorded with the above-mentioned setup, where t_1 is the end of the pump, and t_2 the beginning of the probe. (right) Pump transients recorded with in the same condition by removing the filter and the gain medium, showing that the PL dynamics is not related to the pump profile.

excitation (the probe) passes through after a delay $\Delta_t = t_2 - t_1$.

Because the first excitation will generate long-lived triplets *via* intersystem crossing, one can monitor their decay afterwards by adjusting the delay Δ_t , as shown on Figure 2.4 (left). To be more precise, the idea is to check how the difference $\text{PL}(t_2) - \text{PL}(t_1)$ evolves with time to study the refilling of the ground state, since triplets will eventually decay in a non-radiative way to the S_0 state. The depletion of the T_1 state after $t = t_1$ will be observable *via* the peak fluorescence of the probe at $t = t_2$, which is attributed to a higher and higher density of molecules available to undergo absorption $S_0 \rightarrow S_1$ when Δ_t increases.

Although the pump duration must be long enough to see a quenching of the PL by triplets so that the refilling of the ground state can be processed with enough resolution, the duration of the probe matters less. Indeed, we are at the end only interested in its peak fluorescence at $t = t_2$. A perspective of this setup would then be to build a custom signal using a **F**ield **P**rogrammable **G**ate **A**rray (FPGA) that would include a long initial excitation followed by brief excitations at various delays to keep the sample safe from potential degradation, and also to save time as it would open the way to a full automation of the experiment.

2.2.2 Preparation of the thin films

The dyes used in this study were bought from Exciton in powder form and were diluted in a solution of anisole containing 15% of poly(methyl methacrylate) (PMMA). The desired concentration of active molecule in the PMMA host matrix were obtained by the following formula:

$$C_d = \frac{m_d}{m_d + m_h} \quad (2.5)$$

where C_d and m_d are the final dye doping ratio and mass, respectively. $m_h = 0.15 \times m_s$ is the PMMA host mass, and m_s the mass of the PMMA A15 solution. A proper dilution of the dye was ensured by the use of a magnetic stirrer, with a radio frequency bath in the case of higher concentration.

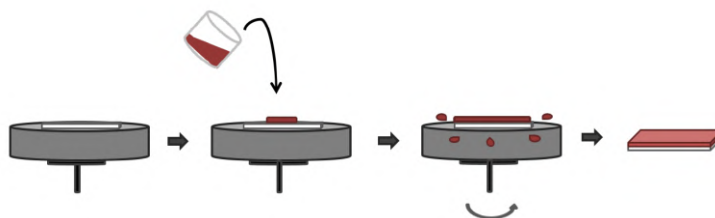


Figure 2.5: Graphical representation of the protocol to create $17 \mu\text{m}$ organic thin films on a glass substrate using a spin coating technique. Figure taken from Reference [205].

The glass microscope plates on which the solutions were to be deposited were washed with ethanol before use. The dye:PMMA solutions were then drop casted on the plates and spin-coated at 850 RPM to obtain $17 \mu\text{m}$ homogeneous films and to ensure the removal of the remaining air bubbles and anisol. Films were then put in the oven for at least 15 minutes at 50°C to solidify the PMMA matrix and remove the residual solvent.

2.2.3 Characterization of thin films

In this subsection, the measurements regarding the absorption and emission spectra of the thin films investigated will be presented, with the evaluation of their fluorescence lifetime.

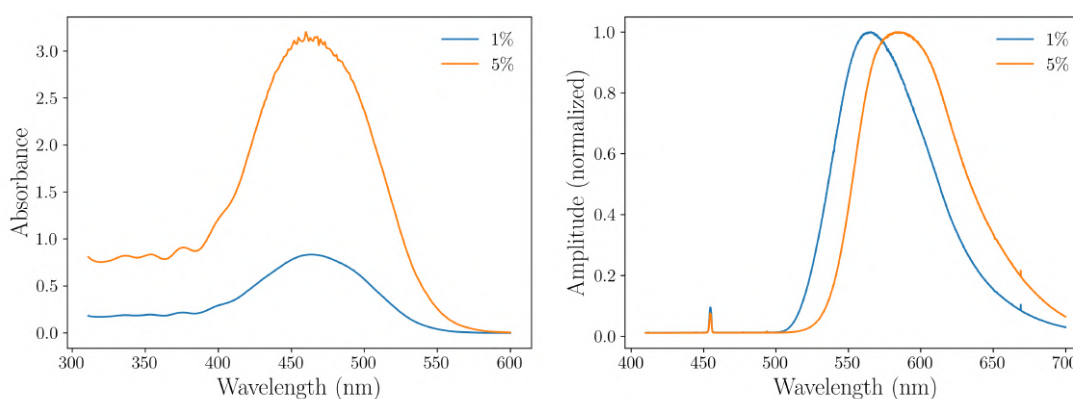


Figure 2.6: Absorption (left) and emission (right) spectra of PMMA:DCM $17 \mu\text{m}$ thin films for different concentrations (wt.%) of DCM.

2.2.3.1 Absorption

The absorbance of the films were measured using a commercial spectrophotometer (Cary 500, Agilent) with a pristine microscope glass plate as the reference. Outputs are shown on Figure 2.6 for different concentrations of DCM in PMMA host matrix. The absorbance OD is then used to estimate the total absorption A of the film as:

$$A = 1 - 10^{-OD} \quad (2.6)$$

to obtain the absorption cross section (m^2) at the pump (the 405/450 nm diodes) wavelengths *via* the following formula:

$$\sigma_{\text{abs}} = \frac{\alpha}{N} = \frac{-\ln(1 - A)}{d \times N} \quad (2.7)$$

where d is the thickness of the gain medium (m). N the total density of active units (m^{-3}) is obtained by:

$$N = \frac{p \times \rho_h \times \mathcal{N}}{M} \quad (2.8)$$

with p the weight concentration of active molecule inside the host matrix, ρ_h the molecular density of the host matrix (kg.m^{-3}), \mathcal{N} is Avogadro's constant and M is the molar mass of the active molecule (kg.mol^{-1}).

2.2.3.2 Emission

To obtain the thin films emission spectra, the gain medium was excited by a 325 nm UV LED and recorded using a fiber spectrometer (USB2000+, 1 nm resolution, OceanOptics) normal to the excitation direction to avoid side-effects. The normalized fluorescence is shown on Figure 2.6 for different concentrations of DCM in PMMA host matrix, where a red-shift of the emission is seen when the concentration increases because of a global polarization effect of the DCM molecules and self-absorption.

2.2.3.3 Fluorescence lifetime

The fluorescence lifetime measurements were performed using a brief 800 ps excitation from the third harmonic of a Nd:YAG laser (Q-switched PowerChip NanoLaser PNP-series, 400 ps, 355 nm, Teem Photonics). The luminescence was recorded after the photoexcitation using an optic fiber linked to a 15 GHz oscilloscope (Tektronix).

The output for a blended (1 wt.%) PMMA:DCM film is shown on Figure 2.6 alongside the instrument response function. Although this setup is limited in sensitivity (two decades versus 5/6 for TCSPC), it is considered enough for this work.

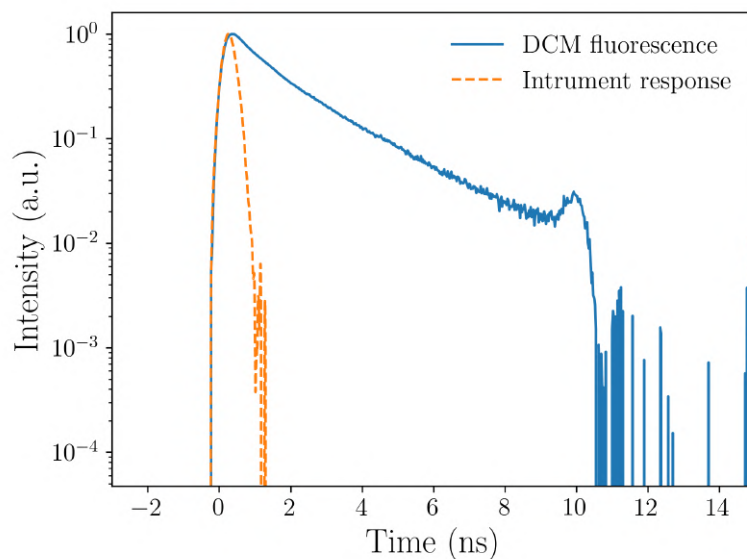


Figure 2.7: Fluorescence of a PMMA:DCM (1 wt.%) after photoexcitation (400 ps, 355 nm). The pump power has been set to a minimum to avoid ASE in the film.

2.2.4 Photoluminescence transients analysis on C521T films

In this section, the proposed protocol towards the measurement of τ_t , k_{ISC} , k_{STA} , and k_{TTA} is presented and discussed in detail using datas obtained from coumarin 521T (C521T) 17 μm blended films.

2.2.4.1 Triplet lifetime and intersystem crossing

The first constant accessible from the photoluminescence transients is the triplet lifetime, which is estimated after the difference in fluorescence intensity between the start of the probe (t_2) and the end of the pump (t_1) similarly to the report of Kogan *et al.* [85] presented in the introduction.

On Figure 2.8 (left) are presented the luminescence transients for various delay between the pump (ending at $t = 0$) and the probe coming afterwards. The quenching of the fluorescence during the excitation time is not as pronounced as on Figure 2.4 because of the lower chromophore concentration and lower associated triplet population. On the right picture, a direct image of the ground state recovery (or indirectly, the depletion of the triplet state) is observable. The fitting of this dynamics by a monoexponential expression gives us a triplet lifetime for this molecule in this configuration of 120 μs .

The noise of the measurement comes from the very low variation of luminescence within the pump pulse points, which is linked to the low concentration. It is also related to the gain medium being shifted between two points to avoid degradation, as mentioned in Section 2.2.5. Nevertheless, changing point between each measurement can lead to slightly different fluorescence intensity if we consider

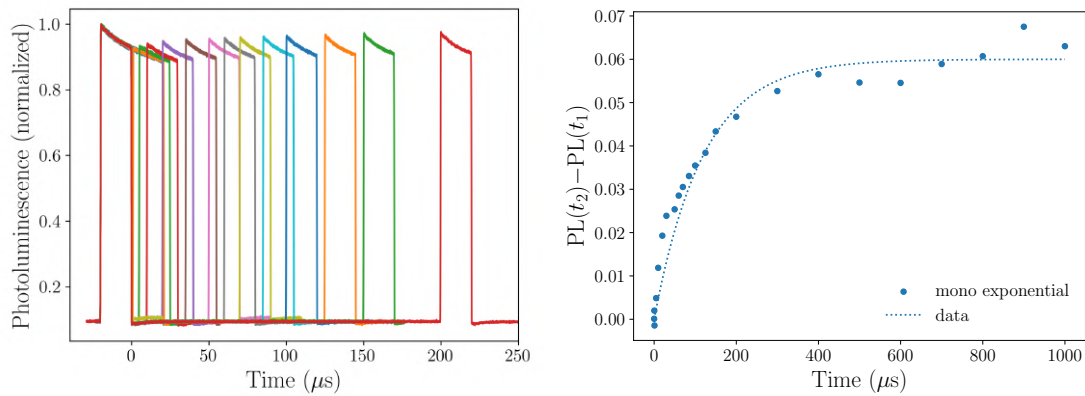


Figure 2.8: Left) Photoluminescence transients of a PMMA:C521T (1 wt.%) 17 μm thin film recorded with the setup evoked in Section 2.2.1. Right) Associated difference of photoluminescence between the end of the pump (ending at $t = 0 \rightarrow t_1$ on Figure 2.4) and the beginning of the probe ($t > 0 \rightarrow t_2$ on Figure 2.4).

that films are not ideally homogeneous. A good way to estimate the uncertainty of these measurements would be to repeat the complete pump-probe experiment several times on the same film to quantify the precision of the setup. It has however not been done for this work.

To be sure that the triplet lifetime we measure is "absolute" and does not depend on other processes or on the concentration, we checked that the transients of a 0.1 wt.% blended film exhibited the same dynamics. Figure 2.9 shows that this is the case, and that therefore only ISC occur in the gain medium. Consequently, a similar triplet lifetime is obtained with this lower concentrated film.

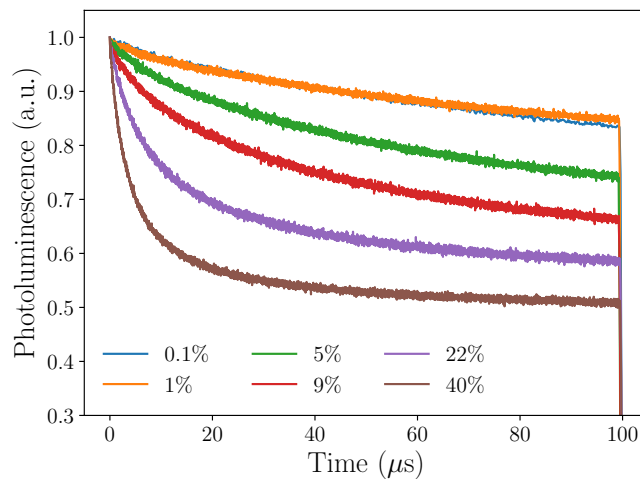


Figure 2.9: Photoluminescence transients of PMMA films with different doping ratios of coumarin 521T. The fluorescence of the film is more and more reduced with time when the concentration of active molecules in the excitation volume increases.

This check leads us to the second part of the protocol: intersystem crossing.

Since it is assumed here that k_{ISC} does not change much with the concentration of active molecules, as it has been discussed in some papers, one can argue that only the creation of long-lived triplets *via* ISC quenches the fluorescence in the 0.1 and 1% films, yielding a roughly linear decrease with time on Figure 2.9 that does not depend on the concentration. With that in mind, the next step is to fit the transients by numerical integration of the population rate equations:

$$\frac{dS_1}{dt} = \sigma_{\text{abs}} I_p S_0 - (k_f + k_{\text{ISC}} + k_{\text{STA}} T_1) S_1 + \zeta k_{\text{TTA}} T_1^2 \quad (2.9)$$

$$\frac{dT_1}{dt} = k_{\text{ISC}} S_1 - k_t T_1 - (1 + \zeta) k_{\text{TTA}} T_1^2 \quad (2.10)$$

where k_{STA} and k_{TTA} are set to zero, leaving k_{ISC} as the only triplet-related adjustable parameter. Results shown on Figure 2.10 are obtained for $k_{\text{ISC}} = 1.7 \times 10^7 \text{s}^{-1}$ which is consistent with the different ISC constants reported (see Section 1.2.4.1).

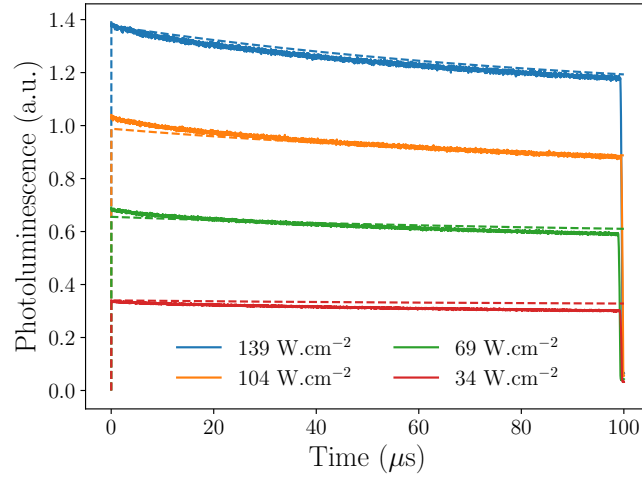


Figure 2.10: Photoluminescence transients (solid) and numerical fit (dashed) of a 1 wt.% PMMA:C521T film at different pump power densities.

2.2.4.2 STA and TTA rates at different concentrations

In this work, singlet-triplet- and triplet-triplet-annihilation are isolated from each other by fitting the PL transients at different times. Indeed, we found out during this study that the PL dynamics of higher concentrated films (an important decrease followed by a saturation as on Figure 2.9) could not be entirely explained neither by ISC nor by the simple addition of STA. Instead, the initial decrease (before $t = 20 \mu\text{s}$ in this case), can be fitted with only ISC and STA, whereas the late stages require a mechanism that depletes the triplet population. We found out that triplet-triplet annihilation is the ideal candidate to explain the saturation

of the triplet population, as it has a negligible influence on the initial decrease of the PL and it occurs only when the concentration of active molecules reaches a sufficient level. A detailed study regarding this conclusion is provided in Section 2.2.5.6 of the discussion.

This reasoning allows us to focus on the fitting of higher concentrated PL within the first $\approx 10 \mu\text{s}$ with k_{STA} as the sole adjustable parameter, since k_{ISC} has been established previously and is assumed not to be concentration dependent.

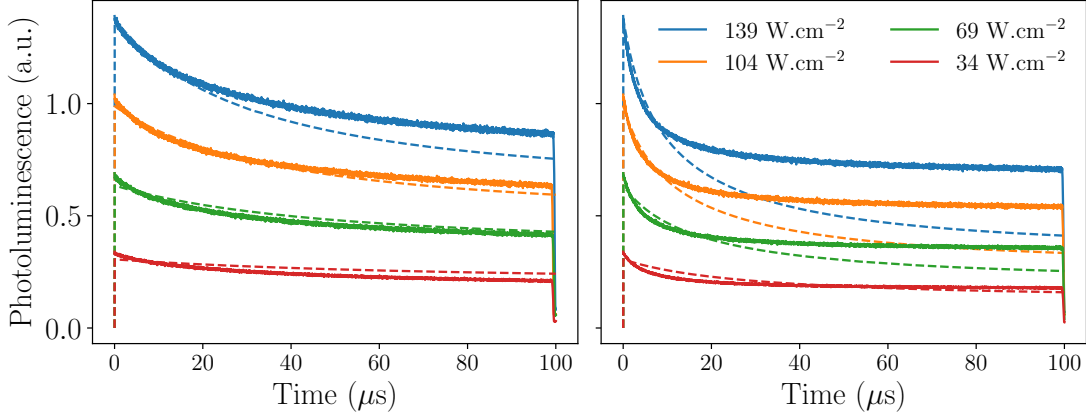


Figure 2.11: Experimental (solid) and numerical (dashed) photoluminescence transients of 22% (left) and 40 wt.% of C521T in PMMA thin films for different pump power densities. k_{ISC} and k_{STA} for each concentration are available in Table 2.1, $k_{\text{TTA}} = 0$.

Figure 2.11 shows the recorded transients and their best numerical fit for two concentrations of C521T in the PMMA $17 \mu\text{m}$ films (22% for the left, and 40% for the right picture) at different excitation power densities. The more important PL quenching at higher doping ratio is attributed to the higher density of triplets, easing the occurrence of bi-exciton processes such as STA. As a matter of fact, k_{STA} rates were found to scale at 6 and $29 \times 10^{-11} \text{ cm}^3 \cdot \text{s}^{-1}$ for concentrations of 22 and 40 wt.%, respectively, suggesting STA as a concentration dependent mechanism rather than an intrinsic parameter of organic molecules.

The best fit is found by minimization of the error between the numerical integration of Equations 2.9 and 2.10, and the experimental data for different values of k_{STA} according to a standard deviation formula:

$$\sigma^2 = \sum_{i=1}^N \frac{(x_i - y_i)^2}{N} \quad (2.11)$$

where x_i and y_i are the i th data and numerical point, respectively. N is the total number of point. σ is afterwards multiplied by 100 to express the error as a percentage, since PL transients are normalized to unity. The complete computations to find the best STA rates are shown on Figure 2.12 (left) for all concentrations of

C521T going from 5 to 40 wt.%. Simulations show that only one k_{STA} minimizes the fitting error, alongside a clear increasing trend with the concentration of active molecules.

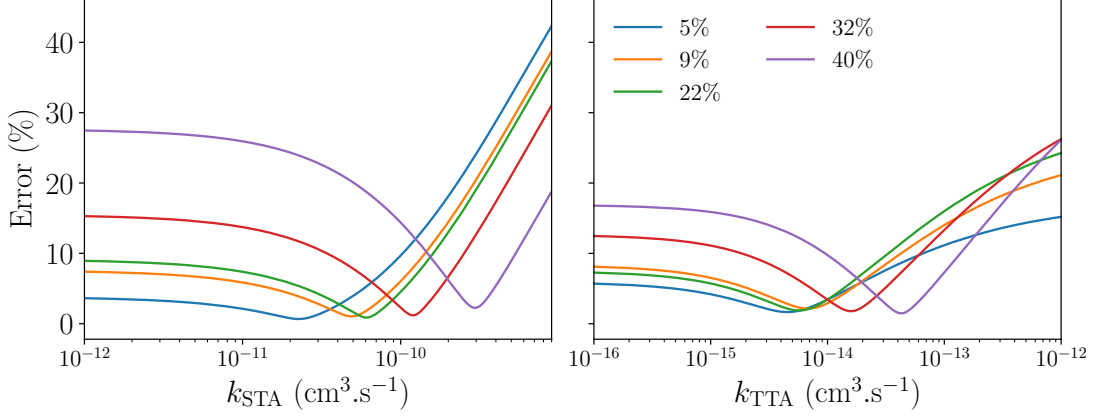


Figure 2.12: Error between the experimental PL and the integration of the equation with k_{STA} (left) and k_{TTA} (right) as adjustable parameters for different doping ratios of C521T in PMMA thin films.

k_{STA} being estimated for highly concentrated films thanks to τ_t and k_{ISC} obtained at low concentration, the last missing constant is the one of TTA, which can be obtained by fitting the PL transients at longer time scales, as we showed that ISC and STA alone were not enough to explain the saturation of the PL after the initial decrease. This can be done, once again, very simply since k_{TTA} is the last and only adjustable parameter. Results for concentrations of 22 and 40 wt.% are presented on Figure 2.13. The numerical PL is to be directly compared with Figure 2.11 where TTA was not taken into account. It shows that TTA can explain the dynamics, and also that it has no influence on the PL at times where only ISC and STA intervene. Rates maximizing the agreement with the experiment scale at 0.57 and $1.6 \times 10^{-14} \text{ cm}^3 \cdot \text{s}^{-1}$ for concentrations of 22 and 40 wt.%, respectively.

Once again, we observe the same behavior for k_{TTA} as with k_{STA} when the doping density of active molecule increases inside the gain medium, as shown on Figure 2.12 and in Table 2.1.

A key advantage of this technique is also the ability to double-check the TTA rate using a second method. Indeed, k_{TTA} can also be obtained from ground state recovery measurements using the pump-probe experiment. At first, it was used to evaluate τ_t by fitting the ground state recovery with a monoexponential. Because it was shown that no other mechanisms but intersystem crossing quenched the PL, the evolution of the triplet density with time after the pump excitation could then be modeled as:

$$\frac{dT_1}{dt} = -k_t T_1 \quad (2.12)$$

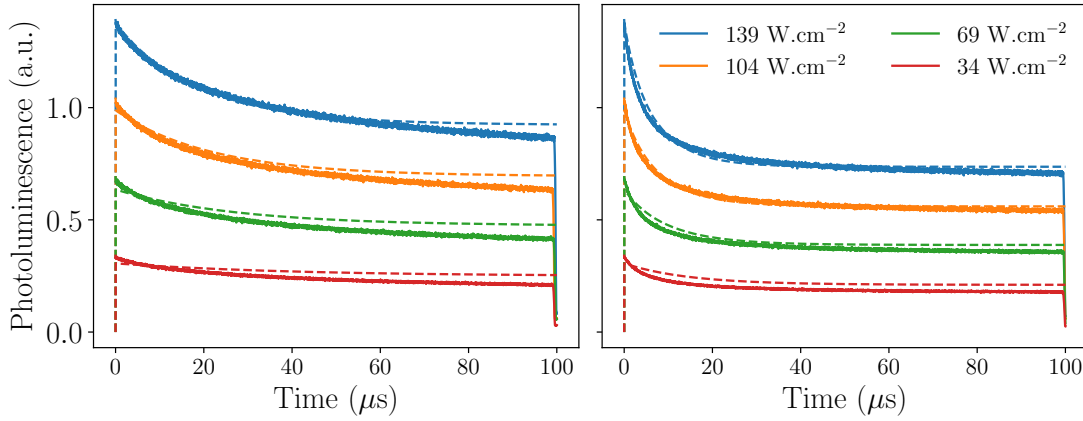


Figure 2.13: Experimental (solid) and numerical (dashed) photoluminescence transients of 22% (left) and 40 wt.% (right) of C521T in PMMA thin films for different pump power densities. k_{ISC} , k_{STA} , and k_{TTA} for each concentration are available in Table 2.1

whose solution is purely exponential since the source term $k_{\text{ISC}}S_1$ is null because of the vanishing of the fluorescence after a few ns. However, when the T_1 density becomes more important because of higher concentrations, TTA has a non-zero probability to occur after the excitation, since no singlets are required in this interaction. As such, the evolution of the population of triplets after the pump is now modeled as:

$$\frac{dT_1}{dt} = -k_t T_1 - (1 + \zeta) k_{\text{TTA}} T_1^2 \quad (2.13)$$

which is known as a Riccati equation and whose decay is no longer ruled by one, unique lifetime. Instead, its analytical solution is expressed as [206]:

$$\frac{T_1(t)}{T_0} = \frac{k_t}{(k_t + (1 + \zeta) k_{\text{TTA}} T_0) \exp(k_t t) - (1 + \zeta) k_{\text{TTA}} T_0} \quad (2.14)$$

where T_0 is the triplet density at the end of the first excitation, at $t = 0$.

The pump-probe PL transients for a PMMA film blended with 40 wt.% of C521T are shown on Figure 2.14, where a much more important quenching of the luminescence can be observed compared to Figure 2.8. This is due, as it has been discussed previously, to a more important singlet-triplet annihilation thanks to more important exciton densities.

The ground state recoveries of various blended films (1, 9, and 40%) are displayed on Figure 2.15. We show that a unique lifetime of 120 μs is sufficient to explain the dynamics for the 1 and 9 wt.% films, whereas the recovery of the higher-concentrated film requires more than one lifetime to be fitted, as shown on Figure 2.15 (right). We found out by minimization of the difference between analytical formula and experiments that a $k_{\text{TTA}} T_0 = 5.7 \times 10^4 \text{ s}^{-1}$ was the best op-

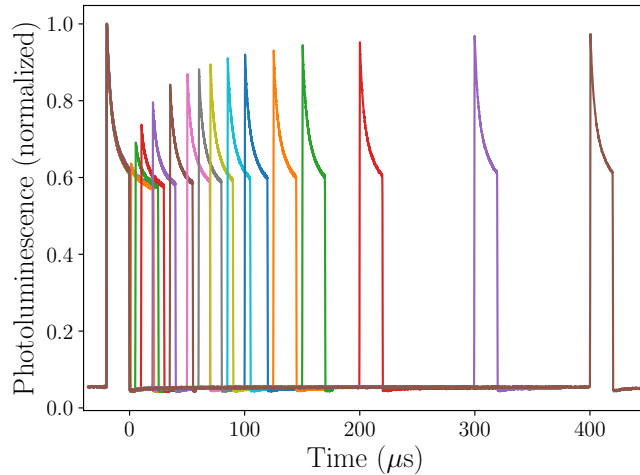


Figure 2.14: Normalized photoluminescence of the pump (ending at $t = 0$) and the probe versus delays between them for a 40 wt.% PMMA:C521T thin film

tion, indicating a strong TTA in play at this concentration. One has to be careful when fitting the ground state recovery with a Ricatti solution, as the adjustable parameter is not k_{TTA} alone but $k_{\text{TTA}}T_0$ (s^{-1}). The complete set of data obtained in this presentation for coumarin 521T are summarized in Table 2.1.

At last, the triplet population at the end of the pump pulse T_0 can be numerically estimated from the fits on the PL transients, leading to a self-consistency check on the TTA rate obtained by fitting longer PL transients. By extracting this value from our simulations, we are able to estimate k_{TTA} from the previously recorded value. As one can see, we could not estimate it when the concentration is less than 22%, which could indicate that the values acquired from long PL transients fitting for lower concentrated films are actually in the noise of this experiment, meaning that no more precise values can be obtained.

doping wt.%	transients			recovery		
	k_{ISC} 10^7 s^{-1}	k_{STA} $10^{-11} \text{ cm}^3 \cdot \text{s}^{-1}$	k_{TTA} $10^{-15} \text{ cm}^3 \cdot \text{s}^{-1}$	τ_t^{eff} μs	$k_{\text{TTA}}T_0$ 10^3 s^{-1}	k_{TTA} $10^{-15} \text{ cm}^3 \cdot \text{s}^{-1}$
1	1.7	120
5		3	5	120
9		5	6	110
22		6	5	90	7.5	3
32		12	16	70	34	26
40		29	42	50	57	69

Table 2.1: triplet-related photophysical constants evaluated in $17 \mu\text{m}$ PMMA films blended with different concentrations of coumarin 521T using two different methods.

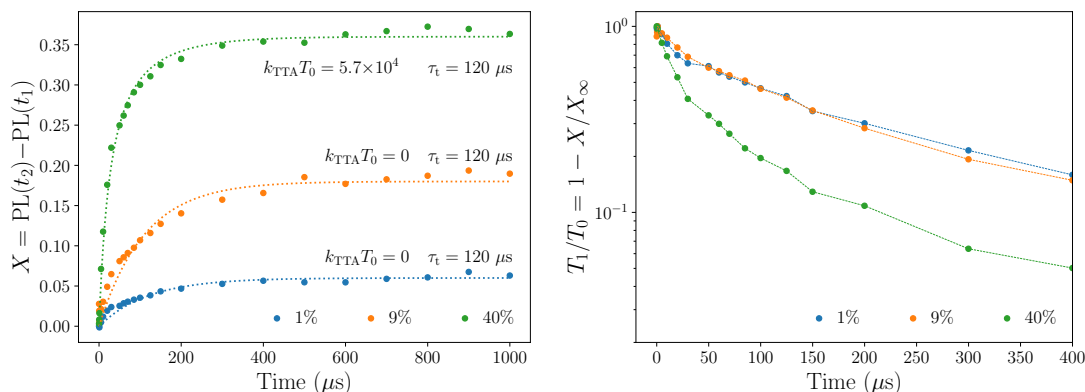


Figure 2.15: Left) Difference in photoluminescence between the end the pump and the beginning of the probe for 17 μm of PMMA with different concentrations of coumarin 521T. Right) Same data reversed, normalized and plotted in log scale to emphasize the different dynamics in high-concentrated films.

2.2.4.3 Summary

The method we present in this thesis to evaluate photophysical constants relies on the combination in a single setup of several approaches based on fluorescence kinetics: the monitoring of the ground state recovery via luminescence kinetics, as reported by Kogan et al. [85] in liquid gain media, and the analysis of longer photoluminescence transients to evaluate bi-molecular processes popularized by Adachi et al. to argue the complete removal of STA thanks to oxygen [153] or mCP-COT [16] for instance.

What our work provides is a step-by-step protocol that allows one to evaluate τ_t , k_{ISC} , k_{STA} , k_{TTA} one after the other at different concentrations, regardless of the pump power density, and without the need of expensive instrument or a spectral resolution. It is graphically presented on Figure 2.17.

First, the triplet lifetime is evaluated by the ground state recovery of a low concentrated gain medium from the pump-probe experiment by varying the delay between the pump and the probe. The refilling of the ground state can then be fitted with a monoexponential expression, since TTA is negligible.

Then, k_{ISC} is obtained by fitting longer transients from the same gain medium. Since the triplet lifetime is now known, the equation only has one adjustable parameter left, as long as STA and TTA do not intervene at such concentrations.

Following the obtention of τ_t and k_{ISC} , k_{STA} can be obtained by fitting the initial decrease of the PL in higher-concentrated films. Doing so showed that STA was not to be taken as an intrinsic parameter of the molecule but rather as a concentration dependent parameter.

At last, k_{TTA} is obtained with the fitting of the PL transients for longer time scales, as ISC and STA cannot explain the dynamics on their own. Figure 2.12 shows the k_{STA} and k_{TTA} that minimize the error with the experiment. This method

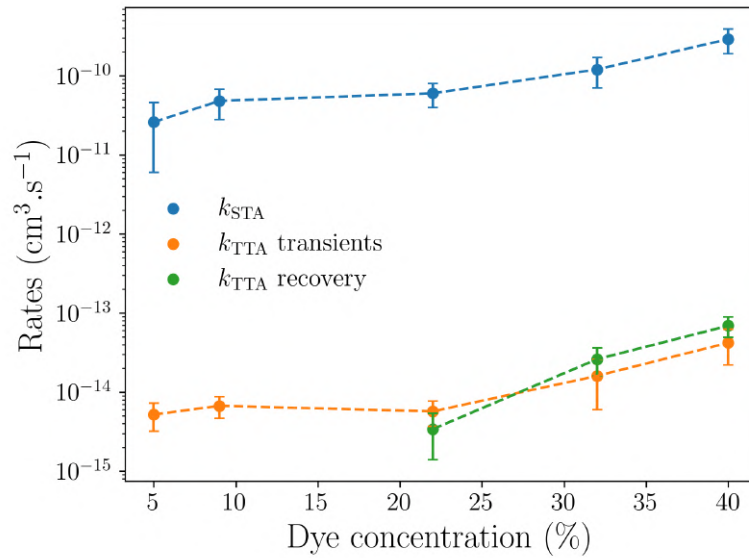


Figure 2.16: STA and TTA rate obtained in this work for PMMA 17 μm films blended with coumarin 521T at different concentrations. Errors are estimated after the depth of the well on Figure 2.12 for each film.

also allows in a second time a self-consistency check on the TTA rate obtained by fitting of the PL transients by fitting the ground state recovery with an updated triplet analytical evolution that does not exhibit one unique lifetime.

The whole set of constant acquired from this protocol for various concentrations of C521T in PMMA films are gathered in Table 2.1. In addition, STA and TTA rates obtained from PL transients and/or ground state recovery are displayed on Figure 2.16. k_{TTA} rates are found to differ only by less than 50% using both methods, which is considered enough regarding the need of the community. Indeed, methods presented in Section 2.1.1 provided results that could vary up to several orders of magnitude.

2.2.5 Discussions on the method

Before showing some results on several dyes of interest, limits and requirements regarding the protocol presented in this chapter will be discussed. This part also includes relevant discussions and interrogations that have emerged during the early study.

2.2.5.1 Requirements

This setup is used to record μs (or at least hundreds of ns) photoluminescence dynamics, there are no special requirements regarding the temporal resolution, as less than a GHz oscilloscope will do fine. Except for the safety of the sample, we have seen that there is also no need for $\text{MW} \cdot \text{cm}^{-2}$ nor $\text{GW} \cdot \text{cm}^{-2}$ pump power

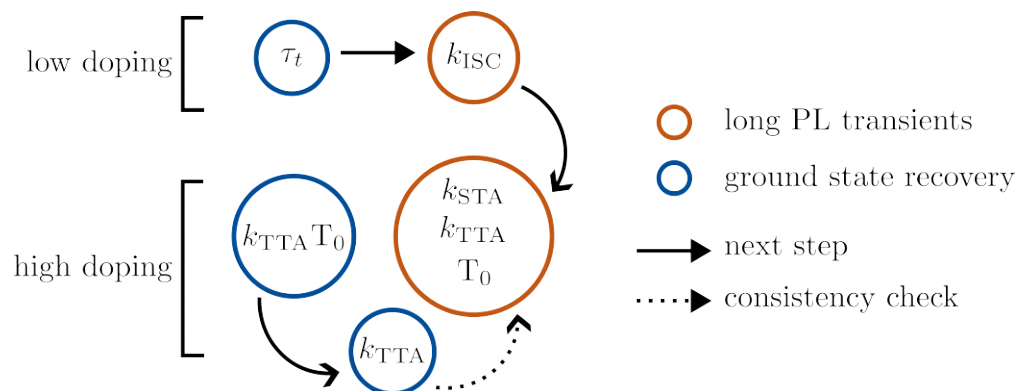


Figure 2.17: Graphical summary of the experimental protocol presented in this thesis to obtain a complete set of data regarding the triplet state of the gain medium.

densities to observe useful dynamics and work with those. However, the pump power density has to be important enough so that triplet population can reach a sufficient level. In other words, the pumping rate R_{ex} has to be greater than k_t , which yields the following condition:

$$I_p = \frac{h\nu_p}{\sigma_{\text{abs}}\tau_t} \quad (2.15)$$

Taking typical values ($\lambda_l = 500$ nm, $\sigma_{\text{abs}} = 10^{-20}$ m², $k_t = 10^4$ s⁻¹) leads to a power density of ≈ 400 W.cm⁻². The excitation of gain media at this power densities during tens of microseconds is then ideal for laser diodes, which explained why this technique was not used until recently. At last, we will see in Section 2.3 that this setup is perfectly capable of working with liquid solutions in cuvettes.

The only requirement of this experiment is that the gain medium exhibits a quenched PL under long optical excitation. To do so as mentioned previously, the pumping rate has to top the rate at which triplets de-excite back to the ground state. If no decrease of the PL is observed either thanks to a high PLQY, a very low doping ratio or the suppression of STA with triplet quencher, the setup has no use.

In fact, we later tried to estimate the triplet lifetime in liquid solutions using the same molecules in order to check in which proportion τ_t would be affected by the state of the gain medium. Unfortunately, we found out that the PL of all compounds investigated previously in liquids was perfectly proportional to the pump at concentrations of 10^{-4} mol.L⁻¹. The only quenching observed was in the case of a highly concentrated (10^{-3} mol.L⁻¹) solution of DCM, whose related results are presented in Section 2.3.

2.2.5.2 Transient absorption spectroscopy measurements

To ensure the reliability of the results obtained from this method, we used a widely used setup to evaluate triplet excited state lifetimes as well as triplet absorption spectra of organic compounds: the **T**ransients **A**bsorption **S**pectroscopy (TAS) experiment, which has been introduced in Section 2.1.1³.

Same PMMA:C521T thin films were employed as test beds for this method, we used samples with similar concentrations of coumarin 521T going from 1 to 40 wt.%. The excitation source on this TAS setup was an **O**ptical **P**arametric **O**scillator (OPO), fixed at 450 nm to match our experiments under diode pumping, pumped at 355 nm by the THG of a Nd:YAG laser. The energy on the samples was 1 mJ with an area of $\approx 4 \text{ mm}^2$. The duration of the excitation was 7 ns, yielding a pump fluence of $\approx 10 \text{ GW}\cdot\text{cm}^{-2}$. The transients after the excitation were analyzed by a photolysis spectrometer (Edinburg Instruments, LP920) and were processed using homemade Python scripts.

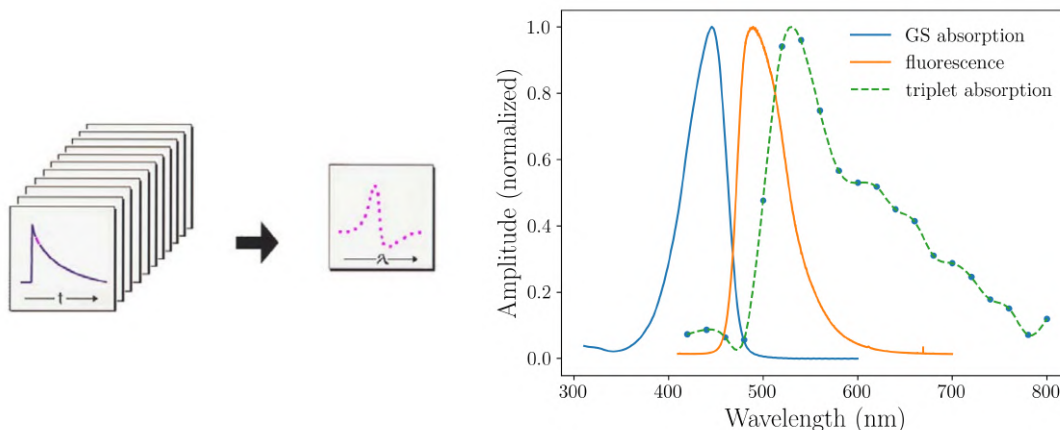


Figure 2.18: Left) Graphical representation of how transients absorption traces are processed to build a triplet absorption spectrum. Right) Ground state absorption, fluorescence and triplet absorption spectra of a $17 \mu\text{m}$ blended PMMA film with 22 wt.% coumarin 521T. The triplet spectrum has been obtained using the TAS experiment at PSSM laboratory. Points are actual outputs, and the dashed line is a cubic interpolation using Python library Scipy.

First, a complete triplet absorption spectrum of the 22 wt.% film, displayed on Figure 2.18 (right), was recorded by tuning the monochromator wavelength detection. The spectrum was obtained *via* absorption transients analysis at a time t after the excitation at different wavelengths, as sketched on the left picture. Points were taken every 20 nm from 400 to 800 nm, and the dashed curve to guide the eyes is a CubicSpline interpolation of the data points coded using the Scipy Python library. As it can be seen, the absorption spectrum shows a well defined peak at

³This experiment has been conducted at the **L**aboratoire de **P**hotophysique et **P**hotochimie **S**upramoléculaires et **M**acromoléculaires (LPPSM) with the help of Gilles Clavier and Arnaud Brosseau.

520 nm that indicate the highest probability of triplet absorption. Moreover, the significant overlap between the fluorescence and the triplet absorption spectra provides a simple explanation to the absence of long pulse lasing observed with this molecule as gain medium.

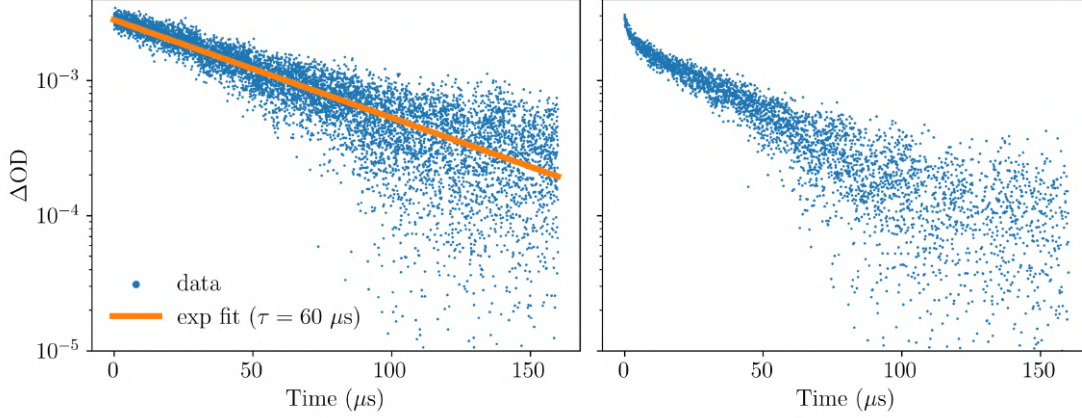


Figure 2.19: Triplet absorption transient of a 17 μm solid PMMA films blended with 9 wt.% (left) and 32 wt.% (right) obtained using the TAS setup at 520 nm.

In a second step, we fixed the detection window of the monochromator at 520 nm to record the absorption transients at different concentrations of C521T, whose raw traces are provided on Figure A23. Figure 2.19 focus on two concentrations: 9 and 32%, and shows that the dynamics below and above 22% is as different as presented in Section 2.2. One can see that indeed the absorption transients of the lowest concentrated film can be perfectly fitted with a monoexponential expression, whereas it is clear that two lifetimes rule the dynamics at higher doping ratio. In fact, it can be seen in the Appendix that for concentrations above 22%, the triplet energy level is depopulated much quicker, suggesting the appearance of an additional process quenching its population density.

Interestingly, the lifetime required to fit the transients at low concentration is different by a factor of 2 compared to the one obtained *via* this work's experiment. This discrepancy could be explained by the tremendous pump power employed for TAS measurement, which scales 10^7 higher than our $\text{kW}\cdot\text{cm}^{-2}$ diode pumping experiment. Although it is not intuitive to picture why the decay of triplet excitons to the ground state should depend on the excitation intensity, the significantly different source term $k_{\text{ISC}}S_1$ brought by this brief excitation results in a much more important triplet population, which could lead a facilitation of the non-radiative de-excitation pathway and short τ_t . Nevertheless, this difference meets the precision requirements for the community, as the important notion is in the first place to estimate at which order of magnitude constants scale and at which concentration second order phenomena occur.

2.2.5.3 Avoid pump-induced degradation of the sample during measurements

As mentioned in the setup description, the pump power densities of the 450 and 405 nm diodes on the samples can reach up to 200 W.cm^{-2} and 3 kW.cm^{-2} , respectively. In both cases, the long duration of the excitation forces one to be careful regarding potential thermal degradation of the sample between measurements. Indeed, the ground state recovery experiment cannot be reliable if the PL transient is not perfectly repeatable pulse after pulse, since the end of the pump ($t = 0$ on Figure 2.20) is used as a reference to study the depletion of the T_1 state. Besides blocking the illumination of the sample when adjusting Δt on the wavefunctions generators, we also took the precaution to mechanically shift the thin films between each measurement, to ensure that the PL had not been damaged by previous excitation. The influence of this precaution is pictured on Figure 2.20 on which the first excitation (ending at $t = t_1$ on Figure 2.4) is plotted for different delays between pump and probe. We show on Figure 2.20 (left) that the excitation of the same point leads to a degradation of the PL (even at a frequency of 10 Hz), which can be seen by its flattening for increasing Δt . Since less S_0 molecules are available due to thermal destruction, less triplets are created and hence the PL appears less quenched.

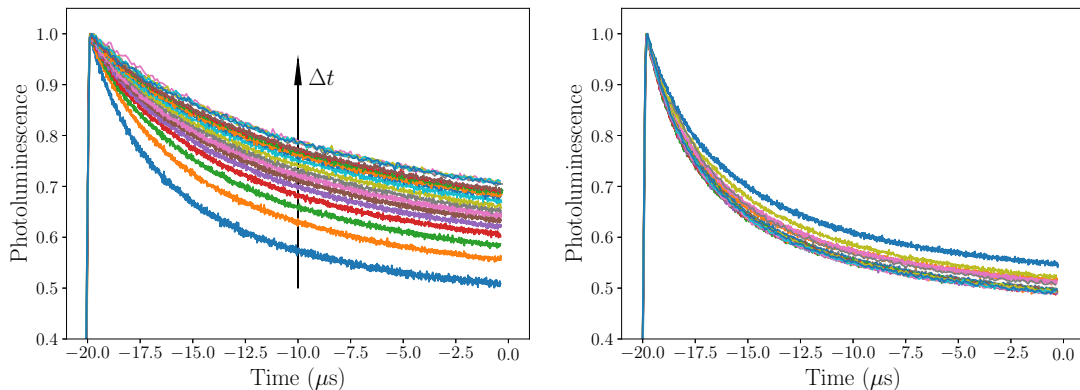


Figure 2.20: Normalized photoluminescence transients of the gain medium after an initial excitation for different delays between pump and probe. On the left, the same area of the film is pumped during the whole experiment, whereas it is changed between each delay on the right, yielding a more reproducible PL transient.

2.2.5.4 Temperature or triplets?

To separate the influence of triplets over temperature is a tricky task in many ways, considering that the typical lifetime for triplet excitons (hundreds of microseconds) is close enough to the typical characteristic time associated with thermal diffusion (ms), meaning that the influence of one sometimes overlaps with the other.

On that matter, Hamja *et al.* [207] showed that the lasing repetition rate of an optically pumped cuvette of propanol-2 containing 10^{-4} M of DCM could be increased from 1 to 14 kHz by putting an aspheric lens between the two mirrors of the cavity, leading to the compensation of the thermal lens.

As discussed in Section 1.3, Sandanayaka *et al.* managed to achieve lasing with BSBCz up to 8 MHz which was ascribed to the reduced influence of triplet excitons [14] but eventually reached 80 MHz thanks to a more efficient thermal management.

The argument presented here to rule out the fact that the PL dynamics is due to thermal effects relies on two neat BSBCz films that have been processed and encapsulated in exactly the same conditions (see Section 2.5 for details). However, the film denoted by "2020 (degrad)" on the absorption spectra from Figure 2.21 exhibited a much less important luminescence than the others, which has been ascribed to a default in the encapsulation of the film, causing the presence of oxygen in the gain medium.

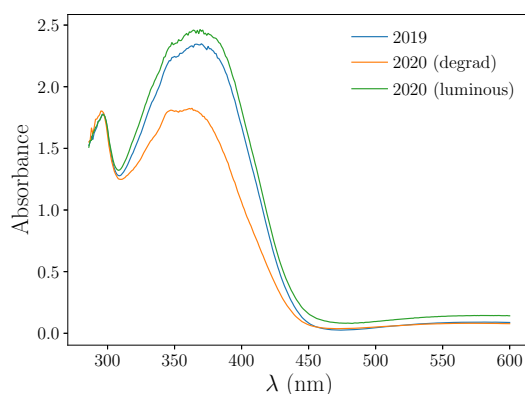


Figure 2.21: Absorption spectra of the pristine and degraded 200 nm BSBCz neat films.

This default is somehow very fortunate in the context of this experiment, as oxygen has been proven to be a very efficient triplet quencher because of its unique ground triplet state [154, 155].

We ran the pump-probe experiment to evaluate the triplet lifetime of both films. The raw PL transients are presented on Figure 2.22 and show dramatically different outputs. First, the relative luminescence of the degraded film (left) is much less quenched than its pristine counterpart (right), which is consistent with oxygen quenching triplets produced *via* ISC. More importantly, the effective triplet lifetime scales at $5 \mu\text{s}$ for the pristine film whereas it decreases to 500 ns for the other.

Since both films have roughly the same absorption at 405 nm and have been excited the same way, such a difference can only be explained by triplets related processes. This conclusion is in agreement with the work of Hubner *et al.* [208] who reported a triplet lifetime two order of magnitudes lower in the presence of

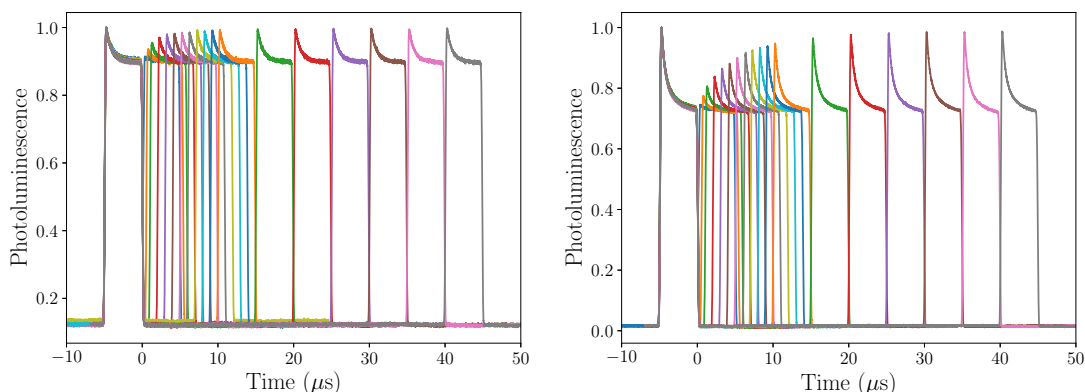


Figure 2.22: Photoluminescence of the pump (ending at $t = 0$) and the probe versus the delay between them for a degraded (left) and pristine (right) BSBCz neat films. The ground state recovery is much faster for the degraded sample because of the quenching of triplets by oxygen in the gain medium.

oxygen in their gain medium, without any impactful variation of neither its k_{ISC} nor its fluorescence lifetime.

2.2.5.5 Pump power density dependency of the triplet lifetime

To check whether or not the triplet lifetime obtained using our setup was dependent of the pump power density, we applied the same method (ground state recovery with low concentrated films then fitting with a monoexponential expression) for different intensity with a 5 wt.% PMMA:C521T film. The results regarding the 1 and 9 wt.% were presented previously to illustrate the protocol and showed that the fluorescence kinetics were similar in both cases *i.e.* both were ruled by a unique lifetime, ruling out TTA at such concentrations (Figure 2.15) and at such power densities.

Figure 2.23 shows that, regardless of the pump power density (varying up to an order of magnitude), we obtained the same dynamics with a unique lifetime of 120 μs . These measurements indicate that the triplet lifetime is not influenced by the excitation intensity, at least in the range of densities investigated.

It is not intuitive in the first place that the decay of the triplet population could depend on the intensity if we consider the triplet equation after the excitation (Equation 2.12), whose analytical solution is

$$T_1(t) = T_0 \times e^{-k_t t} \quad (2.16)$$

T_0 the triplet density at the end of the excitation does depend on the exciton density, but the typical time at which it decays is τ_t in any case. However, it is possible for τ_t itself to be influenced by the exciton density. Similarly to a bucket filled with water with a hole at its base whose flow increases with the level of the water, the triplet lifetime could be decreased by the presence of more triplets

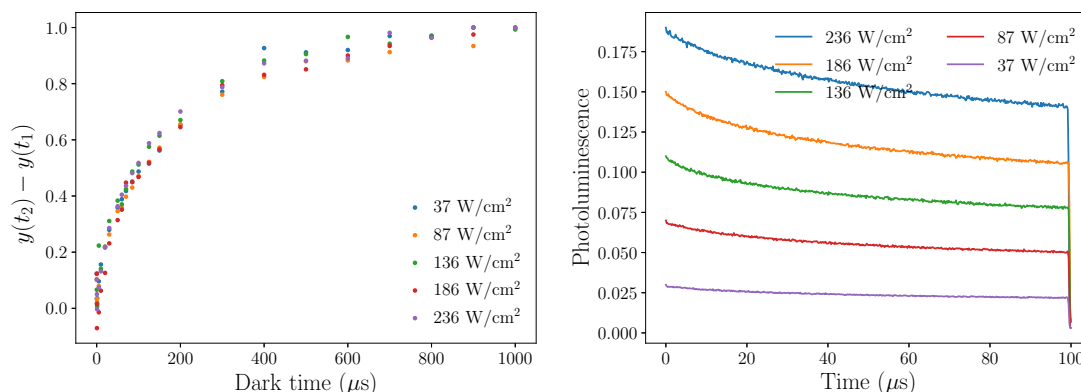


Figure 2.23: Left) Difference in photoluminescence between the end of the pump and the beginning of the probe for 17 μm PMMA:C521T (1 wt.%) at different excitation power density. Right) Long photoluminescence transients for each excitation power density investigated.

inside the gain medium.

2.2.5.6 On the temporal discrimination of STA from TTA

It has been discussed with the obtention of k_{STA} and k_{TTA} in coumarin 521T blended films that the influence of STA and TTA could be isolated from each other in time on the PL transients, which allows this method to have only one adjustable parameter at each step of the protocol. Because there are several interesting points that justify this approach, it is necessary to review in detail how photoluminescence transients can be analyzed. A study of ours that aimed at explaining the outstanding ms lasing emissions obtained by Adachi *et al.* [14, 5] with BSBCz will be presented to that purpose. Two BSBCz solid films were fabricated: a neat one and a secondary containing 17 wt.% of BSBCz in a CBP host matrix.

As shown on Figure 2.24, power densities used in vertical cavities are typically above the $\text{kW}\cdot\text{cm}^{-2}$, the first thoughts were then to evaluate the impact of potential laser-induced thermal effects inside the gain medium that could explain the rapidly decreasing photoluminescence, as it has already been established that temperature can affect several photophysical properties of organic molecules [45, 209]

Here, we modeled a **T**emperature dependent **I**nternal **C**onversion (TIC) using thermals experiments presented in the Appendix. Internal conversion being ruled by vibrational relaxation of molecules, its rate denoted by k_{nr} is expected to vary with the temperature and hence, because the temperature T changes with time in a pulsed mode, to evolve with time in the case of long μs excitations. Taking into account the PLQY versus time measurements and heat conduction simulations⁴

⁴Experiment and simulations regarding the temperature dependency of the PLQY have been done by Fatima Bencheikh from the center for Organic Photonics and Electronics Research (OPERA) at Kyushu University.

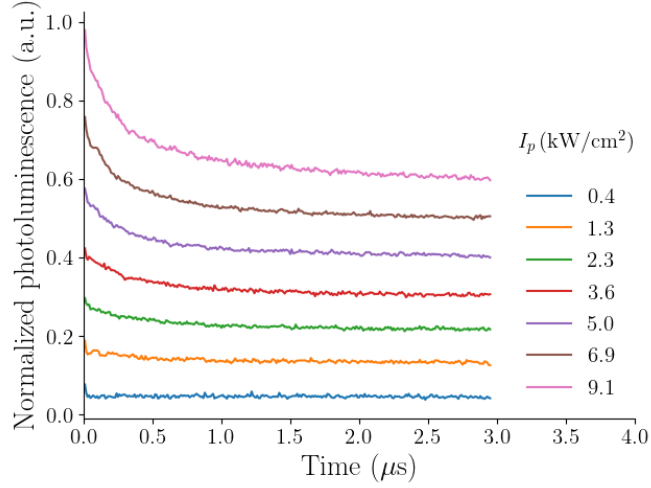


Figure 2.24: Photoluminescence transients divided by the pump profile of a 200 nm BSBCz neat film excited at different pump power densities.

allow us to reach the following expression for k_{nr} by fitting PLQY(T) by a slope:

$$k_{\text{nr}}(t) = \frac{k_{\text{nr}0} - k_r \alpha \Gamma t}{1 + \alpha \Gamma t} \quad (2.17)$$

where α and Γ are adjusted to fit the PLQY measurements, $k_{\text{nr}0}$ is the non-radiative decay rate at room temperature. Details of this derivation are provided in the Appendix. This expression was then implemented in a population rate equation system similar to Equation 2.9 and 2.10 by replacing k_f by $k_r + k_{\text{nr}}(t)$. Results on Figure 2.25 (orange curve) where k_{ISC} , k_{STA} , and k_{TTA} are set to zero show that although the photoluminescence slightly drops, a TIC rate cannot explain the PL transients on its own. Besides, this 10 % drop of the PL is obtained for a pump power density significantly higher than the one used with our setup. It should be noted that these measurements have not been done for the 17 μm films presented in this work. However, thanks to the negligible influence of TIC expected at lower excitation power densities, we consider that this approximation is taken into account in the error regarding the evaluation of the different rates (k_{ISC} , k_{STA} , ..).

This conclusion that thermal effects cannot fit the dynamics is related to the observations in Section 2.2.5.4 where we show that a reduction of the triplet lifetime up to one order of magnitude could be ascribed to the presence of oxygen inside the gain medium, proving that triplets are responsible for the observed quenching of the PL.

Now that thermal quenching has been ruled out, we explored the effects of triplet excitons by enabling intersystem crossing and singlet-triplet annihilation, as the latter is often pointed out as the main limiting process to achieve longer lasing pulses [154, 155, 74]. We show on Figure 2.25 that ISC and STA can only account for the initial decrease of the luminescence, as no combination of k_{ISC}

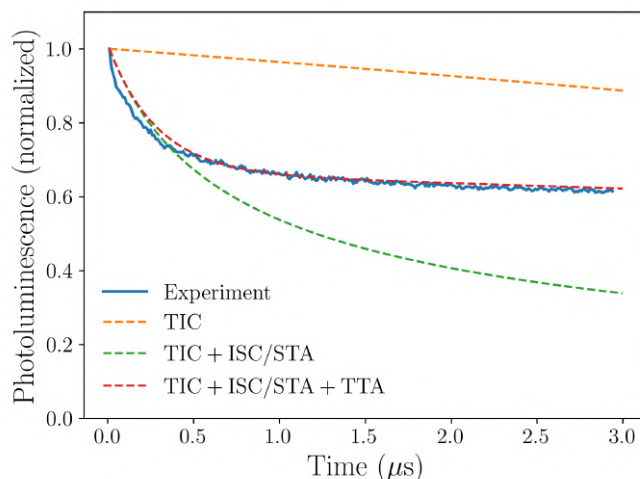


Figure 2.25: Photoluminescence transient (solid line) normalized to the pump profile of a 200 nm BSBCz neat film excited at $9.1 \text{ kW}\cdot\text{cm}^{-2}$. Data are fitted (dashed lines) using different models. TIC: **T**emperature-dependent **I**nternal **C**onversion

and k_{STA} allow a full agreement of the transients. An approach to explain the whole dynamics is to take into account an additional process that will lower the saturation level of the triplet population. Whether it is a lower triplet lifetime or the sign of triplet-triplet annihilation will be discussed afterwards.

Based on these findings, the following discussion will be split in two parts: a first focusing on the early stages of the PL where it abruptly decreases, and the μs scale where the triplet density saturates.

sub-microsecond scale

To properly investigate the influence of ISC and STA on the photoluminescence of BSBCz thin films, we simulated Equation 2.9 and 2.10 for a wide range of k_{ISC} and k_{STA} , in order to highlight the couples of values that could fit the experiments. Two configurations were chosen: a CBP thin film containing 17 wt.% of BSBCz pumped at $23 \text{ kW}\cdot\text{cm}^{-2}$, and a neat BSBCz film pumped at $9.1 \text{ kW}\cdot\text{cm}^{-2}$. The difference between the experiments and simulations are reported on Figure 2.26, where the colormap indicates the inverse of σ the standard deviation, which was computed from Equation 2.11.

Here, the higher, the better. Computations show that two regimes can explain the first 500 ns of the PL transients, regardless of the BSBCz concentration: a first in which they are fitted with only ISC (vertical lines corresponding to high values of k_{ISC} and negligible k_{STA}), and a second for which both ISC and STA are required (oblique lines for lower k_{ISC} and higher k_{STA}). From the cases where k_{STA} is superior to $10^{-12} \text{ cm}^3\cdot\text{s}^{-1}$, a clear relation between both rates can be extracted in the form of:

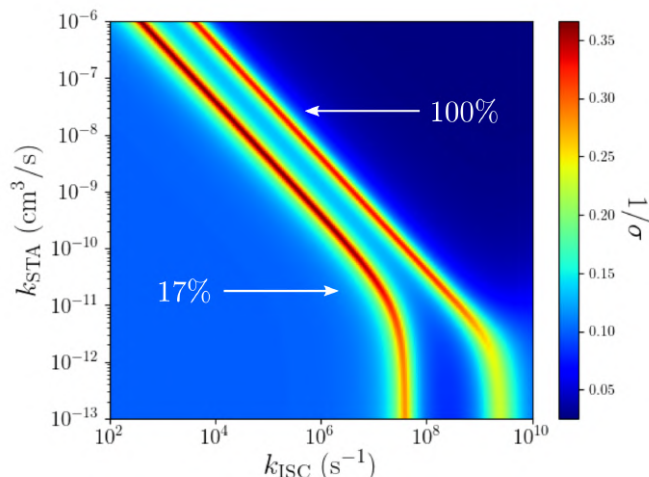


Figure 2.26: Inverse of the standard deviation for the first 500 ns of experimental PL transients (Figure 2.24) and simulations versus k_{ISC} and k_{STA} for two different BSBCz concentrations (17% at 23 kW.cm⁻² and 100% at 9.1 kW.cm⁻²)

$$k_{\text{STA}}k_{\text{ISC}}^{-\alpha} = \beta \quad (2.18)$$

where α is the coefficient of the mentioned lines. It is logical to see ISC and STA being inversely proportional to explain the same dynamic, as the former generates triplets that will quench the PL while the latter indirectly reduce the T_1 population density.

A PLQY of 0.76 in neat film [14] yields an upper limit for k_{ISC} that is above 10^8 s^{-1} , whereas the reported triplet formation quantum yield of 0.04 leads to $k_{\text{ISC}} = 3 \times 10^7 \text{ s}^{-1}$. Projecting these values on Figure 2.26 leads to the conclusion that STA has to be taken into account, and that we have access experimentally to the coefficient β (since we do not have more informations on k_{ISC} or k_{STA}).

Interestingly, it turns out that in the case of Figure 2.26, α is really close to one ($\alpha = 0.98$), meaning that the product $k_{\text{ISC}} \times k_{\text{STA}}$ can be considered constant for each concentration along those lines, regardless of the values chosen individually for k_{ISC} or k_{STA} ⁵.

Unfortunately, the very high fluorescence efficiency of BSBCz does not meet the requirements for our method to be applied, as discussed in Section 2.2.5.1, preventing us from the obtention of k_{ISC} or τ_t at low concentration of BSBCz. Nonetheless, these results show that if one knows either k_{ISC} or k_{STA} in a given configuration, the reciprocal constant can be estimated rather quickly from numerical fits. For the sake of this discussion, the triplet lifetime will be chosen at 175 μs after the report of Sandanayaka *et al.* [14] measured in solution (discussed in

⁵We will see in the Chapter 3 that this product arises naturally when derivating the requirements to achieve a continuous-wave lasing emission in the presence of triplets, making α *a priori* independent of the molecule.

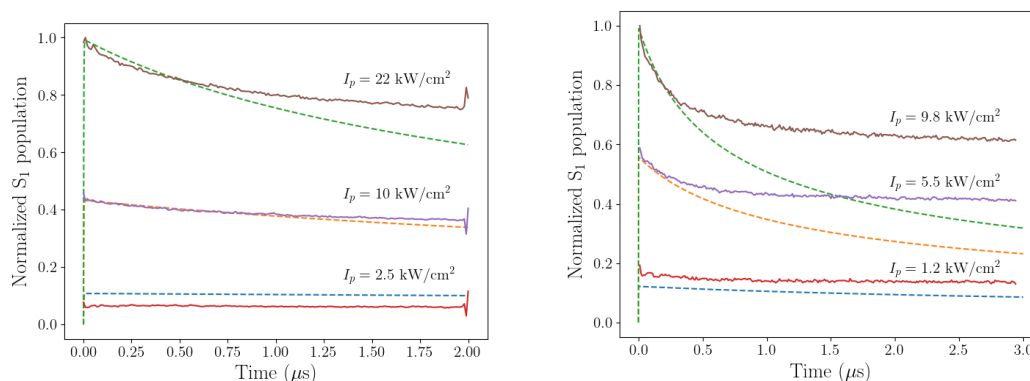


Figure 2.27: Experimental (solid lines) and simulated (dashed lines) photoluminescence transients normalized to the pump profile for 20 wt.% BSBCz in CBP (left) and neat BSBCz film (right). The fits only account for the first 500 ns for an additional process is needed to explain the full dynamics.

Section 2.1.1), as no report can be found for such measurements in solid blended films.

Fitting procedures yield values for β of 0.16×10^{-3} and $4.8 \times 10^{-3} \text{ cm}^3 \cdot \text{s}^{-2}$ for the blended and neat films, respectively, meaning that under the assumption that k_{ISC} does not vary much with the doping ratio ($6 \times 10^6 \text{ s}^{-1}$ for instance), k_{STA} will increase from 2.8 to $68 \times 10^{-11} \text{ cm}^3 \cdot \text{s}^{-1}$.

A trend that is consistent with the results presented in Section 2.2 for coumarin 521T thin films of different concentrations. Photoluminescence transients simulations performed with these STA rates for both films are presented on Figure 2.27, for which k_{TTA} has been set to zero. One can see that simulations only account for the first ≈ 500 ns, as discussed earlier with Figure 2.25. Once again, the rates evaluated from PL transients do not depend on the pump power density.

microsecond scale

To explain the dynamics of the photoluminescence at longer time scales, notably the saturation of the triplet population, triplet-triplet annihilation was implemented into the equations. We evaluate k_{TTA} with the same method described in Section 2.2, by minimizing the error between experiments and simulations at long time scales.

Results presented on Figure 2.28 show that only one TTA rate maximize the agreement with the experiment, and that it scales at 1.2 and $6.7 \times 10^{-13} \text{ cm}^3 \cdot \text{s}^{-1}$ for the blended and neat BSBCz film, respectively. Interestingly, these findings also suggest that TTA is proportional to the concentration of active molecules, contrarily to STA for which the rates increases by more than one order of magnitude from 17 to 100 wt.%. Simulations done with these updated rates can be found on Figure 2.29 for both films and at different pump power densities. It has also been

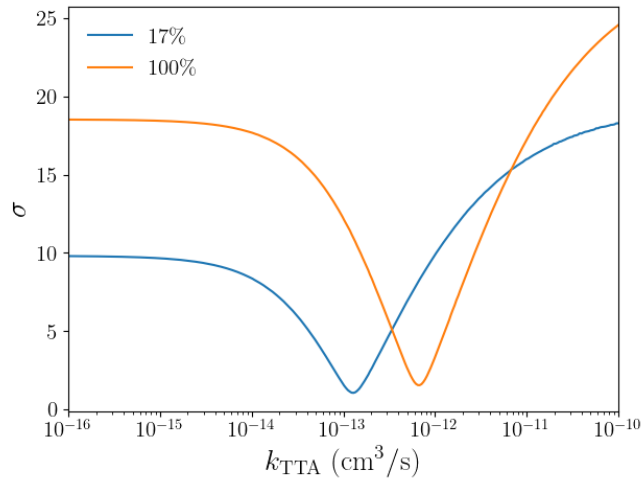


Figure 2.28: Error (%) between experimental and simulation photoluminescence transients of 17 and 100 wt.% of BSBCz in CBP thin films excited at 23 (blue) and 9.1 (orange) $\text{kW}\cdot\text{cm}^{-2}$, respectively.

checked that the k_{TTA} obtained *via* the fitting of the saturation were independent of the values chosen for k_{ISC} and k_{STA} , provided that their product remains similar *i.e.* that they are taken on the same straight lines on Figure 2.26. This checking gives credit to this separation in time to fit the transients, as the two dynamics really are independent.

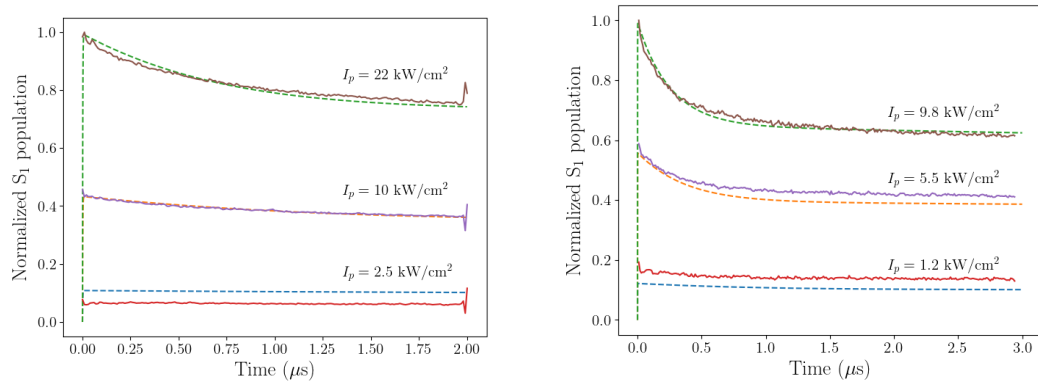


Figure 2.29: Experimental (solid lines) and simulated (dashed lines) photoluminescence transients normalized to the pump profile for 666 nm 20 wt.% BSBCz wt. in CBP (left) and a 200 nm neat BSBCz film (right).

Because Oyama *et al.* [11] recently reported triplet lifetimes of BSBCz and some of its derivatives that would in fact range between tens of nanoseconds to a few hundreds (which differs by several orders of magnitude from the values of 175 μs reported in Reference [14]), we also investigated if the PL transients presented on Figure 2.24 could be entirely explained by an intrinsically low triplet lifetime rather than a usual one being quenched by additional processes. However, our

simulations showed that to account for the whole PL dynamics, τ_t would have to scale at around 450 ns for the neat BSBCz film whereas it would have to reach a few μs for the blended 17 wt.% CBP:BSBCz, strongly suggesting that the reported sub-microsecond lifetimes actually stand for effective ones reduced by triplet-triplet annihilation.

The temporal separation of STA and TTA has been discussed, but one could wonder if a simple fit of the complete dynamics with k_{STA} and k_{TTA} as adjustable parameters would give the same result as long as k_{ISC} is fixed. It would have the advantage of being simpler and more straightforward than the above-mentioned approach. Interestingly, doing so would give the same values as long as k_{ISC} and τ_t are determined, and this is the important point. We have seen in the case of the CBP:BSBCz thin films investigated in this section that fitting the initial decrease gave a large range of possibilities for the couple $(k_{\text{ISC}}, k_{\text{STA}})$ on Figure 2.26. However, if k_{ISC} and τ_t are estimated prior to the fitting of high concentrated films (which our method allows with low concentration fluorescence kinetics), the STA rates obtained would be fixed by k_{ISC} (one point on Figure 2.26 instead of a line), and k_{TTA} would be fixed by $k_{\text{ISC}} \times k_{\text{STA}}$.

2.3 Results for other compounds

In the previous section, special cares were taken to present in the most detailed way the protocol regarding the evaluation of triplet-related constants using coumarin 521T blended PMMA films as an example. Here, the results obtained with other organic compounds with the same setup and subsequent methods are presented. The molecules investigated, sketched on Figure 2.30, were chosen based on their availability and their absorption spectrum which had to match with either the 405 or the 450 nm diode (unfortunately excluding virtually all rhodamine derivatives that could have been interesting to study). Also, the molecule had to be solution processable to be diluted in PMMA, so that the results could be compared with those of C521T films.

The following molecules were studied in the same configuration than for coumarin 521T: Ethyl 1,1,7,7-tetramethyl-11-oxo-2,3,5,6,7,11-hexahydro-1H-pyrano[2,3-f]pyrido[3,2,1-ij]quinoline-10-carboxylate (**coumarin 314T**), 4-Dicyanomethylene-2-methyl-6-p-dimethylaminostyryl-4H-pyran (**DCM**), 2-butyl-6-(butylamino)benzo[de]isoquinoline-1,3-dione (**fluorol 555**), and bis[(N-carbazole)styryl]biphenyl (**BSBCz-EH**). We did not seek the best lasing molecules, but rather various examples from different families.

C314T has been extensively studied in the 90's as a laser dye, owing to its high fluorescence quantum yield [210, 124]. F555 was also used in lasers [211] and was mode-locked in liquid state to achieve 5 ps pulses [212]. Moreover, it has also been used in PMMA films as solar luminescent concentrators [54, 213] thanks to a large Stokes shift and high fluorescence quantum yield [214]. Besides BSBCz-EH

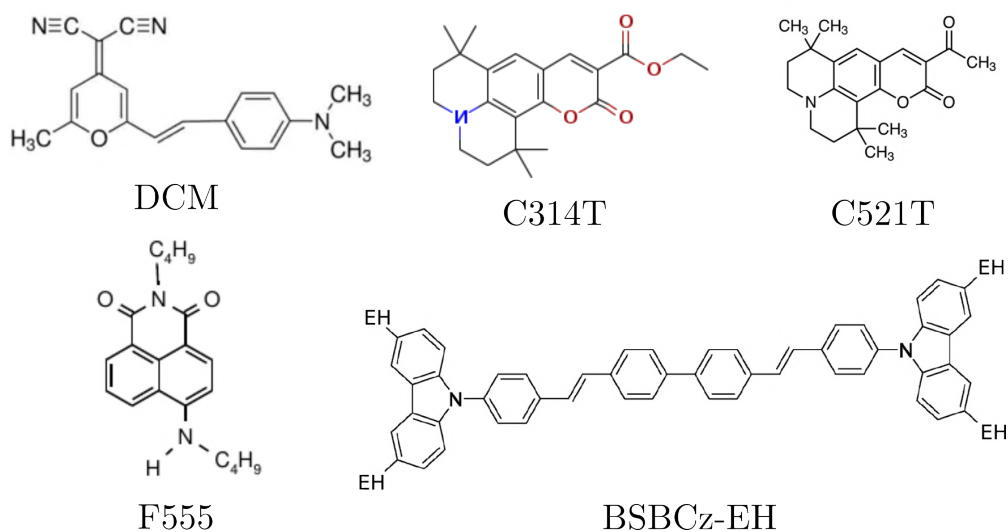


Figure 2.30: Compounds investigated in this work

which was used as a solution-processable alternative to BSBCz [16], DCM is the most known compound investigated in this work. It has been widely used three decades ago as a highly efficient tunable laser in the red (in liquid- and solid-state) thanks to a very low triplet formation quantum yield [215, 216, 217]. Being mixed with Alq₃ in host-guest systems allowed the reaching of novel lasing regimes in solid-state later [165].

This section starts with the presentation of the different triplet state lifetimes for the above-mentioned compounds in addition to a discussion regarding the comparison between lifetimes in solid- and liquid-state using two samples of DCM. It is followed by the evaluation of intersystem crossing rate (k_{ISC}), and of bi-molecular interaction rates (k_{STA} , and k_{TTA}) at different doping ratios when it was possible. Then, the discussion focuses on 200 nm CBP:BSBcz films at different concentrations of BSBCz that were kindly processed by Adachi's lab. By analyzing these films that are very similar to the ones used to achieve 30 ms lasing [5] with our method, we aim to confirm the good properties of the molecules regarding its CW-capabilities.

2.3.1 Triplet state lifetimes

2.3.1.1 Solid PMMA films

The measurement of triplet state lifetimes for each molecule has been done with the same protocol as presented in Section 2.2.4.1 *i.e.*, fitting by a monoexponential expression the ground state recovery kinetics obtained *via* our pump-probe setup. As stated, it has been done at low concentration to avoid the influence of other processes mentioned earlier.

Results are displayed in Table 2.2, alongside the wavelength used to excitate

material	λ_p (nm)	λ_{em} (nm)	τ_f (ns)	τ_t (μs)
DCM	450	575	2.1	160
C521T	450	500	3.7	120
C314T	450	475	3.5	
F555	450	510	4.0	190
BSBCz-EH	405	480	0.9	25

Table 2.2: Some properties of the 17 μm blended PMMA films investigated in this study. Fluorescence lifetime τ_f are obtained by monoexponential fitting of the luminescence (Appendix). Triplet lifetimes τ_t are obtained by monoexponential fitting of the ground state recovery at low concentration 2.34. Emission wavelengths are taken from the peak of the emission spectrum at low concentration for each compound.

each film, their maximum fluorescence wavelength, and their fluorescence lifetime in PMMA. Since emission spectra are red-shifted when the concentration of chromophore increases, λ_{em} has been designated here as the emission peak of the lowest concentrated film for each compound. Fluorescence lifetimes have been measured with the same apparatus as evoked in Section 2.2.3. Complete absorption/emission spectra and fluorescence measurement outputs are provided in Appendix 4.2.

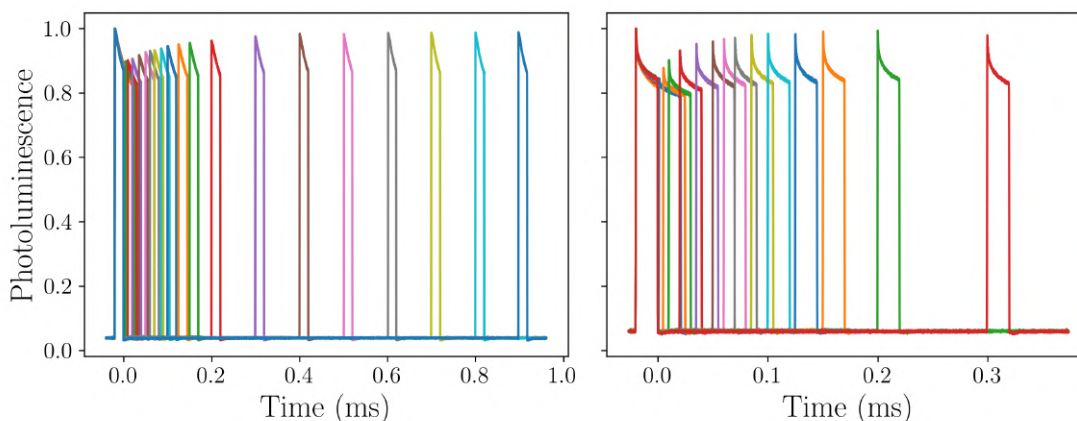


Figure 2.31: Normalized photoluminescence of the pump (ending at $t = 0$) and the probe versus delays between them for 1 wt.% PMMA:DCM (left) and PMMA:BSBCz-EH (right) thin films.

As one can see, there is a clear difference between BSBCz-EH and other compounds. In the case of DCM, coumarin 521T and 314T, and fluorol 555 (or 7GA), triplet lifetimes are found to be above 100 μs with an average of $\approx 150 \mu s$, whereas the one of the PMMA:BSBCz-EH film was measured at 25 μs , almost one order of magnitude lower. This difference is emphasized with Figure 2.31 whereby photoluminescence transients obtained with the pump-probe setup are plotted for DCM

(left) and BSBCz-EH (right) blended (1 wt.%) films. Ground state recoveries exhibit the same dynamics for both molecules but with much different times scales, for the BSBCz-EH fully recovers before 100 μs after the initial excitation whereas it takes DCM more than 400 μs .

We can conclude from this important difference that even though triplet lifetimes of other compounds are found to be quite similar, values are related to neither the gain medium configuration nor the host plastic matrix.

Although this is not really related to triplet lifetime measurements, the BSBCz-EH is also the molecule exhibiting the lowest fluorescence lifetime measured in this work, which can be explained by its high radiative rate constant [16, 14]. This, combined with a lower triplet lifetimes than other compounds in thin films, provides first insights on the CW emission reported using BSBCz by Sandanayaka *et al.* [14, 5]. Because, even though BSBCz-EH is only an alternative, modified version of BSBCz to be solution-processable, it has been shown by Mai *et al.* [16] that the Ethyl-Hexyl (EH) units added to do so had not changed the properties of the pristine molecule.

2.3.1.2 Comparison with liquid dye solution

Comparing lifetimes or any photophysical properties in liquid- and solid-state is no easy task, because of the difference in absorption and in concentration, mainly. Indeed, a standard molar concentration for molecule characterizations is 10^{-4} M, but even a 0.1 wt.% blended film is equivalent to $\approx 10^{-1}$ M. There are therefore only a few studies that were interested on this comparison, and no consensus regarding the alternation of photophysical constants between solid- and liquid-state has been reached yet.

As mentioned previously, an increase of the ISC rate has been reported in different configurations when going from liquid to solid [218, 193]. We can also cite the work of Dzebo *et al.* [219] on this matter, in which they show a significant increase of the TTA-generated delayed fluorescence in solid PMMA matrix compared to a liquid. On triplet state lifetimes, even fewer studies can be found. A common assumption is that it is much shorter in liquid configurations thanks to a much more important diffusion length of molecules, leading to more collision between triplets, oxygen and thus, reducing their lifetime. Furthermore, this reduced lifetime would also be linked to a negligible STA which, coupled with an ISC reportedly much lower, could explain the flat photoluminescence response observed in most dye solutions, even at high pump intensity.

For potentially all of the discussed reasons, we could not observe any decreasing of the photoluminescence (which is a requirement for this method, Section 2.2.5.1 for details) for usual concentration of 10^{-4} M with DCM, but had to reach 10^{-3} M to observe interesting dynamics. The photoluminescence transients obtained with our pump-probe setup on Figure 2.32 (left) show that even though the solution is considered highly concentrated and that the ethanol is almost saturated, the

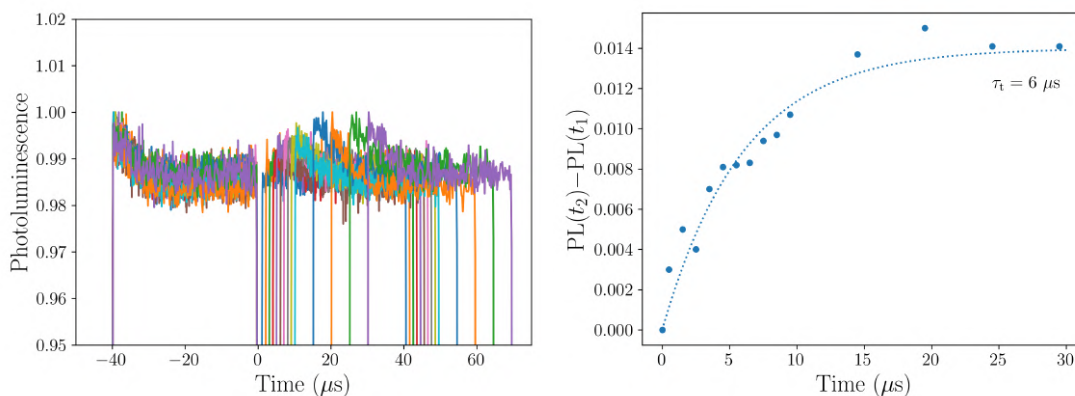


Figure 2.32: Output of the pump-probe experiment for a 10^{-3} M DCM solution in ethanol with left) Normalized photoluminescence of the pump (ending at $t = 0$) and the probe versus delays and right) ground state recovery fitted with a monoexponential expression and a lifetime of $6 \mu\text{s}$.

decrease of the PL with time is still very low compared to Figure 2.31 (left). This difficulty to quench the PL is in agreement with the argument mentioned earlier, if less triplets are created or interact with singlet excitons, there is no reason for the PL to be quenched.

However, the luminescence shown on Figure 2.32 (left) has been quenched enough, although very close to our setup resolution, for a monitoring of the ground state recovery with time. Doing so led us to a triplet lifetime as low as $6 \mu\text{s}$, as displayed on Figure 2.32 (right). If we take as a reference the values of $31 \mu\text{s}$ for DCM triplet state lifetimes [84] (measured in a deaerated solution of DMSO), it is expected to measure shorter ones considering the much higher concentration used here, as well as the finite concentration of O_2 in films. Moreover, the fact that the fluorescence recovery is much faster than in PMMA thin films (6 vs. $160 \mu\text{s}$) tends to agree with the "triplet collision" hypothesis.

2.3.2 Intersystem crossing

Now that triplet lifetimes have been evaluated at low concentration for each compound, longer photoluminescence transients can be used on the same films since k_{ISC} is assumed to be the only adjustable parameter left to explain a decreasing of the PL. Rates obtained are gathered in Table 2.3, and the corresponding PL transients are displayed on Figure 2.33 for DCM, C314T, F555, and BSBCz-EH (left to right, top to bottom) blended films.

For all compounds, k_{ISC} scales in the range of what it usually reported with organic molecules, as discussed in Section 1.2.4.1. The fitting of PL transients reveals quite stronger ISC for DCM, F555, and C314T with rates scaling above 10^8 s^{-1} . Interestingly it also indicates a k_{ISC} of $3 \times 10^7 \text{ s}^{-1}$ for BSBCz-EH, which exhibits similar properties as BSBCz. Although this value is in perfect agreement with the

rate of $3.1 \times 10^7 \text{ s}^{-1}$ reported for BSBCz (from triplet formation quantum yield and fluorescence lifetime measurements as stated in Section 2.1.1), this "typical" value tends to balance the conclusions regarding the CW lasing achieved with this molecule, which were justified with a very low generation of triplet excitons [5], among other arguments.

2.3.3 Bi-molecular interaction rates

Following the measurement of triplet state lifetimes and intersystem crossing rates, higher concentrated films were employed to study whether or not additional bi-annihilation processes were susceptible to influence the PL dynamics. Results (effective lifetimes, annihilation rates) are summarized in Table 2.3 for each compounds and for every concentrations.

Unfortunately, it was not possible to reach weight concentrations as important as with coumarin 521T, mostly because PMMA or anisole were more easily saturated. This is for instance the case of DCM for which it was impossible for us to reach concentration higher than 6/7 wt.%, even with the addition of more anisole to ease the dilution (which would have been ejected when spin-coated on the glass plate) or with the use of long radio frequency baths. In the case of BSBCz-EH however, this limitation to 5 wt.% is due to the limited availability of the material.

Long photoluminescence transients of blended PMMA films with DCM, coumarin 314T, fluorol 555, and BSBCz-EH are displayed on Figure 2.33 for different doping ratios with the associated fitting (dashed lines). Values used to fit the PL are gathered in Table 2.3 for each compound and for each concentration. Similarly to what was observed with coumarin 521T in Section 2.2.4.2, ISC and STA are sufficient to explain the abrupt initial decrease of the photoluminescence in every cases investigated. The same goes for TTA with the saturation of the triplet population, regardless of the time it takes to reach this steady-state regime. Sadly, the above-mentioned limits on the doping ratios prevent us from studying the evolution of k_{STA} and k_{TTA} at very high concentration in this configuration.

If we focus on the transients of the 5 wt.% blended films to compare all molecules, they indicate for most a quenching of PL at around 20 wt.% after 100 μs with a slightly stronger one for DCM. This more dramatic effect with DCM is surprising considering the very weak triplet formation quantum yield of 3×10^{-3} reported in the literature [84]. DCM being widely known for undergoing isomerization rather efficiently could explain this different behavior in our measurements.

On the other hand, experiments also show once again an important discrepancy between BSBCz-EH and others on the dynamics leading to this constant value. While it takes more than 100 μs to reach a steady-state photoluminescence with DCM, F555 and C314T, it only takes less than 10 μs for BSBCz-EH. Taking into account the fluorescence and triplet lifetimes with the ISC constant previously estimated, this faster dynamics can only be explained by the equations with a

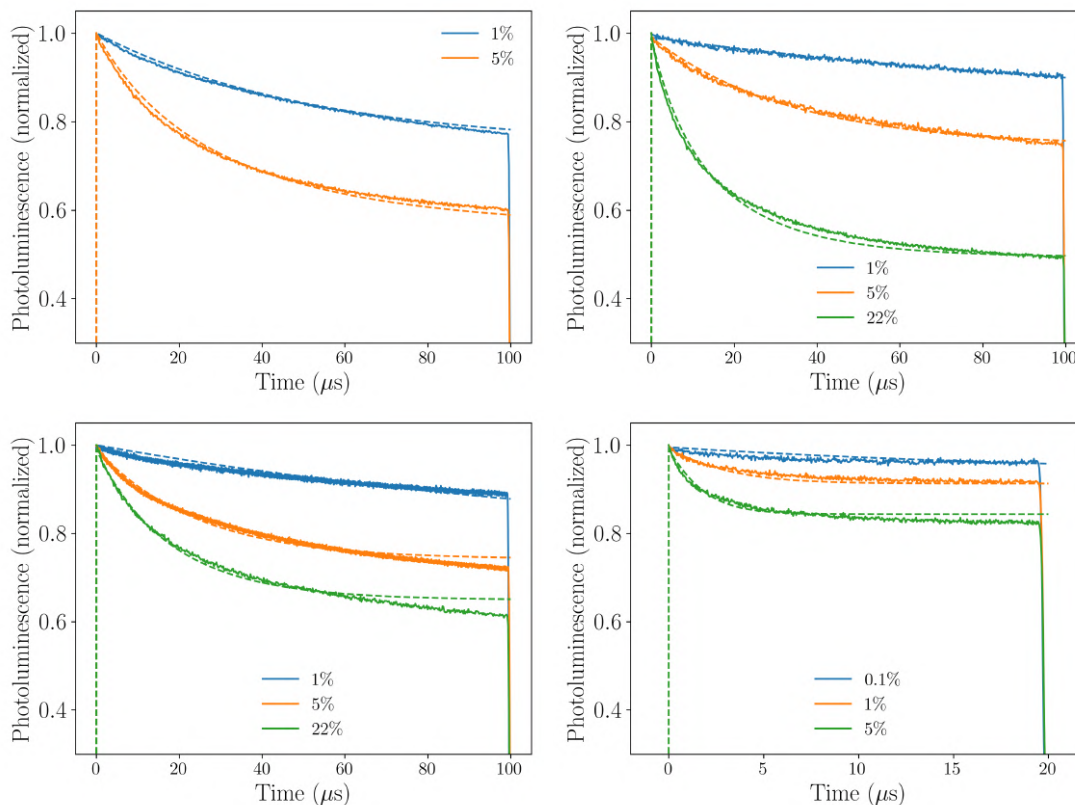


Figure 2.33: Photoluminescence transients of blended PMMA films at different concentrations of (top left) DCM, (top right) coumarin 314T, (bottom left) fluoro 555, and (bottom right) BSBCz-EH. The dashed lines are the associated fits whose values are provided in Table 2.3. Pump power densities used to excite the films: 139 (DCM), 165 (C314T), 139 (F555), and 2600 (BSBCz-EH) $\text{W}\cdot\text{cm}^{-2}$.

more important STA and TTA. Hence, values up to two orders of magnitude higher than other compounds are reported in Table 2.3.

Interestingly, these transients obtained with BSBCz-EH as a gain medium are not consistent with what have been published by Mai *et al.* [16] with the same molecule in neat film. They reported that the photoluminescence is indeed also quenched by approximately 25%, but that the dynamics is remarkably similar to any of the compounds we investigated in this study *i.e.*, a steady-state value reached within more than 100 μs .

This difference could be related to a too short excitation duration in our case that would prevent us from observing similar dynamics at longer time scale, but it has been checked that our results were consistent with a 100 μs excitation. Since we had the BSBCz-EH powder for quite some time before using it in PMMA, it could also be explained by the presence of oxygen inside the recipient, altering the pristine material by easing the triplet quenching. It would explain the shorter lifetime measured at 25 μs in Section 2.3.1 but as we will see in the next subsection, we obtained a similar fast dynamics in the case of encapsulated CBP:BSBCz

blended films.

Assuming that the pump power density linked to a peak power of 2.35 mW is much less important than ours⁶ is also not consistent with what we observed, since no quenching of the PL was observed at all for pump intensity inferior to 800 W.cm⁻².

Because, as it has been discussed previously, STA has been designated numerous times as the mechanism limitating the most the duration of lasing pulses, these strong values obtained in the case of BSBCz:EH blended films do not in the first place seem consistent with the ms lasing achieved with BSBCz [14, 5]. Therefore, it will be interesting to use these rates in Chapter 3 using simulations to study to which extent STA is compatible with CW lasing, and if TTA can help compensating this drastic excited singlets quenching.

In complement to long PL transients and the obtention of k_{STA} and k_{TTA} by fitting of the dynamics, we show on Figure 2.34 the pump-probe setup outputs for the same films. As stated, doing so has several purposes: first, it allows us to estimate the triplet lifetime using low concentrated films, which is then used as an input on Figure 2.33 to find k_{ISC} at the same low concentration. Then, using higher concentrated films provides a robust imaging of the influence of TTA in the gain medium, as the ground state recovery will no longer be fittable by a monoexponential expression with a unique lifetime, but with a more complex solution obtained *via* a Ricatti equation (Equation 2.14), characterized by two different lifetimes.

⁶In their paper, Mai *et al.* do not seem to provide the pump area on the sample in the case of a 355 nm excitation of the films, so that the pump power density cannot be precisely estimated.

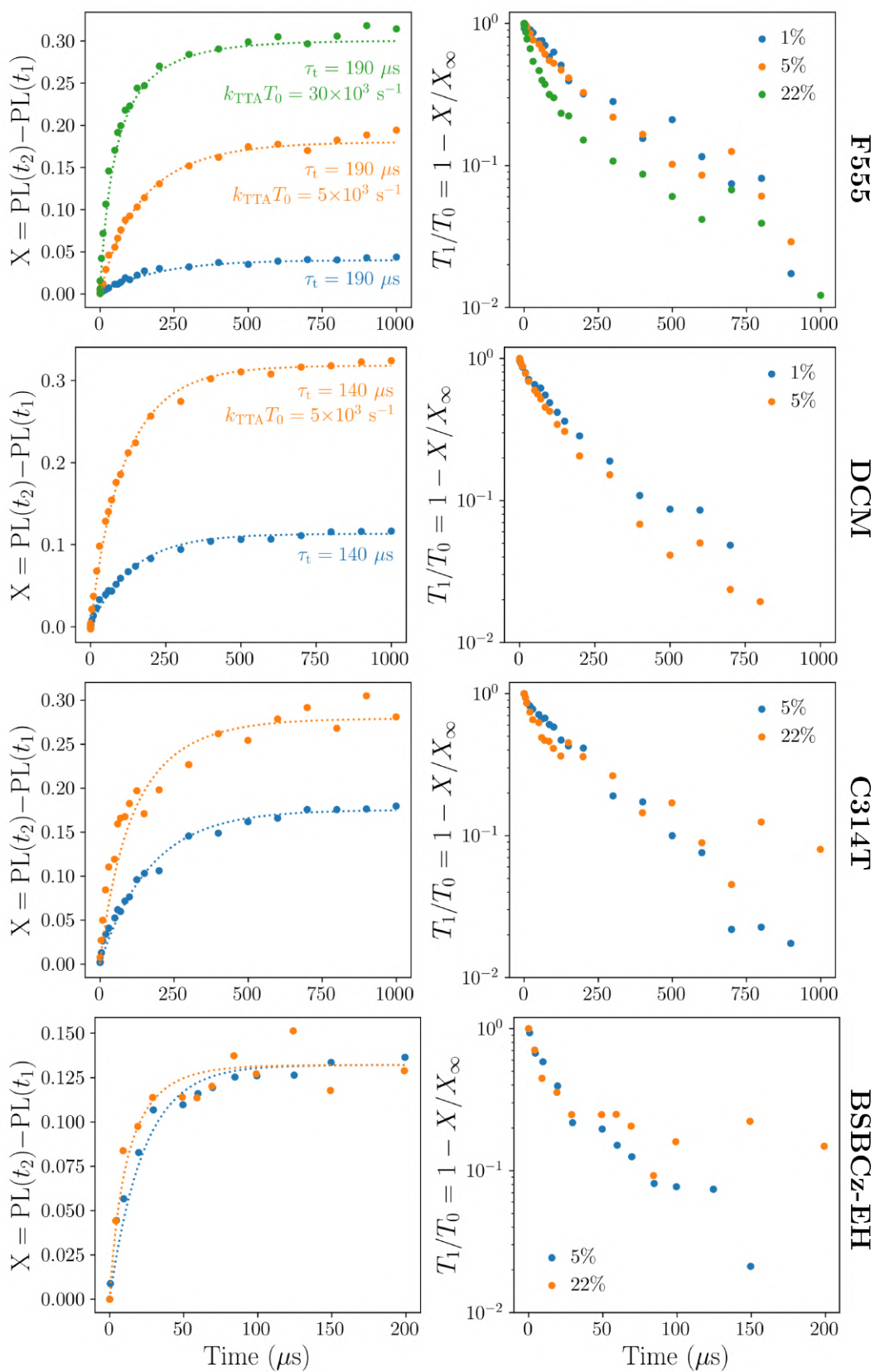


Figure 2.34: Fluorescence recovery kinetics measurements of blended PMMA films at different concentrations. τ_t is the triplet lifetime used to fit the data at low concentration with a monoexponential expression. $k_{\text{TTA}}T_0$ is the adjustable parameter in the triplet analytical solution in Equation 2.14.

On Figure 2.34, the fluorescence kinetic is fitted only with a unique triplet lifetime when no $k_{\text{TTA}}T_0$ is mentioned, meaning that TTA is not likely to occur. Results show that, similarly to what was obtained with coumarin 521T in Section 2.2.4, an increasing chromophore concentration in the gain medium is linked to an increase of TTA. Moreover, while coumarin 314T exhibits the same behavior as coumarin 521T with a meaningful TTA starting at a concentration of 22 wt.%, we see that it happens for concentrations as low as 5 wt.% in DCM, fluorol 555 or BSBCz-EH.

The presence of TTA at "low" concentrations does not seem consistent with its Dexter description, as it has been described in Section 1.2.6.2. However, it can be explained by a non-null probability to find dimers or closely-packed molecules in amorphous thin films.

doping wt.%	transients			τ_t μs	recovery	
	k_{ISC} 10^7 s^{-1}	k_{STA} $10^{-11} \text{ cm}^3 \cdot \text{s}^{-1}$	k_{TTA} $10^{-15} \text{ cm}^3 \cdot \text{s}^{-1}$		$k_{\text{TTA}}T_0$ 10^3 s^{-1}	k_{TTA} $10^{-15} \text{ cm}^3 \cdot \text{s}^{-1}$
C521T						
1	1.7	120
5	1.7	3	5	120
9	1.7	5	6	110
22	1.7	6	5	90	7.5	3
32	1.7	12	16	70	34	26
40	1.7	29	42	50	57	69
C314T						
1	10	170
5	10	8	3	170
22	10	10	2	140	8	1
F555						
1	20	190
5	20	3	3	190	5	2
22	20	3	2.7	190	70	8
DCM						
1	17	160
5	17	2.2	...	160	5	<1
BSBCz-EH						
0.1	7	25
1	7	60	600	25
5	7	60	600	25

Table 2.3: triplet-related photophysical constants evaluated in 17 μm PMMA films blended with different concentrations of coumarin 521T using two different methods.

2.3.4 CBP:BSBCz 200 nm encapsulated films

After applying our method to 17 μm films, we wanted to use it on a compound that has been mentioned numerous times in this thesis in previous sections: the BSBCz. Because as it has been evoked, this molecule cannot be processed in solution to create similar PMMA films, several 200 nm CBP:BSBCz films have been fabricated by a thermal co-evaporation process at the OPERA research center⁷. In order to fully take advantage of the setup presented in this work, films were processed with different concentrations of BSBCz (1, 5, 20, 40, and 100 wt.%) into the CBP host matrix. Doing so allows us not only to estimate constants that are useful for the community, but also to compare with other materials investigated. Besides, these gain media are much more analogous to the ones employed in the recent breakthroughs [5, 14], minus the grating imposed by the DFB resonator. The ideal is therefore to be able to clearly discriminate the properties of BSBCz from others, and also to see in which proportion those constants are similar to the ones of BSBCz-EH.

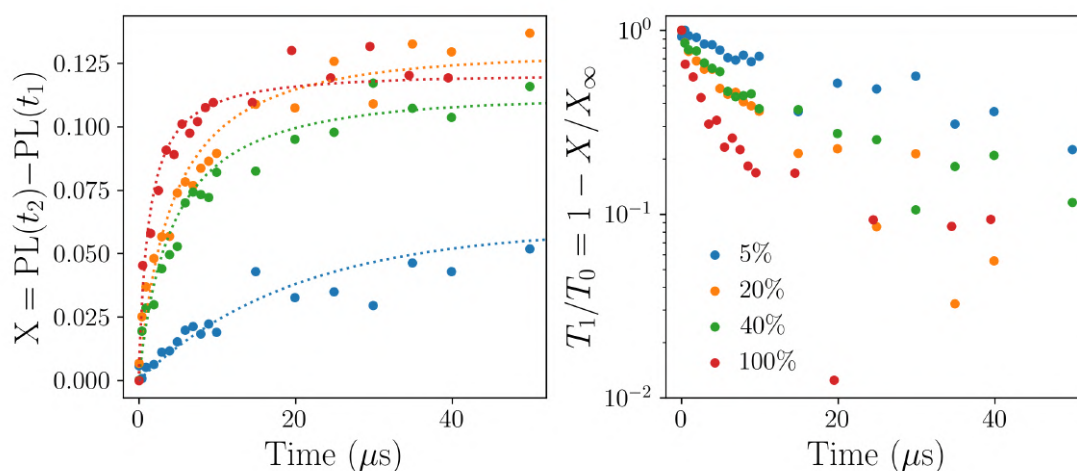


Figure 2.35: Fluorescence recovery kinetics measurements of 200 nm blended CBP:BSBCz films at different concentrations. Fits are obtained using a mono-exponential expression at 5 wt.%, and Equation 2.14 at higher concentration with $k_{\text{TTA}}T_0$ as adjustable parameters.

First, we looked at the fluorescence recovery kinetics at low concentration to estimate the triplet lifetime, and a value of 20 μs was reached. This rate is found to be consistent with the one found for BSBCz-EH, for which τ_t had been estimated at 25 μs . However, it should be noted that contrarily to other previous compounds, the measurements have been carried at a concentration of 5 wt.% because the quenching of the PL was not meaningful enough at lower concentration for the rather low resolution of our setup. It can be seen on Figure 2.36 with the blue curve

⁷We are especially grateful to C.Adachi and T. Xun for the time taken to process the films and to characterize them.

that corresponds to a 1 wt.% concentration, and for which the decreasing of the PL is much less important than for other compounds (Figure 2.33). Measuring the triplet lifetime at a concentration of 5 wt.% is legitimated by the monoexponential decay of the T_1 state at this doping ratio, as showed on Figure 2.35 (right).

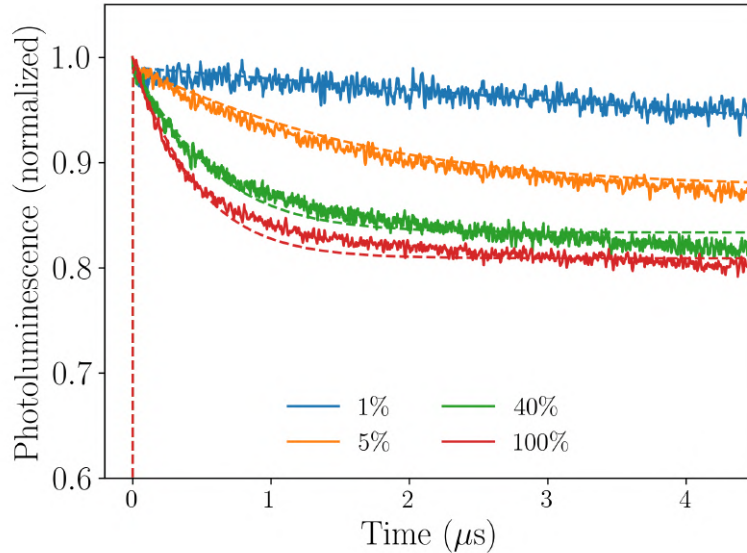


Figure 2.36: Experimental (left) and numerical (right) photoluminescence transients of 200 nm CBP:BSBCz films at different concentrations. $I_p = 2.6 \text{ kW}\cdot\text{cm}^{-2}$.

Such as BSBCz-EH in the previous section, we reached values for k_{STA} and k_{TTA} , in the range of 10^{-9} and $10^{-12} \text{ cm}^3\cdot\text{s}^{-1}$, respectively, in highly concentrated films that are much higher than other compounds whose rates have been evaluated at 10^{-11} and $10^{-14} \text{ cm}^3\cdot\text{s}^{-1}$ for STA and TTA, respectively. This is due to the much faster dynamics in play here, as the triplet population density saturates in less than three microseconds for concentrations higher than 5 wt.%. To simulate this fast recovery, a shorter triplet lifetime is not enough and TTA is required, hence the strong values around $3\times 10^{-12} \text{ cm}^3\cdot\text{s}^{-1}$. Although several options exist to simulate a fast depletion of the T_1 state, TTA is once again found to be the best probable scenario, owing to the non-exponential decay dynamics displayed on Figure 2.35 (right).

Regarding k_{ISC} , the value of $3\times 10^7 \text{ s}^{-1}$ is close enough to the value obtained for PMMA:BSBCz-EH films, and is found to be consistent with the triplet formation quantum yield of 0.04 and the fluorescence lifetime of 1.28 ns reported in [5]. The effective triplet lifetimes presented in Table 2.4 were defined for each concentration as the closest fit of the Ricatti expression (Equation 2.14) with $k_{\text{TTA}}T_0$ set to zero. Although it is a rather crude rough way to fit experimental data, it shows that for concentrations above 20 wt.%, τ_t^{eff} reaches values of less than 10 μs . This, combined with high TTA (despite a high STA), provides useful insights regarding the results obtained by Adachi *et al.* at OPERA that will be discussed in Chapter

4.

doping wt.%	transients			recovery		
	k_{ISC} 10^7 s^{-1}	k_{STA} $10^{-10} \text{ cm}^3 \cdot \text{s}^{-1}$	k_{TTA} $10^{-12} \text{ cm}^3 \cdot \text{s}^{-1}$	τ_t^{eff} μs	$k_{\text{TTA}}T_0$ 10^6 s^{-1}	k_{TTA} $10^{-12} \text{ cm}^3 \cdot \text{s}^{-1}$
1	3	20
5	3	2	2	20
20	3	7	3	7	0.4	2
40	3	9	4	7	0.4	2
100	3	7	3.5	3	1.5	1.5

Table 2.4: Triplet-related photophysical constants evaluated for 200 nm CBP films blended with different concentrations of BSBCz using two different methods. τ_t^{eff} the effective triplet lifetime is estimated by fitting as best as possible the Ricatti dynamics without TTA.

2.4 Conclusions

In this chapter, a method to evaluate triplet-related photophysical constants has been presented. This experimental protocol combines the previous work of Kogan *et al.* [85] and the photoluminescence transients analysis used notably by Adachi *et al.* [16, 83, 153] to study the suppression of singlet-triplet annihilation with the incorporation of triplet quenchers in the gain medium. Using a simple pump-probe setup illustrated on Figure 2.3 with μs , $\text{kW} \cdot \text{cm}^{-2}$ optical excitations and the fit of both ground state recovery *via* fluorescence kinetics and photoluminescence transients allows us to obtain τ_t and k_{ISC} in low concentrated blended films. k_{STA} and k_{TTA} are then estimated at higher concentrations of active molecules.

The expensive and/or complicated setup that is usually required to properly obtain such constants (if possible) were discussed in the first place, as well as the limitations imposed by numerical fitting procedure using too many adjustable parameters. Instead, this work provides an approach that only has one adjustable parameter at each step of the protocol as summarized on Figure 2.17. Besides, no spectral resolution, PLQY measurements, ns resolution is required, making it cheaper and simpler than most methods presented in Section 2.1.1.

First, the triplet lifetime is estimated from the monoexponential fitting of the ground state recovery dynamics at the lowest possible doping ratio. k_{ISC} is estimated afterwards by fitting long PL transients at similarly low concentration, to rule out the influence of concentration quenching and intermolecular interactions. Now that the complete photophysics occurring at such concentration is known, k_{STA} and k_{TTA} can be estimated by fitting PL transients of higher-concentrated blended

films. Although it is not mandatory because k_{ISC} has been fixed previously, but we showed that STA and TTA could be split temporally and that both accounted for different parts of the PL kinetics.

To begin with, the method was presented in detail in the case of blended PMMA films containing different concentrations of coumarin 521T, and was then applied to flurorol 555, coumarin 314T, DCM, and BSBCz-EH in the same configurations. Several interesting key points are worth mentioning: first, triplet lifetime were evaluated at around 150 μs for all compounds but BSBCz-EH. Then, we also showed that k_{STA} and k_{TTA} were much more pronounced in BSBCz-EH too, as stronger rates are necessary to explain the fast saturation of the triplet population density and the ground state recovery. Being able to discriminate one molecule from others with this simple setup provides great insights regarding the lasing capabilities of gain media. Also, the use with C521T of high concentrated films allows us to study the concentration dependence of bi-molecular interactions such as STA and TTA. It should be mentioned that this method does not provide precise values of the rates, but does a great job a providing order of magnitude with errors that are estimated to be less than twofold, which is enough for the need of the community. Indeed, it has been mentioned in the state-of-the-art that actual methods, even though they can be much more expensive and/or complicated, cannot provide values up to a certain degree of precision.

Then, we performed this protocol on 200 nm CBP:BSBCz films at different concentrations, on which similar conclusions as with BSBCz-EH were reached *i.e.*, a triplet lifetime of $\approx 20 \mu\text{s}$ while STA and TTA are very strong with rates reaching values above 10^{-10} and $10^{-12} \text{ cm}^3.\text{s}^{-1}$, respectively.

There are several ways to improve this setup in the future: first, the resolution of the measurements may be significantly improved by the use of an FPGA for instance to automate the recording. Indeed, since only the pump is required to last long enough to build an important population of triplet, implementing a custom analog signal that alternates between long and brief pulses (since we are only interested at the peak fluorescence of the probe) could improve the resolution. Besides, it would also prevent potential permanent bleaching of the gain medium during experiments and obviously save time, as it would become a turnkey system that performs all necessary recording and processing much faster. We could also give more attention to the evolution of the transients with δ_t in cases where there is an existing T_1 population before the probe. If aiming for database-like applications, one of the key point would be to explore new emission wavelengths to be able to screen properties of various new light emitting dyes.

Chapter 3

Continuous-wave lasing conditions of organic lasers

3.1 Motivations

The early motivations to understand what are the optical and photophysical requirements to achieve a (quasi)-continuous wave lasing operation using an optical excitation of an organic thin film came from the breakthroughs reported by Sandanayaka *et al.* [14, 5] with BSBCz in a mix-order DFB resonator. As discussed in Section 1.3, their report on a lasing operation during a 30 ms excitation was the first of its kind and an important step towards the current state-of-the-art. It was ascribed to BSBCz properties (short fluorescence lifetime, very low triplet absorption, high radiative rate and PLQY, and so on.) and an efficient thermal management which allowed the lasing to operate at a repetition rate up to 80 [5] instead of 8 MHz [14].

The idea of our team was then to use the same molecule exhibiting so many CW-friendly properties and incorporate a similar thin film (in concentration and in thickness) into an optically pumped VCSEL-like cavity (the film is mechanically sandwiched between two high-quality mirrors, leaving no empty space inside). Indeed this type of resonator presented in Section 1.1.5 is known to exhibit a near perfect beam quality (with a M factor close to unity), which would allow deeper studies regarding the properties of the beam emitted from the gain material, and pave the way for more practical applications where shapable beams are required.

However, as shown on Figure 3.1, lasing pulses that lasted no longer than one microsecond were obtained with a pump power density of several $\text{kW}\cdot\text{cm}^{-2}$, which is similar to the intensity with which a qCW emission was achieved in DFB. Considering that we used the same molecule at the same concentration in a CBP host matrix, and that we pumped this similar film at approximately the same pump power density, a question emerges: why does the resulting lasing pulses in VCSEL are no different from any classical materials that are not considered CW-friendly?

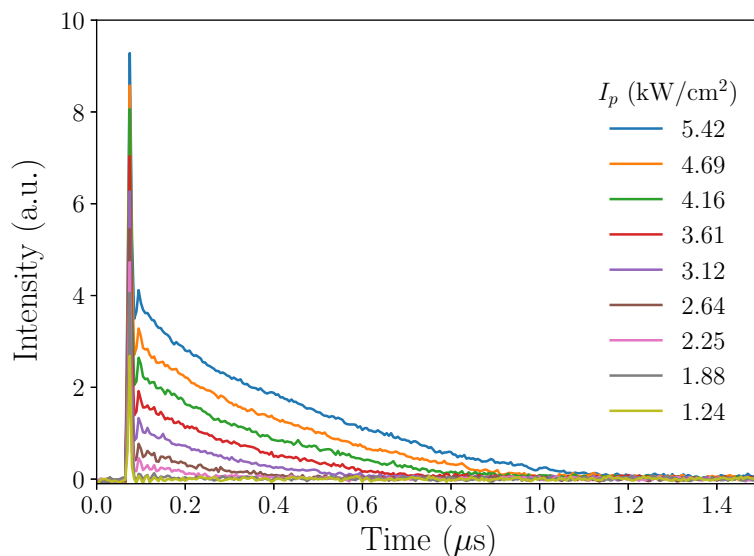


Figure 3.1: Lasing transients of a VCSEL structure composed of two HR mirrors and a 666 nm CBP:BSBCz (20:80 wt.%) at different pump power densities

This very question is at the starting point of this chapter and these numerical studies, in which we included both optical and photophysical losses in our thinking to provide a broader view of the requirements to achieve lasing under (q)CW excitation. This chapter will be presented as follows: First, the theoretical framework (exciton population equations, resonator modeling, ..) will be presented, followed by an extensive discussion regarding the approximations that have been done and the limits of our work. Since our analysis also relies on many analytical expressions, a detailed version of the reasoning is provided using the classical four-system configuration, in which triplets are not taken into account. This illustration has also the purpose to be used as a reference for further comparisons with more complex systems.

Then, the generation of triplet excitons after photoexcitation *via* intersystem crossing is studied, focusing on their influence on the lasing pulse duration. After that, singlet-triplet annihilation and triplet absorption are enabled in the equations and their effects on the populations temporal evolution is addressed, alongside a discussion on whether STA or TA has the most detrimental impact. At last, the influence of beneficial mechanisms such as triplet-triplet annihilation, reverse intersystem crossing, and a low triplet lifetime regarding the above-mentioned loss interactions is also presented.

3.2 Previous investigations

The first report that comes in mind when discussing the modeling of organic lasers is the work of Gärtner *et al.* [96, 38], who studied numerically the thresholds

of OSLEDs and introduced the system of rate equations employed in this work and numerous other papers since. Notably, they explored the influence of bi-exciton annihilations such as STA and TTA on the lasing capabilities of electrically pumped devices. Their work shows among other things that a threshold of 1 kA.cm⁻² would be possible with standard values of k_{STA} and k_{TTA} (which was not obvious since STA was pointed out as an important limitation towards OSLED), provided that other losses such as triplet absorption and thermal effects were efficiently dealt with. Furthermore, they designated the ratio $k_{\text{STA}}/k_{\text{TTA}}$ (*i.e.* the singlets quenched by STA over the ones created *via* TTA) as being an important indicator for electrical stimulation of organic lasers.

Among the methods to harvest triplet excitons back the fluorescence, RISC is a mechanism of choice, and its influence on the lasing pulse duration has been studied in the past. We can cite the work of Abe *et al.* [83] who used numerical simulations to study how the ratio $k_{\text{ISC}}/k_{\text{RISC}}$ affects the exciton statistics and hence, the lasing emission. Their work notably indicates that in order to achieve CW lasing in the presence of optical losses such as triplet absorption, k_{RISC} should be of the same order of magnitude as k_{ISC} , which is not so surprising since both mechanism are exactly reciprocal.

The work of Chua *et al.* [80] also has to be discussed, since it is found to be the closest to this theoretical study, being among the first to actively take into account the cavity characteristics in addition to the photophysical properties of the gain medium to explain lasing behaviors in OSSLEDs. Although they mainly focused on lasing thresholds of nanostructured organic lasers, their work provides great insights regarding the influence of the cavity quality factor Q and confinement factor Γ . To do so, they used system of coupled rate equations as introduced by Gärtner *et al.* [96] but extended to take into account different vibrational sub-levels of each electronic level of interest.

Interestingly, they predict that in a configuration where k_t is equal to k_{ISC} and the photobleaching of the molecules is neglected, a resonator with a quality factor of 5×10^4 would exhibit a lasing threshold as low as 0.7 W.cm⁻². This case seems however utopian, since it means that triplets would no longer be problematic in a system without the help of triplet quencher/manager, considering typical values of 10^7 and 10^3 s⁻¹ for k_{ISC} and k_t , respectively. They also show that no lasing would be possible if k_{ISC}/k_t approaches 10^3 , which is the usual order of magnitude reported in the literature for fluorescent compounds (see Section 1.2.4.1).

Giebink and Forrest [220] studied in 2008 which triplet-related process was the most detrimental regarding the lasing pulse duration, thanks to a simplified system of equations and experimental lasing/PL transients of two DFB resonators with Alq₃:DCM and CBP:BCzVBi (a blue/green dye) as gain media. While they were able to show that the limitation could be ascribed to triplet and not thermal effects thanks to lasing intensity recovery measurements (mentioned in Section 2.1.1), they fitted the temporal dynamics with triplet formation quantum yields

δ_T , defined by

$$\frac{dT_1}{dt} = \delta_T R_p S_0 - k_t T_1 \quad (3.1)$$

which differs from a fixed triplet creation rate as k_{ISC} , R_p being the pumping rate (s^{-1}). Their work contains a quite interesting discussion on the ratio between the time it takes for the triplet population to be relevant (important enough for STA to be meaningful) and the rise time of the singlet population. In other terms, they emphasize that the S_1 population has to reach the density related to the lasing threshold before T_1 excitons are able to quench it. For instance, when taking a low triplet formation quantum yield of 0.03 (meaning that only 3% of the photoexcited molecules will be promoted on the T_1 state), the S_1 density is more important than the T_1 one during the first 50 ns, which gives it the time to be clamped to its threshold value ($1.5 \times 10^{17} \text{ cm}^{-3}$ in their example). After this short time, STA becomes efficient and reduces the singlet excitons density below the threshold, thus terminating stimulated emission. Furthermore, they applied their system to an electrical stimulation of the gain medium (*i.e.* $\delta_T = 0.75$ as discussed in 1.2.4.1). They found out that in this particular case, the T_1 population outnumbered the S_1 one so early that it prevents it from reaching its threshold value. More simulations allowed them to reach the fatal conclusion that STA is not compatible at all with electrical pumping, as it would require a tremendous current combined with a low rising time of the S_1 population, which was unreachable with current materials at that time. Although the equations used here were simplified (not taking into account triplet absorption and triplet-triplet annihilation), the conclusions on the mandatory removal of STA or a better management of triplets were consistent with the recent breakthroughs using BSBCz, 10 years later, whose high performances were attributed to a low triplet formation quantum yield. They also emphasized the importance of a well designed cavity (with losses lower than 150 cm^{-1} , or an equivalent Q higher than $\approx 10^3$, in their case) to reduce the lasing threshold, by reducing the rise time of the S_1 population, which would lead to longer lasing pulses.

Among the system presented in this section, the one used by Chua *et al.* [80,] takes into account neither STA nor TTA, while the one used by Giebink and Forrest [220] is useful for host-guest systems (hence the absence of TTA here too). Overall, both systems are suited for particular applications and are found to be rather complicated. Therefore, there is a need of simpler models that are suited for organic semiconductors such as BSBCz, which is used as the only active molecule in solid films, and where both STA and TTA are thought to occur.

3.3 Theoretical framework

A continuous-wave lasing emission is the result of a certain equilibrium between the populations of energy levels. Thus, it is important to study their dynamics with

time to understand how the different processes in play balance these populations. This part is therefore devoted to the presentation of the theoretical framework within which the CW lasing conditions of organic lasers have been studied.

The system of equations chosen to model the population densities and the intensity inside a resonator will be presented, alongside the different approximations that have been made and the limits of this solution. After a discussion about the quality factor of optical resonators, the algorithm used to discriminate the different regimes of emission will be detailed.

3.3.1 System of equations

3.3.1.1 Energy states populations

The populations of the ground state S_0 , the singlet excited state S_1 and the first excited triplet state T_1 are modeled by Equations 3.2 to 3.4. In addition, most of the pathways involved in this system are illustrated in Figure 1.15. This system is based after the work of Keller *et al.* [221] and Peterson *et al.* [222]. Their approach has been used in numerous studies over the past decades to better understand organic lasers [145, 96, 37, 74, 82].

In this system, exciton populations are expressed in m^{-3} so that every terms are expressed in $\text{m}^{-3}.\text{s}^{-1}$. Molecules in the ground state are excited at a rate $R_{\text{ex}} = \sigma_{\text{abs}}I_p/h\nu_{\text{ex}}$, where σ_{abs} is the absorption cross section of the gain medium at the excitation wavelength (m^2) and I_p the pump power density ($\text{W}.\text{m}^{-2}$). The inverse of the fluorescence lifetime $k_f = k_r + k_{\text{nr}}$ takes into account two de-excitation paths back to the ground state: spontaneous emission of a photon and the non-radiative way. Note that excited singlet excitons can also be transferred in a triplet state *via* intersystem crossing at a rate k_{ISC} (s^{-1}) or feed the photon density by being stimulated at a rate $R_l = \sigma_{\text{em}}I/h\nu_l$, where σ_{em} is the emission cross section of the chromophores at the lasing wavelength (m^2) and I the intensity inside the resonator ($\text{W}.\text{m}^{-2}$) which will be addressed in the next section.

$$\frac{dS_1}{dt} = R_{\text{ex}}S_0 - (k_f + k_{\text{ISC}} + R_l + k_{\text{STA}}T_1)S_1 + \zeta k_{\text{TTA}}T_1^2 \quad (3.2)$$

$$\frac{dS_0}{dt} = -R_{\text{ex}}S_0 + (k_f + R_l + k_{\text{STA}}T_1)S_1 + k_tT_1 + k_{\text{TTA}}T_1^2 \quad (3.3)$$

$$\frac{dT_1}{dt} = k_{\text{ISC}}S_1 - k_tT_1 - (1 + \zeta)k_{\text{TTA}}T_1^2 \quad (3.4)$$

Regarding the triplet population, it is built from the term $k_{\text{ISC}}S_1$ so that the more excited singlets are *created* from the absorption of a photon, the more excitons will be trapped in the dark T_1 state. Their non-radiative de-excitation to the ground state is ruled by the triplet state lifetime k_t^{-1} .

As discussed in Section 1.2.6, molecules located on either singlet or triplet

excited states can also interact with each other *via* different annihilation processes such as STA and TTA. The rates k_{STA} and k_{TTA} of these interactions are expressed in $\text{m}^3 \cdot \text{s}^{-1}$ to take into account the density of the populations. ζ is the proportion of singlet created through TTA, its value has been discussed in Section 1.2.6.2.

3.3.1.2 Photon density

The lasing intensity inside the cavity is modeled after Equation 3.5, whereby two terms account for the gain and two others for the losses. As in every laser, spontaneous emission (I_{sp}) is the feeding term of stimulated (I) emission. The former is defined here as the stimulated emission induced by one photon in the lasing mode [17] and is equal to c/V_l , where c is the speed of light and V_l the volume of the lasing mode. Hence, both terms are proportional to the singlet population density, the emission cross section σ_{em} , and the confinement factor of the lasing mode in the cavity Γ , which is defined as the overlap between the active medium's volume and the lasing mode [37]. It can reach unity in cases where no empty spaces is left between the gain medium and the cavity boundaries, or where the feedback mechanism is parallel to it. It can also be way below one, notably in external cavity where it can be approximated by the ratio d/L , with d the thickness the gain medium and L the distance between mirrors.

$$\frac{dI}{dt} = \frac{c}{n} \Gamma \{ \sigma_{\text{em}} S_1 [I + I_{\text{sp}}] - \sigma_{\text{TA}} T_1 I \} - \frac{2\pi c}{Q \lambda_l} I \quad (3.5)$$

The last two terms stand for very different sources of losses. The first: $\sigma_{\text{TA}} T_1 I$, accounts for the so-called triplet absorption (see Section 1.2.4.3 for details), whereby photons of the lasing mode are absorbed by an excited triplet state to induce a $T_1 \rightarrow T_n$ transition. The probability of this absorption is proportional to the cross section of the transition σ_{TA} (m^2), which is related to the overlap between the lasing peak and the triplet absorption band.

The last term represents the losses due to the resonator itself, mostly driven by its quality factor Q , proportional to the average time during which a lasing photon is trapped inside the cavity boundaries. It can be defined through the following relation:

$$Q = 2\pi \nu \tau_{\text{cav}} = \frac{2\pi}{\lambda \alpha_{\text{cav}}} \quad (3.6)$$

Here, ν is the lasing frequency, τ_{cav} is the photon lifetime in the cavity, and α_{cav} is the associated losses, inversely proportional to τ_{cav} . A more complete discussion about the cavity in this model and the role of its quality factor is addressed in Section 3.3.3.

3.3.2 Limits and approximations

The simplicity of this model comes with a set of approximations that needs to be discussed in order to understand the limits of the equations.

First, we chose not to take into account the vibrational and rotational sub-levels of the different electronic states. This is due to the high efficiency of the non-radiative de-excitations between these sub-levels (ex: $S_{1,m}$) and the nearest ground vibrational level (ex: $S_{1,0}$, or simply S_1), which typically happen at the femtosecond scale [38], much faster than the typical nanosecond fluorescence lifetimes of most dyes. Rovibrational levels can be helpful to target key phenomena or study dynamics at a very short time, but they will not have much influence on the populations in continuous excitations. Furthermore, it will reduce the number of adjustable parameters and ease analytical demonstrations.

Regarding the triplet population, one can see that its only feeding term when the excitation starts is $k_{\text{ISC}}S_1$, implying that the only pathway through which they are created is *via* a fixed intersystem crossing rate when the fluorescence level is populated enough. Although other processes such as **S**inglet **F**ission has been described in Section 1.2.4.1, its presence in our configurations seems unlikely considering a $S_0 \rightarrow S_1$ transition of 2.5 eV in most organic compounds and an average $\Delta E_{\text{ST}} = E(S_1) - E(T_1)$ of 0.7 eV [9, 38, 37]. Furthermore, SSA (see Section 1.2.6.3 for details) will also not be implemented in the population equations, as it has been shown that it accounts for a negligible portion of the quenching of the S_1 state at usual excitation intensity ($\approx \text{kW}\cdot\text{cm}^{-2}$) [38]. Therefore, only ISC will account for the filling of the triplet state.

In this work, the density of active molecules in the film is conserved during the excitation so that at all time, the equality $S_0 + S_1 + T_1 = N$ (where N is the molecular density of the film) stands true. This assumption is supported by the absence of decreasing of the fluorescence intensity observed pulse after pulse in our experiments.

It is worth noticing that this work does not focus on co-doping configurations *i.e.* when two active compounds are mixed in the gain medium to enable, for instance, Förster transfers to seek longer emission wavelengths or to quench the triplet population with a so-called *triplet manager* [223, 157]. Many teams have worked on the subject and it will be an interesting perspective to apply the methodology of this thesis to such problematics but in this simulations, the gain medium is assumed to be dispersed in a neat matrix if nothing says otherwise. This choice is motivated by our desire to better understand CW lasing with BSBCz, which has been directly excited at 405 nm without passing *via* CBP molecules (playing the role of an inert host matrix).

In order to keep the focus of this thesis on triplet-related mechanisms and their influence on the lasing pulse duration, we also chose not to include in the equations the temperature dependence of the photophysical parameters. Indeed, since many processes depend on the vibration and/or rotation of active molecules, temperature

does play a role, especially at high excitation intensity [209, 45]. High-intensity pumping results in a localized heating of the film that can reach several tens of degrees, and sometimes approach the glass transition temperature T_g , which scales at about 120°C. In addition to non-radiative relaxations, an abrupt increase of the temperature inside the gain medium can accelerate the *photobleaching* from the T_1 state. As mentioned by Chua *et al.* [80], the quenching of the chromophore density can be due to several processes, including a high pump intensity resulting in the breaking of the long polymer carbon chains. For the case of low loss cavities however, it has been shown that quasi-continuous wave excitations (several tens of milliseconds) would result in a temperature elevation of less than 10 degrees [5] when the diffusion of the heat is properly dealt with.

At last, one might have noticed that the photon density is ruled by a unique equation, meaning that only one mode is allowed to exist inside the resonator while the spontaneous emission definition used is related to λ^3 multimodal cavities (*i.e.*, $\beta = 10^{-4}$ and the Purcell factor $F_p = 1$). Although the implementation of multimodal equations would be quite interesting to do especially for the screening of mode-locking requirements in OSSLS, the monomode approximation is assumed as this study had for first purpose to explain the different reports on BSBCz [5, 14, 74], which were at the time simulated using this very set of equations.

3.3.3 Resonator

As stated, one of the motivations for this work is to understand the difference between the results of Sandanayaka *et al.* [5, 14] and our results (Figure 3.1), both gain media being composed of a CBP film doped with BSBCz. Even though they have very different feedback mechanisms (see Section 1.1.5), it can eventually be boiled down to two gain media amplifying light between two different types of mirrors. Hence, as a first approach, both can be modeled *via* a confinement factor and a cavity lifetime using the same set of equations.

Since the volume of DFBs and VCSELs are larger than λ^3 , the so-called Purcell effect¹ is not to take into account, their spontaneous emission enhancement factor β will then scale to 10^{-4} . Their confinement factors are also very similar and are found to be between 0.1 and 0.7 [224, 225, 5].

On the other hand, these structures really have different lasing thresholds. Whereas in VCSELs, it scales around 10 kW.cm⁻² [226] or more, DFBs thresholds can top that by several orders of magnitude to reach values as low as 5 W.cm⁻², thanks to their feedback mechanism. Table 3.1 gathers devices whose lasing thresholds were 100 W.cm⁻², all were obtained using several types of DFBs. Hence, this important difference is the central point in this device comparison. Since a resonator quality factor is inversely proportional to its lasing threshold, it is expected

¹When the cavity becomes very short, a more important fraction of the photons emitted spontaneously feed the lasing mode, making it easier to reach the lasing threshold.

for DFBs and VCSELs to have very different Q .

materials	pulse duration (ns)	lasing threshold (W.cm ⁻²)	refs
BBEHP-PPV ^b	4	10	[147]
Fluorene based polymer ^c	10	3.6	[227]
9,9-dioctylfluorene with 9,9-di(2-methyl)butyl ^a	12	30	[228]
pyrene-cored 9,9-dialkylfluorene starbursts ^a	4.2	38-65	[229]
BBEHP-PPV ^b	4	122	[148]
BBEHP-PPV ^c	4	57	[148]
BBEHP-PPV ^c	4	50	[148]
CBP:BSBCz	10 ² -10 ⁶	5-75	[5]
PST-co-VBT doped with laser dye ^b	5	50	[230]
BBEHP-PPV ^b	4	15	[231]

a) 1st order b) 2nd order c) mix-order

Table 3.1: Lowest lasing thresholds reported in organic solid state lasers, where each was obtained using various types of **D**istributed **F**eed**B**ack (DFB) resonator.

3.3.4 Methods

3.3.4.1 Numerical algorithms

A detailed presentation of the numerical methods used in this work is provided in this section. The algorithm developed to discriminate lasing from fluorescence will be presented as well, followed by the techniques to evaluate the duration of a lasing pulse. At last, a typical output figure from these simulations will be displayed as an example and explained, to ease and quicken the interpretation of the following results.

The core of our algorithms relies on the ratio between the intensity inside the cavity, which is proportional to the photon density, and the saturation intensity of the gain medium lasing transition. The saturation intensity I_{sat} is defined as the intra-cavity intensity for which stimulated emission is equal to spontaneous emission. As such, it can be written as:

$$I_{\text{sat}} = \frac{1}{\sigma_{\text{em}}\tau_f} \quad (3.7)$$

where τ_f is the fluorescence lifetime and σ_{em} the stimulated emission cross section. More physically, configurations where the intracavity intensity I is comparable or above I_{sat} can be interpreted as lasing occurring. Therefore, it allows a complete monitoring of the lasing intensity with time and thus ease the computation of the pulse duration. Because it is surprisingly not trivial to discriminate lasing from fluorescence from rates equations, and that this ratio of intensity is rather easy to implement in a program, this approach has been chosen for this work.

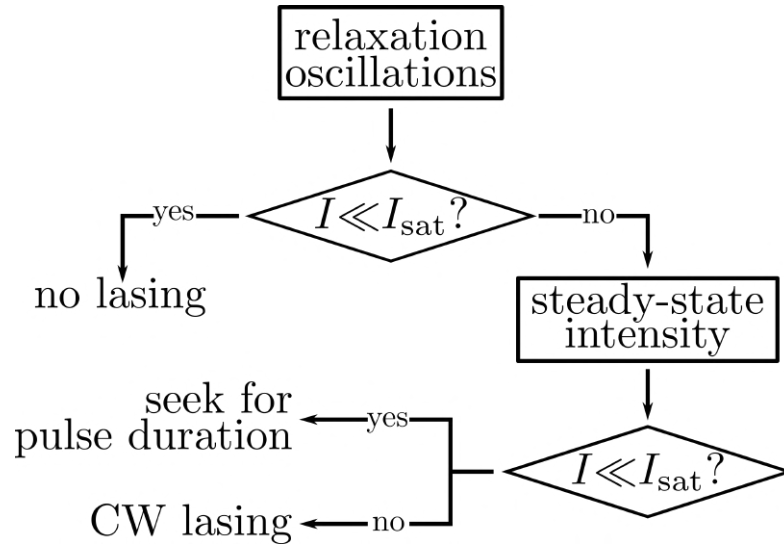


Figure 3.2: Algorithm used in this work to discriminate emission regimes and compute the lasing pulse duration

This paragraph aims at providing every relevant details regarding how the simulations were processed so that everyone can understand the advantages of this method but also its limits. To ease the reading, this documentation is written in the form of a list, where each step will develop one box of Figure 3.2.

The first step for each simulation conducted in this work is the integration of the rate equations for the first 30 nanoseconds. This temporality has been chosen because it matches the end of the relaxation oscillations plus a safety margin. At $t = 30$ ns, the program records the value of the ratio I/I_{sat} and check whether or not it is inferior to 10^{-2} . If it is the case, it is considered that the population inversion imposed by the resonator is too high for lasing to occur, as it can be seen on the blue curve of Figure 3.3. Of course, it could mean that lasing did in fact happen before and lasted only a few nanoseconds, but since this work targets continuous-wave lasing and how long pulsed emissions end, we have no particular interests in working with such short emissions. If, at 30 ns, I/I_{sat} is above 10^{-2} (like orange and green curves on Figure 3.3), it is considered that lasing is happening and the integration can go on for longer times. Although a more proper way to discriminate lasing from fluorescence would rely on the direct detection of relaxation oscillations for it is the clearest sign of lasing, it would also consume a lot more CPU resources considering the millions of points done for this work.

When lasing is "detected", the program will continue to integrate the equation until eventually I/I_{sat} reaches a steady-state value. For the solver to know when to stop, the integration of the system is done 5 microseconds at a time. At the end of each step, the difference in intensity between its last and first point is computed, and it is considered that I/I_{sat} is constant when this difference is lower than 10^{-5} . If it is not, meaning that the intensity is still in a transient dynamics, the solver

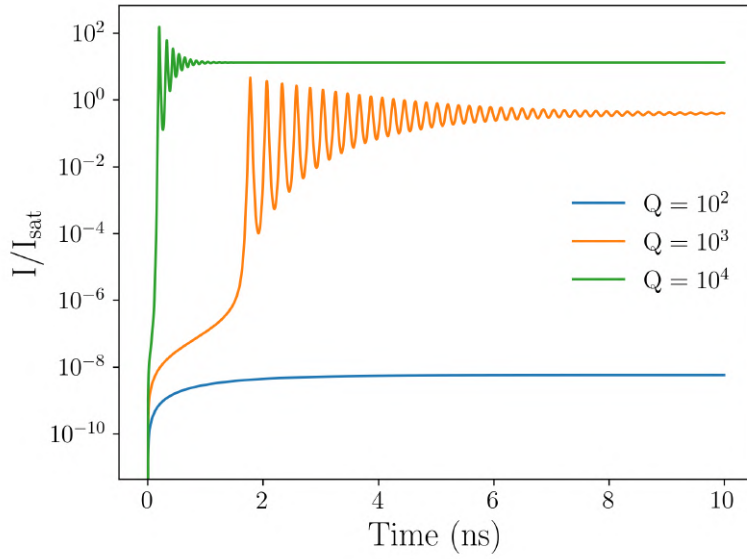


Figure 3.3: Time resolved simulations of the normalized intracavity intensity for different quality factors. The blue case shows only fluorescence whereas the others clearly show lasing. I/I_{sat} allows us to efficiently discriminate the two possibilities.

moves on to the next time step and do the same checkings 5 microseconds later.

The last step depends on the value the intensity reaches when it is stabilized. If it is superior to $10^{-2} \times I_{\text{sat}}$, lasing is considered continuous like for the green curve on Figure 3.4. Otherwise, it is considered a pulsed emission and the duration of this pulse has been evaluated, which would be the case for the orange curve on the same figure. Although this choice is arbitrary, there is always a fundamental difference between these two cases: when I/I_{sat} reaches a very low value, 10^{-7} here, it is always after a brutal decrease of the intensity, indicating the moment where the lasing pulse ended. On this matter, once the program has stated that the intensity corresponds to a lasing pulse that has died, it computes the derivative of the whole temporal signal to find the maximum and interprets it as the end of the lasing pulse. Note that the relaxation oscillations can't be taken into account in this step, as it could result in false data.

In order to save time and CPU resources, the program stops when one of these finalities illustrated on Figure 3.2 is reached. It is especially useful in the case of true continuous-wave lasing, for which the intensity reaches a constant value very soon by definition.

This tutorial ends with an example in the form of Figure 3.5, which represents a typical output of the code we just discussed and contains many informations. Hence, it appears necessary to take a moment and present it in details once and for all. This figure displays the lasing regimes that were reached after an integration time of two milliseconds for different quality factors and pump power densities. In fact, the output of no less than 10000 (100x100) simulations are gathered to draw

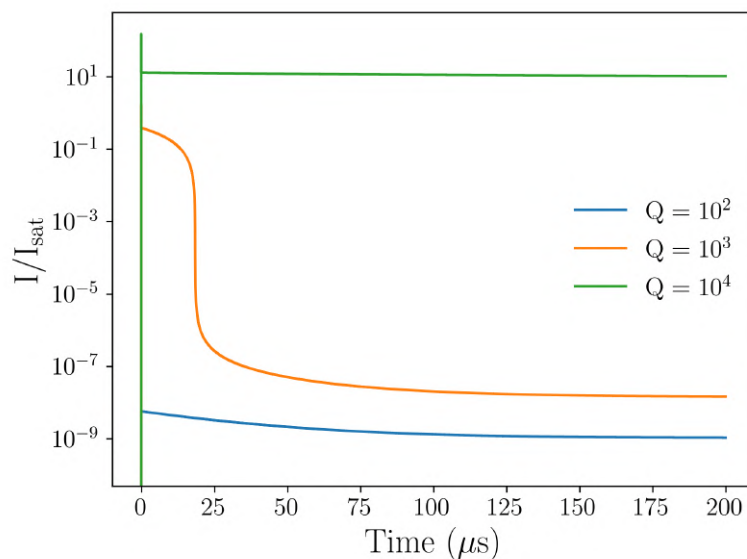


Figure 3.4: Time resolved simulations of the normalized intracavity intensity for different quality factors. The blue case shows only fluorescence whereas the orange curve is a lasing pulse that stops with the vertical fall of I/I_{sat} . The green curve corresponds to CW lasing. I/I_{sat} allows us to efficiently discriminate the two possibilities.

this 2D map of lasing regimes. Each point of this figure comes from temporal simulations and the use of the algorithms mentioned earlier.

Three areas of interest standing for the three finalities sketched on Figure 3.2: the black zone corresponds to configurations of Q and I_p where lasing does not occur, whereas the red zone corresponds to a continuous-wave emission. Finally, the rainbow stands for lasing pulses, whose durations are readable on the colormap at the right of the main plot. So, if we choose a vertical slice of this map for a quality factor of 10^4 and we increase the pump intensity, lasing will be possible for $I_p \approx 700 \text{ W.cm}^{-2}$, whereas one would have to reach 21 kW.cm^{-2} to get a CW lasing emission.

When possible, analytical expressions may be scattered on top of the simulations as the white dots to vouch for the goodness of our algorithms. Since, as it has been said, a few arbitrary choices must be done, it is always a good call to check if an analytical solution match the numerical integration of the equations.

3.3.4.2 Theoretical analysis: the example of the four-level system

It has been mentioned that this work also relies on analytical expressions to provide a greater view of the influence of optical and photophysical parameters on the lasing pulse duration. In order for the reader to fully understand how such-and-such expression is obtained, it is necessary to describe in detail the method that has been used. To do so, we will present it with a simplified version of Equations 3.2-3.5

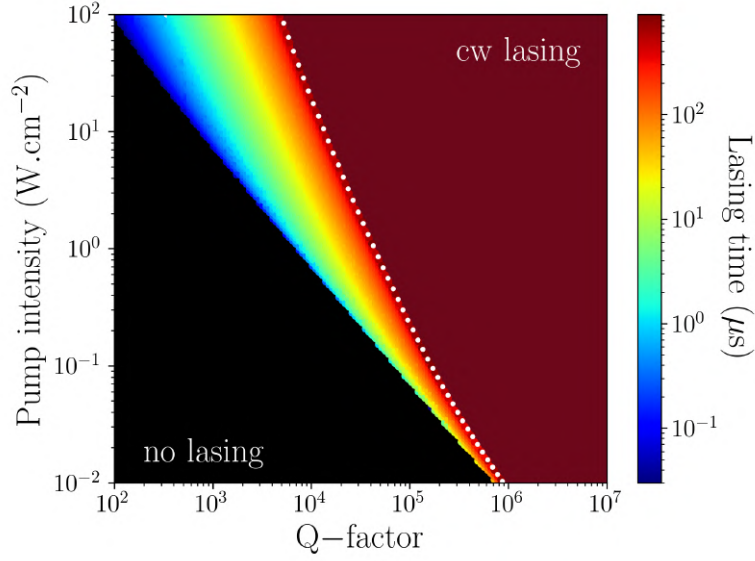


Figure 3.5: Lasing regime achieved as a function of the pump power density and the quality factor of the resonator. Black) no lasing, rainbow) pulsed emission (whose duration is indicated on the colormap), red) CW lasing. White dots correspond to analytical solution of the pump fluence required to enable CW lasing. $k_{\text{ISC}} = 6 \times 10^6 \text{ s}^{-1}$, $k_{\text{STA}} = 10^{-10} \text{ cm}^3 \cdot \text{s}^{-1}$.

in which there are no triplets. This configuration, modeled with Equation 3.8 to 3.10, is commonly mentioned as a *four-level* system, as everything happens between two electronics states (and their rovibrational sub-levels) just as represented on Figure 1.3. Besides the advantage of being much simpler, results obtained from this system will serve as a reference for further comparisons with more complex systems.

In this thesis, triplets are only created by intersystem crossing from S_1 to T_1 , so one just has to zero k_{ISC} to cancel their generation and hence, every subsequent bi-exciton interactions. With triplets being out of the equations, we reach a system that has only two finalities: no lasing at all, or an endless lasing emission, as in the case of inorganic crystals. The initial system of equations can therefore be reduced to:

$$\frac{dS_1}{dt} = R_{\text{ex}}S_0 - (k_f + R_l)S_1 \quad (3.8)$$

$$\frac{dS_0}{dt} = -R_{\text{ex}}S_0 + (k_f + R_l)S_1 \quad (3.9)$$

$$\frac{dI}{dt} = \frac{c}{n}\Gamma\sigma_e S_1(I + I_{\text{sp}}) - \frac{2\pi c}{Q\lambda_l}I \quad (3.10)$$

Zeroing Equation 3.10 gives us S_1^{cav} the clamping of the fluorescence imposed

by the resonator². In other words, when the gain medium is excited, the density of S_1 excitons needed to inverse the populations of the lasing transition will be fixed mostly by the confinement factor of the cavity and its quality factor. By reducing the losses of the cavity, Q increases, making S_1^{cav} lower.

$$S_1^{\text{cav}} = \frac{2\pi n}{\Gamma\lambda_l\sigma_{\text{em}}Q} \quad (3.11)$$

Although S_1^{cav} is an important variable, the comparison with S_1^{th} is even more relevant. This quantity, obtained by zeroing Equation 3.8, accounts for the maximum population inversion one gain medium can provide in order to exhibit a lasing emission.

$$S_1^{\text{th}} = \frac{N}{1 + \frac{k_f}{R_{\text{ex}}} + \frac{R_l}{R_{\text{ex}}}} \quad (3.12)$$

If S_1^{cav} is found to be superior to S_1^{th} (due to poor mirrors for instance), lasing will not be possible. Considering pumping rates from 10^4 to 10^7 s^{-1} (100 $\text{W}\cdot\text{cm}^{-2}$ to 100 $\text{kW}\cdot\text{cm}^{-2}$ for $\sigma_{\text{abs}} = 10^{-20}$ m^2), it is clear that the threshold will be mostly driven by the gain medium photophysical properties, here its fluorescence lifetime through the ratio k_f/R_{ex} .

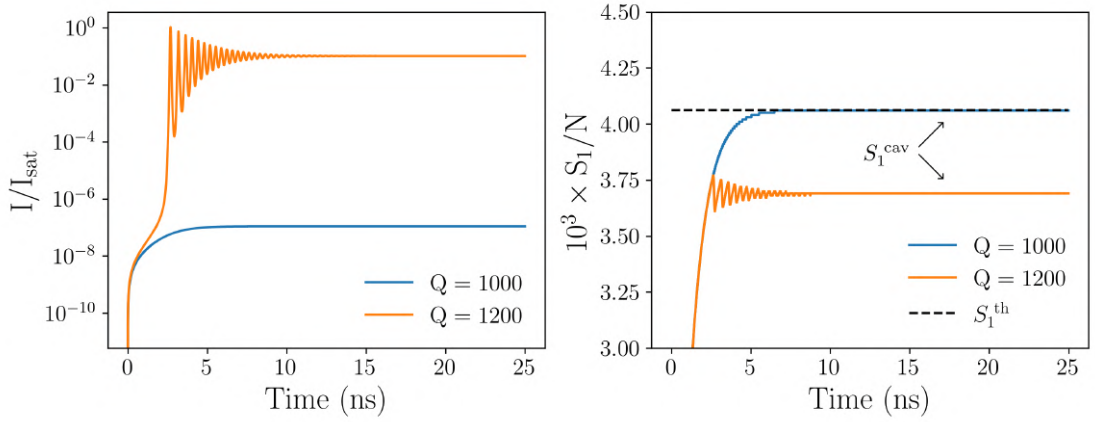


Figure 3.6: Time-resolved simulations of singlets (left) and photons density inside the cavity (right) for different quality factors. $k_f = 10^9$ s^{-1} , $\sigma_{\text{abs}} = 10^{-16}$ cm^2 , $I_p = 20$ $\text{kW}\cdot\text{cm}^{-2}$, $N = 10^{27}$ m^{-3} . S_1^{th} is computed after Equation 3.12.

The relation between S_1^{cav} and S_1^{th} is illustrated on Figure 3.6, where simulations with time of the fluorescence populations and the intra-cavity intensity are presented for various quality factors. When the quality factor is too low, the intra-cavity intensity never reaches the saturation intensity. Hence, only fluorescence through spontaneous emission will occur as described in the previous section.

²It is considered that the intensity emerging from spontaneous emission quickly becomes negligible compared to the intensity coming from stimulated photons

Because it is always more interesting to work with quantities that are easily measurable, these derivations are centered around two reachable parameters: the quality factor Q and the pump power density required to achieve CW I_p^{th} , written in Equation 3.13. It can be obtained by equalizing S_1^{cav} and S_1^{th} and reshaping the expression until the intra-cavity intensity is expressed in the form $I = \eta(I_p - I_p^{\text{th}})$, where η is the quantum efficiency (the slope), I_p the pump power density ($\text{W}\cdot\text{m}^{-2}$). The complete derivation of this result is presented in Appendix 4.2.

$$I_p^{\text{th}} = \frac{k_f}{\sigma_{\text{abs}}} \frac{1}{\frac{N}{S_1^{\text{cav}}} - 1} \quad (3.13)$$

In a configuration without any triplets, it depends only on the fluorescence lifetime, on the absorption cross section of the gain medium, and on the ratio between the population inversion imposed by the resonator and the molecular density of the film. Again, it is visible in this expression that a high quality factor will decrease the lasing threshold of the device, as S_1^{cav} is proportional to $1/Q$.

Since the density of S_1 excitons cannot be superior to the density of active molecules in the gain medium (I_p^{th} would become negative), it is possible to extract the quality factor required to achieve lasing (i.e. satisfy the equality $S_1^{\text{cav}} = S_1^{\text{th}}$). We quickly obtain the following expression:

$$Q \geq Q_{\text{th}} = \frac{2\pi n}{\lambda_l \Gamma \sigma_{\text{em}} N} \quad (3.14)$$

Although it stands very low given the absence of triplets, it is interesting to see that there is a minimal quality factor to have to achieve lasing in this *lossless* configuration. If we choose typical values for each parameters ($\sigma_{\text{em}} = 10^{-20} \text{ m}^2$, $\Gamma = 0.5$, $N = 10^{26} \text{ m}^{-3}$, $\lambda_l = 500 \text{ nm}$, $n = 1.8$), we obtain $Q \approx 50$, but this value can be at least one order of magnitude higher for lower doping ratios.

The next step of this analysis is to use the algorithms presented in Section 3.3.4.1 for a large range of quality factors and pump power densities. The results for this configuration are presented on Figure 3.7. As stated, a system without any triplets comes with two finalities: no lasing (black color) and CW lasing (ref color).

It makes then perfectly sense not to see any pulsed emission regime on this figure. Although the algorithms we developed to discriminate lasing contains a few arbitrary choices, one can see that the exact solution for the threshold in Equation 3.13 is in a perfect agreement with our approximations. Besides the trivial observation that when the quality factor decreases, the pump power needed to achieve lasing increases, the main point of Figure 3.7 is to be used as a reference. Indeed, an important point of this work will be to study how these trends evolve in more complex photophysical configurations.

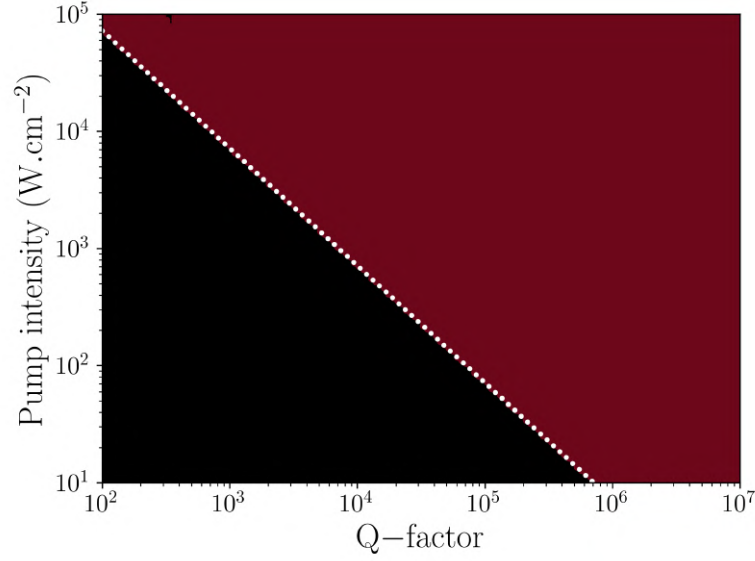


Figure 3.7: Lasing regime achieved as a function of the pump power density and the quality factor of the resonator without any triplets ($k_{\text{ISC}} = 0$). White dots correspond to Equation 3.13.

3.4 Results

This section will be presented in a step-by-step approach, starting from simple configurations to more complex systems where different mechanisms will be turned on to study their influences on the population dynamics.

3.4.1 Enabling the generation of triplet excitons

To understand how triplets affect the lasing capabilities of one device, we will first only consider their generation *via* intersystem crossing (see Section 1.2.4.1), as their role here will be strictly limited to drain the excited singlet state through the term $k_{\text{ISC}}S_1$ (*i.e.* $k_{\text{STA}} = k_{\text{TTA}} = \sigma_{\text{TA}} = 0$) and to decay non-radiatively back the ground state.

Since ISC does not have a direct influence on the photon density, the expression of S_1^{cav} will remain the same as Equation 3.11, meaning that the population inversion required to achieve lasing is imposed by the cavity in any case. On the other side, the upper limit of singlet excitons required by the gain medium to inverse the populations will be different, considering this new loss pathway. Rather than looking for an equilibrium between two levels, the system has to reach a steady-state value for the S_0 , S_1 , and T_1 populations which satisfies the relation $S_1^{\text{cav}} = S_1^{\text{th}}$. This updated threshold is expressed by Equation 3.15.

$$S_1^{\text{th}} = \frac{N}{1 + \frac{k_f}{R_{\text{ex}}} + \frac{R_l}{R_{\text{ex}}} + \frac{k_{\text{ISC}}}{k_t} + \frac{k_{\text{ISC}}}{R_{\text{ex}}}} \quad (3.15)$$

Unlike the simpler case of Equation 3.12, two terms driven by k_{ISC} come to increase the quality factor required to achieve lasing (by lowering S_1^{th}). Considering usual values of R_{ex} ranging between 10^4 and 10^7 s^{-1} (10^2 to 10^5 W.cm^{-2} with σ_{abs} set to 10^{-16} cm^2), and the mentioned typical decay rates for k_{ISC} and k_t (10^7 and 10^3 s^{-1}), both terms $k_{\text{ISC}}/R_{\text{ex}}$ and k_{ISC}/k_t will have an important role.

As presented, we are able from the expressions of S_1^{cav} and S_1^{th} to derive the pump intensity lasing threshold, expressed in this configuration as Equation 3.16. Since k_{ISC} is much smaller than k_f ($\approx 10^9 \text{ s}^{-1}$) in most compounds, the only term that will contribute to the increase of the lasing threshold of one device is k_{ISC}/k_t . This ratio keeps appearing everywhere and there is a good reason for that: it represents the ratio between the growth of the triplet population and its decay. For a system to be efficient, it has either to lower k_{ISC} or to increase k_t . The faucet analogy is very useful here to have a proper view of the problem. If one has a bucket with a hole at its base and a continuous stream of water, he has only two adjustable parameters to vary the level at which the water will stabilize: the flow of the faucet (k_{ISC}) or the hole diameter (k_t).

$$I_p^{\text{th}} = \frac{k_f \left[1 + \frac{k_{\text{ISC}}}{k_f} \right]}{\sigma_{\text{abs}} \left[\frac{N}{S_1^{\text{cav}}} - \left(1 + \frac{k_{\text{ISC}}}{k_t} \right) \right]} \quad (3.16)$$

Interestingly, and even though other loss sources (TA, STA) are not taken into account yet, the minimal quality factor required to obtain CW lasing already appears to be quite high, three to four orders of magnitude higher than the one derived for the four-level system where k_{ISC} was set to zero.

$$Q_{\text{th}} = \frac{2\pi n}{\lambda_l \Gamma \sigma_{\text{em}} N} \left[1 + \frac{k_{\text{ISC}}}{k_t} \right] \quad (3.17)$$

It is considered that the system has reached a steady state, meaning that the populations of the different electronic levels balance each other. Thus, we can go further and derive the total triplet population that the laser must not reach to achieve CW lasing. It is expressed in Equation 3.18 in the form of a ratio between the S_1 and T_1 exciton densities (provided that k_{ISC}/k_t is much larger than unity).

$$\frac{S_1}{T_1} \geq \frac{2\pi n}{N \Gamma \sigma_{\text{em}} \lambda_l Q} \quad (3.18)$$

This expression tells us that if the triplet population becomes too important (due to a high k_{ISC} or a low triplet lifetime), lasing will stop. To illustrate this relation, we plotted on Figure 3.8 the temporal evolution of the S_1 and T_1 populations (normalized to N the total density of active molecule), with the normalized intracavity intensity for different ISC rate constants.

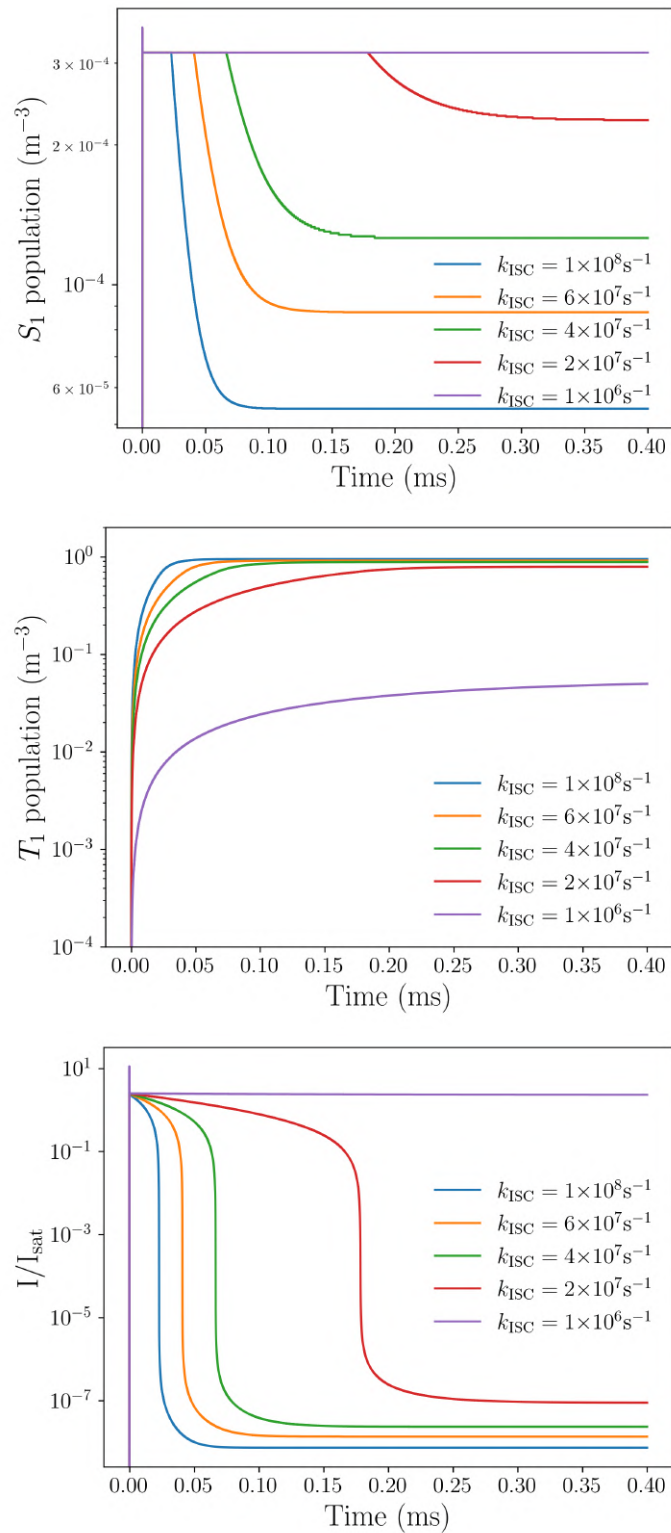


Figure 3.8: Time-resolved simulations of the S_1 and T_1 population densities (top left and right, respectively), and the intracavity intensity (bottom) for different k_{ISC} . $Q = 5 \times 10^3$, $I_p = 5 \text{ kW.cm}^{-2}$.

We see on the top figure that the singlet population, at early times, exhibits oscillation relaxations followed by a steady state. The reason for this clamping value to be independent of k_{ISC} lies in the quantity S_1^{cav} from Equation 3.11, which does not depend on the ISC rate but only on the quality factor of the device (which is the same for every simulations of Figure 3.8). What is interesting is to understand why the clamping stops at one point and what value reaches the S_1 population afterwards but mostly, what are the consequences on the lasing emission.

The monitoring of the triplet population brings some answers. First, its growth with time is explained by this equation:

$$\frac{dT_1}{dt} = k_{\text{ISC}}S_1 - k_tT_1 \quad (3.19)$$

and by the fact that the source term inside is basically constant as long as the clamping is maintained. It is shown here that if k_{ISC} is important enough, the ratio T_1/N quickly reaches unity, the ground state is then completely depleted and no clamping of the population inversion can hold anymore. Moreover, the clamping disappears quicker when k_{ISC} is higher because the triplet population increases much faster, an interpretation that was already discussed in Equation 3.18 with the ratio between the singlet and triplet populations. In the case where $k_{\text{ISC}} = 10^6 \text{ s}^{-1}$, the T_1 density never reaches a critical value that would invalidate Equation 3.18 and therefore, the lasing is continuous over time.

Since lasing is only possible if the population inversion is clamped, this analysis on the exciton density with time explains how the lasing pulse ends at the same time as the brutal decrease of the singlet density. At the end, this is the main difference with a perfect four-level system and this is why they are binary systems: either on or off, no pulse. Because, once you have a high enough quality factor, the population inversion clamping will not be compromised if there is no additional losses such as triplets.

After studying the temporal influences of intersystem crossing on the different excited populations, we worked on a broader image regarding the different emission regimes that could be achieved in the presence of ISC for different quality factors and pump power densities. The results are presented on Figure 3.9 for four different values of k_{ISC} and a fixed value of $175 \mu\text{s}$ for the triplet lifetime. As explained in Section 3.3.4.1, each point of these 2D figures represents a numerical integration of the main system of equations at fixed quality factor Q and pump power density I_p . Doing so for a wide range of values allow us to study how different devices would react to optical and photophysical changes. See section of interest for details about the algorithms used to provide the results.

It has been mentioned in Section 1.3 that Zhang and Forrest [157] reported the existence of two thresholds: the classical lasing threshold leading to pulsed emissions and, with an increase of the excitation density, a threshold leading to a

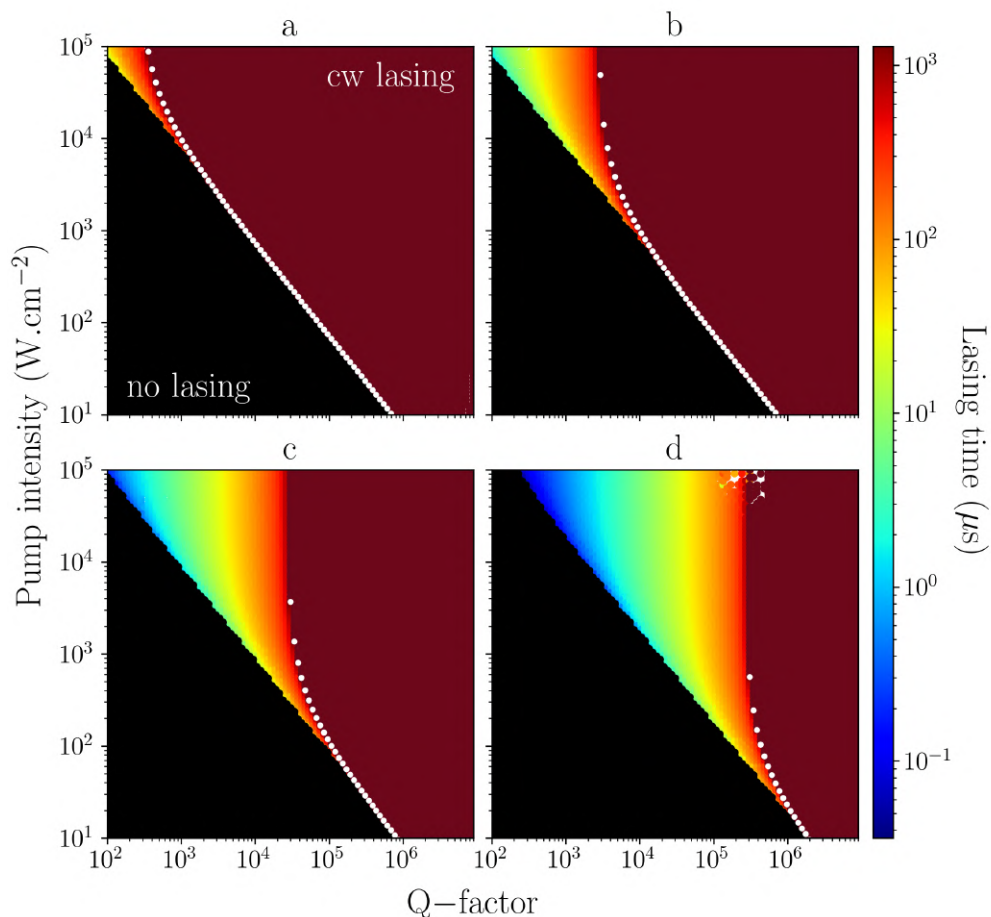


Figure 3.9: Lasing regime achieved as a function of the pump power density and the quality factor of the resonator with $k_{\text{ISC}} =$ a) 10^6 b) 10^7 c) 10^8 d) 10^9 s^{-1} . White dots correspond to Equation 3.16.

CW regime. Both thresholds can be seen for instance on Figure 3.9.c ($k_{\text{ISC}} = 10^8$ s^{-1}) where a resonator with a quality factor of $\approx 3 \times 10^4$ exhibits two clear thresholds symbolized by the black-rainbow frontier (I_{PS} in their paper) and the rainbow-red frontier at higher pump fluence (I_{CW} in their paper). They also emphasize the fact when losses due to triplets become negligible (with the addition of a triplet manager in their case that limits the saturation of the active triplet molecules), both thresholds would merge, which was also obtained by our simulations in the case of a simple monomolecular gain medium. Indeed, keeping the same resonator (its Q-factor) and lowering k_{ISC} as on Figure 3.9.a or 3.9.b results in the deletion of the pulsed regime, making it easier to reach a CW emission.

Moreover, these simulations allows us to provide additional points of interest by actively taking into account the quality factor. First, computations show that an increase of the quality factor allows a merging of the lasing and CW pump threshold, as reported by Zhang and Forrest in the case of triplet-related losses. If

we take again the case above mentioned on Figure 3.9.c, a decrease of the lasing threshold from 100 to $\approx 50 \text{ W.cm}^{-2}$ would allow one to reach a CW emission without the need of a more important pump fluence of elongate more and more lasing pulses. This conclusion can be understood in terms of laser dynamics, since a lower threshold means that less singlet excitons are required to inverse the population of the lasing transition, leading to less triplet created. Eventually when the Q-factor becomes very high, triplets and their influences become negligible.

Another interesting point that has not, to our knowledge, been emphasized previously is the existence of a minimal quality factor for a resonator to have in order to achieve a CW emission, represented by a vertical asymptotes on Figure 3.9. This critical Q-factor corresponds to cases where I_p^{th} from Equation 3.16 tends towards infinity and indicates that no CW lasing could ever be achieved in a given photophysical configuration if the device lasing threshold stands too high. It can also be highlighted that it depends dramatically on k_{ISC} , which was expected based on Equation 3.17 where Q_{th} is mostly ruled by the ratio k_{ISC}/k_t .

Moreover, Equation 3.17 emphasizes that the concentration of active molecules is also to take into account, as N is inversely proportional to Q_{th} . For instance, the difference reaches a factor of 100 for Q_{th} at concentrations of 1 and 100 wt.%, indicating that CW lasing is only possible at high concentrations.

Although this configuration where only ISC intervenes seems utopian (even though the results achieved with BSBCz were ascribed to a complete removal of other triplet-related losses such as STA [14]), these results provides primary insights on the discrimination one can make between such-and-such resonators regarding lasing pulse durations. In this case for instance, if one choose an ISC rate between 10^7 and 10^8 s^{-1} (between Figure 3.9.b and 3.9.c), Q_{th} goes from 4×10^3 to 4×10^4 for lasing thresholds of 1 and 0.2 kW.cm^{-2} , which is below what have been reported for organic VCSELs [226].

3.4.2 Other losses mechanisms

The generation of triplets *via* intersystem crossing and its influence, coupled with those of optical parameters, has been studied in the previous section and is now better understood, the goal is to go further and implement other triplets related losses that are thought to have an important influence on organic lasers. This section will focus on two sources of interest: singlet-triplet annihilation and triplet absorption. Both have been defined in Section 1.2.4.3 and 1.2.6.1 and have been extensively studied in the past for their role in the quenching of lasing emission.

3.4.2.1 Singlet-triplet annihilation

It has been stated in the introduction that when an excited triplet exciton is created, *via* intersystem crossing or *via* other routes, it has the possibility to interact with singlet excitons at long distance [38] in the form of:



Because this annihilation will directly contribute to the loss of one singlet exciton, many teams have worked on proper ways to overcome its influence as it is thought to be a major limitation towards a true continuous-wave lasing in organic lasers [145, 155, 232].

In this work, STA does not appear in the equation governing the triplet state as it is assumed that triplets promoted to a higher excited state T_n will decay back very fast to the T_1 state in a non radiative way. Before dealing with lasing regimes, we focused on the exciton population densities to understand how STA interacts with each level of energy. The equation ruling the population densities can be written as Equation 3.2 to 3.4 with k_{TTA} set to zero.

Figure 3.10 has been obtained by a direct integration of the population equations without any resonator (*i.e.* $\sigma_{\text{em}}I = 0$) and shows a more complex interaction than originally thought. On one hand, STA does contribute to the quenching of the fluorescence because of the term $k_{\text{STA}}S_1T_1$ in the singlet equation. Since it offers an other de-excitation road to the S_1 state, we see that it also contributes to decrease the effective fluorescence lifetime τ_f of the molecule.

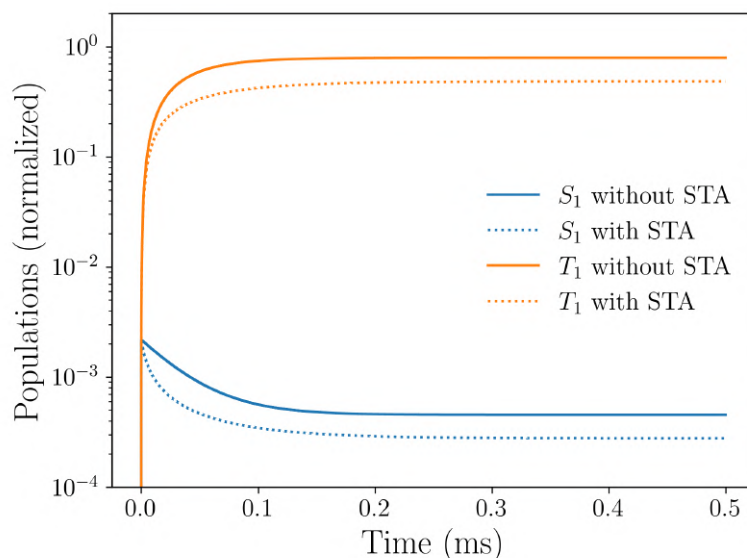


Figure 3.10: Time resolved simulations of the singlet and triplet populations with and without STA. Populations are normalized to the total density of active molecule N in the gain medium. $k_{\text{STA}} = 5 \times 10^{-12} \text{ cm}^3 \cdot \text{s}^{-1}$, $k_{\text{ISC}} = 10^7 \text{ s}^{-1}$.

On the other hand, STA surprisingly contributes to lower the triplet population even though, as said, our model assumes that it does not directly affect the triplet population. It could be explained by a reduced triplet lifetime if k_{STA} was implemented in the triplet equation but it is not. Besides, we do not observe on Figure 3.10 any reduction as we see for the S_1 evolution. This influence on the

triplet population is in fact indirect, as it is just the reflection of the quenching of the fluorescence: if less singlet excitons are available to undergo intersystem crossing, less will be transferred to the triplet state. Even though k_{STA} has been set here to a value that is typically one or two orders of magnitude lower than what has been reported in most organic compounds, it is interesting to see that it is enough to account for the annihilation of about 30% of both singlets and triplets.

Because STA influences both singlet and triplet populations equally, its influence on the lasing intensity is not obvious yet, and a deeper analysis is required to understand it. Since it has no direct influence on the photon density, the equation governing the intracavity intensity will remain unchanged compared to the four-level configuration (Equation 3.10). Although the term $k_{\text{STA}}S_1T_1$ introduces non-linearities in the rate equations, there are still matter to discuss and useful expressions to derive. Hence, zeroing Equation 3.2 gives us the following second order polynomial expression:

$$-\frac{k_{\text{STA}}k_{\text{ISC}}}{k_t}S_1^2 - (R_{\text{ex}} + \frac{k_{\text{ISC}}}{k_t}R_{\text{ex}} + k_f + k_{\text{ISC}} + \sigma_{\text{em}}I)S_1 + R_{\text{ex}}N = 0 \quad (3.21)$$

which leads us to this expression for S_1^{th} the population inversion one resonator has to lower to obtain lasing:

$$S_1^{\text{th}} = \frac{-b - \sqrt{b^2 - 4ac}}{2a} \quad (3.22)$$

with:

$$\begin{cases} a = -\frac{k_{\text{STA}}k_{\text{ISC}}}{k_t} \\ b = -(R_{\text{ex}} + \frac{k_{\text{ISC}}}{k_t}R_{\text{ex}} + k_f + k_{\text{ISC}} + \sigma_{\text{em}}I) \\ c = R_{\text{ex}}N \end{cases} \quad (3.23)$$

Even though the non-linearities prevent the obtention of an expression that could be quantitatively compared to Equation 3.15, it is still interesting to see that k_{STA} is only present in one term and is coupled in a non-intuitive way with the ratio k_{ISC}/k_t . If one equalizes S_1^{th} to S_1^{cav} (whose expression is the same as with only ISC), the quality factor required to achieve lasing versus k_{ISC} and k_{STA} can be expressed as:

$$Q = \frac{2\pi n_{\text{eff}}}{\Gamma\lambda_l\sigma_{\text{em}}S_1^{\text{th}}} \quad (3.24)$$

with S_1^{th} the solution 3.25. For visualization purposes³, we computed Equation

³Meaning that, although it can have useful outcomes, no researcher would ever think this way to engineer a lasing device as it has no practical applications.

3.24 for a wide range of ISC and STA constants. Results are presented on Figure 3.11.

Several points of interest: First, it is necessary in our configuration to have at least a quality factor of 10^3 , regardless of how low k_{ISC} and k_{STA} scale. Then, it is clear that STA will increase the Q required to achieve lasing, it is especially visible with the breaking of the vertical asymptotes, meaning that STA has influence only beyond a certain value that depends on k_{ISC} . If $k_{\text{ISC}} = 10^7 \text{ s}^{-1}$, k_{STA} would have to scale above $10^{-12} \text{ cm}^3 \cdot \text{s}^{-1}$ to account in the photophysics of the gain medium. When k_{ISC} is stronger, the number of triplets generated increases proportionally and hence, a higher k_{STA} is needed to have some influence on the overall exciton statistics. This representation of a simple analytical expression illustrates perfectly how molecules with not so good intrinsic properties could not be used, as the quality factor of the cavity reaches unrealistic values very quickly.

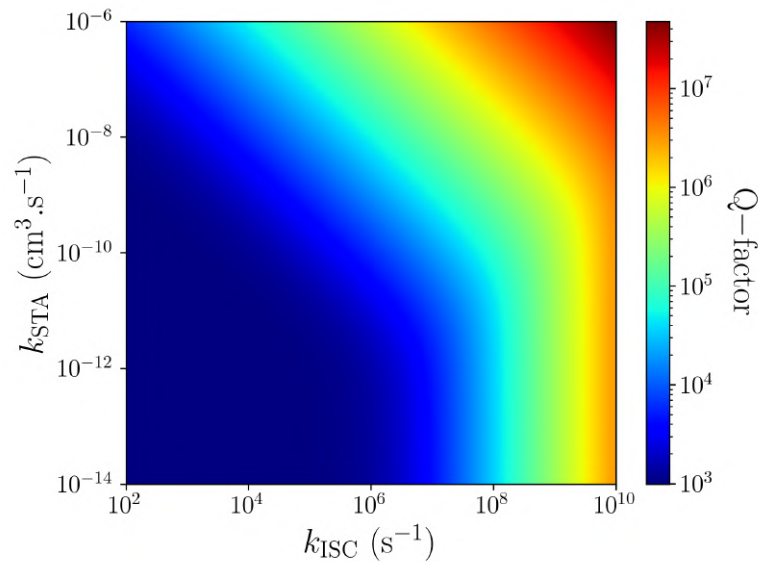


Figure 3.11: Quality factor required to achieve a continuous-wave lasing as a function of ISC and STA constants based on Equation 3.22. $I_p = 10 \text{ kW} \cdot \text{cm}^{-2}$.

As in previous configurations, the pump intensity threshold is a useful quantity to look at to understand one interaction. Fortunately, its derivation in the presence of STA allows the simplification of the non-linearities (with only a few more calculus steps that are detailed in Appendix 4.2) and thus, can be written as:

$$I_p^{\text{th}} = \frac{k_f \left[1 + \frac{k_{\text{ISC}}}{k_f} + \frac{k_{\text{STA}} k_{\text{ISC}}}{k_t k_f} S_1^{\text{cav}} \right]}{\sigma_{\text{abs}} \left[\frac{N}{S_1^{\text{cav}}} - \left(1 + \frac{k_{\text{ISC}}}{k_t} \right) \right]} \quad (3.25)$$

Compared to Equation 3.16 obtained with only ISC taken into account, one

term is added to the numerator containing k_{STA} and the ratio k_{ISC}/k_t that was discussed earlier. Since STA represents a loss of singlets, it is expected that this additional term will increase the CW lasing threshold. If we focus on the efficiency η , as expressed in Equation 3.26, our derivation indicates that it has no influence on it.

$$\eta = \frac{\sigma_{\text{abs}}}{\sigma_{\text{em}}} \times \left[\frac{N}{S_1^{\text{cav}}} - \left(1 + \frac{k_{\text{ISC}}}{k_t}\right) \right] \quad (3.26)$$

Equation 3.25 is plotted on Figure 3.12 for various k_{ISC} and k_{STA} at fixed quality factor, illustrating with the grey area the range of ISC constant for which the denominator of I_p^{th} would be negative, as stated previously in Equation 3.17. Moreover, the important blue zone where I_p^{th} is at the lowest and seems independent of k_{ISC} and k_{STA} is due to the fluorescence lifetime on its denominator, which is in most cases far superior to the ratio k_{ISC}/k_t . The results linked to high k_{ISC} near the limit area in grey are not physical, as they are caused by computational limits

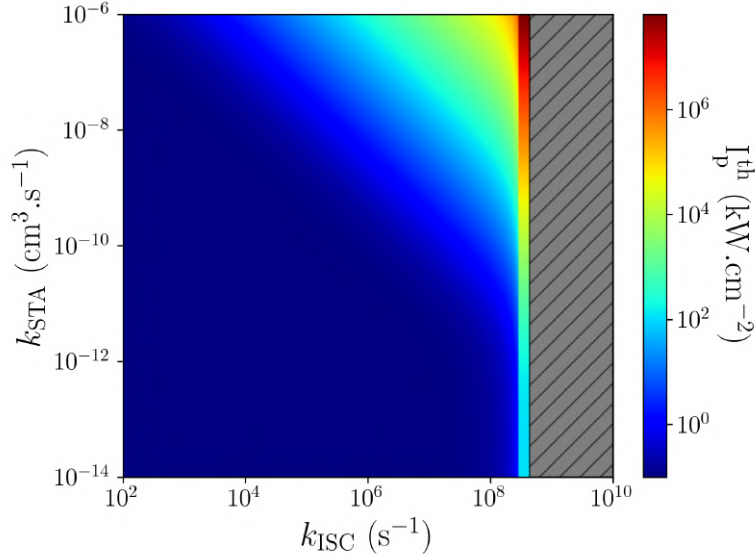


Figure 3.12: Pump intensity required to achieve continuous-wave lasing at fixed quality factor versus k_{ISC} and k_{STA} based on Equation 3.25. Dashed area corresponds to a negative denominator. $Q = 5 \times 10^3$.

More relevant, the lasing pulse durations to expect at fixed conditions of pump intensity and quality factor are sketched on Figure 3.13. Contrarily to Figure 3.11 and 3.12 that are based on analytical expressions, these results (especially the lasing pulse duration) can only be obtained by numerical integration of the main equations since our analysis can only unravel stationary states.

Once again, the white dots shows that our algorithms are in total agreement with the analytical expression of I_p^{th} . We also see that STA does not have any influence below $10^{-12} \text{ cm}^3 \cdot \text{s}^{-1}$ as shown on Figure 3.11. Under this value, the simulations behave as if only intersystem crossing was implemented, hence the min-

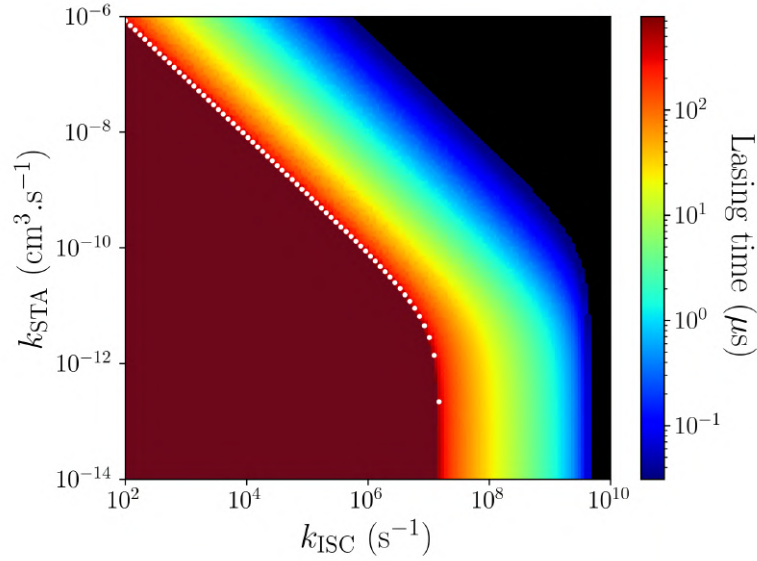


Figure 3.13: Lasing regimes achieved as a function of ISC and STA rates with $I_p = 10 \text{ kW.cm}^{-2}$ and $Q = 5 \times 10^3$. White dots correspond to Equation 3.25.

imum k_{ISC} required to achieve CW lasing which can be evaluated by two means: the ratio S_1/T_1 from Equation 3.18 and the positivity condition on I_p^{th} . Furthermore, the oblique lines suggest that the lasing pulse duration is not dependent of k_{ISC} or k_{STA} but of the product of the two rates. For instance, for the line defining the threshold between pulsed and continuous emission (highlighted by white dots), the quantity $k_{\text{ISC}}k_{\text{STA}}$ is equal to $8 \times 10^{-5} \text{ cm}^3.\text{s}^{-2}$ whether k_{ISC} is set to 10^2 or 10^6 s^{-1} . By extension, one could say that when ISC is coupled with STA, the duration of the lasing pulse is only determined by the quantity $k_{\text{ISC}}k_{\text{STA}}/k_t$. This very finding has already been mentioned in Chapter 2 to explain the abrupt decrease of the photoluminescence with time, for which the quantity $\beta = k_{\text{ISC}} \times k_{\text{STA}}$ was described as an intrinsic parameter of the film.

We then used the same method of analysis as in Section 3.4.1 and computed the rate equations for different quality factors and pump power densities. Doing so for several values of k_{STA} helps understanding how different molecules would react when implemented in a given resonator. Results are presented on Figure 3.14. Based on the previous figures and on their interpretations, it is expected to see that when k_{STA} is set to $10^{-11} \text{ cm}^3.\text{s}^{-1}$, the system is very close to the one of Figure 3.9 where only intersystem crossing was presented. It is especially visible with the so-called vertical asymptote that seems to disappear with higher STA constants.

Interestingly, our results indicate that when k_{STA} is set to its typical reported value of $10^{-10} \text{ cm}^3.\text{s}^{-1}$, the obtention of a long lasing pulse or a CW lasing is still very possible, provided that the resonator has a high enough quality factor.

Moreover, they are found to be consistent with what has been reported by

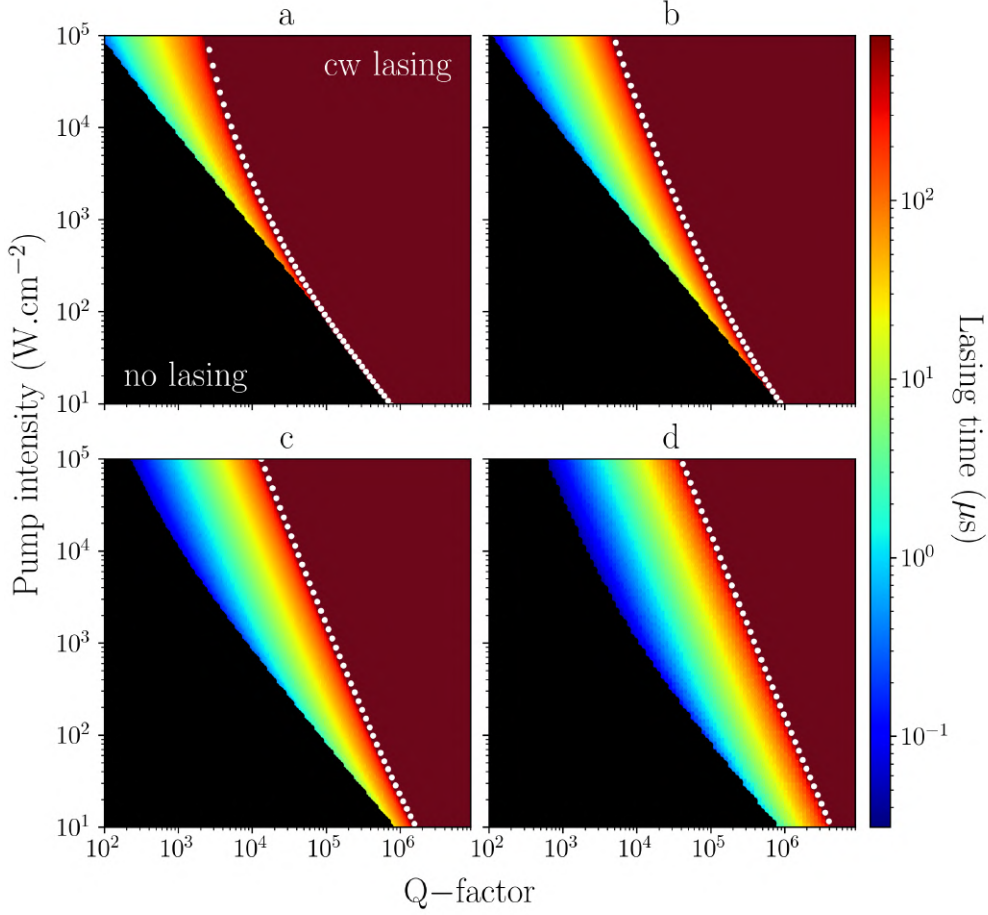


Figure 3.14: Lasing regime achieved as a function of the pump power density and the quality factor of the resonator with $k_{\text{STA}} =$ a) 10^{-11} b) 10^{-10} c) 10^{-9} d) 10^{-8} $\text{cm}^3 \cdot \text{s}^{-1}$. $k_{\text{ISC}} = 6 \times 10^6 \text{ s}^{-1}$. White dots correspond to Equation 3.25.

Zhang and Forrest regarding the decreasing of the CW threshold [157]. Now that our system is more complex and closer to the one they studied (ISC and STA), we can have a more precise look at numbers. In the first case when the concentration of ADN is null, they report pulsed and CW thresholds of 0.93 and $32 \text{ kW} \cdot \text{cm}^{-2}$, respectively. With the informations provided, a loss coefficient α_{cav} for their cavity can be estimated⁴ at around 90 cm^{-1} (obtained with η the fraction of the pump absorbed by the film set to one, as no value seems to be provided), which leads to a quality factor of 1.1×10^4 following this formula:

$$Q = 2\pi\nu_l\tau_{\text{cav}} = \frac{2\pi}{\lambda_l\alpha_{\text{cav}}} \quad (3.27)$$

where $\nu_l = c/\lambda_l$ is the lasing frequency, τ_{cav} the photon cavity lifetime. If this

⁴ $\alpha_{\text{cav}} = \Gamma\sigma_{\text{em}}\eta I_{\text{PS}}/(e_p dk_f)$, where η is the fraction of the pump absorbed, I_{PS} the lasing threshold, e_p the pump photon energy, d the thickness of the gain medium.

values are projected on Figure 3.14.b (the closest to the STA constant of $2.2 \times 10^{-10} \text{ cm}^3 \cdot \text{s}^{-1}$ they chose for the fits), we obtain as well a lasing threshold below $1 \text{ kW} \cdot \text{cm}^{-2}$ and a CW threshold above $20 \text{ kW} \cdot \text{cm}^{-2}$ (32 in their case). Moreover, they report a decreasing of the CW threshold from 32 to $2.2 \text{ kW} \cdot \text{cm}^{-2}$ by increasing the concentration of triplet manager. Although our configuration is not exactly the same, it is straightforward to see that in our case too, if STA is removed, which corresponds to Figure 3.9.b, a CW emission for this Q-factor will be achievable starting from pump fluences at around $1 \text{ kW} \cdot \text{cm}^{-2}$. Of course, thresholds also depend on other molecular properties (fluorescence lifetime, k_{ISC} , and so on) so they differ a little from other reports.

3.4.2.2 Triplet absorption

This section comes right after the singlet-triplet annihilation for two main reasons: First, Triplet Absorption (TA) too represents a quenching of some kind in the framework of organic lasers. Then, many papers have discussed whether STA or TA is responsible for the most dramatic quenching of the lasing intensity to know which one to specifically target when engineering new molecules. So far, no clear answers have been found and it is still unclear how one influences the other and in what proportion. This section has therefore the purposes of not only to understand how $T_1 \rightarrow T_n$ absorption quenches the photon density and to which extent, but also in a second part to compare its influence with the one of STA and thus, give some elements to answer this ongoing debate. For the comparison with the last section to be relevant, only intersystem crossing and triplet absorption will be taken into account in this part.

As presented in Section 1.2.4.3 and 1.2.6.1, TA and STA are different sources of losses. Whereas STA is an annihilation between two excited molecules and therefore only acts on the exciton populations, TA designates the direct absorption of a photon of the lasing mode by an excited triplet state. Although this generated higher excited T_n state is assumed to de-excite very quickly back to the T_1 state (such as the T_n produced *via* singlet-triplet annihilation), at the end, one lasing photon is lost until its energy reaches the ground state so it can be absorbed again. Because of this assumption, the population equations will be the same as in the Section 3.4.1 where only ISC was turned on. As a reminder, the system is written as:

$$\frac{dS_1}{dt} = R_{\text{ex}}S_0 - (k_f + k_{\text{ISC}} + R_l)S_1 \quad (3.28)$$

$$\frac{dS_0}{dt} = -R_{\text{ex}}S_0 + (k_f + R_l)S_1 + k_tT_1 \quad (3.29)$$

$$\frac{dT_1}{dt} = k_{\text{ISC}}S_1 - k_tT_1 \quad (3.30)$$

where k_{STA} and $k_{\text{T TA}}$ are set to zero. On the other hand, the equation for the intracavity intensity will be completed with an additional loss on the stimulated emission and written as Equation 3.31, where σ_{TA} is the triplet absorption cross section, proportional to the overlap between the triplet absorption spectrum and the lasing peak. A first intuition is then that it is easier to avoid than STA, as one "just" has to shift the lasing wavelength away from the TA spectrum by manufacturing the cavity if possible *i.e.*, if TA is not too broad or intense. The whole process is proportional to the triplet population and the intracavity intensity (the photon density of the lasing mode).

$$\frac{dI}{dt} = \frac{c}{n}\Gamma\{\sigma_e S_1 [I + I_{\text{sp}}] - \sigma_{\text{TA}} T_1 I\} - \frac{2\pi c}{Q\lambda_l} I \quad (3.31)$$

Since the populations are ruled by the same equations, the analytical expression of S_1^{th} will be the same as in Equation 3.15, the same applies to the expression of I_p^{th} from Equation 3.16. However, the term S_1^{cav} inside will evolve to take into account triplet absorption and shall be expressed as:

$$S_{1,ta}^{\text{cav}} = \frac{2\pi n}{\Gamma Q \lambda_l \left[\sigma_{\text{em}} - \sigma_{\text{TA}} \frac{k_{\text{ISC}}}{k_t} \right]} \quad (3.32)$$

By setting σ_{TA} to zero, we find back the expression from previous configurations. Being proportional to the in/out ratio of the triplet state, this additional term creates a clear link that was not obvious before between the optical parameters of the resonator and the photophysics of the gain medium. Furthermore, it raises new criteria on the molecule properties that can be addressed as:

$$\sigma_{\text{TA}} \leq \frac{k_t \sigma_{\text{em}}}{k_{\text{ISC}}} \quad (3.33)$$

If typical values of 10^4 and 10^7 s^{-1} are taken for k_t and k_{ISC} , we reach the conclusion that σ_{TA} needs to be at least three order of magnitudes lower than the stimulated emission cross section for CW lasing to be possible, which is not trivial at all. When the values of Table 4.2 are chosen, its upper limit is then $2.6 \times 10^{-19} \text{ cm}^2$. One can also look at this relation from a triplet lifetime perspective. It is then noticeable that if σ_{TA} and σ_{em} are set to 10^{-17} and 10^{-16} cm^2 , respectively, it would have to scale at one microsecond to prevent lasing from dying. Knowing that reported τ_t of numerous organic molecules are up to a few hundred microseconds (above the millisecond for phosphorescent compounds), it really puts a first perspective into the influence TA can have when it is not associated with other "beneficial" process that will be discussed in the next part.

Of course, the ratio of the singlet and triplet population the system has to maintain in order to preserve the population inversion will also be impacted by the same factor, as written in Equation 3.34. As expected, this limit will be more and more difficult to respect if σ_{TA} is important or if triplets are stored for a long

time *i.e.* if k_{ISC} is much larger than k_t .

$$\frac{S_1}{T_1} \geq \frac{2\pi n}{N\Gamma\lambda_l Q \left[\sigma_{\text{em}} - \sigma_{\text{TA}} \frac{k_{\text{ISC}}}{k_t} \right]} \quad (3.34)$$

Actually, it is interesting to derive the criterion for the ratio k_{ISC}/k_t , as it allows one to have good insights about a given molecule and what could be done with it. To do so, we started from the positivity condition of I_p^{th} whose expression matches the case without triplet absorption in Equation 3.16. The mathematics details can be found in Appendix 4.2 but after a few steps one reaches the following expression:

$$\frac{k_{\text{ISC}}}{k_t} \leq \frac{1 - \frac{S_1^{\text{cav}}}{N}}{\frac{\sigma_{\text{TA}}}{\sigma_{\text{em}}} + \frac{S_1^{\text{cav}}}{N}} \approx \left[\frac{\sigma_{\text{TA}}}{\sigma_{\text{em}}} + \frac{S_1^{\text{cav}}}{N} \right]^{-1} \quad (3.35)$$

with S_1^{cav} the population inversion imposed by the resonator without triplet absorption, not to be confused with $S_{1,ta}^{\text{cav}}$ which takes this process into account. This result is obtained under the assumption that the population inversion is much smaller than the total density of active molecules, which is supported by every simulations done for this work. Two terms appears in Equation 3.35: one that accounts for the optical losses and whose interpretation was discussed in Section 3.4.1, and a second one in the form of a ratio between the triplet absorption and the emission cross section, as already seen in other expressions, that account for the gain medium properties.

We saw in Equation 3.33 that σ_{TA} had to be three orders of magnitudes lower than σ_{em} to obtain a CW emission. This statement has to be balanced with the absence of other interactions that would allow more TA by, for instance, creating singlets from other paths than ground state absorption. In fact, **Triplet Absorption Spectroscopy** (TAS) measurements have provided values of σ_{TA} around 10^{-17} cm^2 [233, 234], which would make the ratio $\sigma_{\text{TA}}/\sigma_{\text{em}}$ accounts much more in the lasing pulse duration than S_1^{cav}/N in Equation 3.35.

As it can be seen on Figure 3.15, TA has an influence starting from cross sections as low as 10^{-19} cm^2 . The only solution for a CW emission to be possible when σ_{TA} becomes important (meaning it starts to compete with the emission cross section σ_{em}) is for triplets to be trapped for shorter times, hence k_{ISC} tending towards k_t . As explained, white dots correspond to I_p^{th} the pump power density required to achieve a CW lasing, which in this configuration is expressed as Equation 3.16 with S_1^{cav} being replaced by $S_{1,ta}^{\text{cav}}$ to take into account triplet absorption.

At last, we computed the lasing regimes for different quality factors and pump power densities around the critical value for the triplet absorption cross section established in Equation 3.33. On the left side of Figure 3.16, σ_{TA} is set to $2 \times 10^{-19} \text{ cm}^2$ and it is clear that CW is possible. However, results show that this system ex-

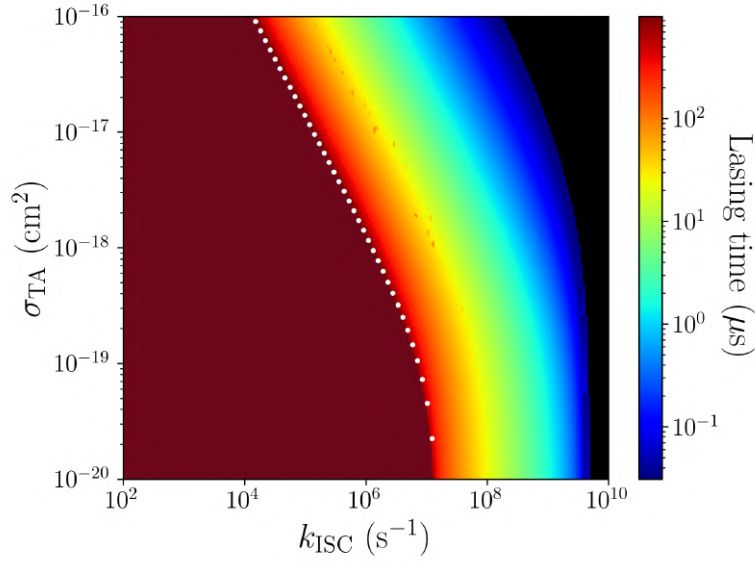


Figure 3.15: Lasing regimes achieved as a function of k_{ISC} and σ_{TA} with $I_p = 10 \text{ kW}\cdot\text{cm}^{-2}$ and $Q = 5 \times 10^3$, $k_t^{-1} = 175 \text{ }\mu\text{s}$. White dots correspond to Equation 3.16 with S_1^{cav} replaced by $S_{1,ta}^{\text{cav}}$.

hibits the same behavior as the "only ISC" configuration (see Figure 3.9) regarding the vertical asymptote for low quality factors. On the contrary, the trend is quite different when it comes to high-Q cavities for which the direct transition between no lasing and a CW emission is broken. Instead, an increase of the pump power density results in longer lasing pulses before reaching the CW regime.

The situation is very different when σ_{TA} is superior to $k_t \sigma_{\text{em}} / k_{\text{ISC}}$. In this context, one can obtain quite long lasing pulses at high quality factor and pump intensity but it will not possible to reach a CW emission since Equation 3.33 is not respected.

After looking at the steady-state values of the intensity it is interesting to look at the temporal evolution of the population and of the photon density. We show on Figure 3.17 the evolution of I/I_{sat} , S_1 and T_1 densities as well as the ratio between both with time. It can be seen that, unlike previous configurations, the excited singlet density is not clamped anymore during the lasing pulse. This surprising behavior is obviously due to triplet absorption, but more precisely to the fact that it adds losses over time that breaks this clamping, meaning that S_1^{cav} is no longer a constant when TA is taken into account.

3.4.2.3 Summary

In this section, three photophysical processes have been studied: intersystem crossing, singlet-triplet annihilation and triplet absorption. It has been shown thanks to the derivation of analytical expressions and the numerical integration of rate equations that those processes all participate in the quenching of the photon den-

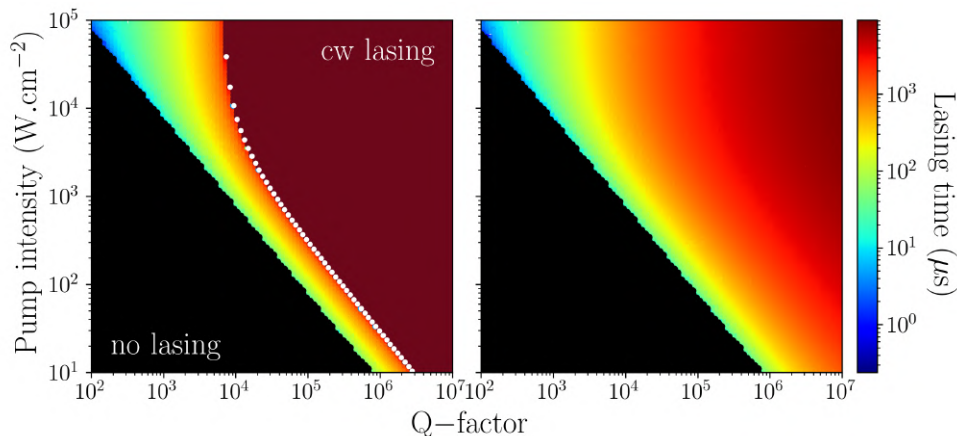


Figure 3.16: Lasing regime achieved as a function of the pump power density and the quality factor of the resonator with $\sigma_{TA} =$ (left) 2×10^{-19} and (right) 3×10^{-19} cm^2 . White dots correspond to Equation 3.16 where S_1^{cav} is replaced by $S_{1,ta}^{\text{cav}}$.

sity of the lasing mode. However, ISC, STA and TA are different mechanisms and therefore, have different and unique ways to influence the dynamics of organic solid-state lasers.

Intersystem crossing is the source of a fast accumulation of triplet state excitons with time via a $S_1 \rightarrow T_1$ transition. This is why the constant k_{ISC} is an interesting characteristic of organic molecules and as a matter of fact, it has been under the spotlight of many works for the past decades, whether it is to lower it in the framework of organic lasers, or to increase it for phosphorescence applications. We saw that, by enabling the generation of triplets with very long lifetime, the T_1 population grows until the clamping of the population inversion can no longer be maintained, as stated in Equation 3.18 and illustrated on Figure 3.8. The only solution for a device to achieve longer pulses is then for the gain medium to have a smaller ratio k_{ISC}/k_t . If it becomes small enough, the triplet population may never reach a critic level and the resulting lasing emission will not stop with time. Also, Figure 3.9 showed that a typical value of 10^7 s^{-1} for k_{ISC} is not incompatible with the achievement of CW lasing. On the other hand, it also showed that this mechanism imposed a minimal quality factor to have to achieve CW lasing which is, contrarily to the common thought, perfectly independant of the pump power density. In the configuration of the simulations for instance, no CW lasing could have been achieved by a resonator with a quality factor lower than 3×10^4 if k_{ISC} was set to 10^7 s^{-1} .

The growth of the triplet population with time enables bi-molecular interactions to occur, singlet-triplet annihilation takes advantage of this and comes in addition of ISC to quench the excited singlet population and thus, the population inversion. Although it is more a complex mechanism because its quenching of the S_1 state also has consequences on the T_1 population (see Figure 3.10), the influence of STA eventually boils down to an increase of the pump intensity required to achieve a

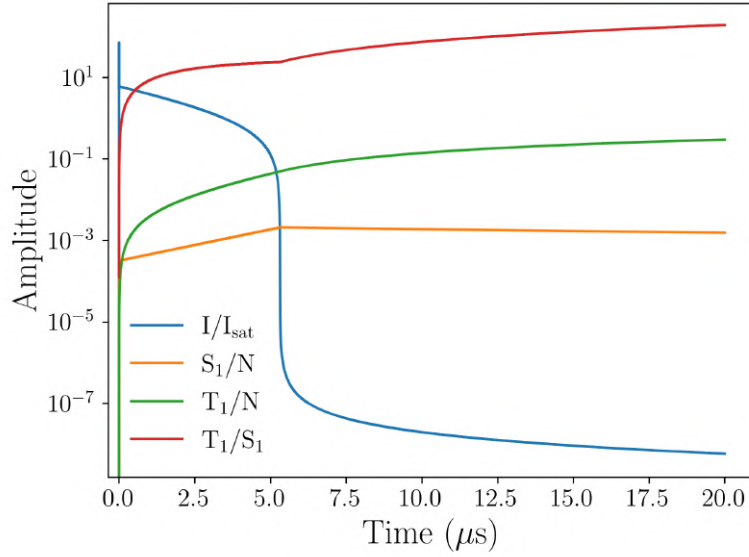


Figure 3.17: Time-resolved simulations of the normalized lasing intensity, S_1 , and T_1 exciton populations with ISC and TA. $k_{\text{ISC}} = 10^7 \text{ s}^{-1}$, $k_t^{-1} = 175 \mu\text{s}$, $\sigma_{\text{TA}} = 10^{-17} \text{ cm}^2$.

continuous emission. It has been explained through Equation 3.25 and Figure 3.14. As matter of fact, results showed that CW lasing was a possibility even if k_{STA} is set to $10^{-10} \text{ cm}^3 \cdot \text{s}^{-1}$, provided that the resonator has a high enough quality factor.

Contrarily to ISC and STA which influence the exciton populations, triplet absorption directly quenches the lasing intensity inside the cavity thanks to the absorption by an excited triplet state of a photon from the lasing mode. Although it has been assumed that this T_1 state that get promoted to a high energy T_n state circles back quickly to the T_1 level (and then accounts for nothing in the population densities distribution), we showed that the loss of photons has dramatic effects on the lasing pulse duration and on the possibility for one system to achieve a CW emission. As we have seen, the most impactful effect of TA is the intervention of molecular properties in the population inversion that one device is able to exhibit, notably through the ratio k_{ISC}/k_t in Equation 3.32. More physically, TA induces time-dependent losses, breaking the clamping of the population inversion and creating a laser whose threshold is increasing over time until losses become too important. Moreover, this new link between optics and photophysics raises new criteria on one device to achieve CW lasing: it was shown by Equation 3.33 and 3.35 that σ_{TA} should scale several (≈ 3) orders of magnitude lower than σ_{em} the emission cross section to allow such emission regimes. These criteria were sketched on Figure 3.16 where we showed that when σ_{TA} did not fulfill the requirements of Equation 3.33, no CW emission were allowed regardless of the quality factor of the resonator.

Even though the absence of other processes that could compensate the influence of STA or TA has to be considered, it is still clear from this results that triplet

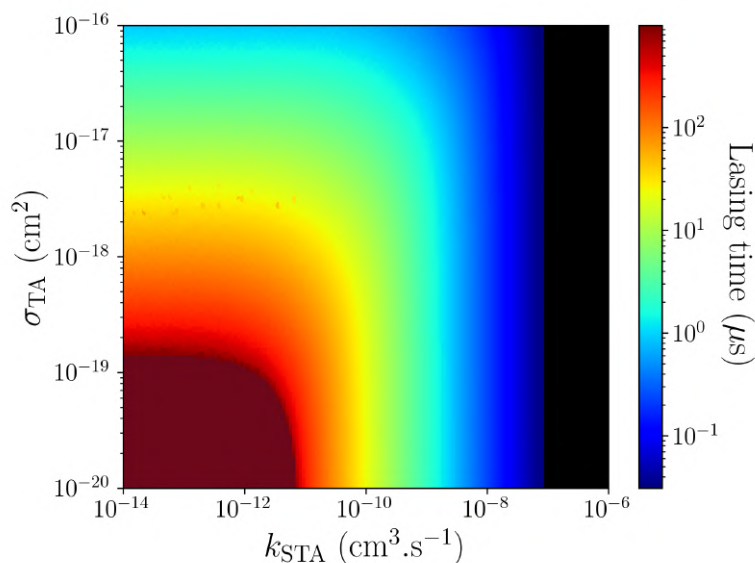


Figure 3.18: Lasing regimes achieved as a function of k_{STA} and σ_{TA} with $I_p = 10 \text{ kW.cm}^{-2}$ and $Q = 5 \times 10^3$. Black means no lasing whereas red is CW lasing.

absorption is much more detrimental than STA when it comes to obtain longer pulses, whether is it by the addition of new requirements or the direct quenching of the photon density of the lasing mode. Finally, we show on Figure 3.18 that a configuration in which both mechanisms are taken into account, the requirements for k_{STA} and σ_{TA} are as difficult to reach as it is expected. In this configuration, the former would have to be lower than $10^{-11} \text{ cm}^3.\text{s}^{-1}$ whereas the latter would have to be under 10^{-19} cm^2 .

3.4.3 CW lasing: A new hope

This part is devoted to interactions that can be seen as beneficial in the framework of organic light emitting devices. Whether it is because it quenches the triplet population or represents a new source of photon density inside the resonator, the point is to understand if it possible to overcome the influences of the processes studied earlier.

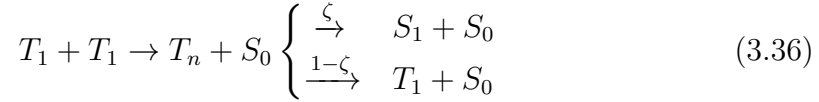
First, triplet-triplet annihilation, which has been described in Section 1.2.6.2, is studied as it has a great potential regarding the quenching the triplet state. Since it is the most direct route from T_1 to the ground state S_0 , it is then interesting to study the consequences of lower and higher values of τ_t . Moreover, the comparison between its effects on the population statistics and the one of a low triplet lifetime will be very helpful to figure out what makes a molecule efficient. At last, **T**hermally **A**ctivated **D**elayed **F**luorescence (TADF) is studied, as it is a recent and promising pathway towards longer lasing pulses from fluorescence materials.

The purpose of this part is to find out if the losses due to photophysical mechanisms can be overcome. Thus, intersystem crossing, singlet-triplet annihilation

and triplet absorption will be taken into account if nothing says otherwise.

3.4.3.1 Triplet-triplet annihilation

As presented in Section 1.2.6.2, this process causes the quenching of the triplet population thanks to the following chain of reactions:



Fortunately, the annihilation of two triplet excitons also results in some proportion in the filling of the singlet population, which is why it has been studied for a long time as a promising lead to overcome the influence of triplets on the intrinsic pulsed emission regime of organic lasers [99, 235].

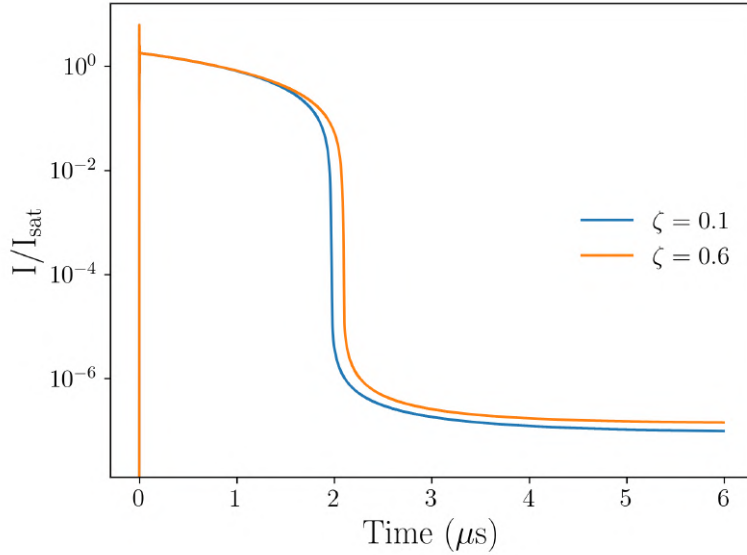


Figure 3.19: Time resolved simulations of the intracavity intensity for different values of ζ the proportion of singlet created *via* TTA. Changing ζ value in Equations 3.2 to 3.4 has no meaningful influence on the lasing pulse duration.

To be sure that this approximated value of 0.25 discussed in the introduction would not affect too hardly the results, we simulated the intensity of the lasing mode for different values of ζ and, as it can be seen on Figure 3.19, it does not have a lot of influence on the pulse duration. This is explained by the fact that in the framework of lasers, the population inversion is clamped and the lasing is mostly kept alive thanks to the ground state absorption. The overall contribution to the term $\zeta k_{\text{TTA}} T_1^2$ in Equation 3.2 on the singlet exciton density becomes then very limited. Debating this value would in fact be much more relevant in configurations without any resonator, for luminescence applications for instance. In such cases,

the values of ζ is important and is actually still debated [236], as 0.1 or 0.5 provides very different outputs since the S_1 population is not clamped.

Here, the influence of TTA will especially be important on the triplet state, as it contributes to the quenching of its population. With TTA taken into account, the triplet equation is written as:

$$\frac{dT_1}{dt} = k_{\text{ISC}}S_1 - k_t T_1 - (1 + \zeta)k_{\text{TTA}}T_1^2 \quad (3.37)$$

with the term proportional to $k_{\text{TTA}}T_1^2$ changing the whole dynamics by the addition of a new loss pathways for the triplet excitons, as it has already been observed in Chapter 2 with the ground state recovery kinetic. If, in previous sections, the evolution of triplets with time was purely exponential (considering that $k_{\text{ISC}}S_1$ is constant), this new term yields a simplified Ricatti equation. As an illustration, we computed the triplet population density with time for different values of k_{TTA} on Figure 3.20. We see that its building at early times is only imposed by k_t the "intrinsic" de-excitation rate of T_1 molecules. Later, the dynamics is affected by triplet-triplet annihilation by reducing the time needed for the population to reach a steady-state value. The late arrival of TTA is due to its need of a certain density of triplet excitons to be efficient.

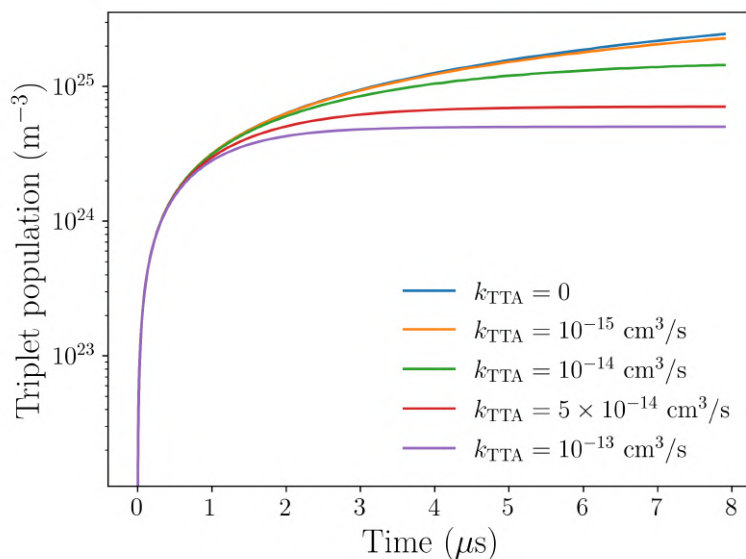


Figure 3.20: Time resolved simulations of the triplet population for different values of k_{TTA} .

Unfortunately, the quadratic form of Equation 3.37 prevents us from any steady-state analysis⁵. Since, to our knowledge, it is not possible to obtain analytical expressions that could be compared to previous configurations, this part will only contain numerical simulations.

⁵It was possible in Chapter 2 to work with analytical expression thanks to the absence of excited singlets after the pump excitation, cancelling the source term $k_{\text{ISC}}S_1$.

To begin with, we computed on Figure 3.21 the ratio I/I_{sat} with time for different TTA constants. Doing so with or without triplet absorption allows a better understanding of how the population densities react in different configurations when TTA is taken into account. On one side, results show that in absence of triplet absorption, TTA increases the lasing pulse duration when going from 0 to $10^{-15} \text{ cm}^3.\text{s}^{-1}$, and allows the achievement of a continuous emission for higher rates. Since the initial lasing regime (in blue) is fixed by k_{ISC} , k_{STA} , k_t and so on, it is expected to see its duration elongated when TTA is enabled, as it decreases more and more triplet state lifetime.

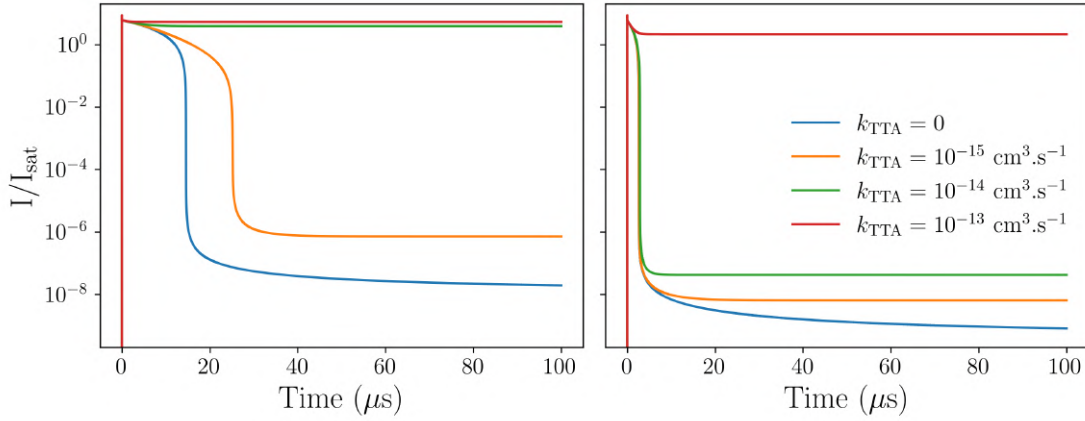


Figure 3.21: Time resolved simulations of the lasing intensity without (left) and with (right) triplet absorption for different values of k_{TTA} . $k_{\text{ISC}} = 10^7 \text{ s}^{-1}$, $k_{\text{STA}} = 10^{-10} \text{ cm}^3.\text{s}^{-1}$, $\sigma_{\text{TA}} = 10^{-17} \text{ cm}^2$, $Q = 5 \times 10^3$, $I_p = 10 \text{ kW.cm}^{-2}$.

On the contrary, Figure 3.21 (right) shows an evolution of the lasing pulse with k_{TTA} that is not at all intuitive, where an increase of k_{TTA} does not lengthen the pulse duration up to a certain point. Instead, only two scenarii are possible: a pulsed emission whose duration is mostly fixed by σ_{TA} ($\approx 3 \mu\text{s}$) and CW lasing when k_{TTA} reaches $10^{-13} \text{ cm}^3.\text{s}^{-1}$. Moreover, in cases where k_{TTA} is set to zero (blue curves), the lasing pulse is reduced from 14 to $3 \mu\text{s}$ (without and with TA, respectively). It also decreases from CW lasing to the same $3 \mu\text{s}$ for the green curve, where TTA is fixed at $10^{-14} \text{ cm}^3.\text{s}^{-1}$. The different behaviors with and without triplet absorption can be explained in terms of triplet population build-up time: Without TA, the lasing intensity depends only on the clamping of the population and therefore on the ratio S_1/T_1 , as we have seen in Section 3.4.2.1. Thus, in this configuration of ISC and STA, the triplet population can be important enough for TTA to be efficient and reduce the triplet states lifetime. This way, the pulse lasts longer and longer until, eventually, this effective τ_t becomes low enough to overcome the generation of T_1 from intersystem crossing and singlet-triplet annihilation.

When triplet absorption is taken into account however, the photon density is reduced directly inside the lasing mode from a $T_1 \rightarrow T_n$ absorption and, as it

has been shown, TA adds drastic criteria towards long lasing pulses. As a result, the duration of the pulse is mostly fixed by σ_{TA} and its influence is difficult to compensate. The only solution in this configuration is to have a very low triplet lifetime, induced by a very strong k_{TTA} like for the red curve on Figure 3.21 (right). If k_t is high enough to overcome the effects of TA, whose influence is far greater than STA, then there is no process to compete with and the population inversion can be maintained indefinitely. Hence, the brutal transition from a lasing pulse with a fixed duration to a continuous-wave emission.

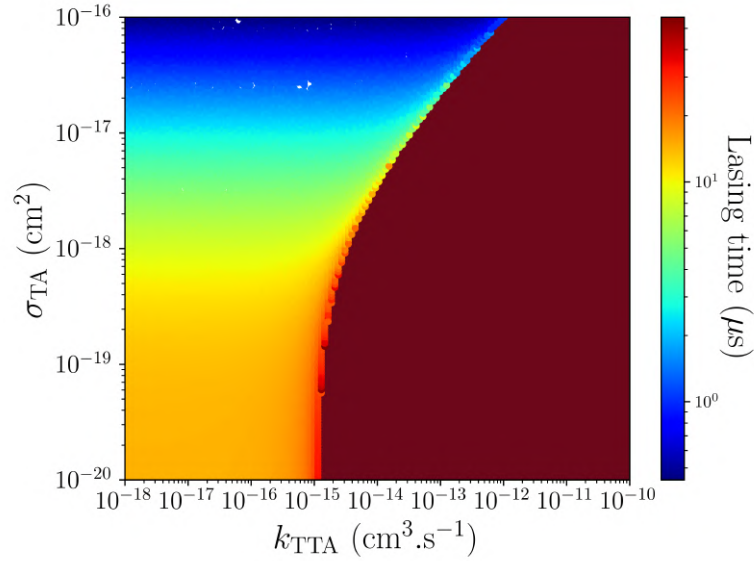


Figure 3.22: Lasing regimes achieved as a function of k_{TTA} and σ_{TA} with $I_p = 10 \text{ kW.cm}^{-2}$, $Q = 5 \times 10^3$, $k_{\text{ISC}} = 10^7 \text{ s}^{-1}$, $k_{\text{STA}} = 10^{-10} \text{ cm}^3.\text{s}^{-1}$.

This interpretation is generalized on Figure 3.22, for which achievable lasing regimes were computed for a large range of k_{TTA} and σ_{TA} in the same condition than Figure 3.21. One can see that, contrarily to Figure 3.15 and 3.13, the duration of the resulting lasing pulse is much shorter, because of last explanations. It can especially be seen when the triplet absorption cross section reaches values above 10^{-17} cm^2 . Here, the pulses are limited to only one or two microseconds and a slight increase of k_{TTA} makes the emission continuous. Moreover, these results make it clear that the maximum value σ_{TA} can have to enable CW lasing established in Equation 3.35 is no longer accurate. Indeed, when compensated by high TTA constants, triplet absorption cross sections can be orders of magnitude higher than the previous limit of $\approx 10^{-19} \text{ cm}^2$.

Because this behavior is expected to be different in the case of cavities with higher quality factors, considering the much lower population inversion they need to enable laser and thus, the low triplet population associated, we integrated the equations with all processes enabled at different pump power densities and quality factors, and plotted the resulting lasing regimes on Figure 3.23. In addition, the

computation has been done for several values of σ_{TA} and k_{TTA} in order to have the clearest view possible on the implication of triplet-triplet annihilation and triplet absorption.

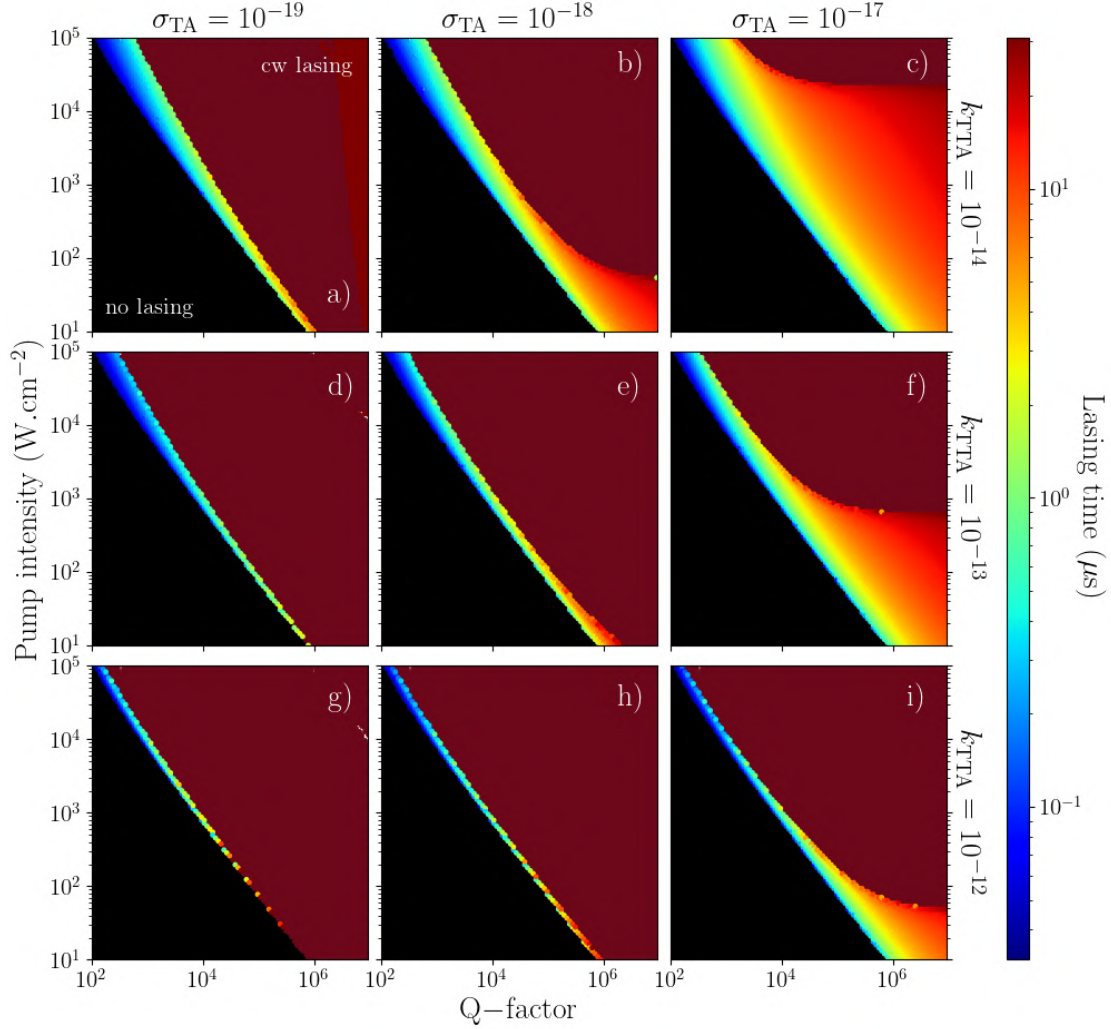


Figure 3.23: Lasing regimes achieved as a function of the pump power density and the quality factor for different values of k_{TTA} (cm³.s⁻¹) and σ_{TA} (cm²). $k_{ISC} = 10^7$ s⁻¹, $k_{STA} = 10^{-10}$ cm³.s⁻¹. $k_t^{-1} = 175$ μs

Simulations show that in the presence of TTA, triplet absorption will mostly affect the pulse duration of high-Q cavities. It is perfectly illustrated on Figure 3.23 (a,b,c) where values of σ_{TA} and k_{TTA} are chosen to be close to what is typically reported in the literature [38, 37]. Starting from 10^{-19} to 10^{-17} cm², TA cancels more and more the possibility of a CW emission especially for quality factors above 10⁴. In such cavities, it exists a CW pump threshold that is not dependent on the quality factor anymore, because the triplet-related losses becomes more important

than the ones induced by the resonator. On the opposite, in the case of low Q cavities where the population inversion stands higher, the proportional creation of triplets allows TTA to be dominant over TA.

Finally, these results show that if k_{TTA} and σ_{TA} are important and low enough, respectively, the system reaches a quasi four-level configuration where only two finalities coexist: no lasing and a continuous-wave emission.

3.4.3.2 Triplet state lifetime

We have seen that in the framework of organic lasers, the influence of TTA eventually boils down to a reduction of the triplet state lifetime, because the singlet population is clamped during the lasing pulse. It is then interesting to ask ourselves if it exists a significant difference between a typical τ_t reduced by TTA and an intrinsically low lifetime regarding the CW capabilities of an OSSL.

An intuitive thought when comparing both configurations might be in favor of the high k_t , as TTA requires an important population of triplet excitons that can trigger subsequent processes, as discussed in the previous section. On the other hand, with a similar k_{ISC} , a short triplet lifetime could prevent in the first place the triplet density to reach an important level and thus prevent TA, STA to occur.

If we look at configurations where only ISC and STA are taken into account ($\sigma_{\text{TA}} = 0$), computation outputs plotted on Figure B1 show at first glance expected results. Indeed, a decrease of τ_t from 500 μs to 500 ns is found to ease CW lasing in every configuration. Besides, it was also expected from the expression of I_p^{th} obtained in Section 3.4.2.1.

Moreover, it is interesting for comparison purposes to go back to Figure 3.22 on which the lasing pulse duration is plotted versus σ_{TA} and k_{TTA} at a pump intensity of 10 $\text{kW}\cdot\text{cm}^{-2}$ and a quality factor of 5×10^3 . Computations showed that CW lasing was obtained without TA for $k_{\text{TTA}} \approx 10^{-15} \text{ cm}^3\cdot\text{s}^{-1}$, as the vertical lines indicating that the influence of triplet absorption is negligible below 10^{-19} cm^2 . Now back to this section and more precisely on Figure B1.a, showing that the same conditions (I_p^{th} , Q , k_{ISC} , and k_{STA}) can be reached without TTA when τ_t is set to 500 ns. What this comparison says is that it exists an equivalence between a TTA constant of $10^{-15} \text{ cm}^3\cdot\text{s}^{-1}$ and a triplet lifetime of 500 ns in this configuration. These findings are very surprising, because it leads to the conclusion that a strikingly low τ_t is required to offer the same possibilities as a k_{TTA} considered quite small, which pretty much invalidates the initial thoughts.

It should however be emphasized that these simulations were performed in neat configuration, so that the total density of active molecule N in the film is here close to 10^{27} m^{-3} . Therefore, this comparison is done in the most extreme case, considering that TTA is proportional to the square of the triplet exciton density. A decrease in the concentration would indeed result in a longer τ_t to compensate the same k_{TTA} , which nuances the conclusion.

Adding triplet absorption to intersystem crossing and singlet-triplet annihilation results in the same analytical formulas as in Section 3.4.2.2. We can use the expression of $S_{1,ta}^{cav}$ (the population inversion that a resonator has to lower to achieve CW lasing in the presence of TA) from Equation 3.32 to extract criteria on k_t . As a reminder, the condition for $S_{1,ta}^{cav}$ not to tend towards infinity can be expressed (in terms of triplet lifetime) as:

$$k_t \geq \frac{\sigma_{TA}}{\sigma_{em}} k_{ISC} \quad (3.38)$$

Setting σ_{TA} and σ_{em} at 10^{-17} and 10^{-16} cm^2 , respectively, and k_{ISC} at 10^7 s^{-1} , the T_1 state has to have a lifetime of less than one microsecond to allow CW lasing. It is straightforward to see that decreasing ISC or TA will allow the same results with a proportionally longer triplet lifetime. Lasing regimes that can be achieved as a function of Q and the pump power density are displayed on Figure 3.24 for two different triplet lifetime of 0.5 and 1.5 μs . Those have been chosen to around the critical value imposed by Equation 3.38 with the values mentioned for σ_{TA} , σ_{em} , and k_{ISC} . Simulations confirms the analytical expression by showing a clear threshold-like phenomenon where a triplet lifetime just slightly below a critical value, the possibility of CW lasing vanishes, regardless of how low the lasing threshold of the resonator scales.

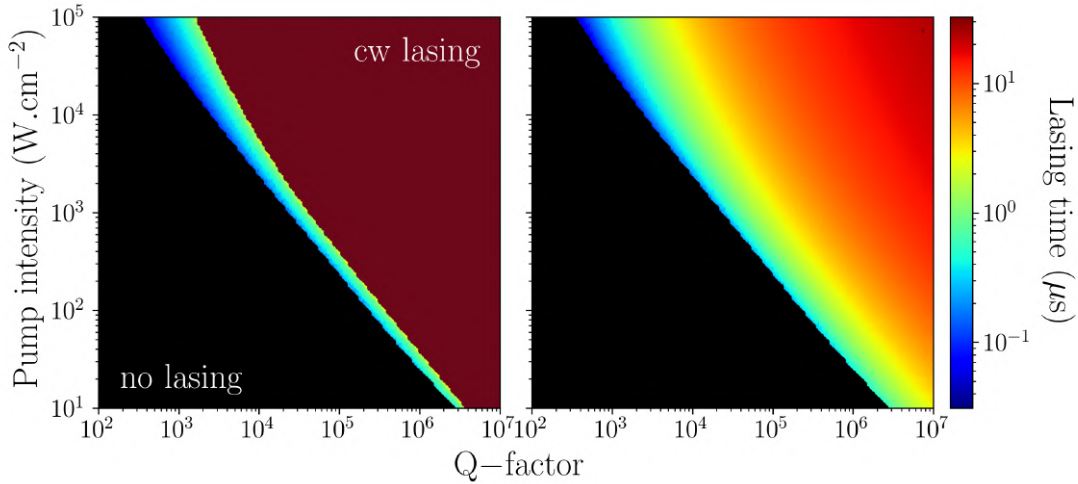


Figure 3.24: Lasing regimes achieved as a function of the resonator quality factor and the pump power density for a triplet lifetime τ_t of (left) 0.5 and (right) 1.5 μs .

Whereas TTA, thanks to its T_1^2 proportionality, could balance the influence of TA for high-Q cavities (Figure 3.23) when Equation 3.38 was not fulfilled, a triplet lifetime cannot.

3.4.3.3 Thermally activated delayed fluorescence

As it has been discussed in details in Section 1.2.4.4, TADF materials have been in the recent years the center of a significant attention from the organic device community as it represents a very promising route for 100% of internal efficiency. Thanks to an energy gap between the first excited singlet and triplet states smaller than for most compounds, excitons promoted on the T_1 state can be upconverted back to the fluorescence level *via* **R**everse **I**nter**S**ystem **C**rossing (RISC).

This part is inspired by two recent papers from Adachi *et al.* [88, 83]. The former deals with exact analytical solutions of a system that takes only into account ISC and RISC. The later on the other hand is closely related to this work as they studied the population dynamics of organic TADF materials from a numerical rate equations approach. Moreover, they reach the conclusion that in order to achieve a CW emission, k_{RISC} must scale at the same order of magnitude than k_{ISC} , which is not that intuitive as a result considering that the density of triplets quickly becomes much more important than the singlet excitons density (see Figure 3.10).

In this work, RISC is implemented in the same way as several references, where triplets are harvested at a constant rate k_{RISC} (s^{-1}) from T_1 states to the fluorescence [98, 237, 238]. The resulting rate equation system is then written as:

$$\frac{dS_1}{dt} = R_p S_0 - (k_f + k_{\text{ISC}} + \sigma_{\text{em}} I + k_{\text{STA}} T_1) S_1 + k_{\text{RISC}} T_1 \quad (3.39)$$

$$\frac{dS_0}{dt} = -R_p S_0 + (k_f + \sigma_{\text{em}} I + k_{\text{STA}} T_1) S_1 + k_t T_1 \quad (3.40)$$

$$\frac{dT_1}{dt} = k_{\text{ISC}} S_1 - (k_t + k_{\text{RISC}}) T_1 \quad (3.41)$$

We chose not to take into account triplet-triplet annihilation for two reasons: Since the purpose of this part is to evaluate to which extend RISC helps to reach longer pulses, a strong mechanism such as TTA would hide the impact of TADF. Furthermore, the absence of TTA in the equations allows us to derive much easier analytical expressions that will be compared to those of previous configurations.

Before dealing with the CW conditions, the temporal evolutions of the intracavity intensity and the triplet population have been plotted on Figure 3.25. As expected from the equations, an increased RISC results in longer lasing pulses because of its influence on the T_1 state. Providing an additional way out, it takes more time for the triplet population to reach a critical level (see discussion on the population ratio requirement with Equation 3.34), increasing the duration during which the population inversion is maintained.

Regarding the intensity inside the cavity, its equation is equivalent to Equation 3.31, as RISC does not directly affects the photons of the lasing mode. However, since the triplet equation has been modified with the addition of the term $k_{\text{RISC}} T_1$, the expression of $S_{1,ta}^{\text{cav}}$ will evolve and will be written as:

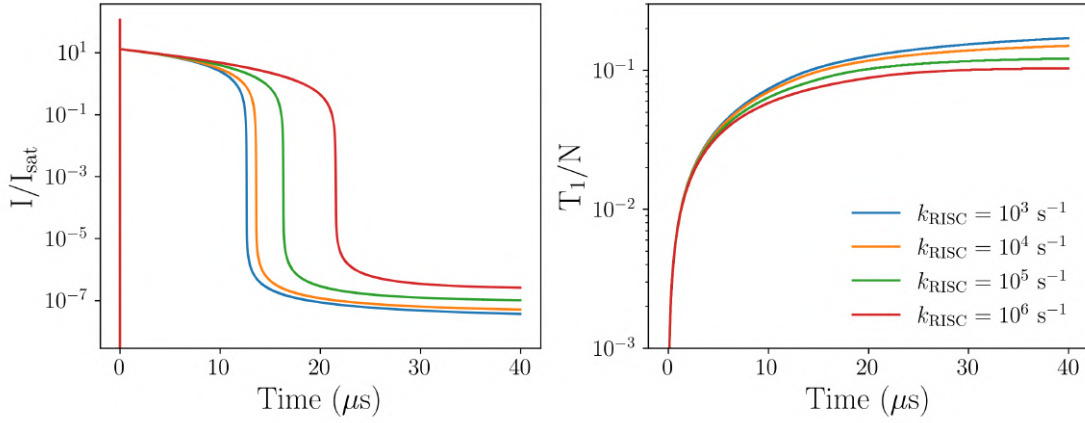


Figure 3.25: Time resolved simulations of the intracavity intensity (left) and the triplet population (right) for different values of k_{RISC} . $k_{\text{ISC}} = 10^8 \text{ s}^{-1}$, $k_{\text{STA}} = 10^{-10} \text{ cm}^3 \cdot \text{s}^{-1}$, $Q = 10^4$, $I_p = 5 \text{ kW} \cdot \text{cm}^{-2}$.

$$S_{1,ta}^{\text{cav}} = \frac{2\pi n}{\Gamma Q \lambda_l (\sigma_{\text{em}} - \sigma_{\text{TA}} \beta)} \quad (3.42)$$

where β is equal to $k_{\text{ISC}}/(k_t + k_{\text{RISC}})$, which means that in the first place, RISC will be impactful only if it scales at the same order of magnitude as k_t . Of course, the requirements on the triplet absorption cross section from Equation 3.33 are also impacted in the case of TADF molecules. Updated criteria can be extracted from Equation 3.42:

$$\frac{\sigma_{\text{em}}}{\sigma_{\text{TA}}} \geq \frac{k_{\text{ISC}}}{k_t + k_{\text{RISC}}} \quad (3.43)$$

confirming that RISC will ease the obtention of a CW lasing in the presence of TA. In fact, if k_{RISC} becomes close to k_{ISC} , triplet absorption would not be a problem any longer and CW lasing would be trivial, as mentioned in Reference [83].

As in previous sections, we derived from Equation 3.39 and 3.41 the pump intensity required to achieve a CW emission, which can be after a few steps detailed in Appendix 4.2 written as:

$$I_p^{\text{th}} = \frac{k_f \left[1 + \frac{k_{\text{ISC}}}{k_f} + \frac{k_{\text{STA}}}{k_f} \beta S_{1,ta}^{\text{cav}} - \frac{k_{\text{RISC}}}{k_f} \beta \right]}{\sigma_{\text{abs}} \left[\frac{N}{S_{1,ta}^{\text{cav}}} - (1 + \beta) \right]} \quad (3.44)$$

It is clear from this expression of I_p^{th} that RISC will participate in its reduction. Because k_{RISC} appears multiple times and is not that trivial to interpret, I_p^{th} has been plotted as a function of the RISC constant on Figure 3.26. To picture how it interacts with different level of triplet populations, we computed Equation 3.44 for multiple values of k_{ISC} .

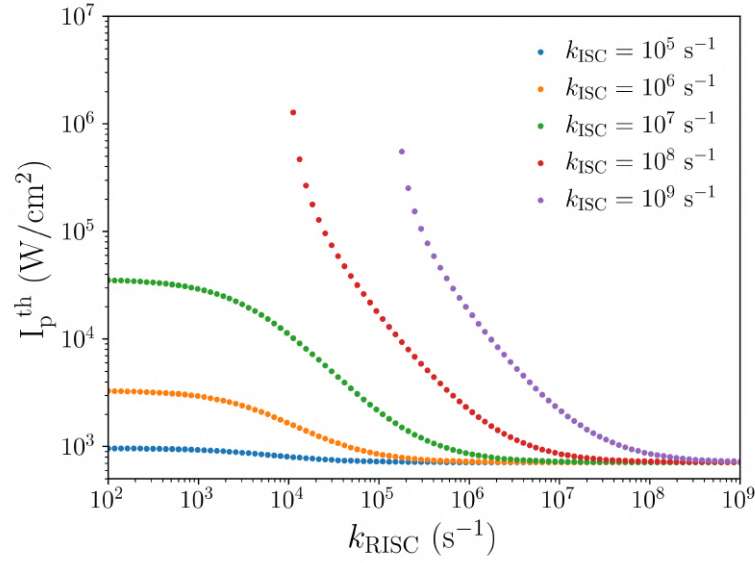


Figure 3.26: Pump intensity required to obtain a continuous-wave lasing emission as a function of k_{RISC} for different values of k_{ISC} . $k_{\text{STA}} = 10^{-10} \text{ cm}^3 \cdot \text{s}^{-1}$, $Q = 10^4$.

First, we see that I_p^{th} converges towards the same value of roughly $10^3 \text{ W} \cdot \text{cm}^{-2}$ when k_{RISC} increases, regardless of its value. It is because when k_{RISC} becomes close to k_{ISC} or higher, the system eventually reaches a state where no triplets are trapped long enough for alternative processes such as STA or TA to occur. Then, the only losses that are still impactful are those linked to the resonator through its quality factor, this is the reason why I_p^{th} does not tend towards zero. For the same reason, when less triplets are generated thanks to a low k_{ISC} , the system also needs a lower k_{RISC} to compensate.

Figure 3.26 also shows two behaviors depending on the value of k_{ISC} : Cases for which I_p^{th} is defined at every value of k_{RISC} , and others where it tends towards infinity below a certain point. The two scenarii can be discriminated thanks to Equation 3.44 and its denominator. Indeed, for ISC constants higher than 10^7 s^{-1} (red and violet curve), it will be impossible to achieve a CW lasing if RISC is not important enough, hence the exponentially increasing value of I_p^{th} . On this matter, it is noticeable that RISC does not have any influence on I_p^{th} below $10^3 \text{ W} \cdot \text{cm}^{-2}$, which roughly corresponds to $k_t/10$. When k_{RISC} becomes very low, the pump intensity threshold is directly driven by the triplet state lifetime. This is why an ISC constant set to 10^5 s^{-1} (blue curve) does not have any significant impact on I_p^{th} , as it is already really close to k_t which is, for this simulations, set to approximately $6 \times 10^3 \text{ s}^{-1}$.

The influence of RISC is even clearer when looking in Appendix 4.2 where lasing pulse durations are plotted for various values of k_{RISC} in different configurations. Figure B2 shows how TADF materials would behave with the only singlet loss channel being ISC, while Figure B3 adds STA in the equations. It is showed

on both that RISC is perfectly equivalent to a decrease of the rates of other interactions, as suggested by Equation 3.44.

3.5 Conclusions

In this chapter, a theoretical study of the requirements for one organic solid-state laser to achieve a continuous-wave emission has been presented. Our approach has been to use a system of coupled rate equations to compute the temporal evolution of S_0 , S_1 , and T_1 population densities as well as the photon density inside the cavity, such as in other reports in this matter [80, 96, 74, 83]. However, the core of its work differs from previous study by explicitly taking into account the influence of the resonator in the lasing pulse duration, notably *via* its quality factor.

At first, previous works that have investigated what are the limitations to overcome towards CW lasing and hence towards practical applications were presented. As it has been discussed, all focused on molecular properties and/or thermal management to improve the current state-of-the-art, with STA often designated as the process to absolutely prevent from occurring during excitation. From that, the first 30 ms lasing in an OSSL has been obtained without the help of triplet quencher [5], and was ascribed to the absence of triplet absorption thanks to a weak overlap between the lasing peak and the triplet band. Heat dissipation was also important in this achievement, allowing Sandanayaka *et al.* to obtain stable lasing from a 8 [14] to 80 MHz [5] repetition rate. But at the end, the current state-of-the-art of 30 ms was topped by Senevirathne *et al.* [6] who achieved one second lasing with a FWHM of 0.4 nm during the whole optical excitation, a three orders of magnitude improvement ascribed to the much lower lasing threshold of their original mix-order circular DFB.

Afterwards, the theoretical framework of this thesis was introduced, with a presentation of the modeling of the different photophysical mechanisms ruling the excitons statistics and of the device resonator. Since the initial purpose of these simulations was to compare the lasing pulses obtained with BSBCz inside two resonators, namely DFB and VCSEL, we chose to describe both mostly by their quality factors to take into account their significantly different lasing thresholds. Special cares were taken regarding the different approximations and limitations of our approach in Section 3.3.2, as there are some. The core of this work is to discriminate different lasing regimes *i.e.* if for some optical and photophysical configuration, the device would achieve a pulsed or a continuous lasing emission (or no lasing at all). To do so, we developed an algorithm that sorts different temporal simulations by comparing the ratio I/I_{sat} where I is the lasing intensity inside the resonator (related to the photon density) and I_{sat} is the saturation intensity of the lasing transition. As an illustration and a reference for comparison with more complex system, we detailed our analytical analysis to derive CW lasing intensity threshold I_p^{th} with the well-established four-level system, in which triplets do not

intervene.

The results of our simulations were presented in a step-by-step approach, by at first including the generation of triplets *via* intersystem crossing but not subsequent interactions ($k_{\text{STA}} = k_{\text{TTA}} = \sigma_{\text{TA}} = 0$). Temporal simulations on Figure 3.8 coupled with Equation 3.18 provided insights on the reasons to the premature death of the lasing in organic devices, which is ascribed to an increasing triplet population that leads to a breaking of the criteria regarding the ratio S_1/T_1 required to keep the population inversion alive. Moreover, we show that in such a system, it exists a minimal quality factor a resonator has to have in order to achieve CW lasing, which is once again not intuitive. Denoted by Q_{th} , it is obtained by making I_p^{th} from Equation 3.16 tend towards infinity and can be visualized on the 2D map of Figure 3.9. Interestingly, and even though this particular configuration without any additional process is somehow utopian, the lasing thresholds (*i.e.* the Q-factor) required to reach CW lasing easily scale above the lowest reported in VCSEL configuration, which gives hints to explain the mentioned difference observed between DFB and VCSEL.

In a second phase, we studied mechanisms that are thought to be detrimental for the lasing emission: singlet-triplet annihilation and triplet absorption. Those two fundamentally differ as the former is a dipole-dipole intermolecular interaction and the latter is the absorption of a photon by a triplet exciton and as such, their influence is also dramatically different. Our simulations showed that the influence of STA eventually boils down to an increase of the pump power required to achieve a CW lasing, notably *via* a term proportional to $k_{\text{ISC}} \times k_{\text{STA}}$ in Equation 3.25 (term that was evoked in the transients PL analysis in Chapter 2). But, as it has been discussed on Figure 3.14, typical values of $10^{-10} \text{ cm}^3 \cdot \text{s}^{-1}$ for k_{STA} do not prevent a device to achieve CW lasing, provided that its lasing threshold scales very low, such as DFB-type resonators. Also, results provide a generalization of the work of Zhang and Forrest [157] regarding the existence of two pump intensity thresholds (pulsed and CW), and especially their conclusion on the reunification of both thresholds if the triplet-related losses are managed. Indeed, this work has shown that a road towards a four-level-like configuration is definitely possible *via* a reduction of the lasing threshold, since the population inversion required is lower, leading to less triplets generated.

On the other hand, triplet absorption will directly influence the population inversion imposed by the resonator as discussed with Equation 3.32, yielding a σ_{TA} that has to be three orders of magnitude lower than σ_{em} the stimulated emission cross section (by taking typical values of k_{ISC} and k_t , see details in Section 3.4.2.2). We showed with simulations that this drastic condition is not easily fulfilled, as CW is no longer possible for cross sections above $3 \times 10^{-19} \text{ cm}^2$ regardless of the pump power density and the lasing threshold. Even if this pessimistic conclusion has to be balanced by the absence of other processes that could hinder or compensate its influence on the photon density, this model does a great job at comparing the

influences of STA and TA, and allows us to reach the conclusion that TA is far more important to avoid than STA regarding CW lasing possibilities.

Then, phenomena that can be seen as beneficial for the lasing pulse (*i.e.* for the excited singlet population) were studied, namely triplet-triplet annihilation, reverse intersystem crossing, in order to see whether the significant quenching induced by TA could be balanced. Moreover, the influence of a short triplet lifetime was also explored.

Results showed that the most rewarding choice to improve the CW lasing capabilities of a device is *via* TTA, as it can overcome limitations imposed by k_{ISC} and σ_{TA} even in the case of strong rates/cross sections. It is especially important for high-Q cavities, for which the low production of triplets makes it very efficient versus triplet absorption. Since it has been discussed that the role TTA is mostly about depleting the triplet state through the term $k_{TTA}T_1^2$, we compared its influence with the one of a shorter triplet lifetime. Even though we showed that a short triplet lifetime has eventually the same overall influence on the lasing pulse duration than TTA, we also show that it would require a very low lifetime of under one microsecond to compensate a TTA rate of only $10^{-15} \text{ cm}^3.\text{s}^{-1}$, designating the latter as far more interesting to work with when aiming at longer lasing pulses. Besides, it has also been derived that in the presence of TA, CW lasing conditions are strictly related to a condition linking k_{isc} , σ_{TA} , and σ_{em} for every resonator. As such, the triplet is drastically limited to below one microsecond with standard values for the system to achieve CW lasing, regardless of the lasing threshold of the laser (this is an important difference with TTA, whose influence differed from one resonator to another).

At last, we reviewed the influence of RISC, which has recently gained a lot of interest and has allowed the third generation of OLED to be efficient over the whole visible region. In the framework of lasing however, we saw that it contributes to decrease the influence of other mechanisms such as ISC and STA. As long as TA is involved, we showed that k_{RISC} ease the reaching of CW lasing as soon as it scales around k_t or higher, nuancing the conclusions of Abe *et al.* [83] on the fact that k_{RISC} had to scale at k_{ISC} for CW lasing to be possible.

More generally, this study has shown that in addition to molecular properties of the gain medium, it is just as important to focus on the resonator. Indeed, reducing its lasing threshold can ease in various ways the obtention of longer lasing pulses: in cases where TA is not taken into account, we have seen that a lower lasing threshold reduced the amount of singlet required to inverse the population of the fluorescence, leading to less triplets, until eventually the lasing and CW thresholds make one. An observation that was already mentioned by Zhang and Forrest [157] but with the losses induced by triplet excitons and not the cavity. When TA is enabled however, we have seen that a high-Q resonator allows TTA to balance triplet absorption above theoretical limits.

Even tough this work has explored many aspects to understand how CW las-

ing could be achieved in different photophysical and optical configurations, there are a few additional key points that are worth studying in order to obtain further insights. As mentioned when discussing the limits of the system, it would be interesting to take into account the heat generated by the long and intense excitation, by implementing related quenchings whether they would be permanent or transient. It is now known that a proper thermal management is mandatory when aiming at longer pulses and higher repetition rate. Furthermore, the role of the concentration of active molecules inside the host matrix has not been fully explored. Indeed, we showed that it accounts in the capabilities of one device, notably in the presence of triplet absorption and bi-molecular interactions, but that it was also a variable to look at in systems where only ISC occurred. In such cases, derivations have shown for instance that a significant decrease of N could lead to inversely proportional higher quality factors required to achieve CW lasing (regardless of the pump power density).

Also, it would be useful to study how our conclusions still stand when going beyond the approximation that only one lasing mode propagates in the cavity. As discussed, it can be seen as the rather crude one considering the size of the cavities investigated. Moreover, including additional lasing modes would be the starting point towards another great topic to explore: the mode-locking of an OSSL. Because, as of today, no studies (numerical or fitting procedure of experimental results) have included the possibilities of several modes to interact with each other, to our knowledge. Besides, mode-to-mode simulations could provide insights on the duration of the lasing pulse required to allow a mode-locking regime to build itself, but those simulations are complicated to perform and are very resource demanding (as the computation time drastically increases with the number of modes).

Chapter 4

On the discrepancy regarding BSBCz lasing pulse duration in different resonators

4.1 Introduction

The method presented in Chapter 2 allowed us for blended CBP:BSBCz 200 nm films to estimate triplet-related photophysical constants such as triplet lifetimes, ISC, STA, and TTA rates. Since the films were similar to the ones used by Sandanayaka *et al.* to demonstrate a 30 ms lasing [5], our conclusions regarding their smaller triplet lifetimes and higher TTA rates as opposed to other dyes (C521T, DCM, ..) provided additional leads to explain such achievements (which are usually ascribed to a negligible triplet absorption and to a low triplet formation quantum yield [15, 14, 5]).

Afterwards, we presented a theoretical study on the requirements to achieve continuous-wave lasing for an OSSL, with an assumed focus on how those conditions evolve for different resonators, which are distinguished mostly through a quality factor. Taking advantage of a widely used system of rate equations governing the different state populations and the photon density inside the cavity, our homemade algorithm allows a fine discrimination of the lasing regimes (no lasing, pulsed, and CW) that one device can achieve for a given excitation intensity.

The purpose of this last short chapter is therefore to combine the usefulness of both previous chapters by implementing in the numerical model the values estimated using the pump-probe setup (τ_t , k_{ISC} , k_{STA} , k_{TTA}) for CBP:BSBCz thin films, and use the algorithms to explain why the achievement of ms lasing pulses are still only limited to DFB resonators. As a reminder, lasing transients displayed on Figure 3.1 showed that BSBCz used in VCSEL configuration at similar concentration and excited at similar fluences yielded pulses that lasted no longer than one microsecond, which is no better than any classical dye investigated before.

Parameters used for these simulations are gathered in Table 4.1. Since there

are constants that cannot be evaluated with our current setup, we chose the other relevant ones directly from the report of Sandanayaka *et al.* [5]. In this paper, σ_{TA} is estimated to scale 10^{-17} cm^2 , but since it is in the noise of their setup, we can consider that this value stands for an upper limit rather than a precise measurement.

Parameters	Value	Unit	References	Description
λ_{abs}	405	nm	[5]	absorption wavelength
λ_{em}	480	nm	[5]	emission wavelength
τ_f	0.9	ns	[5]	fluorescence lifetime
τ_t	20	μs	this work	triplet state lifetime
k_{ISC}	3×10^7	s^{-1}	this work	intersystem crossing
k_{STA}	7×10^{-10}	$\text{cm}^3 \cdot \text{s}^{-1}$	this work	singlet-triplet annihilation
k_{TTA}	2×10^{-12}	$\text{cm}^3 \cdot \text{s}^{-1}$	this work	triplet-triplet annihilation
σ_{abs}	8×10^{-17}	cm^2	[5]	absorption cross section (λ_{abs})
σ_{em}	2×10^{-16}	cm^2	[5]	emission cross section (λ_{em})
σ_{TA}	10^{-17}	cm^2	[5]	triplet absorption cross section (λ_{em})

Table 4.1: Photophysical parameters used for numerical simulations with a blended CBP:BSBCz (80:20 wt.%) as gain medium.

4.2 Results

Similarly to what has been done in Chapter 3, we computed the main system of rate equations for a wide range of quality factors and pump power densities with all relevant mechanisms taken into account (ISC, STA, TTA, and TA). Results obtained using the above-mentioned rates, lifetimes and cross sections are displayed on Figure 4.1.

Several observations that have been discussed in detail in the previous chapter are worth reminding: the influence of a triplet absorption cross section of 10^{-17} cm^2 is balanced by the strong TTA of $10^{-12} \text{ cm}^3 \cdot \text{s}^{-1}$ estimated from long photoluminescence transients with our setup. More details about the balance TA/TTA are available in Section 3.4.3.1. The fact that beyond a certain quality factor, the CW pump threshold I_p^{th} does not vary anymore is also consistent with previous discussion regarding the smaller and smaller generation of triplet excitons. Moreover, the pulse duration is here drastically limited to less than one microsecond for quality factors of 10^4 and below because of triplet absorption and its influence on I_p^{th} . Even in configurations where optical losses are minimized, the duration allowed for the lasing pulse is $\approx 10 \mu\text{s}$, with an abrupt transition to CW lasing when increasing the excitation density, as discussed in Section 3.4.2.2.

To compare the results obtained in a VCSEL and in a DFB configuration, we need to evaluate the quality factor of both resonators. To do so, we used the

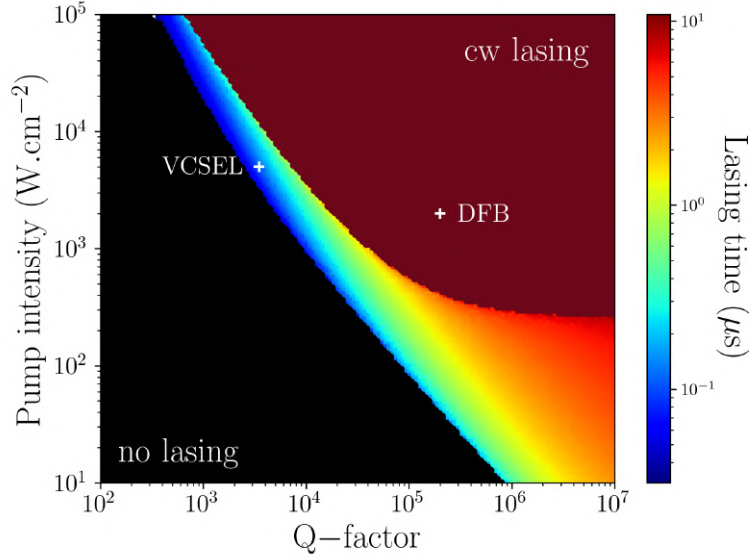


Figure 4.1: Lasing regime as a function of the quality factor of the resonator and the pump power density for a 200 nm CBP:BSBCz (80:20 wt.%) film. Parameters used for the computations are provided in Table 4.1.

equivalence between the lasing threshold and the quality factor of the cavity with the following relation:

$$Q = \frac{2\pi n_{\text{eff}} hc}{\lambda_l \lambda_p \sigma_{\text{em}} \alpha_{\text{abs}} \Gamma I_p^{\text{th}} \tau_f} \quad (4.1)$$

Here, λ_l and λ_p are the absorption and emission wavelength, respectively ; n_{eff} is the effective propagation index ; $\alpha_{\text{abs}} = \sigma_{\text{abs}} N$ the absorption coefficient of the film ; I_p^{th} is the lasing threshold and τ_f is the fluorescence lifetime.

Sandanayaka *et al.* reported a lasing threshold of $\approx 20 \text{ W.cm}^{-2}$, which corresponds to a quality factor of $\approx 3 \times 10^5$. Our VCSEL cavity on the other hand exhibited a threshold of $\approx 2 \text{ kW.cm}^{-2}$, which is linked to a quality factor of 3×10^3 . If we project those values on Figure 4.1, we obtain a clear discrepancy in the lasing regimes achieved for the two configurations investigated. Whereas a CW emission is allowed for the DFB, the VCSEL, excited at similar power density is constrained to lasing pulses that last less than one microsecond, which is consistent with the lasing transients displayed on Figure 3.1.

However, there are some disagreements with what has been reported. First, simulations show that in the DFB case, pulsed and CW thresholds are not similar, meaning that the device should exhibit pulsed emissions (becoming longer when increasing the excitation intensity) before reaching a steady-state lasing emission.

In apparent contradiction with these theoretical predictions, the reports of Sandanayaka *et al.* [5] and others [15, 173] more recently have only shown lasing that is perfectly proportional to the pump profile (when a temporal trace was provided), we can therefore assume that there was an abrupt transition between

no lasing and CW lasing as in a four-level system. Moreover, a closer look on the lasing transients related to the output of Figure 4.1, presented on Figure 4.2 (right), reveals an initial decrease of the lasing intensity before reaching a steady-state value, even for quality factors above 10^5 . A similar scenario was reported experimentally by Zhang and Forrest [157], with a pulse lasting up to 100 μs after an initial overshoot during the first four microseconds. Also, one might notice the presence of relaxation oscillation, even for quality factor this high, which were not reported with BSBCz.

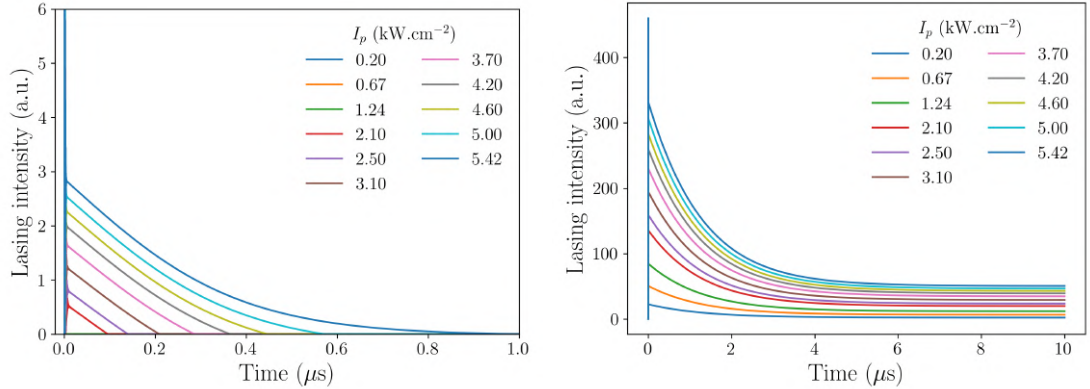


Figure 4.2: Lasing transients corresponding to the VCSEL (left) and DFB (right) points of Figure 4.1. Parameters used are displayed in Table 4.1.

The VCSEL simulations on the other hand show a good agreement with the experiments presented on Figure 3.1, with a slight difference of the slope of the lasing intensity, more pronounced in simulations. However, Figure 4.1 indicates that CW lasing is also perfectly possible for a cavity with a "low" quality factor such as VCSELs, provided a high enough pump power density. This is due to the strong TTA in play here as discussed in Section 3.4.3.1. This result has to be balanced with the fact that such excitation intensities (superior to $10 \text{ kW}\cdot\text{cm}^{-2}$) during such long times would probably result in the permanent damaging of solid-state gain media. Besides, this model do not take into account thermal quenching, whereas VCSELs are much more inclined to thermal effects than DFBs, owing to their geometry. For instance, thermal lenses (a gaussian distribution of the heat that affects lasing modes) have been proven to cause the termination of the lasing pulse in liquid state [207].

These discrepancies between simulations and experiments for the DFB could be explained by several different reasons. Starting with the model, some approximations could lead to results not in phase with reality: the modeling of the resonator using proper DFB equations could change the output, even though it would result in relaxation oscillation anyway [239]. The monomode characteristic of our simulations could also lead to different outputs, especially considering that σ_{TA} (which is proportional to the intensity of the lasing mode) is not precisely known. On that matter, it may also be related to the value of σ_{TA} chosen for the simulations,

which as it has been said corresponds to an upper limit, based on the sensitivity of the measurement. If, instead, we chose the minimal TA cross section of 3×10^{-19} cm^2 required to achieve CW lasing, which is obtained from the following relation:

$$\sigma_{\text{TA}} < \sigma_{\text{em}} \frac{k_t}{k_{\text{ISC}}} \quad (4.2)$$

where the parameters are taken from Table 4.1. We show on Figure 4.3 (left) that such a lower TA cross section (that no measurement can estimate) is more consistent with a transition between no lasing and CW lasing, although pulsed emissions are still predicted. Even if, in this configuration, the lasing intensity still decreases a little bit before reaching a steady-state value, relaxation oscillations are still present.

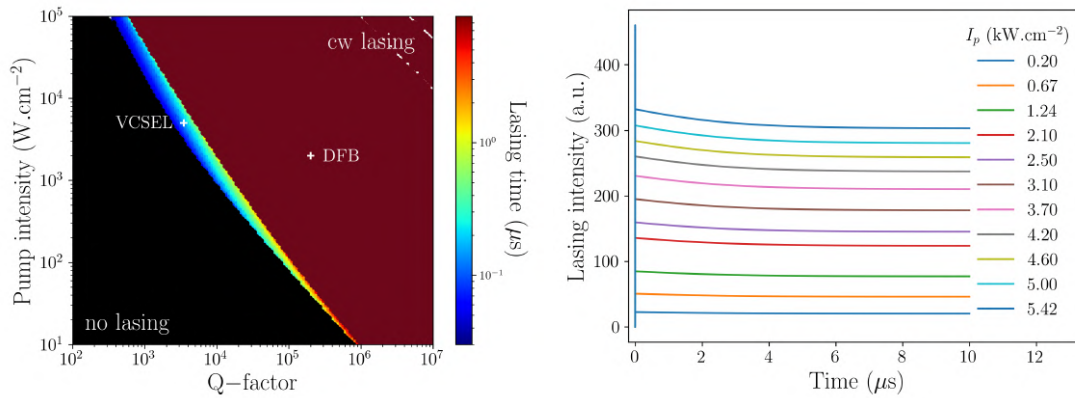


Figure 4.3: (left) Lasing regime as a function of the quality factor of the resonator and the pump power density for a 200 nm CBP:BSBCz (80:20 wt.%) film. Parameters used for the computations are provided in Table 4.1. σ_{TA} has been set to 4×10^{-19} cm^2 according to Equation 4.2. (right) Lasing transients corresponding to the DFB point of the left picture.

The reports themselves could also be debated. Although most papers that reported on CW lasing in OSSLs showed a threshold behavior and a related abrupt reduction of the **F**ull **W**idth at **H**alf **M**aximum (FWHM), the absence of relaxation oscillation from temporal traces could indicate that another regime than lasing is occurring.

Using the values obtained *via* the setup presented in Chapter 2 and our lasing algorithm, this work provides solid arguments to the different lasing pulses achieved in different resonators with BSBCz as the active molecule. Hence, we reach the conclusion that the CW lasing reported by Sandanayaka *et al.* can be explained with the low-threshold resonator, and with a unusually low triplet absorption cross section, emphasizing that both optical and molecular properties shall be taken into account in further studies towards true CW lasing.

Conclusion

It is established that the main limitation towards the achievement of continuous-wave lasing under optical pumping is the inherent building of long-lived triplet excitons with time *via* intersystem crossing. The depletion of the ground state S_0 and triplet-related mechanisms such as singlet-triplet annihilation and triplet absorption had then always hindered OSSs to emit lasing pulses that lasted much than a few hundreds of nanoseconds. However, very recently, a few papers have shown the possibility to overcome those traditional limitations using a class of molecules containing carbazole units (BSBCz [14, 5], BSFCz [15]) and to demonstrate ms qCW lasing. This breakthrough and all subsequent ones using similar compounds and configurations have been ascribed to a weak triplet absorption cross section at the lasing frequency, and to a low triplet formation quantum yield.

In addition to their long lifetime, it is crucial to quantify the different pathways through which triplet excitons can quench the lasing intensity inside a cavity, namely intersystem crossing, singlet-triplet-, triplet-triplet-annihilation, and triplet absorption. However, methods that are used to measure such constants (k_t , k_{ISC} , k_{STA} , k_{TTA} , and σ_{TA}) often require expensive apparatus, complicated setups, or rely on too many adjustable parameters in the case of fitting procedures, leading to discrepancies that can reach several orders of magnitude.

In this manuscript, an experimental method is presented in Chapter 2 that aims at tackling these limitations by taking advantage of a simple, inexpensive setup to almost fully characterize triplet-related constants. To do so, two optical pulses ($\approx 100 \text{ W.cm}^{-2}$, tens of μs) with an adjustable delay between them excite gain media whose photoluminescence is recorded with a PMT and an oscilloscope. By looking at the recovery of the S_0 population density when increasing the delay between the pump and the probe (and hence the depletion of the triplet state), we can estimate the triplet lifetime τ_t . To ensure that no other phenomena influence the non-radiative de-excitation of T_1 excitons, measurements are performed at a concentration which is low enough so that the recovery kinetic is purely monoexponential. Afterwards, k_{ISC} can be estimated at similarly low doping ratios using longer PL transients to fit its almost linear decrease with time, caused by the term $k_{ISC}S_1$. Using the transients PL of higher concentrated gain media allows the fitting of the dynamics with STA and TTA, which are required to explain the initial

abrupt decrease and the further saturation of the triplet population. This method presents the advantages of being easy to build and to adapt to a wide range of absorption wavelength, being limited by the availability of UV laser diode with high enough power to provide the $\approx \text{kW.cm}^{-2}$ of irradiance required to saturate the triplet population. On the other hand, it requires neither a ns resolution (an oscilloscope of 100 MHz was enough for this study, as the dynamics investigated are microseconds long) nor a spectral characterization.

This setup has been employed to study 17 μm blended films of PMMA containing coumarin 521T and 314T, fluorol 555, DCM, and BSBCz-EH, as well as 200 nm films of CBP:BSBCz. Each films were processed at different concentrations to fully take advantage of the step-by-step protocol introduced. Measurements have shown triplet lifetimes around 150 μs for all compounds but BSBCz and its solution-processable derivative, for which τ_t was estimated to scale at around 20 μs . Also, we found out that much stronger STA and TTA were required to explain the faster saturation of the triplet population for BSBCz(-EH) films. Thus, this simple experiment allows clear discriminations between different molecules, and subsequent results tend to ascribe the results achieved with BSBCz to a smaller triplet lifetime and higher TTA rates, which helps depleting the triplet states.

In a second time, we theoretically studied the requirements for OSSs to achieve CW lasing, using a commonly used system of rate equations governing the S_0 , S_1 , and T_1 population densities and the lasing intensity inside the resonator. Moreover, a homemade algorithm allowed us to easily discriminate for each configuration the lasing regime (no lasing, pulsed, CW) that is achievable. In this work, we focus on the photophysical requirements (lifetimes, rates, cross sections) as much as the optical ones, especially *via* the quality factor Q of the cavity, which is inversely proportional to the lasing threshold. Doing it this way has been motivated by the work of Senevirathne *et al.* [6] who outpaced the previous state-of-the-art when reporting a one second qCW lasing using the same BSBCz in a CBP host matrix. However, this two orders of magnitude improvement towards CW lasing was entirely ascribed to the exotic circular mix-order configuration of their DFB, which helped reducing the lasing threshold threefold. However, no pulse lasting longer than one microsecond was obtained by our team with BSBCz in a VCSEL configuration, excited at similar $\approx \text{kW.cm}^{-2}$ pump fluences, suggesting that the duration of the lasing emission is not only related to the molecule but also to the cavity.

Following a discussion on the different approximations used in this work and the limits of the system, simulations and analytical derivation were presented in a step-by-step approach starting with a four-level system, where triplets are not taken into account, for explanation purposes and also to be used as a reference. Then, we studied the influence of a generation of triplet excitons *via* ISC on the lasing capabilities of OSSs, and showed that in this particular condition ($k_{\text{STA}} = k_{\text{TTA}} = \sigma_{\text{TA}} = 0$), it exists a minimal quality factor (Q_{th}) for a device to exhibit in

order to achieve CW lasing, regardless of the excitation power density. Although this system is somewhat utopian, it provides first insights into the different results observed with BSBCz in VCSEL and in DFB, with Q_{th} scaling above 10^4 when k_{ISC} is set to a typical value of 10^7 s^{-1} . Since this Q_{th} corresponds (with the values taken for absorption/emission cross sections, concentration, ..) to a lasing threshold of 1 kW.cm^{-2} , it immediately rules out VCSELs and similar resonators from reaching CW lasing, since power densities higher than $\approx 100 \text{ kW.cm}^{-2}$ will quickly result in the permanent degradation of the gain medium. DFBs on the other hand exhibiting a much lower threshold (thus a higher Q) are less impacted by an increasing ISC, as long as it does not reach values above 10^9 s^{-1} . Moreover, simulations confirm the existence of two distinct thresholds (pulsed, and CW), as reported by Zhang and Forrest [157]. We were also able to generalize the fact that both thresholds merge into one when triplet-induced losses are neglected, as the same behavior can also be observed when optical losses become negligible (in high-Q cavities).

Further, additional processes related to triplet excitons were enabled to study how each of them influences the lasing pulse duration. We showed that the influence of STA mostly consisted in increasing the CW pump threshold by a cross term $k_{\text{ISC}}k_{\text{STA}}/k_t$, and that contrarily to what is usually assumed in the literature [38, 153, 5], STA is compatible with CW emission provided that the resonator has a very low threshold (as it is the case for DFBs). Triplet absorption on the other hand is here designated as a much more dramatic mechanism towards longer lasing pulses. It can be understood because it directly quenches the photon density instead of singlet excitons, but also because of the theoretical limits imposed by the expression of I_p^{th} that was derived. Indeed, we show that in configurations where only ISC and STA are taken into account, σ_{TA} is restricted to values below $3 \times 10^{-19} \text{ cm}^2$ if usual values for k_t , k_{ISC} , and σ_{em} are chosen. What makes this criterion so dramatic is that it prevails regardless of the resonator quality factor, whereas the influence of STA was limited to low-Q cavities.

We then showed that the best candidate to compensate the influence of STA and TA is definitely triplet-triplet annihilation, owing to a twofold influence: the population of the S_1 state and the depletion the triplet state through a strong term proportional to T_1^2 . Our model showed that on this matter, TTA rates of $10^{-13} \text{ cm}^3.\text{s}^{-1}$ allowed the reaching of CW lasing for TA cross section as high as 10^{-17} cm^2 for excitation of 1 kW.m^{-2} . Regarding an intrinsically short value for τ_t that could also be a solution to deal with triplet excitons without requiring TTA, our calculations suggested that a triplet lifetime as low as 500 ns would be required to compensate the influence of a k_{TTA} set only at $10^{-15} \text{ cm}^3.\text{s}^{-1}$ (and a triplet lifetime of 175 μs). Since triplet lifetimes reported in the literature as well as the ones estimated in this work are much longer than one microsecond, increasing the concentration to take advantage of TTA seems like a more rewarding choice to elongate lasing pulses.

At last, we used in Chapter 4 the rates measured with the setup of Chapter 2 on CBP:BSBCz films presented in this thesis and lasing algorithms from Chapter 3 to study whether or not the differences observed with BSBCz in DFB (qCW) and in VCSEL (1 μ s) could be better understood. We reached the conclusion that indeed, the fact that both resonators had such different lasing thresholds was enough to explain the CW lasing reached with the DFB, and the much shorter lasing pulses in VCSEL configuration.

Whether it is from an experimental or theoretical view, this work constitutes a step forward to a better understanding of the requirements to achieve CW lasing in organic solid-state lasers. Except for the triplet absorption cross section, our method allows by a simple pump-probe setup the full characterization of triplet states in organic gain media, which could be useful to the lasing community for molecular properties screening. Besides, this setup is only at its early ages, and the perspectives and possibilities discussed in Section 2.4 would allow one to go further by increasing the resolution of the apparatus, exploring other emission wavelengths, or study a potential photobleaching of the gain medium more precisely. On the other hand, our theoretical work has clearly emphasized that the quality factor has to be taken care of as much as the photophysical properties of the active molecules. We showed for instance that a slight increase of the quality factor could be sufficient in certain configurations to go from tens of microseconds lasing pulses to continuous-wave lasing. The perspectives of taking our experiments to the next step and modeling more finely the excitons dynamics inside a resonator are quite promising, as we are by the day closer and closer to true CW emission in OSSs, paving the way for mode-locking and electrical pumping.

Appendices

Measurement of photophysical constants

Analytical solution of the population density in the absence of intermolecular interactions or resonator

In a configuration without resonator ($\sigma_{\text{em}}I = 0$) where only intersystem crossing is enabled ($k_{\text{STA}} = k_{\text{T TA}} = \sigma_{\text{TA}} = 0$), the system of rate equation used in this work can be expressed as:

$$\begin{cases} \frac{dS_1}{dt} = R_{\text{ex}}S_0 - k_f S_1 - k_{\text{ISC}}S_1 \\ \frac{dT_1}{dt} = k_{\text{ISC}}S_1 - k_t T_1 \\ \frac{dS_0}{dt} = -R_{\text{ex}}S_0 + k_f S_1 + k_t T_1 \end{cases} \quad (4.3)$$

Since there are no cross terms (*e.g.* $k_{\text{T TA}}T_1^2$, $\sigma_{\text{TA}}I$, ...), it can be written in a matrix form:

$$\frac{d}{dt} \begin{bmatrix} S_1 \\ T_1 \\ S_0 \end{bmatrix} = \begin{bmatrix} -k_f - k_{\text{ISC}} & 0 & R_{\text{ex}} \\ k_{\text{ISC}} & -k_t & 0 \\ k_f & k_t & -R_{\text{ex}} \end{bmatrix} \begin{bmatrix} S_1 \\ T_1 \\ S_0 \end{bmatrix} \quad (4.4)$$

Math reminder

Previous equation can be computed as:

$$\frac{d\vec{S}}{dt} = \frac{d}{dt} \begin{bmatrix} S_1(t) \\ T_1(t) \\ S_0(t) \end{bmatrix} = M \vec{S} \quad (4.5)$$

M is diagonalized so that it contains the eigenvalues and eigenvectors of the system. Eigenvalues are the diagonal elements of the matrix D while eigenvectors are the columns of the change-of-basis matrix P , which is defined as $P^{-1}MP = D$ or $PDP^{-1} = M$. The idea is that this differential equation has simple solution

consisting in a sum of exponentials in the eigenbasis. If we define new variables $x(t)$, $y(t)$, and $z(t)$, the system becomes

$$\vec{X} = \begin{bmatrix} x(t) \\ y(t) \\ z(t) \end{bmatrix} = P^{-1} \vec{S} \quad (4.6)$$

It is then straightforward to check that

$$\frac{d\vec{X}}{dt} = P^{-1} M P \vec{X} = D \vec{X} \quad (4.7)$$

If λ_1 , λ_2 , and λ_3 are the three eigenvalues of D , the solution is

$$\begin{bmatrix} x(t) \\ y(t) \\ z(t) \end{bmatrix} = \begin{bmatrix} x(0)e^{\lambda_1 t} \\ y(0)e^{\lambda_2 t} \\ z(0)e^{\lambda_3 t} \end{bmatrix} \quad (4.8)$$

To reach our initial population $S_0(t)$, $S_1(t)$, and $T_1(t)$, one just need to multiply the P since $\vec{S} = P \vec{X}$. We don't need to compute P^{-1} : we don't care about knowing exactly how $x(t)$ and other variables are defined from $\vec{X} = P^{-1} \vec{S}$, we just need P and D . To calculate those, a handy tool is Python's literal computation library, which has been used here to diagonalize the squared matrix M . If we define $\kappa = (k_f^2 + k_{\text{ISC}}^2 + k_t^2 + R_{\text{ex}}^2 + 2k_f k_{\text{ISC}} + 2k_f R_{\text{ex}} - 2k_f k_t - 2k_{\text{ISC}} R_{\text{ex}} - 2k_{\text{ISC}} k_t - 2R_{\text{ex}} k_t)^{1/2}$, calculations yields $M = P D P^{-1}$ with:

$$P = \begin{bmatrix} \frac{R_{\text{ex}}}{k_f + k_{\text{ISC}}} & \frac{2R_{\text{ex}}}{k_f + k_{\text{ISC}} - R_{\text{ex}} - k_t - \kappa} & \frac{2R_{\text{ex}}}{k_f + k_{\text{ISC}} - R_{\text{ex}} - k_t + \kappa} \\ \frac{k_{\text{ISC}} R_{\text{ex}}}{k_t(k_f + k_{\text{ISC}})} & \frac{2k_{\text{ISC}}}{k_f - k_{\text{ISC}} + R_{\text{ex}} - k_t + \kappa} & \frac{2k_{\text{ISC}}}{k_f - k_{\text{ISC}} + R_{\text{ex}} - k_t - \kappa} \\ 1 & 1 & 1 \end{bmatrix} \quad (4.9)$$

and

$$D = \begin{bmatrix} 0 & 0 & 0 \\ 0 & -\frac{k_f + k_{\text{ISC}} + R_{\text{ex}} + k_t}{2} - \frac{\kappa}{2} & 0 \\ 0 & 0 & -\frac{k_f + k_{\text{ISC}} + R_{\text{ex}} + k_t}{2} + \frac{\kappa}{2} \end{bmatrix} \quad (4.10)$$

It is useful to first simplify as much as possible these expressions given the usual orders of magnitude : $k_f \sim 10^9$, $k_{\text{ISC}} \sim 10^7$, $k_t \sim 10^4 s^{-1}$ and $R_{\text{ex}} = \sigma_{\text{abs}} I_p^{\text{photonic}} = \frac{I_p^{\text{energetic}}}{\sigma_{\text{abs}} h\nu_p}$. $I_p^{\text{energetic}}$ scales usually between $\sim 100 \text{ W.cm}^{-2}$ for low-threshold DFB lasers

and up to $\sim 100 \text{ kW.cm}^{-2}$ in VECsOLs, which for a pump wavelength of 400 nm corresponds to pumping rates, with $\sigma_{abs} \sim 10^{-20} \text{ m}^2$, ranging between $2 \times 10^4 \text{ s}^{-1}$ (for 100 W/cm^2) to $2 \times 10^7 \text{ s}^{-1}$ (for 100 kW.cm^{-2}). So, R_{ex} can span a wide range of values, either very low and comparable to k_t , or quite high and comparable to k_{ISC} . With $R_{ex} = 2 \times 10^4 \text{ s}^{-1}$, we get $\kappa = 1.01 \times 10^9 \text{ s}^{-1} \approx k_f$ and with $R_{ex} = 2 \times 10^7 \text{ s}^{-1}$, we get $\kappa = 1.03 \times 10^9 \text{ s}^{-1} \approx k_f$. So it is possible to approximate κ by k_f in all situations, and greatly simplify the above equations

$$P \approx \begin{bmatrix} \frac{R_{ex}}{k_f} & \frac{2R_{ex}}{k_f + k_{ISC} - R_{ex} - k_t - \kappa} & \frac{R_{ex}}{k_f} \\ \frac{k_{ISC}R_{ex}}{k_t k_f} & \frac{k_{ISC}}{k_f} & \frac{2k_{ISC}}{k_f - k_{ISC} + R_{ex} - k_t - \kappa} \\ 1 & 1 & 1 \end{bmatrix} \quad (4.11)$$

and

$$D \approx \begin{bmatrix} 0 & 0 & 0 \\ 0 & -k_f & 0 \\ 0 & 0 & -\frac{k_f + k_{ISC} + R_{ex} + k_t}{2} + \frac{\kappa}{2} \end{bmatrix} \quad (4.12)$$

To further simplify κ , it's important not to neglect too fast seemingly little terms, because the 3rd eigenvalue is in fact very dependent on every term ! Let's go to the maths: if we just rearrange κ to factorize k_f and use $\sqrt{1 + \epsilon} \approx 1 + \frac{\epsilon}{2}$, we get :

$$\kappa \approx k_f + R_{ex} + k_{ISC} - k_t + \frac{k_{ISC}^2}{2k_f} + \frac{k_t^2}{2k_f} + \frac{R_{ex}^2}{2k_f} - \frac{k_{ISC}R_{ex}}{k_f} - \frac{k_{ISC}k_t}{k_f} - \frac{k_tR_{ex}}{k_f} \quad (4.13)$$

Let's see what is the order of magnitude of each of these terms :

- $k_f \sim 10^9, k_{ISC} \sim 10^7, R_{ex} \sim 2 \times 10^4 \rightarrow 2 \times 10^7, k_t \sim 10^4$
- $\frac{k_{ISC}^2}{2k_f} \sim 5 \times 10^4$
- $\frac{k_t^2}{2k_f} \sim 5 \times 10^{-2}$
- $\frac{R_{ex}^2}{2k_f} \sim 2 \times 10^{-1}$ to 2×10^5
- $-\frac{k_{ISC}R_{ex}}{k_f} \sim -2 \times 10^2 \rightarrow -2 \times 10^5$
- $-\frac{k_{ISC}k_t}{k_f} \sim -10^2$
- $-\frac{k_tR_{ex}}{k_f} \sim -2 \times 10^{-1} \rightarrow -2 \times 10^2$

Let's write what is the third engenvalue λ_3 (actually the second one because $\lambda_1 = 0$) :

$$\begin{aligned}
\lambda_3 &= -\frac{k_f + k_{\text{ISC}} + R_{\text{ex}} + k_t}{2} + \frac{\kappa}{2} \\
&\approx -\frac{k_f + k_{\text{ISC}} + R_{\text{ex}} + k_t}{2} \\
&\quad + \frac{k_f + R_{\text{ex}} + k_{\text{ISC}} - k_t + \frac{k_{\text{ISC}}^2}{2k_f} + \frac{k_t^2}{2k_f} + \frac{R_{\text{ex}}^2}{2k_f} - \frac{k_{\text{ISC}}R_{\text{ex}}}{k_f} - \frac{k_{\text{ISC}}k_t}{k_f} - \frac{k_tR_{\text{ex}}}{k_f}}{2} \\
&\approx -k_t + \frac{k_{\text{ISC}}^2}{4k_f} - \frac{k_{\text{ISC}}k_t}{2k_f} + \frac{k_t^2}{4k_f} - \frac{k_{\text{ISC}}R_{\text{ex}}}{2k_f} - \frac{R_{\text{ex}}k_t}{2k_f} + \frac{R_{\text{ex}}^2}{4k_f}
\end{aligned} \tag{4.14}$$

Let's put numbers on all these terms, with typical values already given for photophysical constants. For extremely low pumping rates ($R_{\text{ex}} = 2 \times 10^4 \text{ s}^{-1}$ corresponding to 100 W.cm^{-2}) up to high rates ($R_{\text{ex}} = 2 \times 10^7 \text{ s}^{-1}$ corresponding to 100 kW.cm^{-2}):

$$\begin{aligned}
\lambda_3(I_p = 100 \text{ W/cm}^2) &= -10^4 + 2.5 \times 10^4 - 50 + 2.5 \times 10^{-2} - 10^2 - 10^{-1} + 10^{-1} \\
&= 1.485 \times 10^4 (\text{s}^{-1}) \\
\lambda_3(I_p = 100 \text{ kW/cm}^2) &= -10^4 + 2.5 \times 10^4 - 50 + 2.5 \times 10^{-2} - 10^5 - 10^2 + 10^5 \\
&= 1.485 \times 10^4 (\text{s}^{-1})
\end{aligned} \tag{4.15}$$

In this particular example and completely by chance, both values for λ_3 for two extreme pump powers are equal to roughly 15000, which yields a build-up time of $\lambda_3^{-1} \approx 67 \mu\text{s}$ for a CW regime. However, if we go to the exact calculation we reach $\lambda_3 = -1.02 \times 10^4$ for $R_{\text{ex}} = 2 \times 10^4$ and $\lambda_3 = -2.04 \times 10^5$ for $R_{\text{ex}} = 2 \times 10^7$. The eigenvalues are now *negative* and they correspond to time constants $\lambda_3^{-1} \approx 10 \mu\text{s}$ and $5 \mu\text{s}$, respectively. This shows that we must be very cautious in our attempts to simplify the expression of κ to find analytical expressions.

Then, the diagonal matrix becomes:

$$D = \begin{bmatrix} \lambda_1 & 0 & 0 \\ 0 & \lambda_2 & 0 \\ 0 & 0 & \lambda_3 \end{bmatrix} \approx \begin{bmatrix} 0 & 0 & 0 \\ 0 & -k_f & 0 \\ 0 & 0 & -\frac{k_f + k_{\text{ISC}} + R_{\text{ex}} + k_t}{2} + \frac{k_f + k_{\text{ISC}} + R_{\text{ex}} - k_t + \frac{k_{\text{ISC}}^2}{2k_f} - \frac{k_{\text{ISC}}R_{\text{ex}}}{k_f} + \frac{R_{\text{ex}}^2}{2k_f}}{2} \end{bmatrix} \tag{4.16}$$

and

$$D \approx \begin{bmatrix} 0 & 0 & 0 \\ 0 & -k_f & 0 \\ 0 & 0 & -k_t + \frac{k_{\text{ISC}}^2}{4k_f} - \frac{k_{\text{ISC}}R_{\text{ex}}}{2k_f} + \frac{R_{\text{ex}}^2}{4k_f} \end{bmatrix} \quad (4.17)$$

Experimental setup

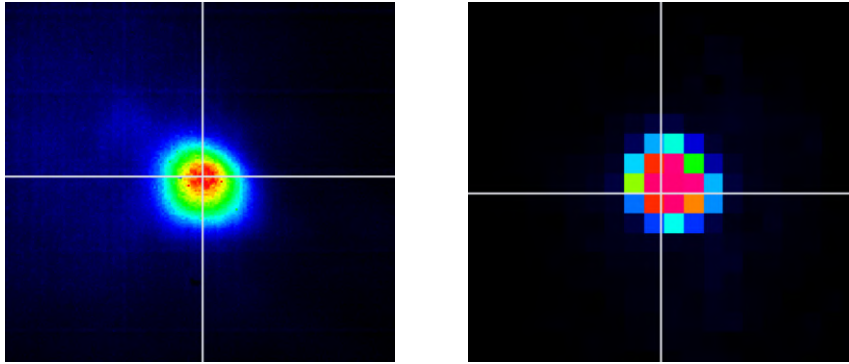


Figure A1: Beam areas on the sample captured with an imagery system and a beam analyzer for the 450 (left) and 405 (right) nm diodes. Pump diameters on the sample have been measured at $320 \mu\text{m}$ (left), and $30 \mu\text{m}$ (right).

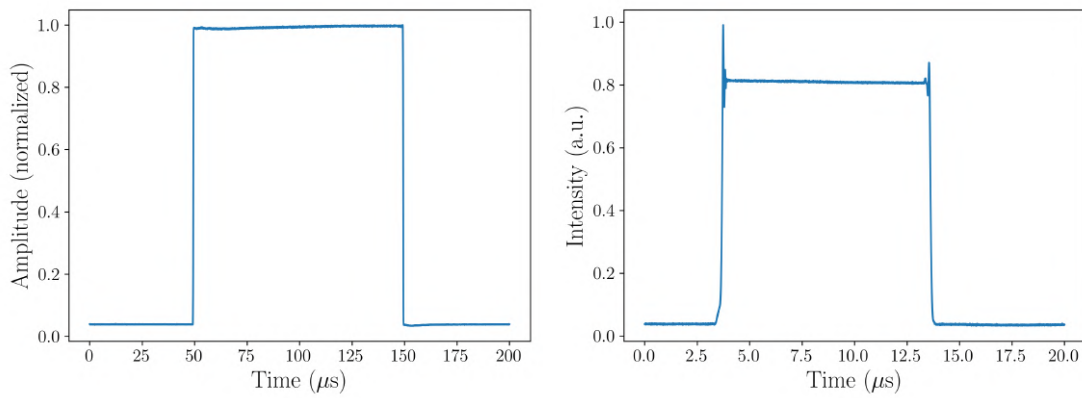


Figure A2: Pump intensity versus time recorded without sample by a PMT and an oscilloscope for the 450 (left) and 405 (right) nm diodes

Coumarin 521T

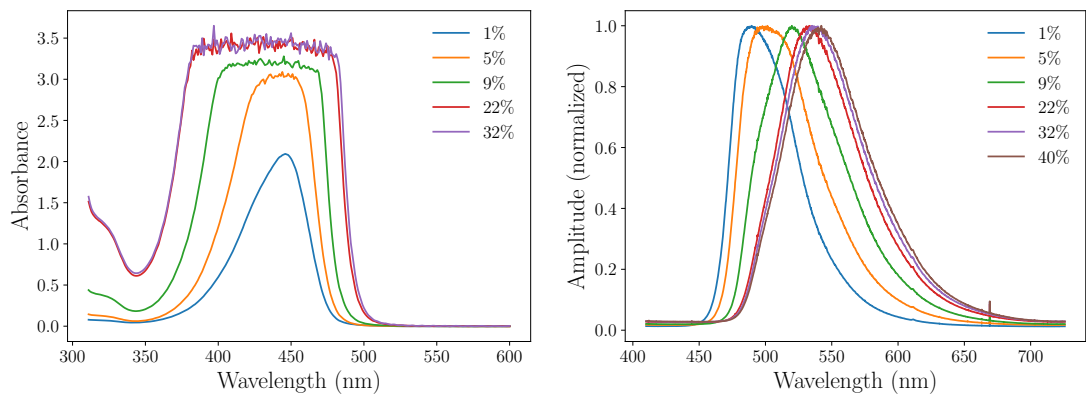


Figure A3: Absorption (left) and emission (right) of $17\mu\text{m}$ PMMA films with different concentrations of coumarin 521T

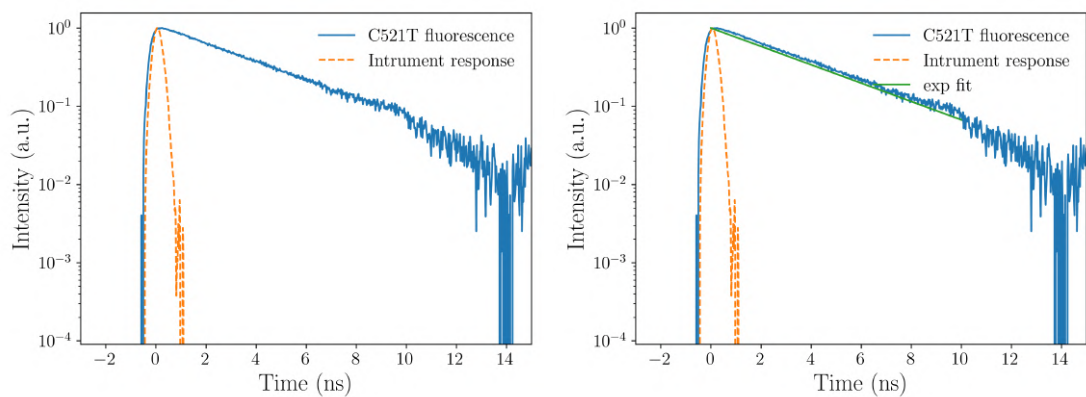


Figure A4: Fluorescence lifetime measurements for a 1 wt.% PMMA:C521T $17\mu\text{m}$ film. The monoexponential fit gives $\tau_f = 3.7$ ns.

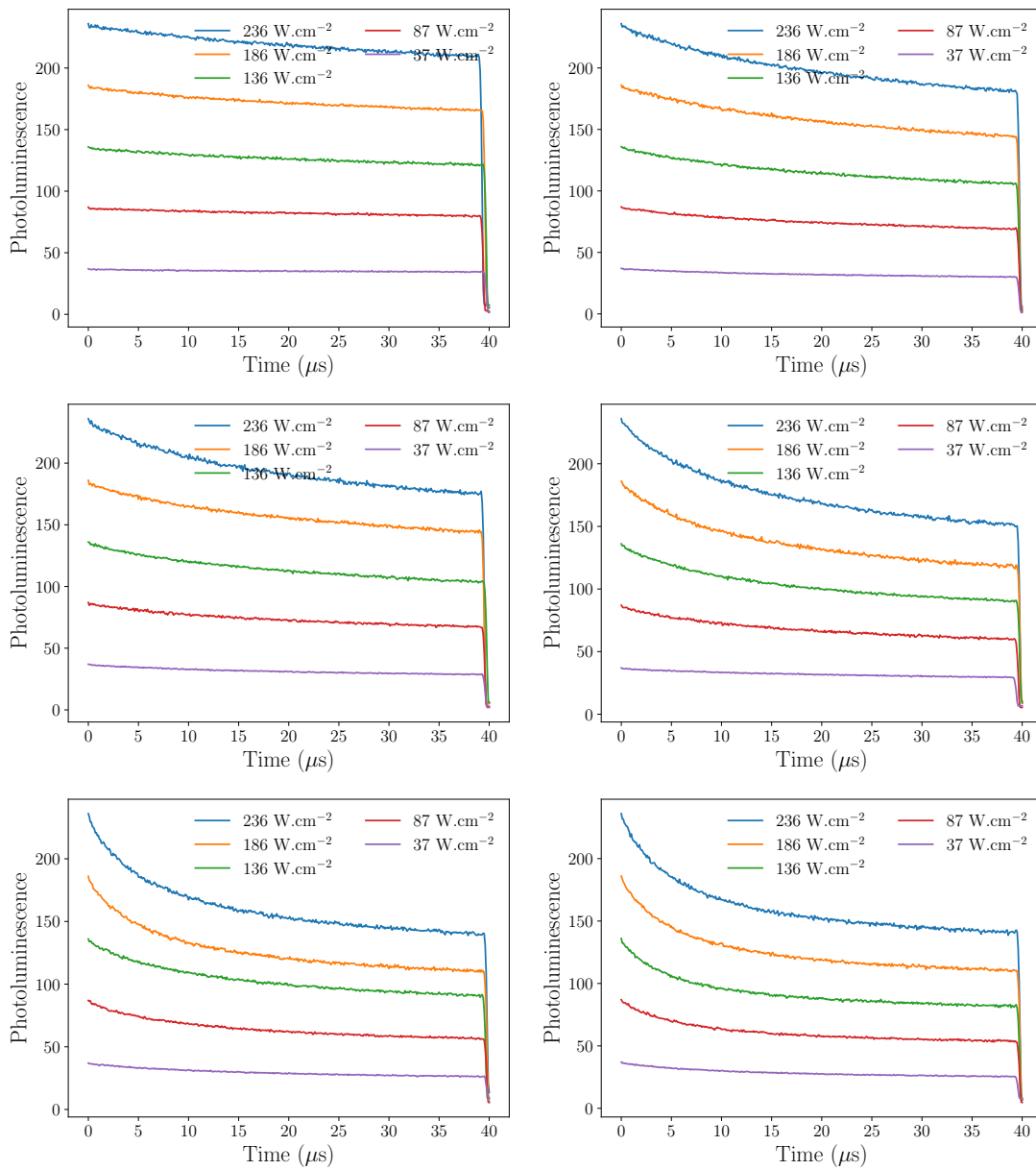


Figure A5: Photoluminescence transients of 17 μ m PMMA films with different concentrations (1, 5, 9, 22, 32, 40 wt.%) of coumarin C521T excited at different pump power densities by a 450 nm diode.

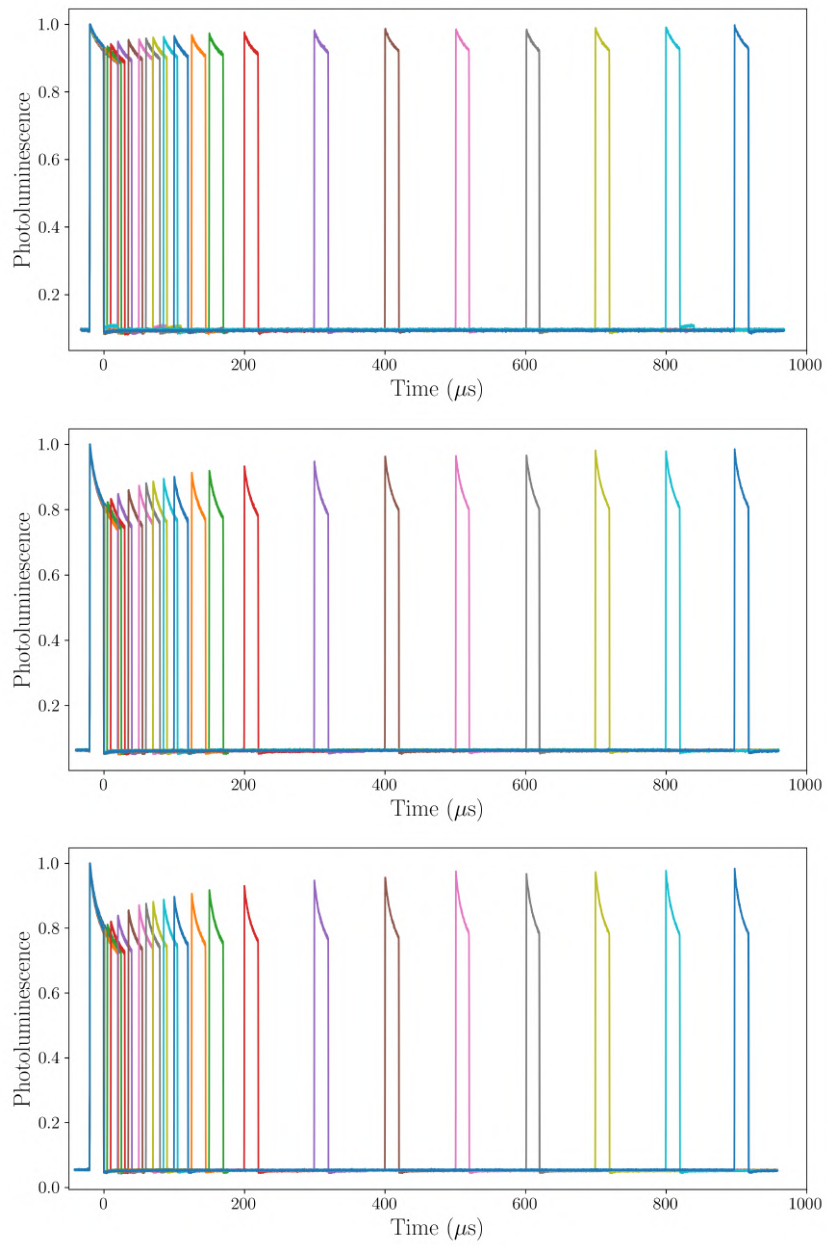


Figure A6: Photoluminescence transients from pump-probe experiment of $17\mu\text{m}$ PMMA films with different concentrations (1, 5, 9 wt.%) of coumarin C521T excited at $236\text{ W}\cdot\text{cm}^{-2}$ with a 450 nm diode.

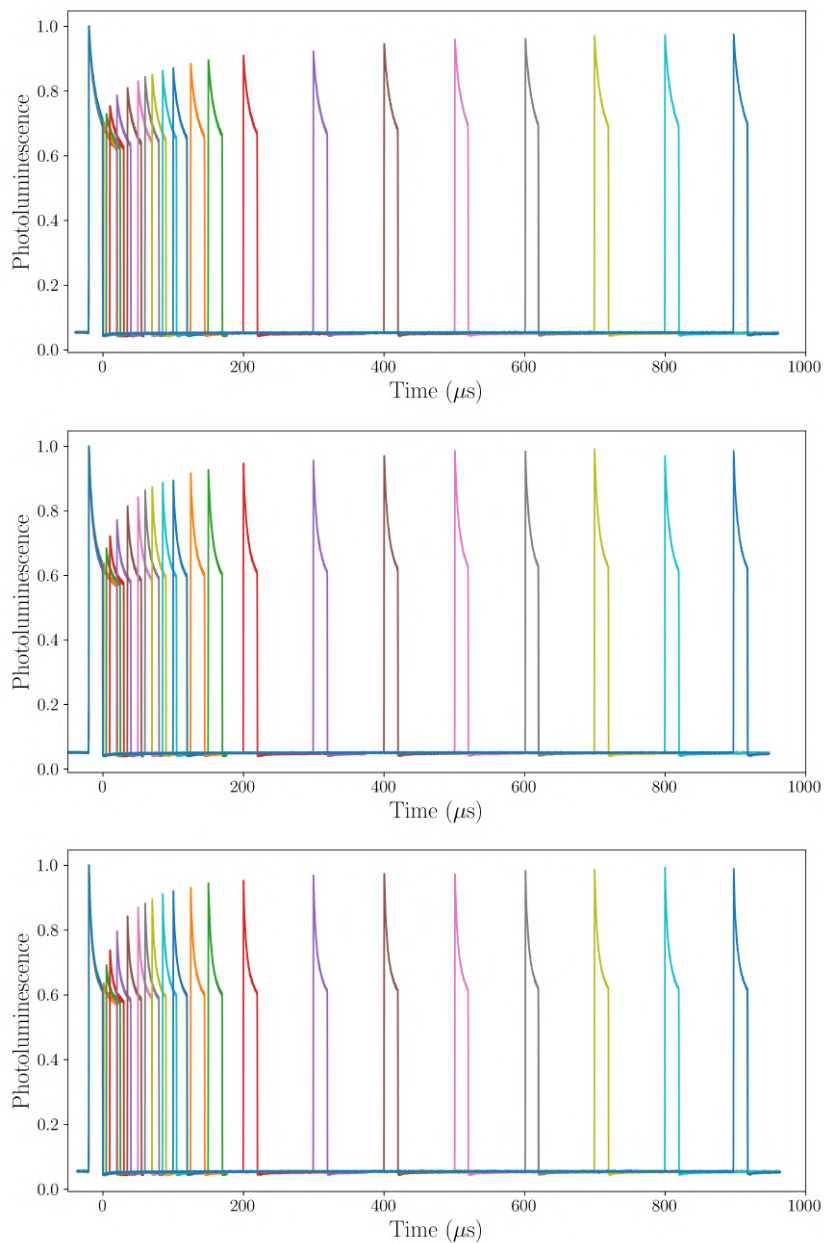


Figure A7: Photoluminescence transients from pump-probe experiment of $17\mu\text{m}$ PMMA films with different concentrations (22, 32, 40 wt.%) of coumarin C521T excited at $236\text{ W}\cdot\text{cm}^{-2}$ with a 450 nm diode.

Coumarin 314T

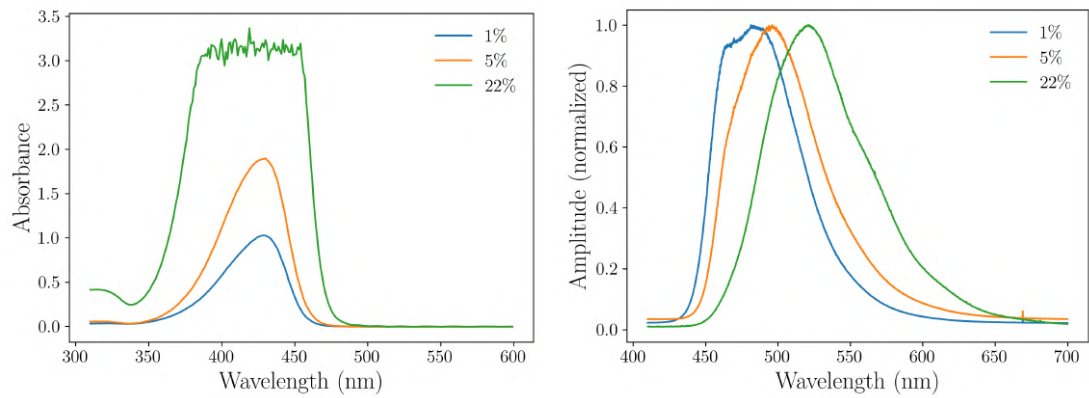


Figure A8: Absorption (left) and emission (right) of $17\mu\text{m}$ PMMA films with different concentrations of coumarin 314T

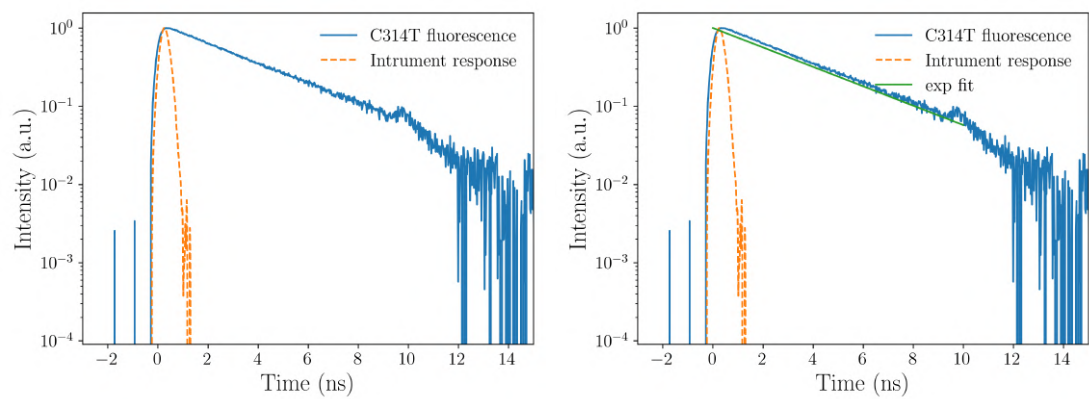


Figure A9: Fluorescence lifetime measurements for a 1 wt.% PMMA:C314T $17\mu\text{m}$ film. The monoexponential fit gives $\tau_f = 3.5$ ns.

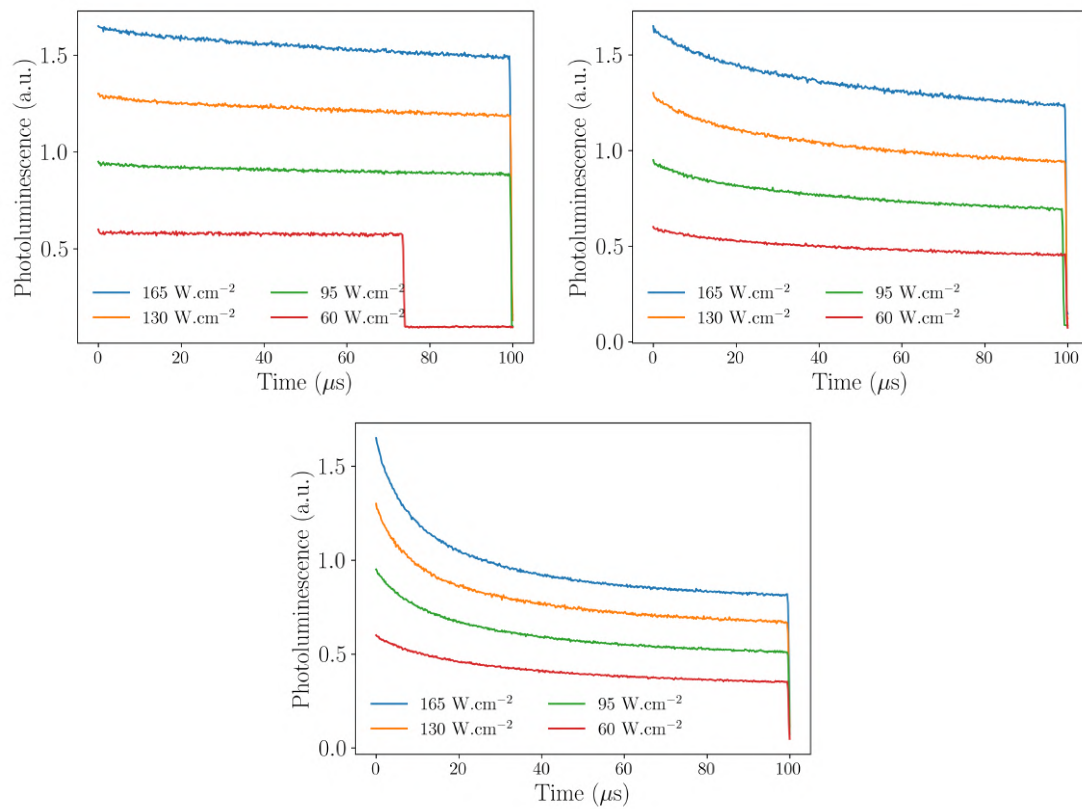


Figure A10: Photoluminescence transients of $17\mu\text{m}$ PMMA films with different concentrations (1, 5, 22 wt.%) of coumarin 314T excited at different pump power densities by a 450 nm diode.

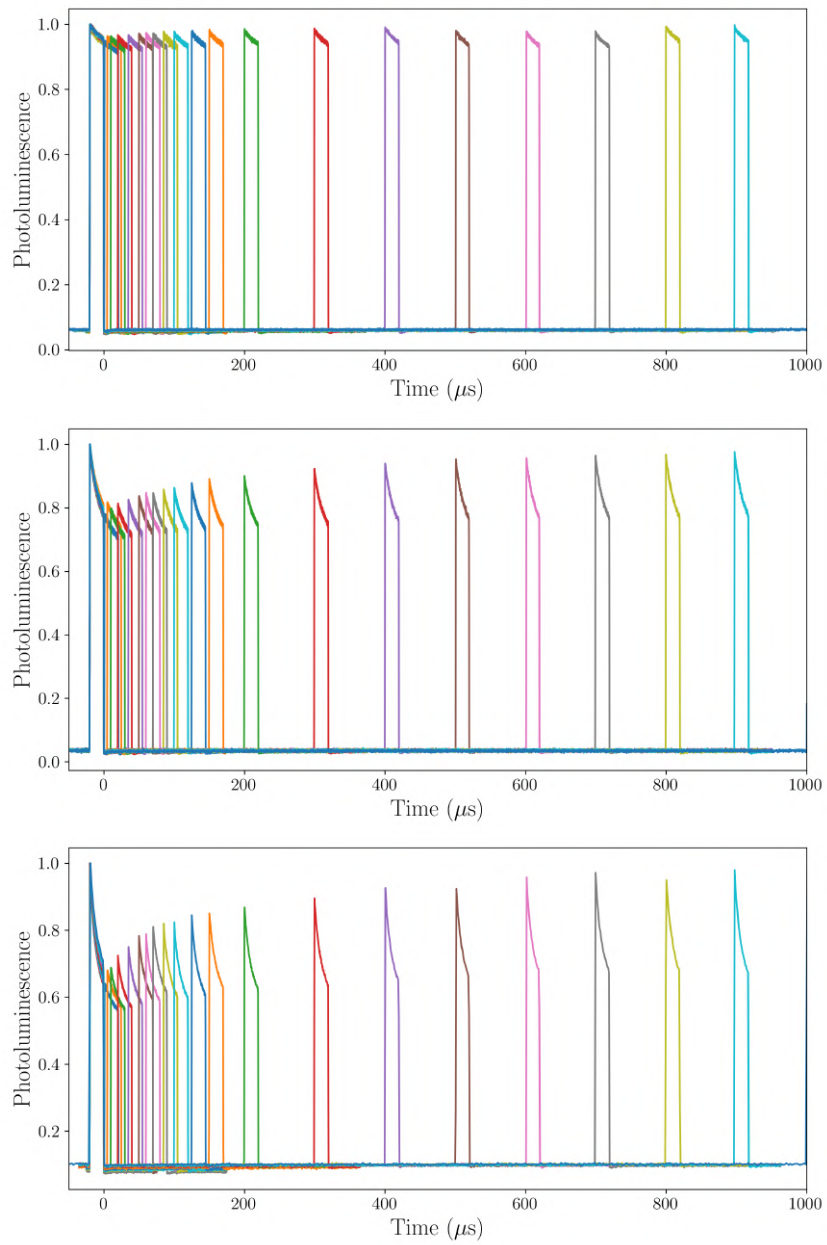


Figure A11: Photoluminescence transients from pump-probe experiment of $17\mu\text{m}$ PMMA films with different concentrations (1, 5, 22 wt.%) of coumarin 314T excited at $165\text{ W}\cdot\text{cm}^{-2}$ with a 450 nm diode.

Fluorol 555

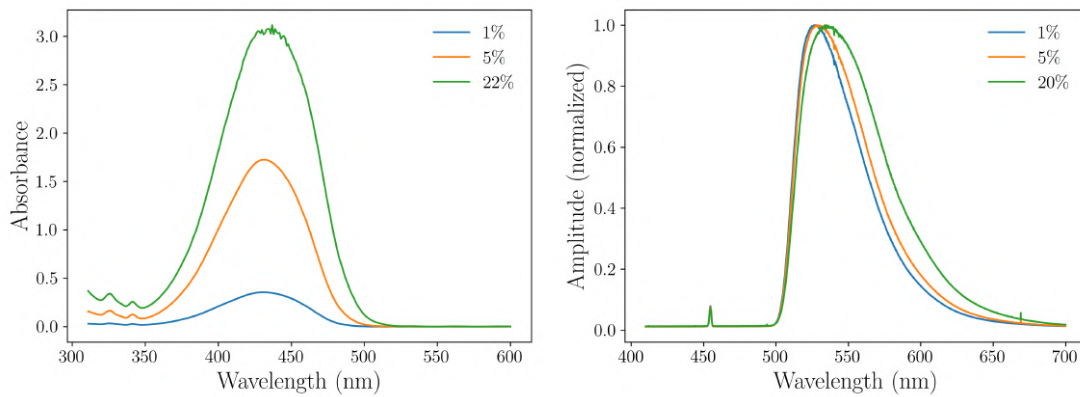


Figure A12: Absorption (left) and emission (right) of $17\mu\text{m}$ PMMA films with different concentrations of fluorol 555

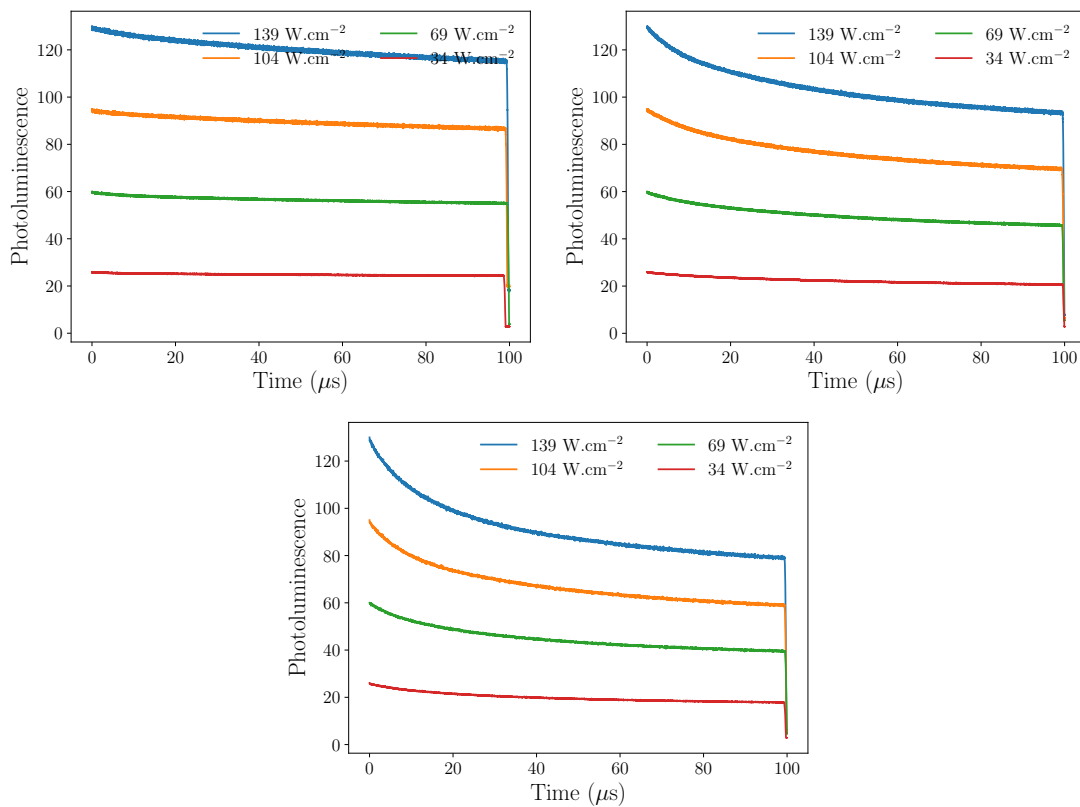


Figure A13: Photoluminescence transients of $17\mu\text{m}$ PMMA films with different concentrations (1, 5, 22 wt.%) of fluorol 555 excited at different pump power densities by a 450 nm diode.

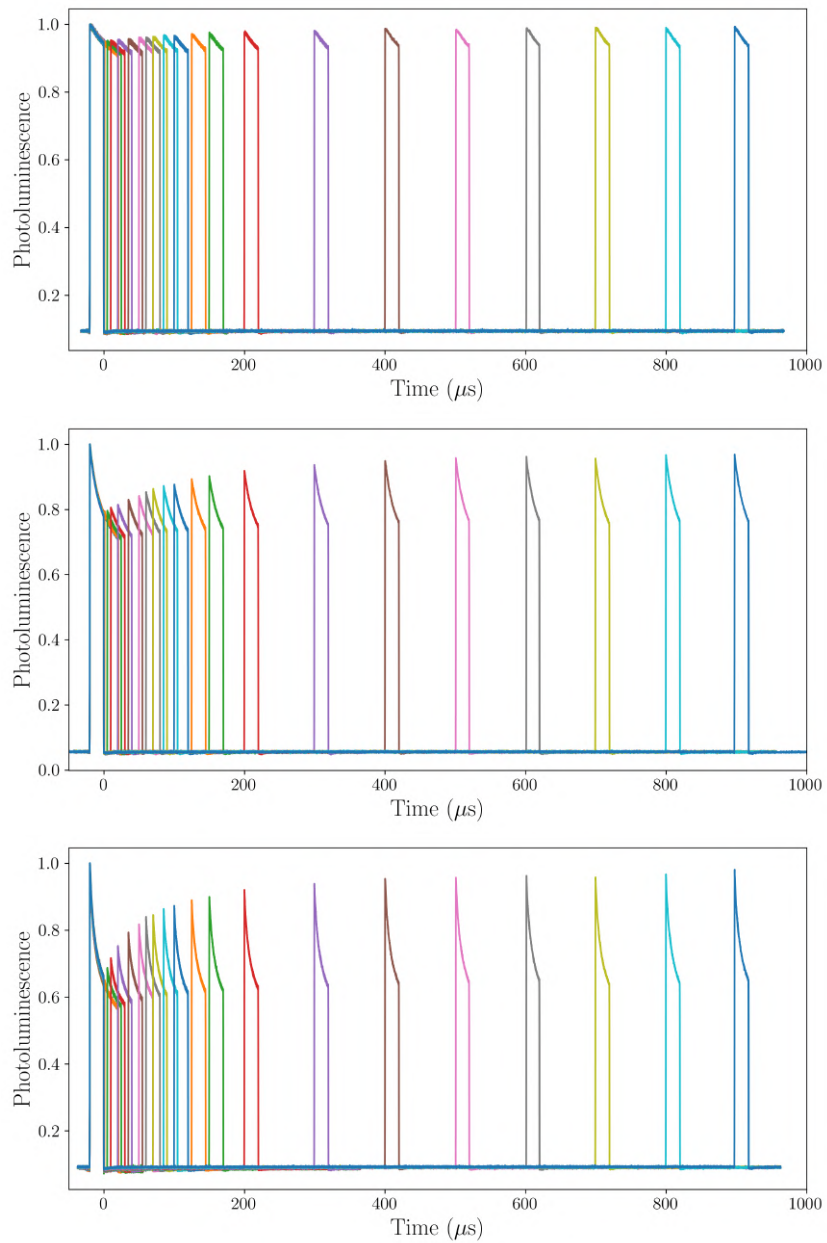


Figure A14: Photoluminescence transients from pump-probe experiment of $17\mu\text{m}$ PMMA films with different concentrations (1, 5, 22 wt.%) of fluorol 555 excited at $139\text{ W}\cdot\text{cm}^{-2}$ with a 450 nm diode.

DCM

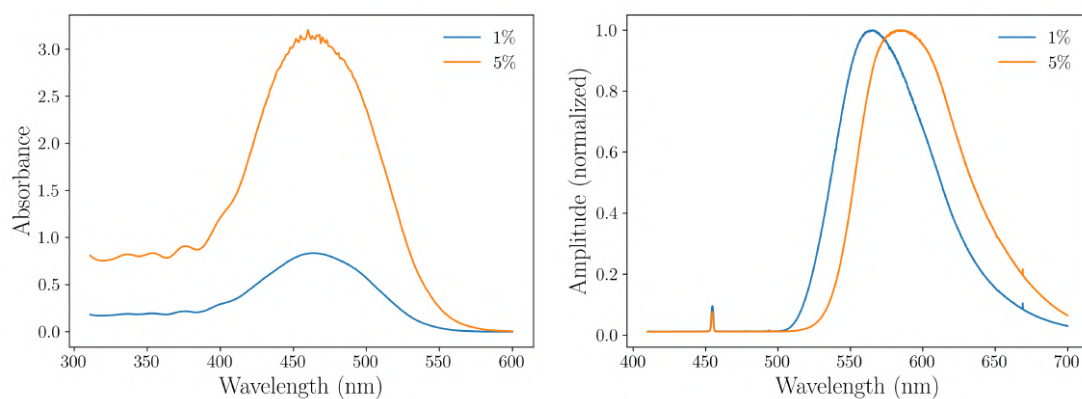


Figure A15: Absorption (left) and emission (right) of $17\mu\text{m}$ PMMA films with different concentrations of DCM

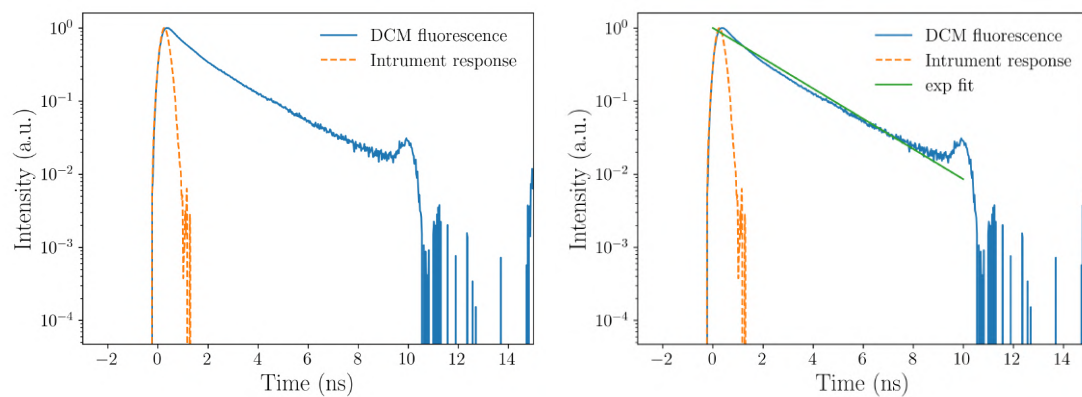


Figure A16: Fluorescence lifetime measurements for a 1 wt.% PMMA:DCM $17\mu\text{m}$ film. The monoexponential fit gives $\tau_f = 2.1$ ns.

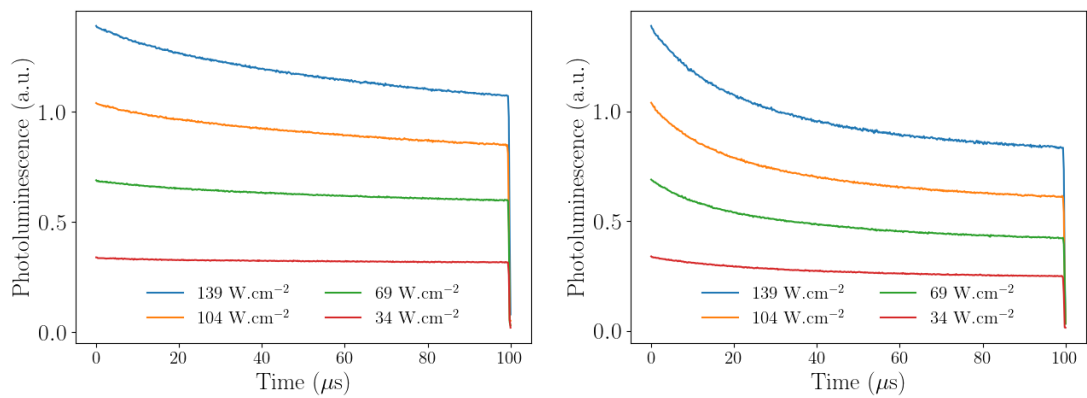


Figure A17: Photoluminescence transients of $17\mu\text{m}$ PMMA films with different concentrations (1, 5, 22 wt.%) of fluoro 555 excited at different pump power densities by a 450 nm diode.

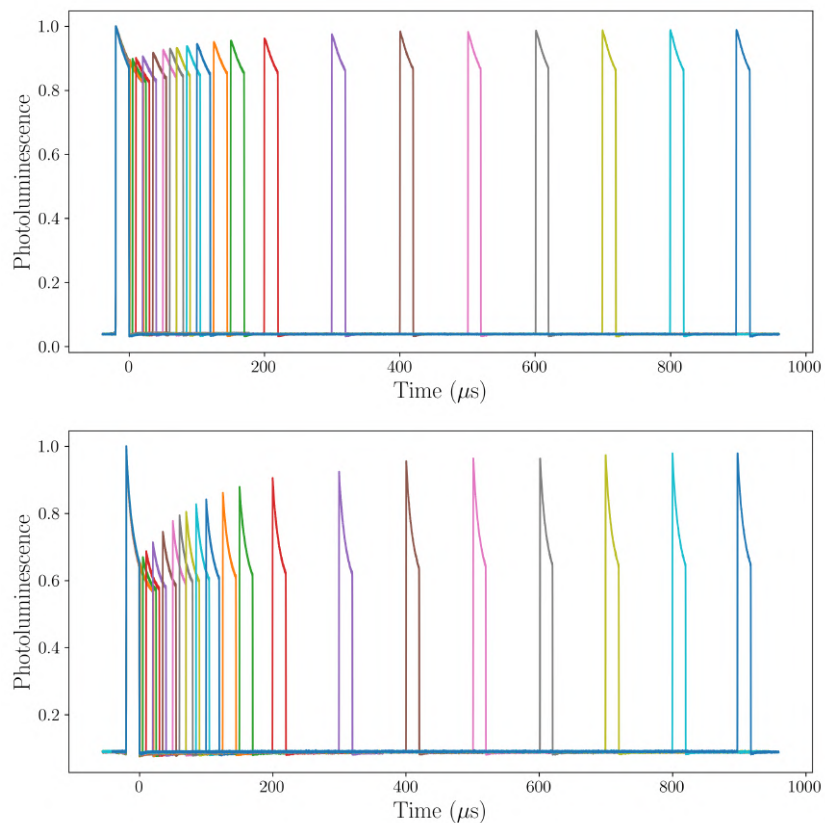


Figure A18: Photoluminescence transients from pump-probe experiment of $17\mu\text{m}$ PMMA films with different concentrations (1, 5, 22 wt.%) of fluoro 555 excited at 139 W.cm^{-2} with a 450 nm diode.

BSBCz-EH

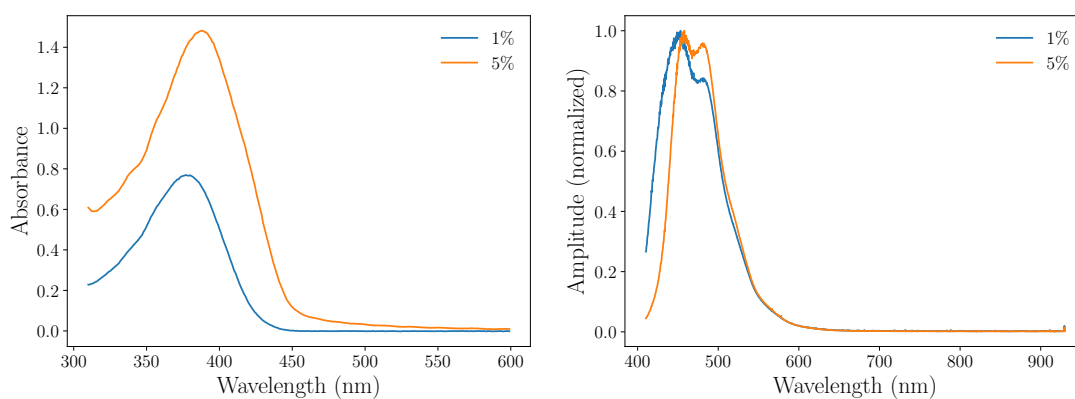


Figure A19: Absorption (left) and emission (right) of $17\mu\text{m}$ PMMA films with different concentrations of BSBCz-EH

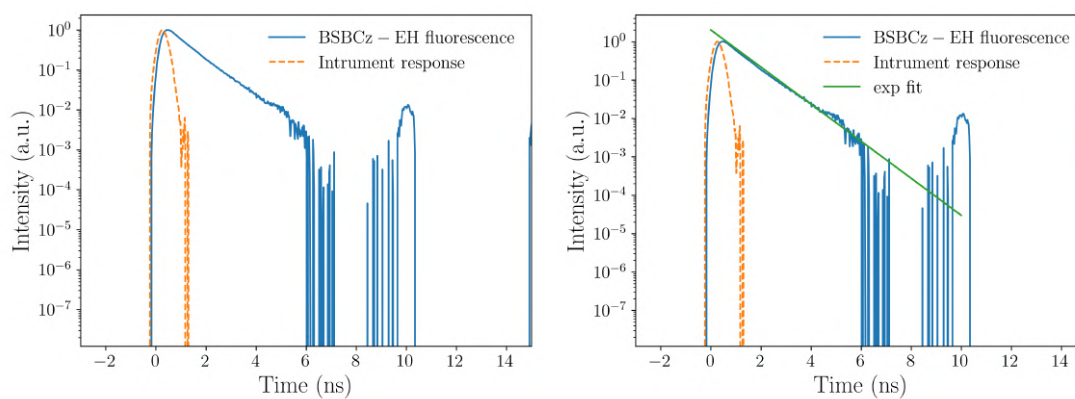


Figure A20: Fluorescence lifetime measurements for a 1 wt.% PMMA:BSBCz-EH $17\mu\text{m}$ film. The monoexponential fit gives $\tau_f = 0.9$ ns.

BSBCz

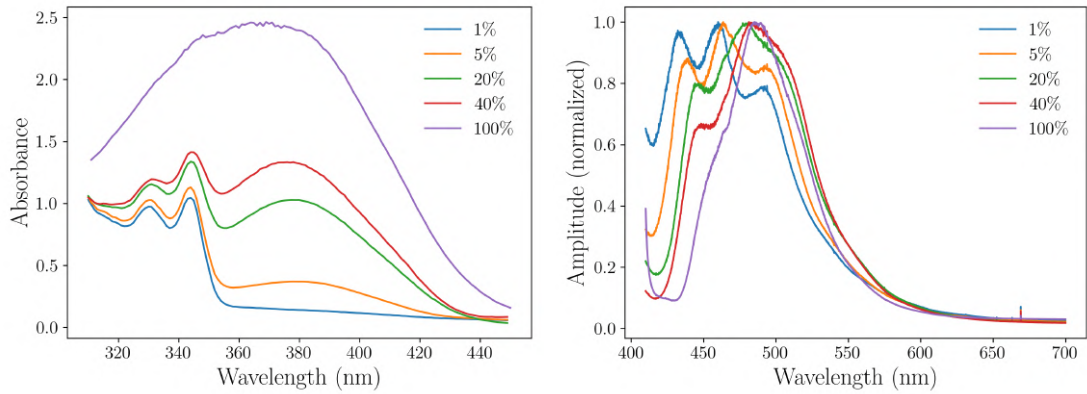


Figure A21: Absorption (left) and emission (right) of 200nm CBP films with different concentrations of BSBCz

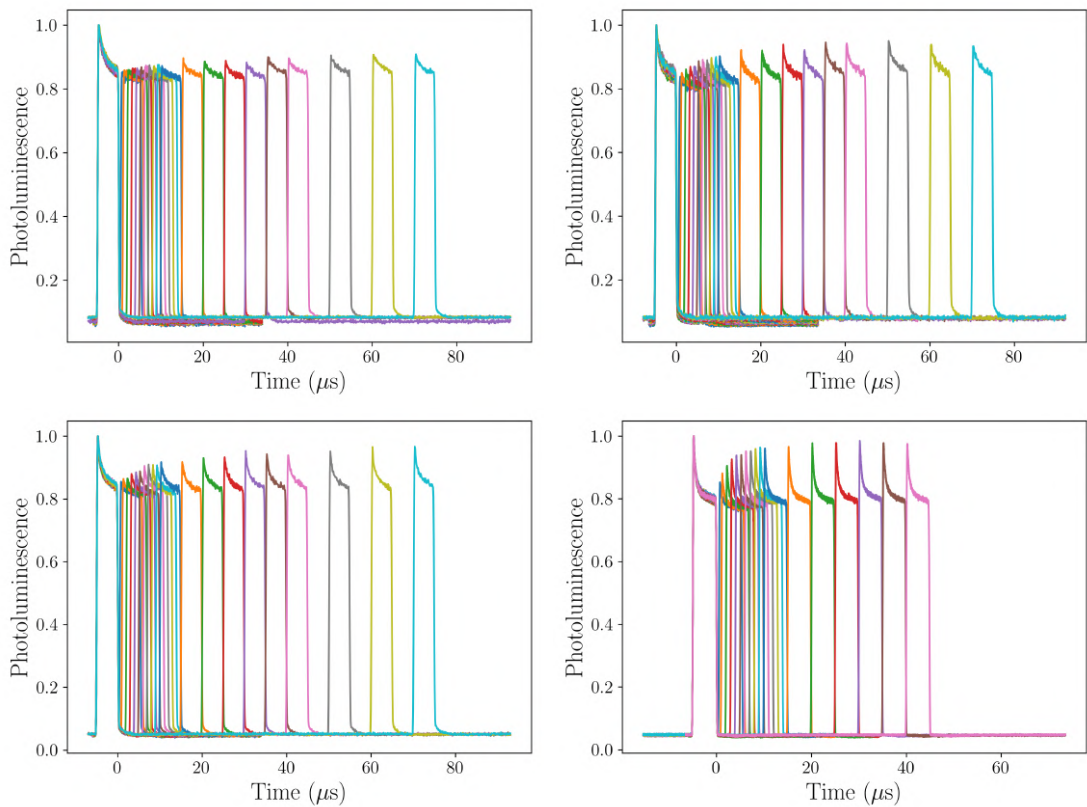


Figure A22: Photoluminescence transients of 200 nm CBP films with 5 (top left), 20 (top right), 40 (bottom left), and 100 wt.% (bottom right) of BSBCz excited at $2.6 \text{ kW}\cdot\text{cm}^{-2}$ with a 405 nm diode.

Transient Absorption Spectroscopy

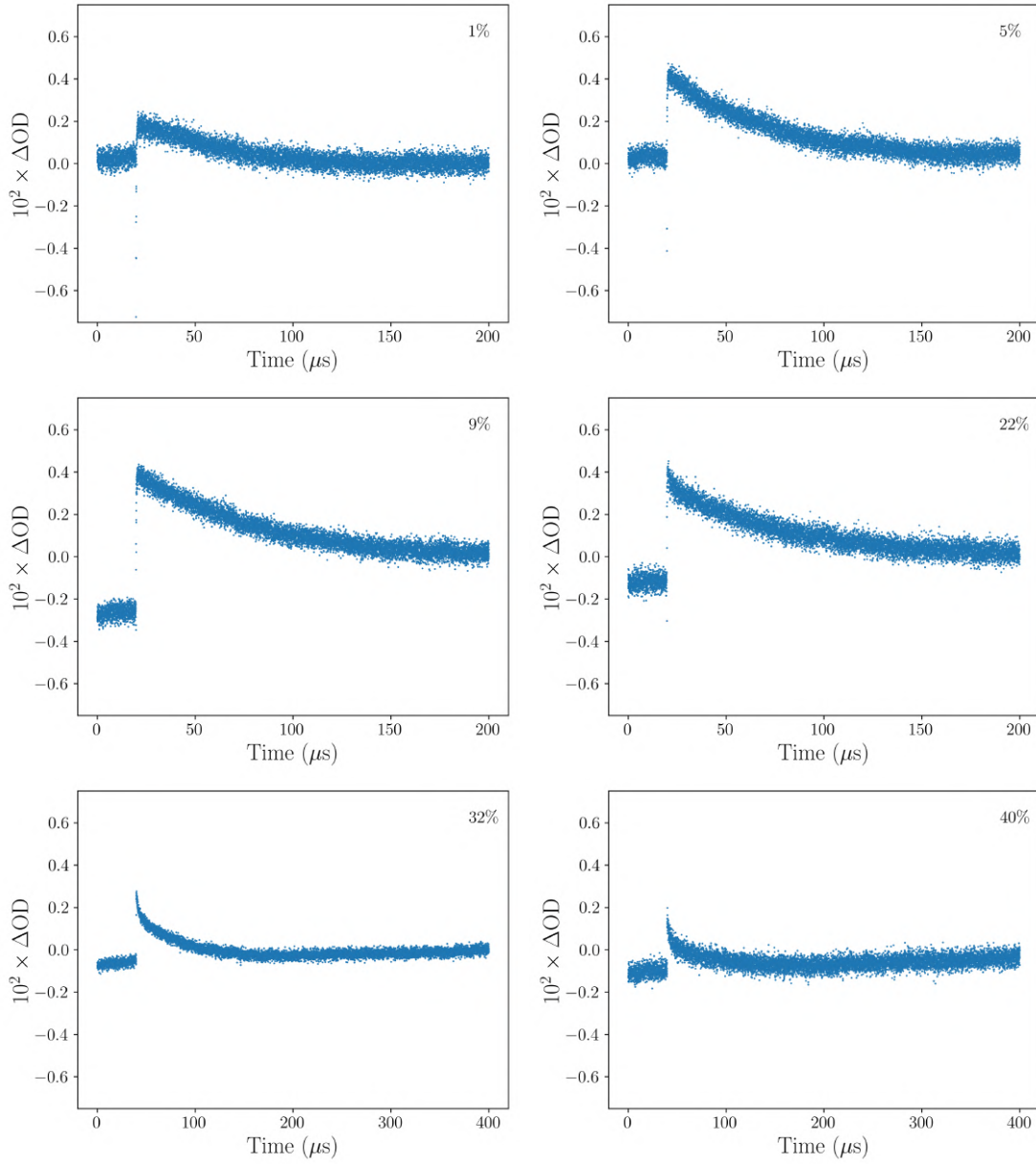


Figure A23: Transient absorption measurements of PMMA:C521T thin films at 520 nm for different concentrations of C521T.

Time-dependent internal conversion derivation

Considering that the temperature inside the gain medium should not exceed 60°C (Figure SX), one can write the PLQY temperature dependence as $\text{PLQY}(T) = 1 + \alpha\Delta T$ where $\alpha < 0$ is the slope coefficient. It can then be expressed as :

$$\frac{\text{PLQY}(T)}{\text{PLQY}(T = T_0)} = \frac{k_r}{k_r + k_{nr}} \frac{k_r + k_{nr0}}{k_r} = 1 + \alpha\Delta T \quad (4.18)$$

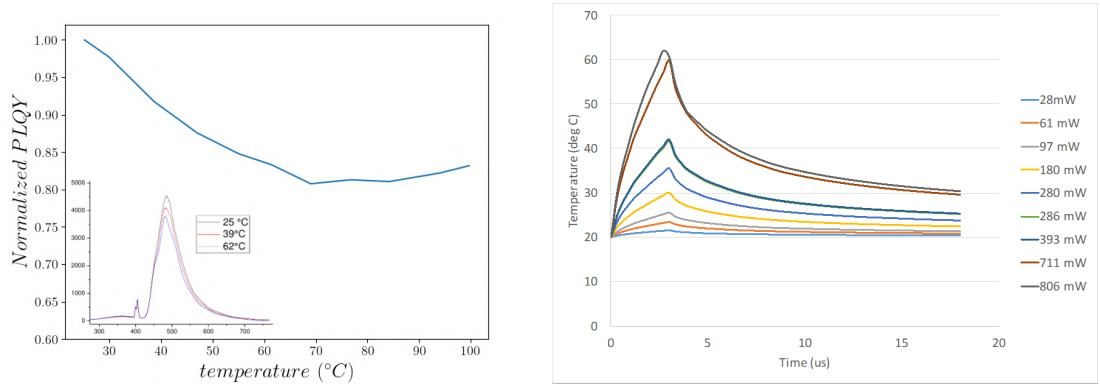


Figure A24: (left) Photoluminescence quantum yield of a 200 nm BSBCz neat film versus temperature inside the film. (right) Time-resolved simulations of the temperature inside a 200 nm neat BSBCz film at different excitation power.

leading to the following nonradiative decay rate :

$$k_{\text{nr}}(T) = \frac{k_r \alpha \Delta T + k_{\text{nr}0}}{1 + \alpha \Delta T} \quad (4.19)$$

Since the PL experiment has been performed using microseconds pumps, the heat diffusion in the gain media can be neglected. The heat equation can then be simplified and solved as:

$$\rho C_p \frac{\partial T}{\partial t} = Q \quad \rightarrow \quad T(t) = \Gamma t + T_0 \quad (4.20)$$

where the term $-k\nabla^2 T$ is cancelled, ρ is the density of the material, C_p its heat coefficient and Q corresponds to the amount of energy brought into the system. From this, a linear variation of the temperature with time can be implemented in equation 4.19 to obtain :

$$k_{\text{nr}}(T(t)) = k_{\text{nr}}(t) = \frac{k_{\text{nr}0} - k_r \alpha \Gamma t}{1 + \alpha \Gamma t} \quad (4.21)$$

CW lasing conditions of organic lasers

Parameters used in this work

Parameters	Value	Unit	Description
τ_f	1.28	ns	fluorescence lifetime
τ_t	175	μs	triplet state lifetime
k_{ISC}	10^7	s^{-1}	intersystem crossing
k_{STA}	10^{-10}	$\text{cm}^3 \cdot \text{s}^{-1}$	singlet-triplet annihilation
k_{TTA}	10^{-14}	$\text{cm}^3 \cdot \text{s}^{-1}$	triplet-triplet annihilation
Γ	0.5	...	confinement factor
λ_p	405	nm	pump wavelength
λ_l	480	nm	lasing wavelength
m	689	$\text{g} \cdot \text{mol}^{-1}$	molar mass
σ_{em}	2×10^{-16}	cm^2	emission cross section (λ_l)
σ_{abs}	8×10^{-17}	cm^2	absorption cross section (λ_p)

Table 4.2: Parameters used for the theoretical study

Expression of the CW pump intensity threshold with ISC, STA, TA, and RISC

Let's start from the system of rates equations for the excitons population densities:

$$\frac{d[S_1]}{dt} = R_{\text{ex}}[S_0] - (k_f + k_{\text{ISC}} + R_l + k_{\text{STA}}[T_1])[S_1] + k_{\text{RISC}}[T_1] \quad (4.22)$$

$$\frac{d[S_0]}{dt} = -R_{\text{ex}}[S_0] + (k_f + R_l + k_{\text{STA}}[T_1])[S_1] + k_t[T_1] \quad (4.23)$$

$$\frac{d[T_1]}{dt} = k_{\text{ISC}}[S_1] - (k_t + k_{\text{RISC}})[T_1] \quad (4.24)$$

Zeroing Equation 4.22 gives:

$$R_{\text{ex}}[S_0^{\text{ss}}] - (k_f + k_{\text{ISC}} + \sigma_{\text{em}}I + k_{\text{STA}}[T_1^{\text{ss}}])[S_1^{\text{ss}}] + k_{\text{RISC}}[T_1^{\text{ss}}] = 0 \quad (4.25)$$

Zeroing Equation 4.24 gives the steady state solution of the triple state:

$$[T_1^{\text{ss}}] = \frac{k_{\text{ISC}}}{k_t + k_{\text{RISC}}}[S_1^{\text{ss}}] = \beta[S_1^{\text{ss}}] \quad (4.26)$$

We can then implement it in Equation 4.25 and replace S_0 with $N - [S_1^{\text{ss}}] - [T_1^{\text{ss}}]$ to obtain the following second order polynomial expression.

$$-k_{\text{STA}}\beta[S_1^{\text{ss}}]^2 - (R_{\text{ex}} + k_f + k_{\text{ISC}} + \sigma_{\text{em}}I + [R_{\text{ex}} - k_{\text{RISC}}]\beta)[S_1^{\text{ss}}] + R_{\text{ex}}N = 0 \quad (4.27)$$

Let's simplify these expressions for a moment:

$$\begin{cases} a = -k_{\text{STA}}\beta \\ b = -(R_{\text{ex}} + k_f + k_{\text{ISC}} + \sigma_{\text{em}}I + [R_{\text{ex}} - k_{\text{RISC}}]\beta) \\ c = R_{\text{ex}}N \end{cases} \quad (4.28)$$

Since a and b are negative, the only positive root of this polynome is:

$$[S_1^{\text{ss}}] = \frac{-b - \sqrt{b^2 - 4ac}}{2a} \quad (4.29)$$

The point is now is isolate the lasing intensity I which is contained in b . With the next steps, we get around the problem of having b and b^2 in the same expression:

$$2a[S_1^{\text{ss}}] + b = -\sqrt{b^2 - 4ac} \quad (4.30)$$

$$4a^2[S_1^{\text{ss}}]^2 + b^2 + 4a[S_1^{\text{ss}}]b = b^2 - 4ac \quad (4.31)$$

$$-b = \frac{c}{[S_1^{\text{ss}}]} + a[S_1^{\text{ss}}] \quad (4.32)$$

We can now express I :

$$\sigma_{\text{em}}I = R_{\text{ex}}\frac{N}{[S_1^{\text{ss}}]} - k_{\text{STA}}\beta[S_1^{\text{ss}}] - k_f - k_{\text{ISC}} - R_{\text{ex}} - R_{\text{ex}}\beta + k_{\text{RISC}}\beta \quad (4.33)$$

and replace R_{ex} with $\sigma_{\text{abs}}I_p$ gives:

$$\frac{\sigma_{\text{em}}}{\sigma_{\text{abs}}}I = I_p \left[\frac{N}{[S_1^{\text{ss}}]} - (1 + \beta) \right] - \frac{1}{\sigma_{\text{abs}}}(k_f + k_{\text{ISC}} + k_{\text{STA}}\beta[S_1^{\text{ss}}] - k_{\text{RISC}}\beta) \quad (4.34)$$

At last, the intensity can be expressed in the form of $I = \eta(I_p - I_p^{\text{th}})$:

$$\frac{\sigma_{\text{em}}}{\sigma_{\text{abs}}}I = \left[\frac{N}{[S_1^{\text{ss}}]} - (1 + \beta) \right] \left\{ I_p - \frac{k_f + k_{\text{ISC}} + k_{\text{STA}}\beta[S_1^{\text{ss}}] - k_{\text{RISC}}\beta}{\sigma_{\text{abs}} \left[\frac{N}{[S_1^{\text{ss}}]} - (1 + \beta) \right]} \right\} \quad (4.35)$$

ending this derivation with the most complete solvable expression one can have from this system of equation with the expression of the pump power density required to achieve a continuous-wave lasing:

$$I_p^{\text{th}} = \frac{k_f + k_{\text{ISC}} + k_{\text{STA}}\beta[S_1^{\text{ss}}] - k_{\text{RISC}}\beta}{\sigma_{\text{abs}} \left[\frac{N}{[S_1^{\text{ss}}]} - \left(1 + \frac{k_{\text{ISC}}}{k_t}\right) \right]} \quad (4.36)$$

Since this expression represents a threshold, $[S_1^{\text{ss}}]$ can be replaced S_1^{cav} whose expression is obtained by zeroing the equation ruling the photon density:

$$\frac{dI}{dt} = \frac{c}{n} \Gamma \{ \sigma_e [S_1^{\text{ss}}] [I + I_{\text{sp}}] - \sigma_{\text{TA}} [T_1^{\text{ss}}] I \} - \frac{2\pi c}{Q\lambda_l} I \quad (4.37)$$

to obtain if triplet absorption is taken into account the following expression:

$$S_1^{\text{cav}} = \frac{2\pi n}{\Gamma Q \lambda_l \left[\sigma_{\text{em}} - \sigma_{\text{TA}} \frac{k_{\text{ISC}}}{k_t} \right]} \quad (4.38)$$

Triplet state lifetime

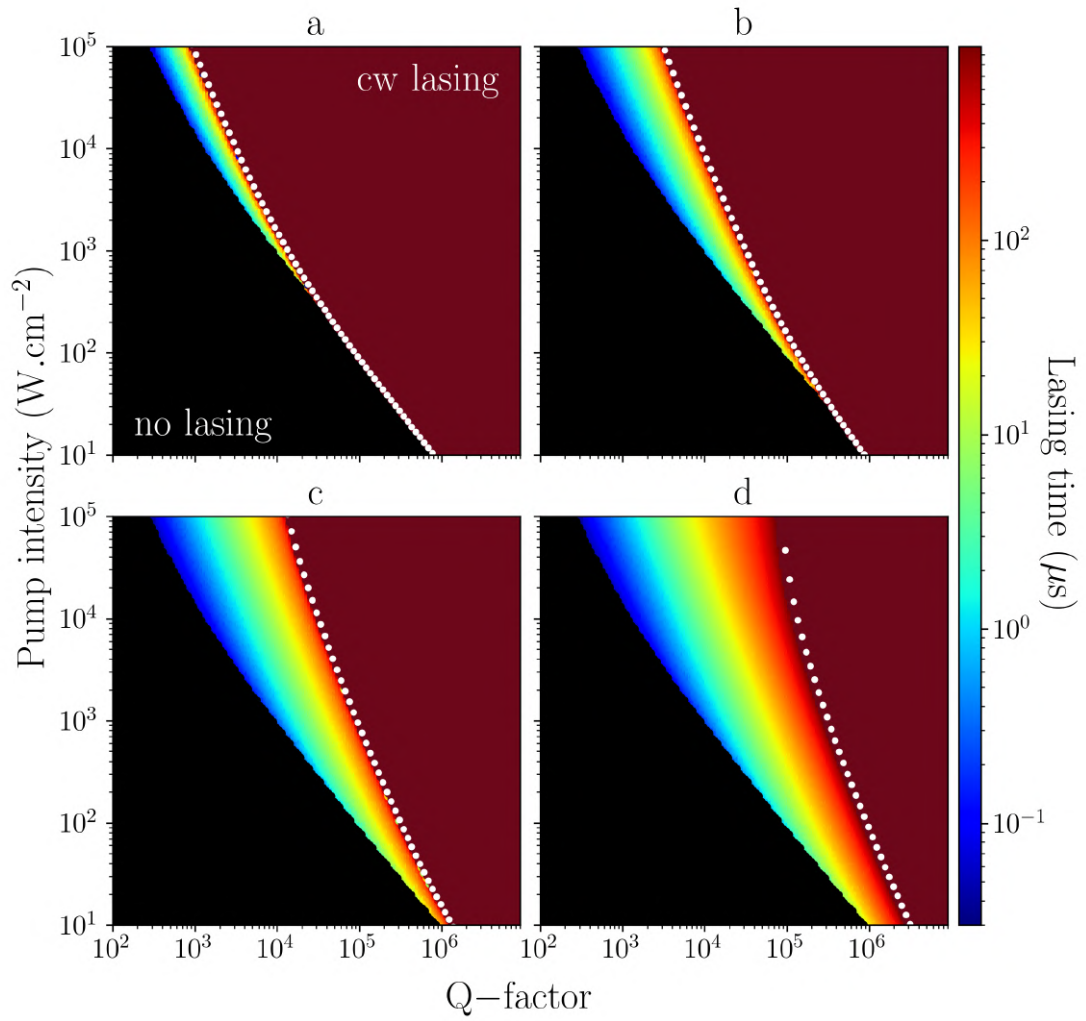


Figure B1: Lasing achieve for different triplet state lifetimes versus the cavity quality factor and the pump power density. $\tau_t =$ a) 0.5, b) 5, c) 50, and d) 500 μs .

Thermally activated delayed fluorescence (TADF)

Lasing regimes achievable in the presence of ISC

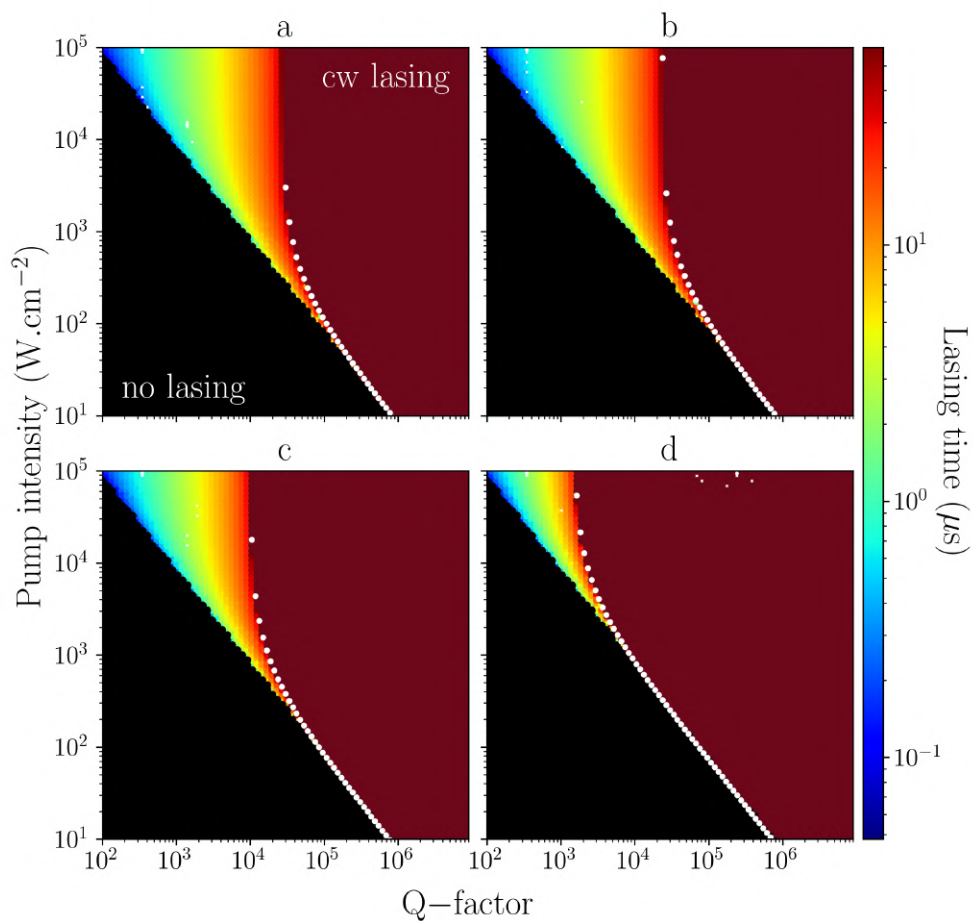


Figure B2: Lasing regime achieved as a function of the pump power density and the quality factor of the resonator with $k_{\text{RISC}} =$ a) 10^2 b) 10^3 c) 10^4 d) 10^5 s^{-1} . $k_{\text{ISC}} = 10^8$ s^{-1} . White dots correspond to Equation 3.44.

Lasing regimes achievable in the presence of STA

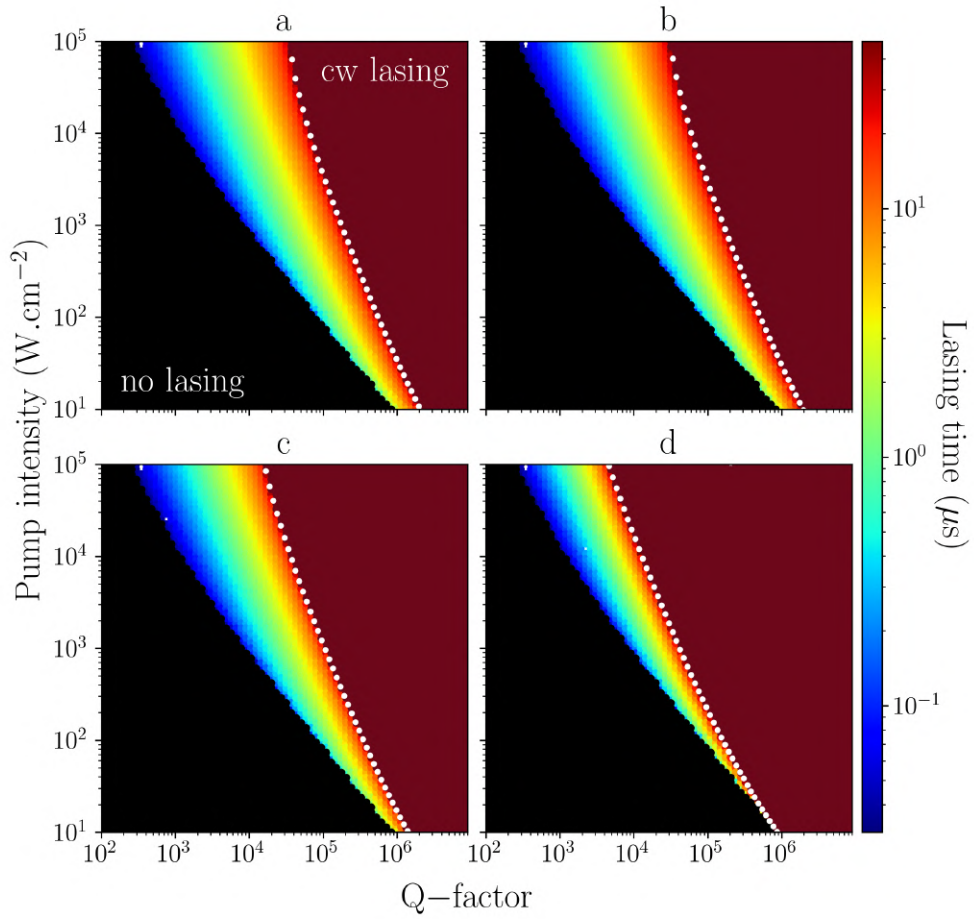


Figure B3: Lasing regime achieved as a function of the pump power density and the quality factor of the resonator with $k_{\text{RISC}} =$ a) 10^2 b) 10^3 c) 10^4 d) 10^5 s⁻¹. $k_{\text{ISC}} = 10^8$ s⁻¹, $k_{\text{STA}} = 10^{-10}$ cm³.s⁻¹. White dots correspond to Equation 3.44.

List of Figures

1	Galaxy Flip 4	1
2	Illustration of the three level electronic configuration of organic molecules.	2
1.1	Illustration of a typical Fabry-Pérot resonator	6
1.2	Illustration of the main light-matter interaction processes	7
1.3	Left: Illustration of a four-level electronic system with non-radiative de-excitation (curved), spontaneous emission (dashed), absorption and stimulated emission (bold). $\nu_{l,p}$ are the laser and pump transition frequency, respectively.	9
1.4	Illustration of the Stokes-Shift of molecules: the example of coumarin 521T	10
1.5	Emission spectrum of a commercial 450 nm diode used in Chapter 2 recorded before (blue) and after (orange) its lasing threshold. The lasing spectrum appears much narrower than the fluorescence emission.	11
1.6	Illustration of the broadness of absorption spectra	12
1.7	Jablonski-Perrin diagram of a typical two-level system.	13
1.8	(left) V ertical- C avity S urface- E mitting L aser (VCSEL) and (right) D istributed F eed B ack (DFB) resonator.	15
1.9	Left) a classical, unstable Fabry-Pérot resonator in which only low-order transverse modes are supported. Right) Specially designed stable cavity with curved mirrors to support high-order transverse modes. Figure taken from Reference [35].	15
1.10	(a) Schematic of single-cell laser, where different types of brain cells were sandwiched within a FP microcavity. Laser modes emit from the FP cavity upon excitation. (b) Schematic of hyperspectral imaging setup. Hyperspectral images of laser modes were obtained using an imaging spectrometer, in which a CCD was used to record the laser modes with different wavelengths after the laser emission beam was diffracted by a grating Figure taken from Reference [36].	16
1.11	Chemical formula of ethane (left), ethylene (center), and ethyne (right).	18

1.12	Electron configuration of carbon: ground state (top left), sp^3 - (top right), sp^2 - (down left) and sp -hybridization (down right). For the ground state, the 1s- and the 2s- orbitals are occupied by two electrons and two 2p-orbitals are occupied by one electron. Hybrid orbitals are formed by superposition of s- and p-orbitals. Figure taken from Reference [38].	19
1.13	Topological representation of the butadi-1,3-ene, for which the alternation of single and double bounds allows the delocalization of the π -electrons to be along the whole carbon backbone of the molecule thanks to the overlap between 2p-orbitals.	20
1.14	Energy levels of molecular orbitals in formaldehyde and possible electronics transitions. Figure taken from Reference [40].	21
1.15	Jablonski-Perrin diagram of organic molecules.	23
1.16	Illustration of two pumping methods: Optical and electrical injection	26
1.17	Illustration of two methods to generate triplet excitons: Intersystem crossing and singlet fission	27
1.18	Chemical structure of some well-known organic TADF compounds .	30
1.19	Illustration of the delayed fluorescence induced by reverse intersystem crossing. Figure taken from Reference [88].	31
1.20	Illustration of FRET mechanism	32
1.21	Illustration of Förster transfer in host-guest systems. Higher emission wavelengths are reachable with the same excitation source thanks to the overlap (colored in grey) between the donor emission spectrum and the acceptor absorption spectrum. Dashed lines: emission spectra ; Solid lines: absorption spectra.	33
1.22	Dexter energy transfer	34
1.23	Illustration of the different generations of OLED and what mechanisms are used to emit light. Figure taken from Edinburgh Instruments website.	38
1.24	Schematic representation of a circular flowing configuration of the gain medium and a dispersive element inside the cavity to tune the emission wavelength	41
1.25	Graphical representation of the different pathways for excitons (S: singlets, T: triplets) inside the gain medium during the excitation. Figure taken from Reference [157].	43
1.26	Chemical structure of bis[(N -carbazole)styryl]biphenyl (BSBCz). .	45
1.27	Fabrication method of the organic DFB laser with BSBCz as a gain medium, which is sandwiched between a glass substrate and a 2 μm layer of CYTOP to encapsulate it. A thick layer of Sapphire is deposited on top of the CYTOP to ensure an efficient heat conductivity. Figure taken from Reference [14].	46

1.28	2D DFB resonator structures were designed to improve laser performance. (a) Second-order 2D square lattice, (b) second-order 2D cross double, (c) circular second order, and (d) circular mixed-order grating structures. Arrows represent the feedback directions of each structure. All these 2D DFBs provide a surface-emitting laser. Figure taken from Reference [6].	49
2.1	(left) Stimulated emission and triplet absorption cross section spectra of BSBCz. Emission spectra of DFB laser were measured from the BSBCz neat film above the threshold. (right) Triplet absorption spectra were measured in a solution containing BSBCz under Ar. Figure taken from Reference [5].	54
2.2	Setup for TA measurement introduced by Lehnhardt <i>et al.</i> [145].	60
2.3	Experimental setup used in this work	62
2.4	(left) Photoluminescence transients of a PMMA:C521T (32 wt.%) 17 μm thin film recorded with the above-mentioned setup, where t_1 is the end of the pump, and t_2 the beginning of the probe. (right) Pump transients recorded with in the same condition by removing the filter and the gain medium, showing that the PL dynamics is not related to the pump profile.	63
2.5	Illustration of the protocol used to create homogeneous 17 μm organic thin films	64
2.6	Absorption (left) and emission (right) spectra of PMMA:DCM 17 μm thin films for different concentrations (wt.%) of DCM.	64
2.7	Fluorescence of a PMMA:DCM (1 wt.%) after photoexcitation (400 ps, 355 nm). The pump power has been set to a minimum to avoid ASE in the film.	66
2.8	Left) Photoluminescence transients of a PMMA:C521T (1 wt.%) 17 μm thin film recorded with the setup evoked in Section 2.2.1. Right) Associated difference of photoluminescence between the end of the pump (ending at $t = 0 \rightarrow t_1$ on Figure 2.4) and the beginning of the probe ($t > 0 \rightarrow t_2$ on Figure 2.4).	67
2.9	Photoluminescence transients of PMMA films with different doping ratios of coumarin 521T.	67
2.10	Photoluminescence transients (solid) and numerical fit (dashed) of a 1 wt.% PMMA:C521T film at different pump power densities.	68
2.11	Experimental photoluminescence transients fitted with k_{STA} the only adjustable parameters for different concentrations of C521T in PMMA thin films	69
2.12	Error between the experimental PL and the integration of the equation with k_{STA} (left) and k_{TTA} (right) as adjustable parameters for different doping ratios of C521T in PMMA thin films.	70

2.13	Experimental (solid) and numerical (dashed) photoluminescence transients of 22% (left) and 40 wt.% (right) of C521T in PMMA thin films for different pump power densities. k_{ISC} , k_{STA} , and k_{TTA} for each concentration are available in Table 2.1	71
2.14	Normalized photoluminescence of the pump (ending at $t = 0$) and the probe versus delays between them for a 40 wt.% PMMA:C521T thin film	72
2.15	Left) Difference in photoluminescence between the end the pump and the beginning of the probe for 17 μm of PMMA with different concentrations of coumarin 521T. Right) Same data reversed, normalized and plotted in log scale to emphasize the different dynamics in high-concentrated films.	73
2.16	STA and TTA rate obtained in this work for PMMA 17 μm films blended with coumarin 521T at different concentrations. Errors are estimated after the depth of the well on Figure 2.12 for each film.	74
2.17	Graphical summary of the experimental protocol presented in this thesis to obtain a complete set of data regarding the triplet state of the gain medium.	75
2.18	Left) Graphical representation of how transients absorption traces are processed to build a triplet absorption spectrum. Right) Ground state absorption, fluorescence and triplet absorption spectra of a 17 μm blended PMMA film with 22 wt.% coumarin 521T. The triplet spectrum has been obtained using the TAS experiment at PSSM laboratory. Points are actual outputs, and the dashed line is a cubic interpolation using Python library Scipy.	76
2.19	Triplet absorption transient of a 17 μm solid PMMA films blended with 9 wt.% (left) and 32 wt.% (right) obtained using the TAS setup at 520 nm.	77
2.20	Normalized photoluminescence transients of the gain medium after an initial excitation for different delays between pump and probe. On the left, the same area of the film is pumped during the whole experiment, whereas it is changed between each delay on the right, yielding a more reproducible PL transient.	78
2.21	Absorption spectra of the pristine and degraded 200 nm BSBCz neat films.	79
2.22	Photoluminescence of the pump (ending at $t = 0$) and the probe versus the delay between them for a degraded (left) and pristine (right) BSBCz neat films. The ground state recovery is much faster for the degraded sample because of the quenching of triplets by oxygen in the gain medium.	80

2.23	Left) Difference in photoluminescence between the end of the pump and the beginning of the probe for 17 μm PMMA:C521T (1 wt.%) at different excitation power density. Right) Long photoluminescence transients for each excitation power density investigated.	81
2.24	Photoluminescence transients divided by the pump profile of a 200 nm BSBCz neat film excited at different pump power densities.	82
2.25	Photoluminescence transient (solid line) normalized to the pump profile of a 200 nm BSBCz neat film excited at $9.1 \text{ kW}\cdot\text{cm}^{-2}$. Data are fitted (dashed lines) using different models. TIC: Temperature-dependent Internal Conversion	83
2.26	Inverse of the standard deviation for the first 500 ns of experimental PL transients (Figure 2.24) and simulations versus k_{ISC} and k_{STA} for two different BSBCz concentrations (17% at $23 \text{ kW}\cdot\text{cm}^{-2}$ and 100% at $9.1 \text{ kW}\cdot\text{cm}^{-2}$)	84
2.27	Experimental (solid lines) and simulated (dashed lines) photoluminescence transients normalized to the pump profile for 20 wt.% BSBCz in CBP (left) and neat BSBCz film (right). The fits only account for the first 500 ns for an additional process is needed to explain the full dynamics.	85
2.28	Error between experimental and simulated BSBCz thin film PL transients versus k_{TTA} with k_{ISC} and k_{STA} fixed.	86
2.29	Experimental (solid lines) and simulated (dashed lines) photoluminescence transients normalized to the pump profile for 666 nm 20 wt.% BSBCz wt. in CBP (left) and a 200 nm neat BSBCz film (right).	86
2.30	Compounds investigated in this work	88
2.31	Normalized photoluminescence of the pump (ending at $t = 0$) and the probe versus delays between them for 1 wt.% PMMA:DCM (left) and PMMA:BSBCz-EH (right) thin films.	89
2.32	Output of the pump-probe experiment for a 10^{-3} M DCM solution in ethanol with left) Normalized photoluminescence of the pump (ending at $t = 0$) and the probe versus delays and right) ground state recovery fitted with a monoexponential expression and a lifetime of $6 \mu\text{s}$	91
2.33	Photoluminescence transients of blended PMMA films at different concentrations of (top left) DCM, (top right) coumarin 314T, (bottom left) fluorol 555, and (bottom right) BSBCz-EH. The dashed lines are the associated fits whose values are provided in Table 2.3. Pump power densities used to excite the films: 139 (DCM), 165 (C314T), 139 (F555), and 2600 (BSBCz-EH) $\text{W}\cdot\text{cm}^{-2}$	93

2.34	Fluorescence recovery kinetics measurements of blended PMMA films at different concentrations. τ_t is the triplet lifetime used to fit the data at low concentration with a monoexponential expression. $k_{\text{TTA}}T_0$ is the adjustable parameter in the triplet analytical solution in Equation 2.14.	95
2.35	Fluorescence recovery kinetics measurements of 200 nm blended CBP:BSBCz films at different concentrations. Fits are obtained using a monoexponential expression at 5 wt.%, and Equation 2.14 at higher concentration with $k_{\text{TTA}}T_0$ as adjustable parameters. . . .	97
2.36	Experimental (left) and numerical (right) photoluminescence transients of 200 nm CBP:BSBCz films at different concentrations. $I_p = 2.6 \text{ kW.cm}^{-2}$	98
3.1	Lasing transients of a VCSEL structure composed of two HR mirrors and a 666 nm CBP:BSBCz (20:80 wt.%) at different pump power densities	102
3.2	Algorithm used in this work to discriminate lasing regimes	110
3.3	Time resolved simulations of the photon density to show how lasing and fluorescence can be discriminated at early stages.	111
3.4	Time resolved simulations of the normalized intracavity intensity for different quality factors. The blue case shows only fluorescence whereas the orange curve is a lasing pulse that stops with the vertical fall of I/I_{sat} . The green curve corresponds to CW lasing. I/I_{sat} allows us to efficiently discriminate the two possibilities.	112
3.5	Lasing regime achieved as a function of the pump power density and the quality factor of the resonator. Black) no lasing, rainbow) pulsed emission (whose duration is indicated on the colormap), red) CW lasing. White dots correspond to analytical solution of the pump fluence required to enable CW lasing. $k_{\text{ISC}} = 6 \times 10^6 \text{ s}^{-1}$, $k_{\text{STA}} = 10^{-10} \text{ cm}^3.\text{s}^{-1}$	113
3.6	Time-resolved simulations of singlets (left) and photons density inside the cavity (right) for different quality factors. $k_f = 10^9 \text{ s}^{-1}$, $\sigma_{\text{abs}} = 10^{-16} \text{ cm}^2$, $I_p = 20 \text{ kW.cm}^{-2}$, $N = 10^{27} \text{ m}^{-3}$. S_1^{th} is computed after Equation 3.12.	114
3.7	Lasing regimes in a configuration without triplets for different quality factors and pump power densities	116
3.8	Time-resolved simulations of the S_1 and T_1 population densities, and the intracavity intensity for different k_{ISC}	118
3.9	Lasing regime achieved as a function of the pump power density and the quality factor of the resonator with $k_{\text{ISC}} =$ a) 10^6 b) 10^7 c) 10^8 d) 10^9 s^{-1} . White dots correspond to Equation 3.16.	120

3.10	Time-resolved simulations of the S_1 and T_1 populations with and without STA.	122
3.11	Quality factor required to achieve lasing in the presence of ISC and STA at fixed pump power density.	124
3.12	Pump intensity required to achieve continuous-wave lasing at fixed quality factor versus k_{ISC} and k_{STA}	125
3.13	Lasing regimes achieved as a function of ISC and STA rates with the pump power density and the quality fixed.	126
3.14	Lasing regimes for different k_{STA}	127
3.15	Lasing regimes achieved as a function of k_{ISC} and σ_{TA} with $I_p = 10$ kW.cm ⁻² and $Q = 5 \times 10^3$, $k_t^{-1} = 175$ μ s. White dots correspond to Equation 3.16 with S_1^{cav} replaced by $S_{1,\text{ta}}^{\text{cav}}$	131
3.16	Lasing regime achieved as a function of the pump power density and the quality factor of the resonator with $\sigma_{\text{TA}} =$ (left) 2×10^{-19} and (right) 3×10^{-19} cm ² . White dots correspond to Equation 3.16 where S_1^{cav} is replaced by $S_{1,\text{ta}}^{\text{cav}}$	132
3.17	Time-resolved simulations of the normalized lasing intensity, S_1 , and T_1 exciton populations with ISC and TA. $k_{\text{ISC}} = 10^7$ s ⁻¹ , $k_t^{-1} = 175$ μ s, $\sigma_{\text{TA}} = 10^{-17}$ cm ²	133
3.18	Lasing regimes achieved as a function of k_{STA} and σ_{TA} with $I_p = 10$ kW.cm ⁻² and $Q = 5 \times 10^3$. Black means no lasing whereas red is CW lasing.	134
3.19	Time resolved simulations of the intracavity intensity for different values of ζ the proportion of singlet created <i>via</i> TTA. Changing ζ value in Equations 3.2 to 3.4 has no meaningful influence on the lasing pulse duration.	135
3.20	Time resolved simulations of the triplet population for different values of k_{TTA}	136
3.21	Time resolved simulations of the lasing intensity without (left) and with (right) triplet absorption for different values of k_{TTA} . $k_{\text{ISC}} = 10^7$ s ⁻¹ , $k_{\text{STA}} = 10^{-10}$ cm ³ .s ⁻¹ , $\sigma_{\text{TA}} = 10^{-17}$ cm ² , $Q = 5 \times 10^3$, $I_p = 10$ kW.cm ⁻²	137
3.22	Lasing regimes achieved as a function of k_{TTA} and σ_{TA} with $I_p = 10$ kW.cm ⁻² , $Q = 5 \times 10^3$, $k_{\text{ISC}} = 10^7$ s ⁻¹ , $k_{\text{STA}} = 10^{-10}$ cm ³ .s ⁻¹	138
3.23	Lasing regimes achieved as a function of the pump power density and the quality factor for different values of k_{TTA} (cm ³ .s ⁻¹) and σ_{TA} (cm ²). $k_{\text{ISC}} = 10^7$ s ⁻¹ , $k_{\text{STA}} = 10^{-10}$ cm ³ .s ⁻¹ . $k_t^{-1} = 175$ μ s	139
3.24	Lasing regimes achieved as a function of the resonator quality factor and the pump power density for a triplet lifetime τ_t of (left) 0.5 and (right) 1.5 μ s.	141
3.25	Time resolved simulations of the intracavity intensity and the triplet population for different values of k_{RISC}	143

3.26	Pump intensity required to obtain a continuous-wave lasing emission as a function of k_{RISC}	144
4.1	Lasing regime as a function of the quality factor of the resonator and the pump power density for a 200 nm CBP:BSBCz (80:20 wt.%) film. Parameters used for the computations are provided in Table 4.1.	151
4.2	Lasing transients corresponding to the VCSEL (left) and DFB (right) points of Figure 4.1. Parameters used are displayed in Table 4.1.	152
4.3	(left) Lasing regime as a function of the quality factor of the resonator and the pump power density for a 200 nm CBP:BSBCz (80:20 wt.%) film. Parameters used for the computations are provided in Table 4.1. σ_{TA} has been set to $4 \times 10^{-19} \text{ cm}^2$ according to Equation 4.2. (right) Lasing transients corresponding to the DFB point of the left picture.	153
A1	Beam areas on the sample captured with an imagery system and a beam analyzer for the 450 (left) and 405 (right) nm diodes. Pump diameters on the sample have been measured at $320 \mu\text{m}$ (left), and $30 \mu\text{m}$ (right).	163
A2	Pump intensity versus time recorded without sample by a PMT and an oscilloscope for the 450 (left) and 405 (right) nm diodes	163
A3	Absorption (left) and emission (right) of $17 \mu\text{m}$ PMMA films with different concentrations of coumarin 521T	164
A4	Fluorescence lifetime measurements for a 1 wt.% PMMA:C521T $17 \mu\text{m}$ film. The monoexponential fit gives $\tau_f = 3.7 \text{ ns}$	164
A5	Photoluminescence transients of $17 \mu\text{m}$ PMMA films with different concentrations (1, 5, 9, 22, 32, 40 wt.%) of coumarin C521T excited at different pump power densities by a 450 nm diode.	165
A6	Photoluminescence transients from pump-probe experiment of $17 \mu\text{m}$ PMMA films with different concentrations (1, 5, 9 wt.%) of coumarin C521T excited at 236 W.cm^{-2} with a 450 nm diode.	166
A7	Photoluminescence transients from pump-probe experiment of $17 \mu\text{m}$ PMMA films with different concentrations (22, 32, 40 wt.%) of coumarin C521T excited at 236 W.cm^{-2} with a 450 nm diode.	167
A8	Absorption (left) and emission (right) of $17 \mu\text{m}$ PMMA films with different concentrations of coumarin 314T	168
A9	Fluorescence lifetime measurements for a 1 wt.% PMMA:C314T $17 \mu\text{m}$ film. The monoexponential fit gives $\tau_f = 3.5 \text{ ns}$	168
A10	Photoluminescence transients of $17 \mu\text{m}$ PMMA films with different concentrations (1, 5, 22 wt.%) of coumarin 314T excited at different pump power densities by a 450 nm diode.	169

A11	Photoluminescence transients from pump-probe experiment of $17\mu\text{m}$ PMMA films with different concentrations (1, 5, 22 wt.%) of coumarin 314T excited at 165 W.cm^{-2} with a 450 nm diode.	170
A12	Absorption (left) and emission (right) of $17\mu\text{m}$ PMMA films with different concentrations of fluoro 555	171
A13	Photoluminescence transients of $17\mu\text{m}$ PMMA films with different concentrations (1, 5, 22 wt.%) of fluoro 555 excited at different pump power densities by a 450 nm diode.	171
A14	Photoluminescence transients from pump-probe experiment of $17\mu\text{m}$ PMMA films with different concentrations (1, 5, 22 wt.%) of fluoro 555 excited at 139 W.cm^{-2} with a 450 nm diode.	172
A15	Absorption (left) and emission (right) of $17\mu\text{m}$ PMMA films with different concentrations of DCM	173
A16	Fluorescence lifetime measurements for a 1 wt.% PMMA:DCM $17\mu\text{m}$ film. The monoexponential fit gives $\tau_f = 2.1 \text{ ns}$	173
A17	Photoluminescence transients of $17\mu\text{m}$ PMMA films with different concentrations (1, 5, 22 wt.%) of fluoro 555 excited at different pump power densities by a 450 nm diode.	174
A18	Photoluminescence transients from pump-probe experiment of $17\mu\text{m}$ PMMA films with different concentrations (1, 5, 22 wt.%) of fluoro 555 excited at 139 W.cm^{-2} with a 450 nm diode.	174
A19	Absorption (left) and emission (right) of $17\mu\text{m}$ PMMA films with different concentrations of BSBCz-EH	175
A20	Fluorescence lifetime measurements for a 1 wt.% PMMA:BSBCz-EH $17\mu\text{m}$ film. The monoexponential fit gives $\tau_f = 0.9 \text{ ns}$	175
A21	Absorption (left) and emission (right) of 200nm CBP films with different concentrations of BSBCz	176
A22	Photoluminescence transients of 200 nm CBP films with 5 (top left), 20 (top right), 40 (bottom left), and 100 wt.% (bottom right) of BSBCz excited at 2.6 kW.cm^{-2} with a 405 nm diode.	176
A23	Transient absorption measurements of PMMA:C521T thin films at 520 nm for different concentrations of C521T.	177
A24	178
B1	Lasing achieve for different triplet state lifetimes versus the cavity quality factor and the pump power density. $\tau_t =$ a) 0.5, b) 5, c) 50, and d) $500 \mu\text{s}$	182
B2	Lasing regimes as a function of the cavity quality factor and the pump power density for different k_{RISC}	183
B3	Lasing regimes as a function of the cavity quality factor and the pump power density for different k_{RISC}	184

List of Tables

1.1	Some fluorescence lifetimes reported in the literature for different organic compounds.	24
1.2	Some triplet state lifetimes reported in the literature for different compounds.	29
2.1	triplet-related photophysical constants evaluated in 17 μm PMMA films blended with different concentrations of coumarin 521T using two different methods.	72
2.2	Somes properties of the 17 μm blended PMMA films investigated in this study. Fluorescence lifetime τ_f are obtained by monoexponential fitting of the luminescence (Appendix). Triplet lifetimes τ_t are obtained by monoexponential fitting of the ground state recovery at low concentration 2.34. Emission wavelengths are taken from the peak of the emission spectrum at low concentration for each compound.	89
2.3	triplet-related photophysical constants evaluated in 17 μm PMMA films blended with different concentrations of coumarin 521T using two different methods.	96
2.4	Triplet-related photophysical constants evaluated for 200 nm CBP films blended with different concentrations of BSBCz using two different methods. τ_t^{eff} the effective triplet lifetime is estimated by fitting as best as possible the Ricatti dynamics without TTA.	99
3.1	Lowest organic lasers lasing thresholds	109
4.1	Photophysical parameters used for numerical simulations with a blended CBP:BSBCz (80:20 wt.%) as gain medium.	150
4.2	Parameters used for the theoretical study	179

Bibliography

- [1] Leiping Duan and Ashraf Uddin. Progress in Stability of Organic Solar Cells. *Advanced Science*, 7(11):1903259, June 2020.
- [2] Yuanbao Lin, Begimai Adilbekova, Yuliar Firdaus, Emre Yengel, Hendrik Faber, Muhammad Sajjad, Xiaopeng Zheng, Emre Yarali, Akmaral Seitkhan, Osman M. Bakr, Abdulrahman El-Labban, Udo Schwingenschlögl, Vincent Tung, Iain McCulloch, Frédéric Laquai, and Thomas D. Anthopoulos. 17% Efficient Organic Solar Cells Based on Liquid Exfoliated WS₂ as a Replacement for PEDOT:PSS. *Advanced Materials*, 31(46):1902965, November 2019.
- [3] Shu-Jen Wang, Michael Sawatzki, Ghader Darbandy, Felix Talnack, Jörn Vahland, Marc Malfois, Alexander Kloes, Stefan Mannsfeld, Hans Kleemann, and Karl Leo. Organic bipolar transistors. *Nature*, 606(7915):700–705, June 2022.
- [4] Marco Fattori, Simone Cardarelli, Joost Fijn, Pieter Harpe, Micael Charbonneau, Denis Locatelli, Stephanie Lombard, Christelle Laugier, Laurent Tournon, Stephanie Jacob, Krunoslav Romanjek, Romain Coppard, Herbert Gold, Manfred Adler, Martin Zirkl, Jonas Groten, Andreas Tschepp, Bernhard Lamprecht, Markus Postl, Barbara Stadlober, Josephine Socratous, and Eugenio Cantatore. A printed proximity-sensing surface based on organic pyroelectric sensors and organic thin-film transistor electronics. *Nature Electronics*, 5(5):289–299, May 2022.
- [5] Atula S. D. Sandanayaka, Toshinori Matsushima, Fatima Bencheikh, Kou Yoshida, Munetomo Inoue, Takashi Fujihara, Kenichi Goushi, Jean-Charles Ribierre, and Chihaya Adachi. Toward continuous-wave operation of organic semiconductor lasers. *Science Advances*, 3(4):e1602570, April 2017.
- [6] Chathuranganie A. M. Senevirathne, Atula S. D. Sandanayaka, Buddhika S. B. Karunathilaka, Takashi Fujihara, Fatima Bencheikh, Chuanjiang Qin, Kenichi Goushi, Toshinori Matsushima, and Chihaya Adachi. Markedly Improved Performance of Optically Pumped Organic Lasers with Two-Dimensional Distributed-Feedback Gratings. *ACS Photonics*, page acsphotronics.0c01728, March 2021.

- [7] Ying Yang, Graham A. Turnbull, and Ifor D. W. Samuel. Sensitive Explosive Vapor Detection with Polyfluorene Lasers. *Advanced Functional Materials*, 20(13):2093–2097, May 2010.
- [8] Markus Karl, James M. E. Glackin, Marcel Schubert, Nils M. Kronenberg, Graham A. Turnbull, Ifor D. W. Samuel, and Malte C. Gather. Flexible and ultra-lightweight polymer membrane lasers. *Nature Communications*, 9(1):1525, December 2018.
- [9] A. Köhler and H. Bässler. Triplet states in organic semiconductors. *Materials Science and Engineering: R: Reports*, 66(4-6):71–109, November 2009.
- [10] Stephen R. Forrest. *Organic electronics: foundations to applications*. Oxford University Press, Oxford [England] ; New York, NY, 2020.
- [11] Yuya Oyama, Masashi Mamada, Atul Shukla, Evan G. Moore, Shih-Chun Lo, Ebinazar B. Namdas, and Chihaya Adachi. Design Strategy for Robust Organic Semiconductor Laser Dyes. *ACS Materials Letters*, pages 161–167, January 2020.
- [12] Yuya Oyama, Masashi Mamada, Akihiro Kondo, and Chihaya Adachi. Advantages of naphthalene as a building block for organic solid state laser dyes: smaller energy gaps and enhanced stability. *Journal of Materials Chemistry C*, 9(12):4112–4118, 2021.
- [13] Chathuranganie A. M. Senevirathne, Seiya Yoshida, Morgan Auffray, Masayuki Yahiro, Buddhika S. B. Karunathilaka, Fatima Bencheikh, Kenichi Goushi, Atula S. D. Sandanayaka, Toshinori Matsushima, and Chihaya Adachi. Recycling of Triplets into Singlets for High-Performance Organic Lasers. *Advanced Optical Materials*, page 2101302, October 2021.
- [14] Atula S. D. Sandanayaka, Kou Yoshida, Munetomo Inoue, Chuanjiang Qin, Kenichi Goushi, Jean-Charles Ribierre, Toshinori Matsushima, and Chihaya Adachi. Quasi-Continuous-Wave Organic Thin-Film Distributed Feedback Laser. *Advanced Optical Materials*, 4(6):834–839, June 2016.
- [15] Van T N Mai, Atul Shukla, A M Chathuranganie Senevirathne, Ilene Allison, Hyunsoo Lim, Romain J Lepage, Sarah K M McGregor, Michael Wood, Toshinori Matsushima, Evan G Moore, Elizabeth H Krenske, Atula S D Sandanayaka, Chihaya Adachi, Ebinazar B Namdas, and Shih-Chun Lo. Lasing Operation under Long-Pulse Excitation in Solution-Processed Organic Gain Medium: Toward CW Lasing in Organic Semiconductors. *Advanced Optical Materials*, page 9, 2020.

- [16] Van T. N. Mai, Viqar Ahmad, Masashi Mamada, Toshiya Fukunaga, Atul Shukla, Jan Sobus, Gowri Krishnan, Evan G. Moore, Gunther G. Andersson, Chihaya Adachi, Ebinazar B. Namdas, and Shih-Chun Lo. Solid cyclooctatetraene-based triplet quencher demonstrating excellent suppression of singlet-triplet annihilation in optical and electrical excitation. *Nature Communications*, 11(1):5623, December 2020.
- [17] Anthony E. Siegman. *Lasers*. Univ. Science books, Mill Valley, Calif, 1986.
- [18] P. F. Moulton. Spectroscopic and laser characteristics of Ti:Al₂O₃. *Journal of the Optical Society of America B*, 3(1):125, January 1986.
- [19] J. E. Geusic, H. M. Marcos, and L. G. Van Uitert. Laser oscillations in Nd-doped Yttrium Aluminium, Yttrium Gallium and Gadolinium garnets. *Applied Physics Letters*, 4(10):182–184, May 1964.
- [20] V V Apollonov, S Yu Kazantsev, V F Oreshkin, and K N Firsov. Feasibility of increasing the output energy of a nonchain HF (DF) laser. *Quantum Electronics*, 27(3):207–209, March 1997.
- [21] J. C. Polanyi. Proposal for an Infrared Maser Dependent on Vibrational Excitation. *The Journal of Chemical Physics*, 34(1):347–348, January 1961.
- [22] Jerome V. V. Kasper and George C. Pimentel. HCl Chemical Laser. *Physical Review Letters*, 14(10):352–354, March 1965.
- [23] D. J. Spencer, T. A. Jacobs, H. Mirels, and R. W. F. Gross. Continuous-wave chemical laser. *International Journal of Chemical Kinetics*, 1(5):493–494, September 1969.
- [24] T. H. Maiman. Stimulated Optical Radiation in Ruby. *Nature*, 187(4736):493–494, August 1960.
- [25] Albert Einstein. On the quantum mechanics of radiation. *Physikalische Zeitschrift*, 18(121.128), 1917.
- [26] K. Iga. Surface-emitting laser-its birth and generation of new optoelectronics field. *IEEE Journal of Selected Topics in Quantum Electronics*, 6(6):1201–1215, November 2000.
- [27] Holger Moench, Ralf Conrads, Carsten Deppe, Guenther Derra, Stephan Gronenborn, Xi Gu, Gero Heusler, Johanna Kolb, Michael Miller, Pavel Pekarski, Jens Pollmann-Retsch, Armand Pruijmboom, and Ulrich Weichmann. High-power VCSEL systems and applications. page 93480W, San Francisco, California, United States, March 2015.

- [28] Alexandre Laurain, Isak Kilen, Jorg Hader, Antje Ruiz Perez, Peter Ludewig, Wolfgang Stolz, Sadvikas Addamane, Ganesh Balakrishnan, Stephan W. Koch, and Jerome V. Moloney. Modeling and experimental realization of modelocked VECSEL producing high power sub-100 fs pulses. *Applied Physics Letters*, 113(12):121113, September 2018.
- [29] Lin Mao, Xiaojian Zhang, Renjiang Zhu, Tao Wang, Lijie Wang, and Peng Zhang. Widely tunable external-cavity surface-emitting laser using various methods. *Applied Optics*, 60(22):6706, August 2021.
- [30] M. Rahim, A. Khair, M. Fill, F. Felder, and H. Zogg. Continuously tunable singlemode VECSEL at 3.3 [micro sign]m wavelength for spectroscopy. *Electronics Letters*, 47(18):1037, 2011.
- [31] Yuliang Liu, Wentao Zhang, Tuanwei Xu, Jun He, Faxiang Zhang, and Fang Li. Fiber laser sensing system and its applications. *Photonic Sensors*, 1(1):43–53, March 2011.
- [32] Ensieh Khalkhal, Majid Rezaei-Tavirani, Mohammad Reza Zali, and Zahra Akbari. The Evaluation of Laser Application in Surgery: A Review Article. *Journal of Lasers in Medical Sciences*, 10(5):S104–S111, December 2019.
- [33] Gerhard A. Koepf, Robert G. Marshalek, and David L. Begley. Space Laser Communications: A Review of Major Programs in the United States. *AEU - International Journal of Electronics and Communications*, 56(4):232–242, January 2002.
- [34] Denis Guilhot and Pol Ribes-Pleguezuelo. Laser Technology in Photonic Applications for Space. *Instruments*, 3(3):50, September 2019.
- [35] Kyungduk Kim, Stefan Bittner, Yongquan Zeng, Stefano Guazzotti, Ortwin Hess, Qi Jie Wang, and Hui Cao. Massively parallel ultrafast random bit generation with a chip-scale laser. *Science*, 371(6532):948–952, February 2021.
- [36] Zhen Qiao, Wen Sun, Na Zhang, Randall Ang, Wenjie Wang, Sing Yian Chew, and Yu-Cheng Chen. Brain Cell Laser Powered by Deep-Learning-Enhanced Laser Modes. *Advanced Optical Materials*, 9(22):2101421, November 2021.
- [37] Sébastien Forget and Sébastien Chénais. *Organic solid-state lasers*. Number 175 in Springer series in optical sciences. Springer, Heidelberg, 2013. OCLC: 857988630.
- [38] Christian Gärtner. *Organic laser diodes: modelling and simulation*. Universitätsverlag, Karlsruhe, 2009.

- [39] Hiroo Inokuchi. The discovery of organic semiconductors. Its light and shadow. *Organic Electronics*, 7(2):62–76, April 2006.
- [40] Bernard Valeur and M. N. Berberan-Santos. *Molecular fluorescence: principles and applications*. Wiley-VCH Verlag GmbH & Co. KGaA, Weinheim, Germany, second edition edition, 2013.
- [41] Gary L. Miessler and Donald A. Tarr. *Inorganic chemistry*. Prentice Hall, Upper Saddle River, N.J., 2nd ed edition, 1999.
- [42] M. Born and R. Oppenheimer. Zur Quantentheorie der Molekeln. *Annalen der Physik*, 389(20):457–484, 1927.
- [43] S. J. Strickler and Robert A. Berg. Relationship between Absorption Intensity and Fluorescence Lifetime of Molecules. *The Journal of Chemical Physics*, 37(4):814–822, August 1962.
- [44] The relations between the fluorescence and absorption properties of organic molecules. *Proceedings of the Royal Society of London. Series A. Mathematical and Physical Sciences*, 275(1360):135–148, August 1963.
- [45] Zhuang Zhao, Oussama Mhibik, Tatiana Leang, Sébastien Forget, and Sébastien Chénais. Thermal effects in thin-film organic solid-state lasers. *Optics Express*, 22(24):30092, December 2014.
- [46] Kevin K. Smith and Kenneth J. Kaufmann. Solvent dependence of the non-radiative decay rate of methyl salicylate. *The Journal of Physical Chemistry*, 85(20):2895–2897, October 1981.
- [47] Joscha Hoche, Alexander Schulz, Lysanne Monika Dietrich, Alexander Humeniuk, Matthias Stolte, David Schmidt, Tobias Brixner, Frank Würthner, and Roland Mitric. The origin of the solvent dependence of fluorescence quantum yields in dipolar merocyanine dyes. *Chemical Science*, 10(48):11013–11022, 2019.
- [48] Kelly G. Casey and Edward L. Quitevis. Effect of solvent polarity on non-radiative processes in xanthene dyes: Rhodamine B in normal alcohols. *The Journal of Physical Chemistry*, 92(23):6590–6594, November 1988.
- [49] Mikhail Y. Berezin and Samuel Achilefu. Fluorescence Lifetime Measurements and Biological Imaging. *Chemical Reviews*, 110(5):2641–2684, May 2010.
- [50] A.-C Ribou, J Vigo, and J.-M Salmon. Synthesis and characterization of (1'-pyrene butyl)-2-rhodamine ester: a new probe for oxygen measurement in the mitochondria of living cells. *Journal of Photochemistry and Photobiology A: Chemistry*, 151(1-3):49–55, August 2002.

- [51] Aparna V. Deshpande and Uday Kumar. Correlation between photophysical properties and lasing performances of Rhodamine-19 in three types of solgel glass hosts. *Journal of Luminescence*, 128(7):1121–1131, July 2008.
- [52] K. A. Selanger, J. Falnes, and T. Sikkeland. Fluorescence lifetime studies of Rhodamine 6G in methanol. *The Journal of Physical Chemistry*, 81(20):1960–1963, October 1977.
- [53] Paul C. Beaumont, David G. Johnson, and Barry J. Parsons. Photophysical properties of laser dyes: picosecond laser flash photolysis studies of Rhodamine 6G, Rhodamine B and Rhodamine 101. *Journal of the Chemical Society, Faraday Transactions*, 89(23):4185, 1993.
- [54] Michael L. Lesiecki and J. Michael Drake. Use of the thermal lens technique to measure the luminescent quantum yields of dyes in PMMA for luminescent solar concentrators. *Applied Optics*, 21(3):557, February 1982.
- [55] Zhigang Shuai and Qian Peng. Organic light-emitting diodes: theoretical understanding of highly efficient materials and development of computational methodology. *National Science Review*, 4(2):224–239, March 2017.
- [56] Chelsea R. Martinez and Brent L. Iverson. Rethinking the term pi-stacking. *Chemical Science*, 3(7):2191, 2012.
- [57] Darren W. Johnson and Fraser Hof, editors. *Aromatic interactions: frontiers in knowledge and application*. Number no. 20 in Monographs in supramolecular chemistry. The Royal Society of Chemistry, Cambridge, 2017. OCLC: ocn952386178.
- [58] Frank Würthner. Perylene bisimide dyes as versatile building blocks for functional supramolecular architectures. *Chem. Commun.*, (14):1564–1579, 2004.
- [59] Mariusz Szabelski, Douglas Ilijev, Pabak Sarkar, Rafal Luchowski, Zygmunt Gryczynski, Peter Kapusta, Rainer Erdmann, and Ignacy Gryczynski. Collisional quenching of erythrosine b as a potential reference dye for impulse response function evaluation. *Appl. Spectrosc.*, 63(3):363–368, Mar 2009.
- [60] Thomas J. Penfold, Etienne Gindensperger, Chantal Daniel, and Christel M. Marian. Spin-Vibronic Mechanism for Intersystem Crossing. *Chemical Reviews*, 118(15):6975–7025, August 2018.
- [61] Michael. Kasha. Phosphorescence and the Role of the Triplet State in the Electronic Excitation of Complex Molecules. *Chemical Reviews*, 41(2):401–419, October 1947.

- [62] M. A. Baldo, D. F. O'Brien, Y. You, A. Shoustikov, S. Sibley, M. E. Thompson, and S. R. Forrest. Highly efficient phosphorescent emission from organic electroluminescent devices. *Nature*, 395(6698):151–154, September 1998.
- [63] Chihaya Adachi, Marc A. Baldo, Mark E. Thompson, and Stephen R. Forrest. Nearly 100% internal phosphorescence efficiency in an organic light-emitting device. *Journal of Applied Physics*, 90(10):5048–5051, November 2001.
- [64] Jie Zhang, Lei Wang, Aiguo Zhong, Guobo Huang, Fengshou Wu, Dan Li, Mingyu Teng, Jiali Wang, and Deman Han. Deep red PhOLED from dimeric salophen Platinum(II) complexes. *Dyes and Pigments*, 162:590–598, March 2019.
- [65] Hai-Feng Xiang, Siu-Chung Chan, Kitty Kit-Ying Wu, Chi-Ming Che, and P. T. Lai. High-efficiency red electrophosphorescence based on neutral bis(pyrrole)-diimine platinum(ii) complex. *Chemical Communications*, 71(11):1408, 2005.
- [66] Semyon Cogan, Yehuda Haas, and Shmuel Zilberg. Intersystem crossing at singlet conical intersections. *Journal of Photochemistry and Photobiology A: Chemistry*, 190(2-3):200–206, August 2007.
- [67] Donald L. Pavia, Gary M. Lampman, George S. Kriz, and Randall G. Engel. *A small-scale approach to organic laboratory techniques*. Cengage Learning laboratory series for organic chemistry. Cengage Learning, Boston, MA, fourth edition edition, 2016.
- [68] T. A. Ford, I. Avilov, D. Beljonne, and N. C. Greenham. Enhanced triplet exciton generation in polyfluorene blends. *Physical Review B*, 71(12):125212, March 2005.
- [69] Gordon J. Hedley, Arvydas Ruseckas, and Ifor D. W. Samuel. Ultrafast Intersystem Crossing in a Red Phosphorescent Iridium Complex. *The Journal of Physical Chemistry A*, 113(1):2–4, January 2009.
- [70] Li Yang, Xijun Wang, Guozhen Zhang, Xiaofeng Chen, Guoqing Zhang, and Jun Jiang. Aggregation-induced intersystem crossing: a novel strategy for efficient molecular phosphorescence. *Nanoscale*, 8(40):17422–17426, 2016.
- [71] S. Singh, W. J. Jones, W. Siebrand, B. P. Stoicheff, and W. G. Schneider. Laser Generation of Excitons and Fluorescence in Anthracene Crystals. *The Journal of Chemical Physics*, 42(1):330–342, January 1965.
- [72] V. Barzda, V. Gulbinas, R. Kananavicius, V. Cervinskas, H. van Amerongen, R. van Grondelle, and L. Valkunas. Singlet-Singlet Annihilation Kinetics in

- Aggregates and Trimers of LHCII. *Biophysical Journal*, 80(5):2409–2421, May 2001.
- [73] Eduard Fron, Gerd Schweitzer, Josemon Jacob, Antoine Van Vooren, David Beljonne, Klaus Müllen, Johan Hofkens, Mark Van der Auweraer, and Frans C. De Schryver. SingletSinglet Annihilation Leading to a Charge-Transfer Intermediate in Chromophore-End-Capped Pentaphenylenes. *ChemPhysChem*, 8(9):1386–1393, June 2007.
- [74] F. Bencheikh, A. S. D. Sandanayaka, T. Fukunaga, T. Matsushima, and C. Adachi. Origin of external quantum efficiency roll-off in 4,4'-bis[(*N*-carbazole)styryl]biphenyl (BSBCz)-based inverted organic light emitting diode under high pulsed electrical excitation. *Journal of Applied Physics*, 126(18):185501, November 2019.
- [75] R.E. Merrifield, P. Avakian, and R.P. Groff. Fission of singlet excitons into pairs of triplet excitons in tetracene crystals. *Chemical Physics Letters*, 3(6):386–388, June 1969.
- [76] C.E. Swenberg and W.T. Stacy. Bimolecular radiationless transitions in crystalline tetracene. *Chemical Physics Letters*, 2(5):327–328, September 1968.
- [77] Millicent B. Smith and Josef Michl. Recent Advances in Singlet Fission. *Annual Review of Physical Chemistry*, 64(1):361–386, April 2013.
- [78] Julian Messelberger, Annette Grünwald, Piermaria Pinter, Max M. Hansmann, and Dominik Munz. Carbene derived diradicaloids building blocks for singlet fission? *Chemical Science*, 9(28):6107–6117, 2018.
- [79] David Casanova. Theoretical Modeling of Singlet Fission. *Chemical Reviews*, 118(15):7164–7207, August 2018.
- [80] Song-Liang Chua, Bo Zhen, Jeongwon Lee, Jorge Bravo-Abad, Ofer Shapira, and Marin Soljai. Modeling of threshold and dynamics behavior of organic nanostructured lasers. *Journal of Materials Chemistry C*, 2(8):1463, 2014.
- [81] Amani Ouirimi, Alex Chamberlain Chime, Nixson Loganathan, Mahmoud Chakaroun, Alexis P.A. Fischer, and Daan Lenstra. Threshold estimation of an organic laser diode using a rate-equation model validated experimentally with a microcavity OLED submitted to nanosecond electrical pulses. *Organic Electronics*, 97:106190, October 2021.
- [82] Sahar Alasvand Yazdani, Amir Mikaeili, Fatima Bencheikh, and Chihaya Adachi. Impact of excitonic and photonic loss mechanisms on the threshold and slope efficiency of organic semiconductor lasers. *Japanese Journal of Applied Physics*, June 2022.

- [83] Ayano Abe, Kenichi Goushi, Atula S. D. Sandanayaka, Ryutaro Komatsu, Takashi Fujihara, Masashi Mamada, and Chihaya Adachi. Numerical Study of Triplet Dynamics in Organic Semiconductors Aimed for the Active Utilization of Triplets by TADF under Continuous-Wave Lasing. *The Journal of Physical Chemistry Letters*, pages 1323–1329, February 2022.
- [84] Martine. Meyer, Jean Claude. Mialocq, and Bruno. Perly. Photoinduced intramolecular charge transfer and trans-cis isomerization of the DCM styrene dye: picosecond and nanosecond laser spectroscopy, high-performance liquid chromatography, and nuclear magnetic resonance studies. *The Journal of Physical Chemistry*, 94(1):98–104, January 1990.
- [85] B. Ya. Kogan, A. V. Butenin, and A. P. Galov. Measurement of lifetimes of triplet states of organic molecules by fluorescence recovery kinetics. *Optics and Spectroscopy*, 120(2):280–282, February 2016.
- [86] Marcus Lehnhardt, Thomas Riedl, Torsten Rabe, and Wolfgang Kowalsky. Room temperature lifetime of triplet excitons in fluorescent host/guest systems. *Organic Electronics*, 12(3):486–491, March 2011.
- [87] Bryan R Henry and Robert V Hunt. Triplet-triplet absorption studies on coumarin and related molecules. *Journal of Molecular Spectroscopy*, 39(3):466–470, September 1971.
- [88] Youichi Tsuchiya, Stefan Diesing, Fatima Bencheikh, Yoshimasa Wada, Paloma L. dos Santos, Hironori Kaji, Eli Zysman-Colman, Ifor D. W. Samuel, and Chihaya Adachi. Exact Solution of Kinetic Analysis for Thermally Activated Delayed Fluorescence Materials. *The Journal of Physical Chemistry A*, page acs.jpca.1c04056, September 2021.
- [89] Hiroki Uoyama, Kenichi Goushi, Katsuyuki Shizu, Hiroko Nomura, and Chihaya Adachi. Highly efficient organic light-emitting diodes from delayed fluorescence. *Nature*, 492(7428):234–238, December 2012.
- [90] Hajime Nakanotani, Youichi Tsuchiya, and Chihaya Adachi. Thermally-activated Delayed Fluorescence for Light-emitting Devices. *Chemistry Letters*, 50(5):938–948, May 2021.
- [91] Th. Förster. Zwischenmolekulare Energiewanderung und Fluoreszenz. *Annalen der Physik*, 437(1-2):55–75, January 1948.
- [92] Enrico Fermi. *Nuclear physics*. Univ. of Chicago Press, Chicago, rev. ed., reprint edition, 1974.
- [93] Robert M. Clegg. Chapter 1 Förster resonance energy transfer FRET what is it, why do it, and how it's done. In *Laboratory Techniques in Biochemistry and Molecular Biology*, volume 33, pages 1–57. Elsevier, 2009.

- [94] H. Edelhoich, L. Brand, and M. Wilchek. Fluorescence Studies with Tryptophyl Peptides *. *Biochemistry*, 6(2):547–559, February 1967.
- [95] D. L. Dexter. A Theory of Sensitized Luminescence in Solids. *The Journal of Chemical Physics*, 21(5):836–850, May 1953.
- [96] Christian Gärtner, Christian Karnutsch, Uli Lemmer, and Christof Pflumm. The influence of annihilation processes on the threshold current density of organic laser diodes. *Journal of Applied Physics*, 101(2):023107, January 2007.
- [97] C. A. Parker and C. G. Hatchard. Delayed Fluorescence from Solutions of Anthracene and Phenanthrene. *Proceedings of the Royal Society of London Series A*, 269:574–584, October 1962. ADS Bibcode: 1962RSPSA.269..574P.
- [98] Bas Zee, Yungui Li, Gert-Jan A. H. Wetzelaer, and Paul W. M. Blom. Origin of the Efficiency Roll-Off in Single-Layer Organic Light-Emitting Diodes Based on Thermally Activated Delayed Fluorescence. *Advanced Optical Materials*, 9(19):2100249, October 2021.
- [99] Denis Y. Kondakov. Triplet-triplet annihilation in highly efficient fluorescent organic light-emitting diodes: current state and future outlook. *Philosophical Transactions of the Royal Society A: Mathematical, Physical and Engineering Sciences*, 373(2044):20140321, June 2015.
- [100] David G. Bossanyi, Yoichi Sasaki, Shuangqing Wang, Dimitri Chekulaev, Nobuo Kimizuka, Nobuhiro Yanai, and Jenny Clark. Spin Statistics for Triplet-Triplet Annihilation Upconversion: Exchange Coupling, Intermolecular Orientation, and Reverse Intersystem Crossing. *JACS Au*, 1(12):2188–2201, December 2021.
- [101] Bernhard Dick and Bernhard Nickel. Accessibility of the lowest quintet state of organic molecules through triplet-triplet annihilation; an in do ci study. *Chemical Physics*, 78(1):1–16, July 1983.
- [102] Angelo Monguzzi, Riccardo Tubino, Sajjad Hoseinkhani, Marcello Campione, and Francesco Meinardi. Low power, non-coherent sensitized photon up-conversion: modelling and perspectives. *Physical Chemistry Chemical Physics*, 14(13):4322, 2012.
- [103] M. A. Baldo, D. F. OBrien, M. E. Thompson, and S. R. Forrest. Excitonic singlet-triplet ratio in a semiconducting organic thin film. *Physical Review B*, 60(20):14422–14428, November 1999.
- [104] Hajime Nakanotani, Hiroyuki Sasabe, and Chihaya Adachi. Singlet-singlet and singlet-heat annihilations in fluorescence-based organic light-emitting

- diodes under steady-state high current density. *Applied Physics Letters*, 86(21):213506, May 2005.
- [105] Max Gmelch, Heidi Thomas, Felix Fries, and Sebastian Reineke. Programmable transparent organic luminescent tags. *Science Advances*, 5(2):eaau7310, February 2019.
- [106] Max Gmelch, Tim Achenbach, Ausra Tomkeviciene, and Sebastian Reineke. High-Speed and Continuous-Wave Programmable Luminescent Tags Based on Exclusive Room Temperature Phosphorescence (RTP). *Advanced Science*, 8(23):2102104, December 2021.
- [107] Shogo Amemori, Yoichi Sasaki, Nobuhiro Yanai, and Nobuo Kimizuka. Near-Infrared-to-Visible Photon Upconversion Sensitized by a Metal Complex with Spin-Forbidden yet Strong $S_0 \rightarrow T_1$ Absorption. *Journal of the American Chemical Society*, 138(28):8702–8705, July 2016.
- [108] Yoichi Sasaki, Mio Oshikawa, Pankaj Bharmoria, Hironori Kouno, Akiko Hayashi-Takagi, Moritoshi Sato, Itsuki Ajioka, Nobuhiro Yanai, and Nobuo Kimizuka. Near-Infrared Optogenetic Genome Engineering Based on Photon-Upconversion Hydrogels. *Angewandte Chemie International Edition*, 58(49):17827–17833, December 2019.
- [109] Xiao Wang, Huifang Shi, Huili Ma, Wenpeng Ye, Lulu Song, Jie Zan, Xiaokang Yao, Xiangyu Ou, Guohui Yang, Zhu Zhao, Manjeet Singh, Chongyang Lin, He Wang, Wenyong Jia, Qian Wang, Jiahuan Zhi, Chaomin Dong, Xueyan Jiang, Yongan Tang, Xiaoji Xie, Yang (Michael) Yang, Jianpu Wang, Qiushui Chen, Yu Wang, Huanghao Yang, Guoqing Zhang, Zhongfu An, Xiaogang Liu, and Wei Huang. Organic phosphors with bright triplet excitons for efficient X-ray-excited luminescence. *Nature Photonics*, January 2021.
- [110] André Bernanose and Paul Vouaux. Électroluminescence organique : étude du mode d'émission. *Journal de Chimie Physique*, 50:261–263, 1953.
- [111] André Bernanose, Marcel Comte, and Paul Vouaux. Sur un nouveau mode d'émission lumineuse chez certains composés organiques. *Journal de Chimie Physique*, 50:64–68, 1953.
- [112] André Bernanose. Sur le mécanisme de lélectroluminescence organique. *Journal de Chimie Physique*, 52:396–400, 1955.
- [113] H. Kallmann and M. Pope. Bulk Conductivity in Organic Crystals. *Nature*, 186(4718):31–33, April 1960.
- [114] H. Kallmann and M. Pope. Positive Hole Injection into Organic Crystals. *The Journal of Chemical Physics*, 32(1):300–301, January 1960.

- [115] Peter Mark and Wolfgang Helfrich. Space-Charge-Limited Currents in Organic Crystals. *Journal of Applied Physics*, 33(1):205–215, January 1962.
- [116] Hideo Akamatu and Hiroo Inokuchi. On the Electrical Conductivity of Violanthrone, Iso-Violanthrone, and Pyranthrone. *The Journal of Chemical Physics*, 18(6):810–811, June 1950.
- [117] W. Helfrich and W. G. Schneider. Recombination Radiation in Anthracene Crystals. *Physical Review Letters*, 14(7):229–231, February 1965.
- [118] Fritz P. Schäfer, Werner Schmidt, and Jürgen Volze. ORGANIC DYE SOLUTION LASER. *Applied Physics Letters*, 9(8):306–309, October 1966.
- [119] John R. Whinnery. Laser measurement of optical absorption in liquids. *Accounts of Chemical Research*, 7(7):225–231, July 1974.
- [120] E. Ippen, C. Shank, and A. Dienes. Rapid photobleaching of organic laser dyes in continuously operated devices. *IEEE Journal of Quantum Electronics*, 7(4):178–179, April 1971.
- [121] B.B. Snavely. Flashlamp-excited organic dye lasers. *Proceedings of the IEEE*, 57(8):1374–1390, 1969.
- [122] O. G. Peterson, S. A. Tuccio, and B. B. Snavely. cw OPERATION OF AN ORGANIC DYE SOLUTION LASER. *Applied Physics Letters*, 17(6):245–247, September 1970.
- [123] J. M. Yarborough. cw dye laser emission spanning the visible spectrum. *Applied Physics Letters*, 24(12):629–630, June 1974.
- [124] G.A. Reynolds and K.H. Drexhage. New coumarin dyes with rigidized structure for flashlamp-pumped dye lasers. *Optics Communications*, 13(3):222–225, March 1975.
- [125] A. Dienes, E. P. Ippen, and C. V. Shank. A Mode-Locked cw Dye Laser. *Applied Physics Letters*, 19(8):258–260, October 1971.
- [126] E.P. Ippen, C.V. Shank, and A. Dienes. Passive mode locking of the cw dye laser. *Applied Physics Letters*, 21(8):348–350, October 1972.
- [127] F. O'Neill. Picosecond pulses from a passively mode-locked cw dye laser. *Optics Communications*, 6(4):360–363, December 1972.
- [128] C. V. Shank and E. P. Ippen. Subpicosecond kilowatt pulses from a mode-locked cw dye laser. *Applied Physics Letters*, 24(8):373–375, April 1974.

- [129] C. V. Shank, J. E. Bjorkholm, and H. Kogelnik. TUNABLE DISTRIBUTED-FEEDBACK DYE LASER. *Applied Physics Letters*, 18(9):395–396, May 1971.
- [130] M. B. Denton and H. V. Malmstadt. TUNABLE ORGANIC DYE LASER AS AN EXCITATION SOURCE FOR ATOMIC-FLAME FLUORESCENCE SPECTROSCOPY. *Applied Physics Letters*, 18(11):485–487, June 1971.
- [131] B. H. Soffer and B. B. McFarland. CONTINUOUSLY TUNABLE, NARROW-BAND ORGANIC DYE LASERS. *Applied Physics Letters*, 10(10):266–267, May 1967.
- [132] T. W. Hänsch, I. S. Shahin, and A. L. Schawlow. High-Resolution Saturation Spectroscopy of the Sodium D Lines with a Pulsed Tunable Dye Laser. *Physical Review Letters*, 27(11):707–710, September 1971.
- [133] J.G. Morelli, O.T. Tan, R. Margolis, Y. Seki, J. Boll, J.M. Carney, R.R. Anderson, J.A. Parrish, H. Furumoto, and J. Garden. Tunable dye laser (577 nm) treatment of port wine stains. *Lasers in Surgery and Medicine*, 6(1):94–99, 1986.
- [134] Herman Solomon, Leon Goldman, Bruce Henderson, Daniel Richfield, and Marilyn Franzen. Histopathology of the laser treatment of port-wine lesions: biopsy studies of treated areas observed up to three years after laser impacts. *Journal of Investigative Dermatology*, 50(2):141–146, 1968.
- [135] John M. Telle and C. L. Tang. Very rapid tuning of cw dye laser. *Applied Physics Letters*, 26(10):572–574, May 1975.
- [136] O.G. Peterson and B.B. Snavely. STIMULATED EMISSION FROM FLASHLAMP-EXCITED ORGANIC DYES IN POLYMETHYL METHACRYLATE: *Applied Physics Letters*: Vol 12, No 7. *Applied Physics Letter*, 1968.
- [137] A. Costela, F. Florido, I. Garcia-Moreno, R. Duchowicz, F. Amat-Guerri, J. M. Figuera, and R. Sastre. Solid-state dye lasers based on copolymers of 2-hydroxyethyl methacrylate and methyl methacrylate doped with rhodamine 6G. *Applied Physics B Laser and Optics*, 60(4):383–389, April 1995.
- [138] A. Costela, I. Garcia-Moreno, J. M. Figuera, F. Amat-Guerri, R. Mallavia, M. D. Santa-Maria, and R. Sastre. Solid-state dye lasers based on modified rhodamine 6G dyes copolymerized with methacrylic monomers. *Journal of Applied Physics*, 80(6):3167–3173, September 1996.

- [139] G Somasundaram and A Ramalingam. Gain studies of Rhodamine 6G dye doped polymer laser. *Journal of Photochemistry and Photobiology A: Chemistry*, 125(1-3):93–98, August 1999.
- [140] E. J. Schimitschek, J. A. Trias, P. R. Hammond, and R. L. Atkins. Laser performance and stability of fluorinated coumarin dyes. *Optics Communications*, 11(4):352–355, August 1974.
- [141] John M. McKiernan, Stacey A. Yamanaka, Ed Knobbe, Jean-Claude Pouxviel, Soraya Parvaneh, Bruce Dunn, and Jeffrey I. Zink. Luminescence and laser action of coumarin dyes doped in silicate and aluminosilicate glasses prepared by the sol-gel technique. *Journal of Inorganic and Organometallic Polymers*, 1(1):87–103, March 1991.
- [142] Arnaud Dubois, Michael Canva, Alain Brun, Frédéric Chaput, and Jean-Pierre Boilot. Photostability of dye molecules trapped in solid matrices. *Applied Optics*, 35(18):3193, June 1996.
- [143] S Popov. Influence of pump repetition rate on dye photostability in a solid-state dye laser with a polymeric gain medium. *Pure and Applied Optics: Journal of the European Optical Society Part A*, 7(6):1379–1388, November 1998.
- [144] Mark A. Stevens, Carlos Silva, David M. Russell, and Richard H. Friend. Exciton dissociation mechanisms in the polymeric semiconductors poly(9,9-dioctylfluorene) and poly(9,9-dioctylfluorene-co-benzothiadiazole). *Physical Review B*, 63(16):165213, April 2001.
- [145] M. Lehnhardt, T. Riedl, T. Weimann, and W. Kowalsky. Impact of triplet absorption and triplet-singlet annihilation on the dynamics of optically pumped organic solid-state lasers. *Physical Review B*, 81(16):165206, April 2010.
- [146] N. Tessler, G. J. Denton, and R. H. Friend. Lasing from conjugated-polymer microcavities. *Nature*, 382(6593):695–697, August 1996.
- [147] Aimée Rose, Zhengguo Zhu, Conor F. Madigan, Timothy M. Swager, and Vladimir Bulovi. Sensitivity gains in chemosensing by lasing action in organic polymers. *Nature*, 434(7035):876–879, April 2005.
- [148] Johannes Herrnsdorf, Yue Wang, Jonathan J. D. McKendry, Zheng Gong, David Massoubre, Benoit Guilhabert, Georgios Tsiminis, Graham A. Turnbull, Ifor D. W. Samuel, Nicolas Laurand, Erdan Gu, and Martin D. Dawson. Micro-LED pumped polymer laser: A discussion of future pump sources for organic lasers: Micro-LED pumped polymer laser. *Laser & Photonics Reviews*, 7(6):1065–1078, November 2013.

- [149] Hans-Heinrich Hoerhold, Hartwig Tillmann, Cornelia Bader, Elisabeth Klemm, Wolfgang Holzer, and Alfons Penzkofer. MEH-PPV and thianthrene-containing PPV-derivatives as efficient polymeric materials for solid-state lasers. page 317, San Diego, CA, USA, February 2002.
- [150] Fumitomo Hide, Benjamin J. Schwartz, María A. Díaz-García, and Alan J. Heeger. Laser emission from solutions and films containing semiconducting polymer and titanium dioxide nanocrystals. *Chemical Physics Letters*, 256(4-5):424–430, July 1996.
- [151] G. Kranzelbinder, E. Toussaere, J. Zyss, A. Pogantsch, E. W. J. List, H. Tillmann, and H.-H. Hörhold. Optically written solid-state lasers with broadly tunable mode emission based on improved poly (2,5-dialkoxy-phenylene-vinylene). *Applied Physics Letters*, 80(5):716–718, February 2002.
- [152] M Rodriguez, A Costela, I Garcia-Moreno, F Florido, J M Figuera, and R Sastre. A simple rotating system to avoid early degradation of solid-state dye lasers. *Measurement Science and Technology*, 6(7):971–978, July 1995.
- [153] Munetomo Inoue, Toshinori Matsushima, Hajime Nakanotani, and Chihaya Adachi. Introduction of oxygen into organic thin films with the aim of suppressing singlet-triplet annihilation. *Chemical Physics Letters*, 624:43–46, March 2015.
- [154] Li Zhao, Munetomo Inoue, Kou Yoshida, Atula S. D. Sandanayaka, Ju-Hyung Kim, Jean-Charles Ribierre, and Chihaya Adachi. Singlet-Triplet Exciton Annihilation Nearly Suppressed in Organic Semiconductor Laser Materials Using Oxygen as a Triplet Quencher. *IEEE Journal of Selected Topics in Quantum Electronics*, 22(1):26–34, January 2016.
- [155] Atula S. D. Sandanayaka, Li Zhao, Delphine Pitrat, Jean-Christophe Mulatier, Toshinori Matsushima, Chantal Andraud, Ju-Hyung Kim, Jean-Charles Ribierre, and Chihaya Adachi. Improvement of the quasi-continuous-wave lasing properties in organic semiconductor lasers using oxygen as triplet quencher. *Applied Physics Letters*, 108(22):223301, May 2016.
- [156] F. Schindler, J.M. Lupton, J. Feldmann, and U. Scherf. Controlled Fluorescence Bursts from Conjugated Polymers Induced by Triplet Quenching. *Advanced Materials*, 16(7):653–657, April 2004.
- [157] Yifan Zhang and Stephen R. Forrest. Existence of continuous-wave threshold for organic semiconductor lasers. *Physical Review B*, 84(24):241301, December 2011.
- [158] Yifan Zhang, Michael Slights, and Stephen R. Forrest. Enhanced efficiency in high-brightness fluorescent organic light emitting diodes through triplet management. *Applied Physics Letters*, 99(22):223303, November 2011.

- [159] Toshinori Matsushima, Seiya Yoshida, Ko Inada, Yu Esaki, Toshiya Fukunaga, Hiroyuki Mieno, Nozomi Nakamura, Fatima Bencheikh, Matthew R. Leyden, Ryutaro Komatsu, Chuanjiang Qin, Atula S. D. Sandanayaka, and Chihaya Adachi. Degradation Mechanism and Stability Improvement Strategy for an Organic Laser Gain Material 4,4'-Bis[(*N*-carbazole)styryl]biphenyl (BSBCz). *Advanced Functional Materials*, 29(10):1807148, March 2019.
- [160] W. H. Melhuish and R. Hardwick. Lifetime of the triplet state of anthracene in lucite. *Transactions of the Faraday Society*, 58:1908, 1962.
- [161] A. A. Gorman, I. Hamblett, M. Irvine, P. Raby, M. C. Standen, and S. Yeates. Pulse radiolysis study of the cycloheptatriene triplet state: lifetime, relaxation and nonvertical excitation. *Journal of the American Chemical Society*, 107(15):4404–4411, July 1985.
- [162] Bernard Zietek, Piotr Targowski, Andrzej Baczynski, and Janusz Bissinger. Cyclooctatetraene As A Triplet Quencher In Dye Lasers. In Ryszard S. Romaniuk, Bohdan K. Wolczak, and Wieslaw L. Wolinski, editors, *Laser Technology II*, volume 0859, pages 25 – 29. International Society for Optics and Photonics, SPIE, 1987.
- [163] F.C. Strome and S.A. Tuccio. Triplet quenching and continuous laser action in three fluorescein dyes. *Optics Communications*, 4(1):58–59, September 1971.
- [164] Masashi Mamada, Toshiya Fukunaga, Fatima Bencheikh, Atula S. D. Sandanayaka, and Chihaya Adachi. Low Amplified Spontaneous Emission Threshold from Organic Dyes Based on Bis-stilbene. *Advanced Functional Materials*, 28(32):1802130, August 2018.
- [165] T. Rabe, K. Gerlach, T. Riedl, H.-H. Johannes, W. Kowalsky, J. Niederhofer, W. Gries, J. Wang, T. Weimann, P. Hinze, F. Galbrecht, and U. Scherf. Quasi-continuous-wave operation of an organic thin-film distributed feedback laser. *Applied Physics Letters*, 89(8):081115, August 2006.
- [166] G. Heliotis, R. Xia, G.A. Turnbull, P. Andrew, W.L. Barnes, I.D.W. Samuel, and D.D.C. Bradley. Emission Characteristics and Performance Comparison of Polyfluorene Lasers with One- and Two-Dimensional Distributed Feedback. *Advanced Functional Materials*, 14(1):91–97, January 2004.
- [167] Hajime Nakanotani, Chihaya Adachi, Sadayuki Watanabe, and Ryuzi Kato. Spectrally narrow emission from organic films under continuous-wave excitation. *Applied Physics Letters*, 90(23):231109, June 2007.

- [168] F. J. H. van Assche, R. T. Vangheluwe, J. W. C. Maes, W. S. Mischke, M. D. Bijker, F. C. Dings, M. F. J. Evers, W. M. M. Kessels, and M. C. M. van de Sanden. P-111: A Thin Film Encapsulation Stack for PLED and OLED Displays. *SID Symposium Digest of Technical Papers*, 35(1):695, 2004.
- [169] J.D. Affinito, M.E. Gross, C.A. Coronado, G.L. Graff, I.N. Greenwell, and P.M. Martin. A new method for fabricating transparent barrier layers. *Thin Solid Films*, 290-291:63–67, December 1996.
- [170] A. P. Ghosh, L. J. Gerenser, C. M. Jarman, and J. E. Fornalik. Thin-film encapsulation of organic light-emitting devices. *Applied Physics Letters*, 86(22):223503, May 2005.
- [171] S. Richardson, O. P. M. Gaudin, G. A. Turnbull, and I. D. W. Samuel. Improved operational lifetime of semiconducting polymer lasers by encapsulation. *Applied Physics Letters*, 91(26):261104, December 2007.
- [172] Atul Shukla, Van T. N. Mai, A. M. Chathuranganie Senevirathne, Ilene Allison, Sarah K. M. McGregor, Romain J. Lepage, Michael Wood, Toshinori Matsushima, Evan G. Moore, Elizabeth H. Krenke, Atula S. D. Sandanayaka, Chihaya Adachi, Ebinazar B. Namdas, and ShihChun Lo. Low Amplified Spontaneous Emission and Lasing Thresholds from Hybrids of Fluorenes and Vinylphenylcarbazole. *Advanced Optical Materials*, 8(20):2000784, October 2020.
- [173] Buddhika S. B. Karunathilaka, Umamahesh Balijapalli, Chathuranganie A. M. Senevirathne, Yu Esaki, Kenichi Goushi, Toshinori Matsushima, Atula S. D. Sandanayaka, and Chihaya Adachi. An Organic Laser Dye having a Small Singlet-Triplet Energy Gap Makes the Selection of a Host Material Easier. *Advanced Functional Materials*, 30(30):2001078, July 2020.
- [174] George S. Hammond and Jack. Saltiel. **Photosensitized $\langle b \rangle$ *Cis-Trans* Isomerization of the Stilbenes $\langle /b \rangle$.** *Journal of the American Chemical Society*, 84(24):4983–4984, December 1962.
- [175] Min Cao, Zhi Cai, Xiaosong Chen, Kongyang Yi, and Dacheng Wei. Photo-switchable field-effect transistors based on two-dimensional stilbene oligomer crystals. *Journal of Materials Chemistry C*, 5(37):9597–9601, 2017.
- [176] Qi Ou, Qian Peng, and Zhigang Shuai. Computational screen-out strategy for electrically pumped organic laser materials. *Nature Communications*, 11(1):4485, December 2020.
- [177] Musubu Ichikawa, Kiyoshi Nakamura, Masamitsu Inoue, Hiromi Mishima, Takeshi Haritani, Ryota Hibino, Toshiki Koyama, and Yoshio Taniguchi.

- Photopumped laser oscillation and charge-injected luminescence from organic semiconductor single crystals of a thiophene/phenylene co-oligomer. *Applied Physics Letters*, 87(22):221113, November 2005.
- [178] Donald S. McClure. Triplet-Singlet Transitions in Organic Molecules. Lifetime Measurements of the Triplet State. *The Journal of Chemical Physics*, 17(10):905–913, October 1949.
- [179] J. S. Wilson, A. Köhler, R. H. Friend, M. K. Al-Suti, M. R. A. Al-Mandhary, M. S. Khan, and P. R. Raithby. Triplet states in a series of Pt-containing ethynylenes. *The Journal of Chemical Physics*, 113(17):7627–7634, November 2000.
- [180] Jiamo Guo, Hideo Ohkita, Hiroaki Bente, and Shinzaburo Ito. Near-IR Femtosecond Transient Absorption Spectroscopy of Ultrafast Polaron and Triplet Exciton Formation in Polythiophene Films with Different Regioregularities. *Journal of the American Chemical Society*, 131(46):16869–16880, November 2009.
- [181] Rudi Berera, Rienk van Grondelle, and John T. M. Kennis. Ultrafast transient absorption spectroscopy: principles and application to photosynthetic systems. *Photosynthesis Research*, 101(2-3):105–118, September 2009.
- [182] A. Maciejewski, R. Naskrecki, M. Lorenc, M. Ziolk, J. Karolczak, J. Kubicki, M. Matysiak, and M. Szymanski. Transient absorption experimental set-up with femtosecond time resolution. Femto- and picosecond study of DCM molecule in cyclohexane and methanol solution. *Journal of Molecular Structure*, 555(1-3):1–13, November 2000.
- [183] Katrin E. Oberhofer, Mikayel Musheghyan, Sebastian Wegscheider, Martin Wörle, Eleonora D. Iglev, Rositca D. Nikolova, Reinhard Kienberger, Petko St. Pekov, and Hristo Iglev. Individual control of singlet lifetime and triplet yield in halogen-substituted coumarin derivatives. *RSC Advances*, 10(45):27096–27102, 2020.
- [184] Tor Sandén, Gustav Persson, Per Thyberg, Hans Blom, and Jerker Widengren. Monitoring Kinetics of Highly Environment Sensitive States of Fluorescent Molecules by Modulated Excitation and Time-Averaged Fluorescence Intensity Recording. *Analytical Chemistry*, 79(9):3330–3341, May 2007.
- [185] Nirmalya Bag and Thorsten Wohland. Imaging Fluorescence Fluctuation Spectroscopy: New Tools for Quantitative Bioimaging. *Annual Review of Physical Chemistry*, 65(1):225–248, April 2014.
- [186] Jerker Widengren. Fluorescence-based transient state monitoring for biomolecular spectroscopy and imaging. *Journal of The Royal Society Interface*, 7(49):1135–1144, August 2010.

- [187] Thiemo Spielmann, Lei Xu, Annica K. B. Gad, Sofia Johansson, and Jerker Widengren. Transient state microscopy probes patterns of altered oxygen consumption in cancer cells. *The FEBS Journal*, 281(5):1317–1332, March 2014.
- [188] Matthias Geissbuehler, Thiemo Spielmann, Aurélie Formey, Iwan Märki, Marcel Leutenegger, Boris Hinz, Kai Johnsson, Dimitri Van De Ville, and Theo Lasser. Triplet Imaging of Oxygen Consumption during the Contraction of a Single Smooth Muscle Cell (A7r5). *Biophysical Journal*, 98(2):339–349, January 2010.
- [189] Leonardo De Boni, Paulo L. Franzen, Pablo J. Gonçalves, Iouri E. Borissevitch, Lino Misoguti, Cleber R. Mendonça, and Sergio C. Zilio. Pulse train fluorescence technique for measuring triplet state dynamics. *Optics Express*, 19(11):10813, May 2011.
- [190] Jerker Widengren, Uelo Mets, and Rudolf Rigler. Fluorescence correlation spectroscopy of triplet states in solution: a theoretical and experimental study. *The Journal of Physical Chemistry*, 99(36):13368–13379, September 1995.
- [191] Jerker Widengren, Johannes Dapprich, and Rudolf Rigler. Fast interactions between Rh6G and dGTP in water studied by fluorescence correlation spectroscopy. *Chemical Physics*, 216(3):417–426, April 1997.
- [192] Jerker Widengren and Petra Schwille. Characterization of Photoinduced Isomerization and Back-Isomerization of the Cyanine Dye Cy5 by Fluorescence Correlation Spectroscopy. *The Journal of Physical Chemistry A*, 104(27):6416–6428, July 2000.
- [193] S. M. King, C. Rothe, D. Dai, and A. P. Monkman. Femtosecond ground state recovery: Measuring the intersystem crossing yield of polyspirobifluorene. *The Journal of Chemical Physics*, 124(23):234903, June 2006.
- [194] Larissa Bergmann, Gordon J. Hedley, Thomas Baumann, Stefan Bräse, and Ifor D. W. Samuel. Direct observation of intersystem crossing in a thermally activated delayed fluorescence copper complex in the solid state. *Science Advances*, 2(1):e1500889, January 2016.
- [195] A. Penzkofer, A. Beidoun, and M. Daiber. Intersystem-crossing and excited-state absorption in eosin Y solutions determined by picosecond double pulse transient absorption measurements. *Journal of Luminescence*, 51(6):297–314, May 1992.
- [196] H.E. Lessing, D. Richardt, and A. Von Jena. Quantitative triplet photo-physics by picosecond photometry. *Journal of Molecular Structure*, 84(3-4):281–292, October 1982.

- [197] R. C. Johnson, R. E. Merrifield, P. Avakian, and R. B. Flippen. Effects of Magnetic Fields on the Mutual Annihilation of Triplet Excitons in Molecular Crystals. *Physical Review Letters*, 19(6):285–287, August 1967.
- [198] R. E. Merrifield. Theory of Magnetic Field Effects on the Mutual Annihilation of Triplet Excitons. *The Journal of Chemical Physics*, 48(9):4318–4319, May 1968.
- [199] M. A. Baldo, C. Adachi, and S. R. Forrest. Transient analysis of organic electrophosphorescence. II. Transient analysis of triplet-triplet annihilation. *Physical Review B*, 62(16):10967–10977, October 2000.
- [200] Sergei M. Bachilo and R. Bruce Weisman. Determination of Triplet Quantum Yields from Triplet-Triplet Annihilation Fluorescence. *The Journal of Physical Chemistry A*, 104(33):7711–7714, August 2000.
- [201] Atul Shukla, Monirul Hasan, Gangadhar Banappanavar, Viqar Ahmad, Jan Sobus, Evan G. Moore, Dinesh Kabra, Shih-Chun Lo, and Ebinazar B. Nandas. Controlling triplet-triplet upconversion and singlet-triplet annihilation in organic light-emitting diodes for injection lasing. *Communications Materials*, 3(1):27, December 2022.
- [202] G. D. Hale, S. J. Oldenburg, and N. J. Halas. Observation of triplet exciton dynamics in conjugated polymer films using two-photon photoelectron spectroscopy. *Physical Review B*, 55(24):R16069–R16071, June 1997.
- [203] Nobuhiro Yanai, Kengo Suzuki, Taku Ogawa, Yoichi Sasaki, Naoyuki Harada, and Nobuo Kimizuka. Absolute Method to Certify Quantum Yields of Photon Upconversion via Triplet-Triplet Annihilation. *The Journal of Physical Chemistry A*, 123(46):10197–10203, November 2019.
- [204] Taku Ogawa, Nobuhiro Yanai, Saiya Fujiwara, Thuc-Quyen Nguyen, and Nobuo Kimizuka. Aggregation-free sensitizer dispersion in rigid ionic crystals for efficient solid-state photon upconversion and demonstration of defect effects. *Journal of Materials Chemistry C*, 6(21):5609–5615, 2018.
- [205] Sébastien Chenais, Frédéric DU Burck, Elena Ishow, Mélanie Lebental, and Bernard Ratier. Etude des phénomènes de photodégradation et de polarisation dans les lasers organiques solides à cavité verticale externe. page 213, 2014.
- [206] W. Holzer, A. Penzkofer, and T. Tsuboi. Absorption and emission spectroscopic characterization of Ir(ppy)₃. *Chemical Physics*, 308(1-2):93–102, January 2005.

- [207] A. Hamja, R. Florentin, S. Chénais, and S. Forget. Highly photo-stable, kHz-repetition-rate, diode pumped circulation-free liquid dye laser with thermal lens management. *Applied Physics Letters*, 120(11):113301, March 2022.
- [208] Christian G. Hübner, Alois Renn, Indrek Renge, and Urs P. Wild. Direct observation of the triplet lifetime quenching of single dye molecules by molecular oxygen. *The Journal of Chemical Physics*, 115(21):9619–9622, December 2001.
- [209] Xinyu Wang, Weitao Wang, Chao Yang, Dan Han, Hongzhao Fan, and Jingchao Zhang. Thermal transport in organic semiconductors. *Journal of Applied Physics*, 130(17):170902, November 2021.
- [210] F. J. Duarte, D. R. Foster, and C. H. Chen. *Higher efficiency excimer laser pumped blue-green dye laser*. January 1990. Conference Name: Lasers '89 Pages: 373-375 ADS Bibcode: 1990lase.conf..373D.
- [211] Melissa Lambropoulos. Fluorol 7GA: An efficient yellow-green dye for flashlamp-pumped lasers. *Optics Communications*, 15(1):35–37, September 1975.
- [212] E. Lill, S. Schneider, and F. Dörr. Passive mode-locking of a flashlamp-pumped fluorol 7GA dye laser in the green spectral region. *Optics Communications*, 20(2):223–224, February 1977.
- [213] M. Carrascosa, S. Unamuno, and F. Agullo-Lopez. Monte Carlo simulation of the performance of PMMA luminescent solar collectors. *Applied Optics*, 22(20):3236, October 1983.
- [214] M. Hayashibara and M. Tsukamoto. CONCENTRATORS USING FLUORESCENT SUBSTANCES. *International Journal of Solar Energy*, 8(2):71–79, January 1990.
- [215] Wentao Hu, Hui Ye, Chuangdong Li, Zhonghong Jiang, and Fuzheng Zhou. All-solid-state tunable DCM dye laser pumped by a diode-pumped Nd:YAG laser. *Applied Optics*, 36(3):579, January 1997.
- [216] Peter Hammond and Diane Cooke. Continuous-wave dye lasers in the DCM region. *Applied Optics*, 31(33):7095, November 1992.
- [217] E.G. Marason. Laser dye DCM: CW, synchronously pumped, cavity pumped and single-frequency performance. *Optics Communications*, 37(1):56–58, April 1981.
- [218] S.V. Frolov, W. Gellermann, Z.V. Vardeny, M. Ozaki, and K. Yoshino. Picosecond photophysics of luminescent conducting polymers from excitons to polaron pairs. *Synthetic Metals*, 84(1-3):493–496, January 1997.

- [219] Damir Dzebo, Karl Börjesson, Victor Gray, Kasper Moth-Poulsen, and Bo Albinsson. Intramolecular Triplet-Triplet Annihilation Upconversion in 9,10-Diphenylanthracene Oligomers and Dendrimers. *The Journal of Physical Chemistry C*, 120(41):23397–23406, October 2016.
- [220] N. C. Giebink and S. R. Forrest. Temporal response of optically pumped organic semiconductor lasers and its implication for reaching threshold under electrical excitation. *Physical Review B*, 79(7):073302, February 2009.
- [221] R. Keller. Effect of quenching of molecular triplet states in organic dye lasers. *IEEE Journal of Quantum Electronics*, 6(7):411–416, July 1970.
- [222] O. G. Peterson, J. P. Webb, W. C. McColgin, and J. H. Eberly. Organic Dye Laser Threshold. *Journal of Applied Physics*, 42(5):1917–1928, April 1971.
- [223] Sarah Schols, Andrey Kadashchuk, Paul Heremans, Anke Helfer, and Ullrich Scherf. Triplet Excitation Scavenging in Films of Conjugated Polymers. *ChemPhysChem*, 10(7):1071–1076, May 2009.
- [224] M. Koschorreck, R. Gehlhaar, V. G. Lyssenko, M. Swoboda, M. Hoffmann, and K. Leo. Dynamics of a high-Q vertical-cavity organic laser. *Applied Physics Letters*, 87(18):181108, October 2005.
- [225] F. Bencheikh, A. S. D. Sandanayaka, T. Matsushima, J. C. Ribierre, and C. Adachi. Influence of the organic film thickness on the second order distributed feedback resonator properties of an organic semiconductor laser. *Journal of Applied Physics*, 121(23):233107, June 2017.
- [226] Yongsheng Hu, Fatima Bencheikh, Sébastien Chénais, Sébastien Forget, Xingyuan Liu, and Chihaya Adachi. High performance planar microcavity organic semiconductor lasers based on thermally evaporated top distributed Bragg reflector. *Applied Physics Letters*, 117(15):153301, October 2020.
- [227] C. Karnutsch, C. Pflumm, G. Heliotis, J. C. deMello, D. D. C. Bradley, J. Wang, T. Weimann, V. Haug, C. Gärtner, and U. Lemmer. Improved organic semiconductor lasers based on a mixed-order distributed feedback resonator design. *Applied Physics Letters*, 90(13):131104, March 2007.
- [228] Boon Kar Yap, Ruidong Xia, Mariano Campoy-Quiles, Paul N. Stavrinou, and Donal D. C. Bradley. Simultaneous optimization of charge-carrier mobility and optical gain in semiconducting polymer films. *Nature Materials*, 7(5):376–380, May 2008.
- [229] Ruidong Xia, Wen-Yong Lai, Peter A. Levermore, Wei Huang, and Donal D. C. Bradley. Low-Threshold Distributed-Feedback Lasers Based

- on Pyrene-Cored Starburst Molecules with 1,3,6,8-Attached Oligo(9,9-Dialkylfluorene) Arms. *Advanced Functional Materials*, 19(17):2844–2850, September 2009.
- [230] Gerald Kranzelbinder, Eric Toussaere, Joseph Zyss, Thomas Kavc, Gregor Langer, and Wolfgang Kern. Organic surface emitting laser based on a deep-ultraviolet photopolymer containing thiocyanate groups. *Applied Physics Letters*, 82(14):2203–2205, April 2003.
- [231] Emiliano R. Martins, Yue Wang, Alexander L. Kanibolotsky, Peter J. Skabara, Graham A. Turnbull, and Ifor D. W. Samuel. Low-Threshold Nanoimprinted Lasers Using Substructured Gratings for Control of Distributed Feedback. *Advanced Optical Materials*, 1(8):563–566, August 2013.
- [232] Buddhika S. B. Karunathilaka, Umamahesh Balijapalli, Chathuranganie A. M. Senevirathne, Seiya Yoshida, Yu Esaki, Kenichi Goushi, Toshinori Matsushima, Atula S. D. Sandanayaka, and Chihaya Adachi. Suppression of external quantum efficiency rolloff in organic light emitting diodes by scavenging triplet excitons. *Nature Communications*, 11(1):4926, December 2020.
- [233] C. R. Lambert, H. Stiel, D. Leupold, M. C. Lynch, and I. E. Kochevar. Intensity-Dependent Enzyme Photosensitization Using 532 nm Nanosecond Laser Pulses. *Photochemistry and Photobiology*, 63(2):154–160, February 1996.
- [234] A. V. Buettner. Radiationless Transitions in Cyanine Dyes. *The Journal of Chemical Physics*, 46(4):1398–1401, February 1967.
- [235] Zilong Wu, Shaoxin Song, Xiangyu Zhu, Hao Chen, Jiajin Chi, Dongge Ma, Zujin Zhao, and Ben Zhong Tang. Highly efficient deep-blue fluorescent OLEDs based on anthracene derivatives with a triplet-triplet annihilation mechanism. *Materials Chemistry Frontiers*, 5(18):6978–6986, 2021.
- [236] Andrew J. Musser and Jenny Clark. Triplet-Pair States in Organic Semiconductors. *Annual Review of Physical Chemistry*, 70(1):323–351, June 2019.
- [237] Emma V. Puttock, Chandana Sampath Kumara Ranasinghe, Mohammad Babazadeh, Jos C. M. Kistemaker, Junhyuk Jang, Mile Gao, David M. Huang, Chihaya Adachi, Paul L. Burn, and Paul E. Shaw. Thermally activated delayed fluorescence poly(dendrimer)s detraping excitons for reverse intersystem crossing. *Journal of Materials Chemistry C*, page 10.1039.D1TC05151B, 2022.

- [238] In Seob Park, Hideaki Komiyama, and Takuma Yasuda. Pyrimidine-based twisted donoracceptor delayed fluorescence molecules: a new universal platform for highly efficient blue electroluminescence. *Chemical Science*, 8(2):953–960, 2017.
- [239] Xun Li and Wei-Ping Huang. Simulation of DFB semiconductor lasers incorporating thermal effects. *IEEE Journal of Quantum Electronics*, 31(10):1848–1855, October 1995.